Universiteit Gent
Faculteit Toegepaste Wetenschappen
Vakgroep Civiele Techniek
Laboratorium voor Hydraulica

Diastologie

Inzichten uit Modelstudies en Klinische Waarnemingen met Kleuren M-mode Doppler Echocardiografie

Diastology

Insights from Model Studies and Clinical Observations using Color M-Mode Doppler Echocardiography

ir. Stefaan De Mey

Promotor: Prof. dr. ir. Pascal Verdonck

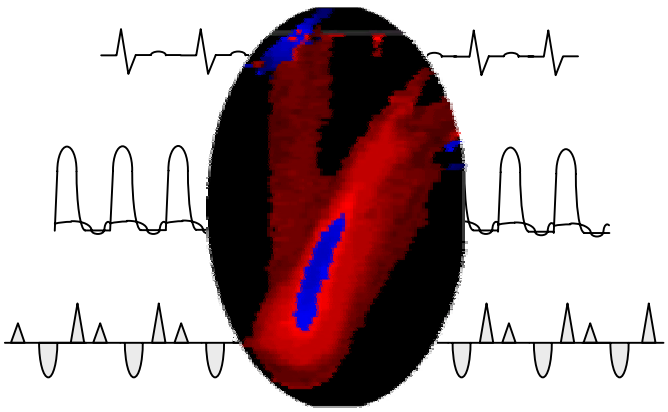

Proefschrift tot het verkrijgen van de graad van
Doctor in de Toegepaste Wetenschappen
Academiejaar 2001-2002

Promotor: Prof. dr. ir. P. Verdonck

Laboratorium voor Hydraulica
Vakgroep Civiele Techniek (TW15V)
Faculteit Toegepaste Wetenschappen
Universiteit Gent
St.-Pietersnieuwstraat 41
B-9000 Gent

Dit onderzoek is uitgevoerd in het kader van een specialisatiebeurs van het Instituut voor de aanmoediging van Innovatie door Wetenschap en Technologie in Vlaanderen, IWT-961097.

Voorwoord

Het schrijven van dit voorwoord geeft een vreemd gevoel. Het geeft een goed gevoel, want de sprong in het ijle, nu zowat vier jaar geleden, was blijkbaar niet in het niets. Het geeft een zuur gevoel, want het betekent een onherroepelijk einde van een mooie periode.

Het resultaat dat nu voorligt zou echter nooit zijn wat het is, zonder tal van mensen die mij op mijn weg de juiste richting wezen. In de eerste plaats mijn promotor Pascal Verdonck. Hij opende de deuren van ’t labo, om mij wegwijs te maken in de boeiende wereld van multidisciplinair onderzoek en nog veel meer.

Als bouwkundig ingenieur voelde ik mij nooit verloren in het medisch doolhof. De verdienste hiervoor ligt bij een aantal leermeesters. De gesprekken met dr. Rik Verhaaren, dr. Hans Pasteuning, dr. Tine De Bakker en dr. Pieter Vandervoort waren onvervangbaar. De gave van Jan Vierendeels om dit alles ook nog eens in een ingenieurscontext te plaatsten maakte de cirkel rond.

En passant introduceerde Pieter Vandervoort mij dan ook nog in “zijn” Cleveland Clinic. Gewapend met gastvrijheid en openheid, voor en na de uren, duwden dr. Jim Thomas en ir. Neil Greenberg er het onderzoek in een definitieve plooi.

Niet dat er dichter bij huis geen mensen met interesse mijn activiteiten volgden. Neem nu dr. Johan De Sutter en Marc De Buyzere. Hun suggesties en hulp bij het uitwerken van ideeën, maar ook hun aanhoudend enthousiasme om nog maar eens een manuscript te doorworstelen werden enorm op prijs gesteld.

Bij dit alles zou ik nog het zenuwcentrum vergeten: de Penthouse. Ietwat op de achtergrond, maar toch altijd nadrukkelijk aanwezig was Patrick. Zijn zin voor realisme was een vertrouwd rustpunt. Steeds op de voorgrond, maar in de eindfase afwezig wegens verhuis naar Leuven, was Peter. In zijn eigen stijl toonde hij me voor hoe het moest, zowel op als naast het veld. De vriendschap van Sunny, Dirk, Stijn, Kris, Fadi, Koen, Luc, Robert, en Marc vormden het peper en zout op het labogerecht, klaargemaakt in de keuken van driesterren chef prof. Ronny Verhoeven. Ook de bijdrage van mijn thesisstudenten heb ik erg gewaardeerd: Sara, Christophe, Jimmy, Kris, Annelien en Dieter, bedankt!

Ondertussen stond de wereld thuis ook niet stil. Dorothée, mijn ouders en familie volgden de vooruitgang met interesse. Steeds was er begrip voor mijn afwezige aanwezigheid (of was het omgekeerd?). Dit werk wordt dan ook aan hen opgedragen.

En zo beland ik finaal weer aan de deur van ‘t labo. Deze keer overschrijd ik de drempel in de andere richting. Het geeft een warm gevoel te weten dat ik een huis vol vrienden achterlaat. Gelukkig is de wereld klein.

Stefaan.

Gent, September 2001.

SINCE ARISTOTLE,
EVERYTHING IS TO BE CLEAVED
INTO TWO POSSIBILITIES:
TRUE OR FALSE, YES OR NO…

NATURE HAS NOWHERE DRAWN SUCH A LINE.

Table of Contents

Nederlandstalige Synthese

Inhoudstafel Nederlandstalige Synthese

Doelstelling en Opbouw van het Proefschrift

Doelstelling

Congestief hartfalen is een belangrijke doodsoorzaak in de Westerse maatschappij. Twee verschillende mechanismen kunnen mede aan de grondslag liggen: systolische disfunctie en diastolische disfunctie. Het kunnen onderscheiden van systolisch en diastolisch hartfalen vormt een essentiële voorwaarde voor een accurate behandeling. De optimale therapie voor één bepaalde toestand kan immers een negatief effect hebben op de andere. In tegenstelling tot systolisch hartfalen, is de definitieve diagnose van diastolisch hartfalen in de klinische praktijk moeilijk te stellen.

Diastologie is de wetenschap die zich toelegt op de studie van een gestoorde LV vulling. Meer dan enkel het achterhalen van de mechanismen aan de grondslag voor diastolisch hartfalen, wordt ook gestreefd naar een integratie van de resultaten in klinisch bruikbare technieken. De voorbije jaren zijn belangrijke basismechanismen van diastolisch hartfalen bestudeerd. Tezelfdertijd zijn parameters afkomstig van zowel invasieve als niet-invasieve metingen geïntroduceerd als merkers van diastolische disfunctie. Invasieve drukmetingen laten toe diastolisch hartfalen onweerlegbaar vast te stellen. Het gebruik van invasieve technieken in grote groepen patiënten is echter duur en houdt ook risico's in. Het gebruik van alternatieve technieken, hoofdzakelijk snelheidsmetingen met Doppler echocardiografie, vormt het onderwerp van intens onderzoek. De interpretatie van Doppler parameters wordt echter bemoeilijkt door

het feit dat ze nooit los van omgevingsfactoren zoals vullingsdruk en hartritme mogen worden beschouwd .

Het doel van dit proefschrift is om een bijdrage te leveren tot de integratie van niet-invasieve technieken, i.h.b. kleuren M-mode Doppler echocardiografie, ter bepaling van diastolisch hartfalen in de klinische praktijk. De aandacht zal voornamelijk toegespitst worden op de invloed van fysiologische eigenschappen op de hemodynamica van het cardiovasculair systeem. Hierbij zal gebruik worden gemaakt van hydraulische en mathematische modellen. De resultaten worden getoetst aan data afkomstig van experimenten in honden en van patiëntenpopulaties.

Opbouw

Het proefschrift omvat 12 Engelstalige hoofdstukken, voorafgegaan door een **Nederlandstalige synthese** conform het reglement van de Faculteit Toegepaste Wetenschappen van de Universiteit Gent. De Nederlandstalige synthese bundelt een inleiding tot diastolisch hartfalen en een overzicht van de wetenschappelijke resultaten. De **12 Engelstalige hoofdstukken** kunnen onderverdeeld worden in drie delen: (1) Inleiding, (2) Methodologische aspecten en (3) Resultaten van modelstudies en klinische waarnemingen.

DEEL 1: INLEIDING

Hoofdstuk 1 biedt een inleiding tot het cardiovasculair systeem. Bijzondere aandacht wordt besteed aan de systolische en diastolische functie van het hart. Congestief hartfalen wordt geïntroduceerd en de problematiek van de diagnosestelling van diastolisch hartfalen in de klinische praktijk wordt geschetst. In **Hoofdstuk 2** wordt de lezer vertrouwd gemaakt met de technische achtergrond van de voor dit proefschrift meest relevante meettechnieken: katheteriseren, (Doppler) echocardiografie en single photon emission computed tomography (SPECT). Tenslotte wordt in hoofdstukken 3 en 4 dieper ingegaan op de huidige stand van zaken op het gebied van de evaluatie van diastolische disfunctie. **Hoofdstuk 3** bespreekt de invasieve technieken en de reeds vrij goed ingeburgerde doch beperkte standaard Doppler technieken. **Hoofdstuk 4**

behandelt uitvoerig de evaluatie van de linker ventrikel vulling met kleuren M-mode Doppler echocardiografie.

DEEL 2: METHODOLOGISCHE ASPECTEN

In deel twee worden een aantal methodologische aspecten in detail uitgewerkt. **Hoofdstuk 5** gaat dieper in op de verschillende methodes voor de berekening van de tijdsconstante van de linker ventrikel relaxatie. **Hoofdstuk 6** beschrijft de mogelijke alternatieve methodes voor de berekening van de voortplantingssnelheid van de vroege vullingsgolf in de linker ventrikel met behulp van kleuren M-mode Doppler echocardiografie. Hiertoe is de nodige software ontwikkeld om bestaande algoritmen automatisch door te rekenen. **Hoofdstuk 7** geeft een aanloop naar een mogelijke alternatieve kwantitatieve verwerking van de snelheidsinformatie in een kleuren M-mode Doppler beeld. **Hoofdstuk 8** gaat tenslotte dieper in op de beperkingen van de gepulste Doppler techniek voor het berekenen van drukgradiënten over vernauwingen. De theorie wordt hierbij getoetst aan een reëel klinisch probleem: de post-operatieve evaluatie van een aortacoarctatie.

DEEL 3: MODELSTUDIES EN KLINISCHE WAARNEMINGEN

Het derde deel bundelt de experimentele en klinische resultaten in de hoofdstukken 9 tot 12. In **hoofdstuk 9** wordt een nieuw hydraulisch model voor de studie van de vulling van de linker ventrikel voorgesteld. Met behulp van dit model is de invloed van de diastolische linker ventrikel eigenschappen op de voortplantingssnelheid van de vullingsgolf onderzocht. **Hoofdstuk 10** toetst de bevindingen van hoofdstuk 9 aan numerieke simulaties. **Hoofdstuk 11** beschrijft gedetailleerde drukmetingen in een hondenstudie. De ruimtelijke verschillen in relaxatie en druk worden in detail bestudeerd. De oorsprong van de intraventriculaire drukgradiënten wordt herbekeken. De waarnemingen worden getoetst aan en de besluiten onderbouwd met metingen in het hydraulisch model, beschreven in hoofdstuk 9. **Hoofdstuk 12** beschrijft de resultaten van een klinische toepassing. Diastolische vullingkarakteristieken worden in verband gebracht met inspanningsparameters enerzijds en infarctgroottes anderzijds.

Een **conclusie** met overzicht van originele bijdragen en mogelijk toekomstig onderzoek vormen de sluitsteen van dit proefschrift.

Deel I
Inleiding

I.1. Overzicht

Dit eerste deel van de Nederlandstalige synthese verschaft de lezer een inleiding tot:

- Het cardiovasculair systeem en diastolische en systolische functie.
- Congestief hartfalen in het algemeen en diastolisch hartfalen in het bijzonder.
- Een stand van zaken betreffende de invasieve en niet-invasieve evaluatie van diastolische disfunctie in experimentele modellen en de klinische praktijk.

I.2. Fysiologie van de Linker Ventrikel Functie

I.2.1. INLEIDING

De functie van het hart bestaat erin om het bloed in het lichaam rond te pompen om de organen en weefsels van voedingsstoffen en zuurstof te voorzien. Koolstofdioxide en afvalstoffen worden verwijderd. Het hart is een pulserende pomp met twee onderscheiden fasen: systole en diastole. Gedurende de systole pompt het hart bloed in de slagaders, gedurende de diastole vullen de hartkamers met bloed.

I.2.2. FYSIOLOGIE VAN DE HARTCYCLUS

Figuur 1 toont het stromingspatroon doorheen de hartkamers. De vena cava brengt zuurstofarm bloed van het lichaam naar het rechter atrium (RA). Via het rechter ventrikel (RV) en de pulmonale arterie pompt het hart dit bloed naar de longen. Zuurstofrijk bloed stroomt van de longen via de pulmonale venen het linker atrium (LA) binnen. Via de linker ventrikel (LV) stuwt het hart het bloed vervolgens door de aorta naar het hele lichaam. Vier kleppen garanderen de éénrichtingsstroming binnen de hartkamers: de tricuspide klep (T), de pulmonaalklep (P), de mitraalklep (M) en de aortaklep (A).

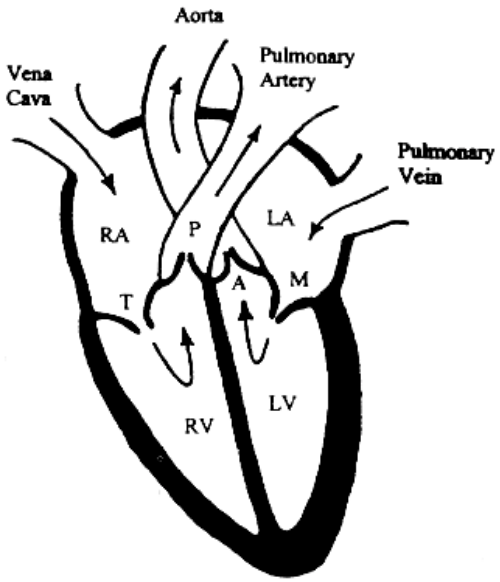

Figuur 1: De stroming doorheen de hartkamers (Bronzino 1995).

Een LV hartcyclus kan beschreven worden met behulp van het druk-volume verband zoals voorgesteld in figuur 2. De ventriculaire systole start met de isovolumetrische contractie en het sluiten van de mitraalklep op het punt B van de lus. De ventriculaire druk stijgt zeer snel gedurende deze isovolumetrische contractie. Op het ogenblik C opent de aortaklep en start de ejectiefase van de systole. Deze fase wordt gekenmerkt door een afname van de LV volume totdat de LV druk daalt tot onder de aortadruk. In het punt D heeft de LV haar minimaal of eind-systolisch volume (ESV) bereikt en sluit de aortaklep. Tussen D en A daalt de druk bij gelijkblijvend volume (isovolumetrische relaxatie). In het punt A opent de mitraalklep. De LV druk wordt dan lager dan de LA druk. De LV vulling gebeurt tussen punten A en B. In punt B bereikt de LV haar maximaal of eind-diastolisch volume (EDV) en sluit de mitraalklep. Bij het sluiten van de mitraalklep begint de volgende hartcyclus.

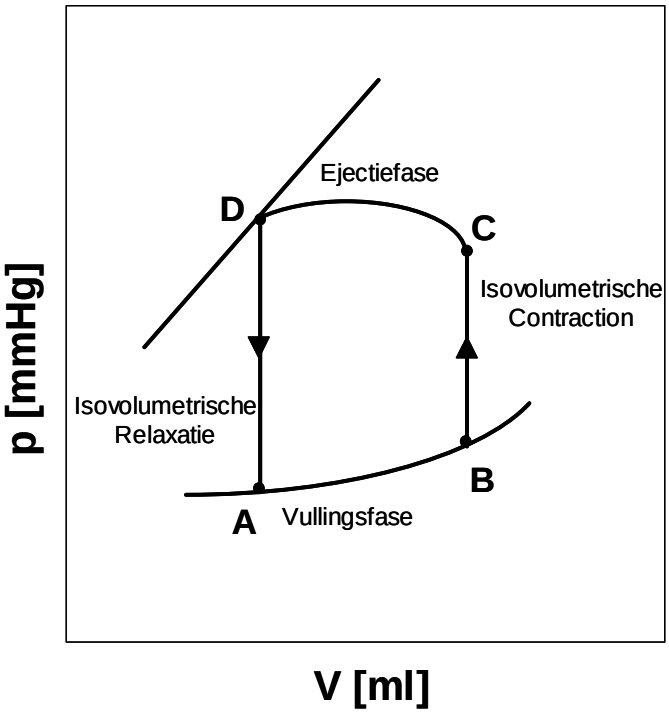

Figuur 2: Ventriculair druk-volume verband gedurende een hartcyclus;
p: LV druk, V: LV volume.

Op basis van het druk-volume verband wordt de hartcyclus ingedeeld in systole (B-C-D) en diastole (D-A-B). Figuur 3 toont een overzicht van de drukken, volumes en snelheden in het cardiovasculair systeem gedurende een hartcyclus.

Figuur 4 toont een karakteristiek snelheidsverloop van de stroming doorheen de mitraalklep tijdens de vullingsfase (Fase A-B in figuur 2), gemeten met gepulste Doppler echocardiografie. Het snelheidsverloop wordt typisch gekarakteriseerd door een bifasisch patroon. Op basis van dit patroon kan men de vullingsfase van de diastole indelen in: (1) de vroege vullingsfase, (2) de diastase en (3) de vulling tijdens atriale contractie. De eerste golf of vroege vullingsgolf (E-golf, early filling wave) komt tot stand door het drukverschil tussen LA en LV als gevolg van de isovolumetrische relaxatie van de LV waardoor de druk in de LV daalt tot onder de druk in het LA. De tweede golf (A-golf, atrial contraction wave) is het gevolg van de LA contractie waardoor de druk in het LA verhoogd wordt tot boven de druk in de LV. De diastase is de periode tussen deze twee vullingsgolven. Gedurende de diastase is het drukverschil tussen LA en LV minimaal.

I.2.3. CELLULAIRE MECHANISMEN VAN CONTRACTIE EN RELAXATIE (PRICE AND WILSON 1992)

De hartspierwand is samengesteld uit hartspiercellen (myocyten), collageenvezels en elastinevezels. De laatste twee componenten zijn belangrijk voor de celoriëntatie en de passieve elasticiteitseigenschappen van het hart. De ventriculaire myocyten hebben een lengte van 100 μm en een diameter van 20 μm. Ze zijn samengesteld uit myofibrillen, die op hun beurt een verzameling sarcomeren zijn. De sarcomeren zijn de kleinste contractiele eenheid van de hartspier en variëren in lengte tussen de 1.6 μm en 2.2 μm.

Ieder sarcomeer bestaat uit een reeks dikke myosine filamenten, elk omringd door zes dunne actine filamenten. De interactie tussen deze twee filamenten veroorzaakt een kracht die leidt tot de verkorting van de myocyt. De myocyten bevatten ook een belangrijk aandeel mitochondriën (tot 20% volume). Deze celorganellen zijn verantwoordelijk voor de productie van energie onder de vorm van ATP (adenosine trifosfaat).

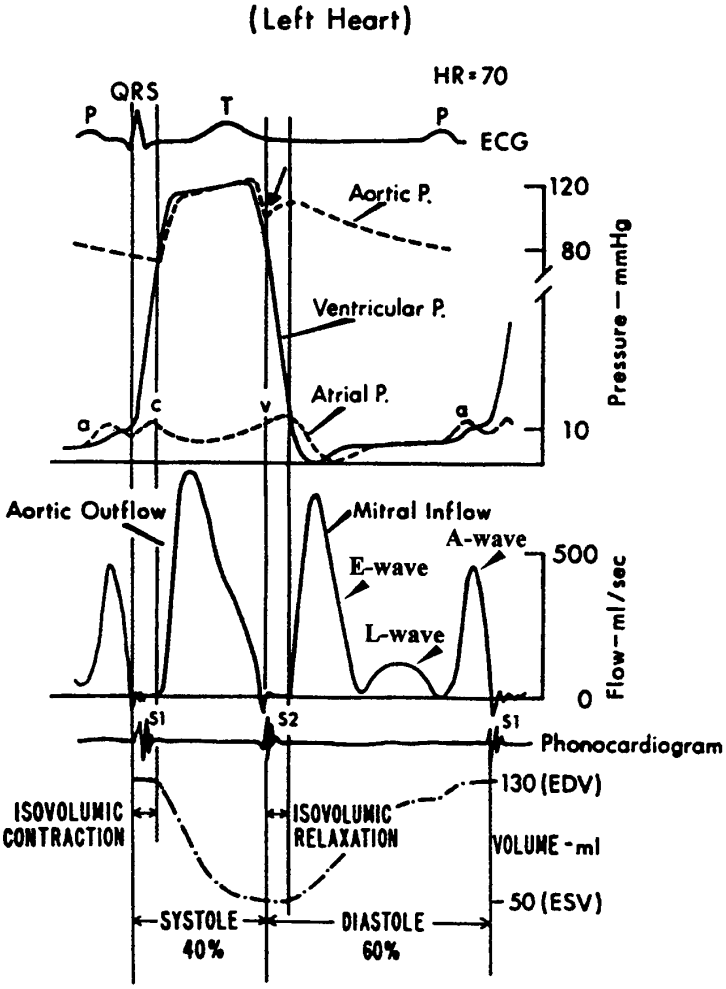

Figuur 3: Druk- , snelheids- en volumeverloop gedurende een hartcyclus zoals geschetst door Yellin et al. (Yellin 1995).

Figuur 4: Snelheidsverloop van het ventriculaire vullingspatroon gedurende twee hartcycli, gemeten met Doppler echocardiografie.

Een myocyt is omringd door een oppervlakte membraan, het sarcolemma. Ionische concentratiegradiënten worden gehandhaafd over dit membraan. Intracellulair is er een grotere concentratie aan kalium (K^+), extracellulair een grotere concentratie aan natrium (Na^+). De concentratiegradiënt wordt onderhouden door enerzijds de "natrium-kalium pomp" en anderzijds een ATP afhankelijke "calcium pomp". Troponine en tropomyosine zijn regulerende proteïnen op het actine filament. Het troponine bevat een component (troponine C) dat calcium bindt. Deze binding veroorzaakt een structuurwijziging in het tropomyosine die toelaat dat brugverbindingen kunnen gemaakt worden tussen de actine en myosine filamenten. De brugverbindingen schuiven de actine filamenten tussen de myosine filamenten en veroorzaken de spierverkorting. In de myocyten wordt het calcium cyclisch vanuit een intracellulair buizennetwerk, het sarcoplasmatisch reticulum, naar de actine filamenten gebracht. Het transport van het calcium over het membraan van het reticulum gebeurt door het membraangebonden proteïne fosfolambane. Het verwijderen van de calcium verbreekt de brugverbindingen en veroorzaakt de relaxatie van de spier. De snelheid van de afname van de spierspanning houdt rechtstreeks verband met de snelheid waarmee calcium van het troponine wordt verwijderd. Dit proces vergt energie. Vanuit het perspectief van de cel is het relaxatieproces dus een actief proces. Bovendien start de LV relaxatie reeds tijdens de ejectiefase. Deze feiten ondersteunen een alternatieve definitie van systole en diastole waarbij de volledige relaxatieperiode en vroege vullingsfase gerekend wordt bij de systole (Brutsaert and Sys 1989, Gillebert and Sys 1994). In deze definitie bestaat diastole enkel uit diastase en LA contractie. Deze zienswijze verschaft nuttige inzichten voor fysiologen, maar werkt verwarrend voor clinici die een indeling maken op basis van fenomenologische feiten en ervan uitgaan dat de diastole start bij het sluiten van de aortaklep en de systole start bij het sluiten van de mitraalklep.

I.2.4. CARDIOVASCULAIRE FUNCTIE

De functie van het hart bestaat erin om het bloed in het lichaam rond te pompen om zo in de metabolische behoeften van het lichaam te voorzien. De hoeveelheid rondgepompt bloed per minuut wordt hartminuutvolume (cardiac output, CO) genoemd en wordt gegeven door vergelijking 1:

$$CO = HR \cdot SV \qquad [V.\ 1]$$

Hierin is HR het hartritme en SV het slagvolume. Het slagvolume is de verpompte hoeveelheid bloed in een hartslag en kan in het geval van intakte hartkleppen berekend worden als het verschil tussen eind-diastolisch en eind-systolisch volume (SV = EDV – ESV). De ejectiefractie (EF) is de verplaatste hoeveelheid, in verhouding tot het eind-diastolische volume (EF = SV/EDV).

De cardiale functie wordt in essentie bepaald door hartritme en slagvolume (vergelijking 1). Het hartritme wordt grotendeels bepaald door hormonale en neurogene activatie. Gezien het pulsatiel karakter van de hartpomp kan en moet het slagvolume vanuit twee perspectieven benaderd worden: systole en diastole. Immers, wenst het hart een bepaald slagvolume te realiseren, dan zal het niet alleen in staat moeten zijn dit slagvolume te kunnen uitpersen tegen de perifere weerstand tijdens systole, maar zal het hart evenzeer in staat moeten zijn om ditzelfde slagvolume te kunnen ontvangen tijdens de voorafgaande diastole. Men spreekt van systolische versus diastolische functie.

I.2.4.1. Systolische Functie

De systolische functie wordt voornamelijk bepaald door vullingssdruk (voorbelasting), inotropische effecten (contractiliteit) en de perifere weerstand (nabelasting).

Voorbelasting

Het verband tussen voorbelasting en hartminuutvolume wordt “de wet van het hart” genoemd en werd reeds beschreven door Starling (Starling 1918) in het begin van de 20^{e} eeuw. Het mechanisme is een gevolg van de typische actine-myosine structuur van de sarcomeren, waarbij bij het uitrekken van de sarcomereren tengevolge van een hogere voorbelasting meer bindingsplaatsen vrijkomen, en vertaalt zich in een positief verband tussen rek (of eind-diastolisch volume) en ontwikkelde kracht. Experimenten bij isovolumetrische en isotonische contracties in kikkerharten uitgevoerd door Frank enerzijds (Frank 1895), en onderzoek naar het gedrag van LV volume en EF bij wisselende veneuze instroming en perifere weerstand door Starling anderzijds (Starling 1918), lagen aan de basis van de ontdekking van dit mechanisme, dat dan ook bekend staat als het “Frank-Starling mechanisme”.

Contractiliteit

Contractiliteit verwijst naar veranderingen in krachtontwikkeling van de hartspiercel tijdens contractie, onafhankelijk van veranderingen in de lengte van de sarcomeren. Een stijging in contractiliteit kan het gevolg zijn van een versterking van de interactie tussen de bindingen tussen actine en myosine, zonder dat het aantal beschikbare bindingsplaatsen toeneemt. De intensiteit van de bindingen houden rechtstreeks verband met de concentratie van intracellulaire vrije calcium ionen.

Nabelasting

De nabelasting kan gedefinieerd worden als de spanning die de LV wand moet ontwikkelen tijdens de systole om de aortaklep te openen en bloed te ejecteren in de systeemcirculatie. Wanneer men de geometrie van de LV beschouwd als een dunwandige bol met straal r en wanddikte h, kan een eenvoudig verband tussen wandspanning (σ) en druk (p) opgesteld worden ("wet van Laplace", (Shintani and Glantz 1994)):

$$\sigma = \frac{p \cdot r}{2 \cdot h} \qquad [V.\ 2]$$

Dit eenvoudige model kan uitgebreid worden naar meer complexe niet-dunwandige geometrieën. De rekken worden dan verkregen door veronderstellingen te maken omtrent de visco-elastische eigenschappen van de hartspierwand (Arts et al. 1993).

I.2.4.2. Diastolische Functie

Belangrijke determinanten voor de diastolische functie zijn vullingsdruk (voorbelasting), ventriculaire relaxatie en passieve LV eigenschappen.

Voorbelasting

De stroming van LA naar LV wordt rechtstreeks bepaald door het drukverschil over de mitraalklep in combinatie met de weerstand, gevormd door de mitraalklep. De voorbelasting of LA druk is aldus ook voor de diastolische functie een kritische factor.

Afhankelijk van de fase in de hartcyclus varieert de LA functie van reservoir functie tijdens ventriculaire systole (gesloten mitraalklep) over doorvoerleiding tijdens de diastasis tot pompfunctie tijdens LA systole (Arakawa et al. 1989).

In normale omstandigheden is de weerstand van de mitraalklep minimaal. Dit houdt in dat de klepblaadjes zelf nauwelijks weerstand bieden en voornamelijk de stroming volgen. De weerstand wordt in hoofdzaak bepaald door de geometrie (diameter) van de klep t.o.v. de afmetingen van LA en LV (Verdonck et al. 1996).

Relaxatie

In het normale hart start de ventriculaire relaxatie in de tweede helft van de systole en loopt door tot het eerste derde deel van de vroege vulling. De relaxatie gaat gepaard met een exponentiële drukdaling van drukken op het eind-systolische niveau tot drukken, lager dan de LA druk. Aangezien de mitraalklep enkel opent op het moment dat de LV druk daalt tot onder de LA druk, zijn de start, snelheid en de mate van relaxatie belangrijke determinanten voor de diastolische vulling en functie. De relaxatie van de hartspiercellen is rechtstreeks afhankelijk van calcium transport. Fysiologische determinanten zijn hartritme, temperatuur, neuronhormonale stimulatie (Lenihan 1995), maar ook belasting (Gillebert et al. 1997).

Passieve LV Eigenschappen

Tijdens diastase en LA contractie is de vulling hoofdzakelijk afhankelijk van het passief druk-volume verband. Het centrale uitgangspunt is dat de netto druk binnen de LV het resultaat is van het evenwicht tussen de drukkrachten binnenin de LV holte en de weerstandbiedende krachten tengevolge van de elasticiteit van het myocardium. De interne druk zorgt voor een expansie van de LV, de wandspanning werkt de expansie tegen. Tijdens de diastole kan dit verband benaderd worden met de vergelijking 3:

$$p = b \cdot e^{k_c \cdot V} \qquad [V.\ 3]$$

Hierin is p de druk in de hartcaviteit, V het volume; b en k_c zijn constanten (Gaasch 1994). Dit exponentieel verband resulteert in een lineair verband tussen de ogenblikkelijke stijfheid (“operating stiffness”) dp/dV en de druk volgens de vergelijking 4:

$$\frac{dp}{dV} = k_c \cdot (b \cdot e^{k_c \cdot V}) = k_c \cdot p \qquad [V.\ 4]$$

De parameter k_c is aldus een index voor de stijfheid. De stijfheid is het reciproque van de compliantie. De stijfheid karakteriseert het volledige LV. Inzicht in functionele en structurele afwijkingen van het myocard kunnen het best onderzocht worden door studie van de spanning-rek verbanden van de wand van de LV (cf. supra: Laplace wet).

I.2.5. VULLING VAN DE LV: ACTIEF OF PASSIEF PROCES?

Inleiding

Verscheidene factoren zoals de actieve relaxatie, elasticiteitskarakteristieken van het myocardium en de karakteristieken van het pericardium bepalen in belangrijke mate het diastolische druk-volume verband (Gaasch and Le Winter 1994). De vraag is in welke mate, wanneer tijdens de vulling en hoelang de verschillende invloedsfactoren een significant effect uitoefenen op het diastolisch druk-volume verband. Zoals hoger uiteengezet kan de diastolische fase van de hartcyclus onderverdeeld worden in vier onderscheiden perioden. Gedurende elk van deze perioden zullen bepaalde karakteristieken in meer of mindere mate een invloed uitoefenen op de LV vulling. Tijdens de isovolumetrische relaxatie en het eerste deel van de vroege vullingsfase (E-golf, early filling wave) zal voornamelijk de relaxatie van de hartspier een belangrijke rol spelen. Hoe verder de diastole vordert en hoe meer het actieve relaxatieproces vermindert, hoe meer de passieve materiaaleigenschappen van de LV het verdere verloop van de vulling zullen bepalen. Onderzoek (Brecher and Kissen 1957, Nikolic et al. 1988, Yellin and Nicolic 1994) geeft echter aanwijzingen dat de passieve LV eigenschappen ook tijdens de vroege vullingsfase reeds aan de orde kunnen zijn. Volgens deze theorie kan onder specifieke omstandigheden de vroege vulling geïnitieerd worden door een combinatie van krachten tengevolge van het actieve relaxatieproces en het vrijkomen van elastische energie uit de tijdens de systole samengedrukte LV wand. Dit laatste mechanisme wordt in de literatuur “elastische terugvering” ("elastic recoil") genoemd.

Experimentele Onderbouwing

Een eerste experiment om het concept van elastische terugvering te onderbouwen werd reeds uitgevoerd in 1957 door Brecher en Kissen (Brecher and Kissen 1957) en wordt geïllustreerd in figuur 5. De grafiek toont het passief druk-volume

verband van een geïsoleerd hondenhart, bekomen door het toevoegen, respectievelijk onttrekken van een hoeveelheid vloeistof. Het evenwichtsvolume (V_0) wordt gedefinieerd als het volume waarbij in de LV een nuldruk heerst. De negatieve drukken bij volumes kleiner dan het evenwichtsvolume vormen de basis voor het concept van elastische terugvering. Op basis van deze negatieve drukken gewaagt men ook te spreken van diastolische zuigkrachten ("diastolic suction").

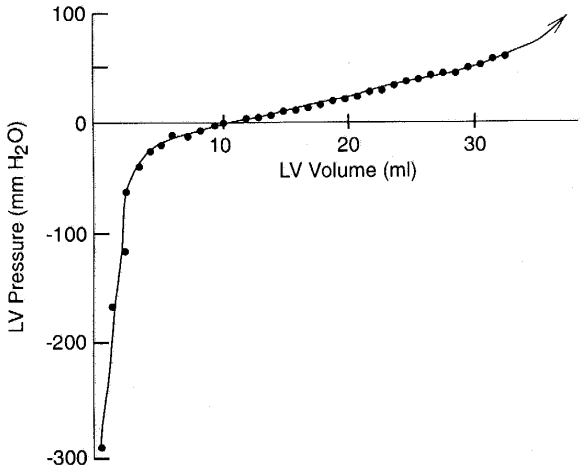

Figuur 5: Passief druk-volume verband van de LV zoals opgemeten door Brecher en Kissen (Brecher and Kissen 1957).

In een kloppend hart worden echter geen onderdrukken waargenomen. Overtuigd van het concept van zuigkrachten, ontwikkelden Yellin et al. (Yellin et al. 1986) daarom een nieuw experiment met het doel aan te tonen dat de stroming tijdens de vulling van de linker hartcaviteit de aanwezige zuigkracht verdoezelt. In essentie werd in dit experiment in een kloppend hondenhart het drukverloop in de LV gemeten tijdens een niet-vullende hartslag. De verhindering van de vulling werd bekomen met behulp van een speciaal daartoe ontworpen elektromagnetisch gestuurde klem. De onderzoekers kregen aldus de mogelijkheid om een LV druk te meten die niet beïnvloed wordt door de vulling van het LV en de LA druk. De drukdaling is enkel te wijten aan de relaxatie en het vrijkomen van de energie, opgeslagen in de LV wand. De hoofdconclusie van de experimenten was dat in de afwezigheid van vulling en vertrekkende van een ESV beneden het evenwichtsvolume V_0, de LV druk gedurende de relaxatie evolueert naar een

negatieve waarde. De uiteindelijke negatieve eindwaarde schrijven de onderzoekers toe aan het vrijkomen van elastische energie, opgeslagen in de hartwand.

Tonen de experimenten van Yellin et al. wel aan dat passieve LV wandeigenschappen ook tijdens de vroege vullingsfase een invloed uitoefenen, dan mag het begrip zuigkracht in deze context echter niet letterlijk gehanteerd worden. Deze discussie wordt samengevat in figuur 6.

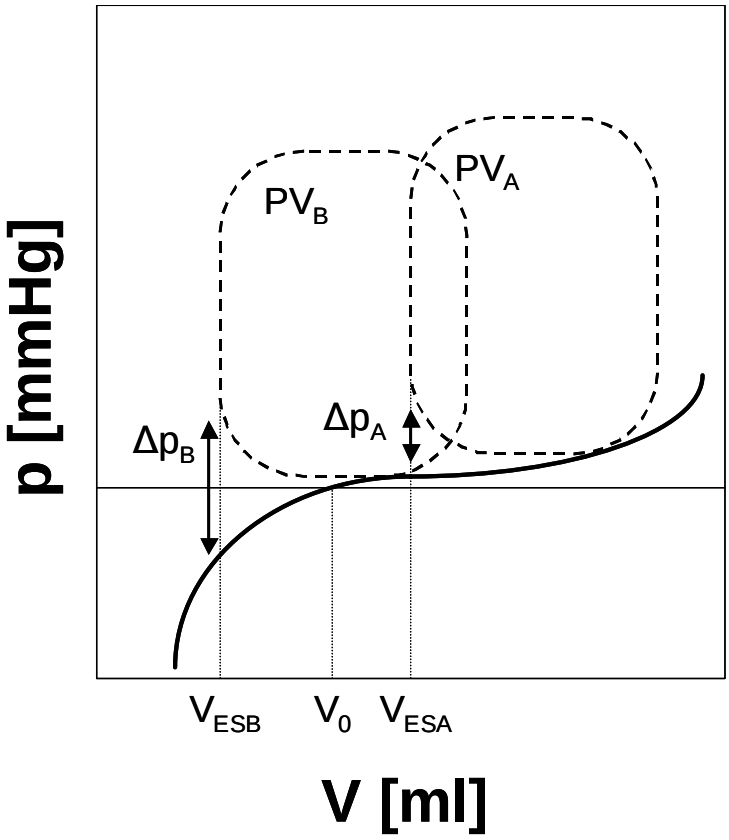

Figuur 6: Druk-volume verbanden in de LV.

De grafiek toont schematisch een passief druk-volume verband van de LV (volle lijn) en twee realistische druk-volume verbanden (PV_A en PV_B, onderbroken lijnen) van een actieve LV hartcyclus. Het ESV van PV_A (V_{ESA}) is groter dan het evenwichtsvolume (V_0). Het ESV van PV_B (V_{ESB}) is kleiner dan V_0. De drukken zijn in beide gevallen gedurende de volledige lus positief. Per definitie is de term zuigkracht dus niet van toepassing in het geval van een normaal relaxerend en vullend LV. Eerder dan een zuigkracht kan men spreken van een drijvende kracht

tengevolge van het verschil in werkelijke diastolische druk, zoals aangegeven door de effectieve druk-volume verbanden PV_A en PV_B, en de theoretische drukken die bekomen kunnen worden bij een niet-vullende hartslag, zoals kan afgelezen worden van het passieve druk-volume verband. In figuur 6 worden deze drukverschillen voor PV_A en PV_B respectievelijk aangeduid met Δp_A en Δp_B. Afhankelijk of het ESV groter dan wel kleiner is dan het evenwichtsvolume situeren deze drukverschillen zich al dan niet deels langs de negatieve zijde van de drukas. Enkel de absolute grootte van het drukverschil kan echter een invloed hebben op de vulling.

De cruciale vraag bij dit alles is hoe groot dit drukverschil moet zijn om een adequate vulling te bekomen bij een gezond hart. Een andere vraag is of een goed functionerend hart het grote drukverschil, in het geval van een ESV veel kleiner dan het evenwichtsvolume, werkelijk nodig heeft en benut. Verdonck et al. met een 1D model (Verdonck et al. 1999) en Vierendeels et al. (Vierendeels et al. 2000) met een 2D model voor de LV vulling hebben immers aangetoond dat voor volumes groter dan het evenwichtsvolume, d.i. voor een vulling zonder zogenaamde “zuigkracht”, fysiologisch normale vullingpatronen kunnen optreden.

I.3. Congestief Hartfalen en Diastolische Disfunctie

I.3.1. CONGESTIEF HARTFALEN

Een klassieke definitie van congestief hartfalen (CHF) is het falen van het hart om in rust en tijdens inspanning een adequaat hartminuutvolume te genereren om aan de metabole behoeften van het lichaam te voldoen bij normale (lage) vullingsdrukken (Braunwald 1992).

Vroeger werd CHF zeer vaak herleid tot systolisch hartfalen (SHF). Het mogelijke belang van een verstoorde diastolische functie, diastolisch hartfalen (DHF), werd lange tijd niet onderkend. Dit is mede het gevolg van de moeilijkheid om diastolisch hartfalen op een eenvoudige manier vast te stellen. Voorbelasting werd immers algemeen gebruikt om de systolische functie te evalueren via het Frank-Starling mechanisme. Zoals hoger uiteengezet is voorbelasting echter een determinant van zowel de systolische als diastolische functie.

Het maken van een onderscheid tussen DHF en SHF is belangrijk omdat beide pathologische toestanden verschillende oorzaken hebben en ook een andere behandelingswijze vergen. Sterker, de gepaste behandelingswijze voor de ene vorm van hartfalen kan contraproductief werken op de andere.

Studies in Europa en de verenigde staten schatten de prevalentie van CHF op 3 tot 21 per 1000 voor de volledige populatie en 23 tot 130 per 1000 voor personen ouder dan 65 jaar (Murdoch and McMurray 1998). Verder tonen studies aan dat tot 40% van de patiënten met CHF een normale systolische functie hebben (Mandinov et al. 2000).

I.3.2. DIASTOLISCHE DISFUNCTIE (PRICE AND WILSON 1992)

Tal van factoren kunnen de vulling en dus de diastolische functie verstoren. (Tabel 1). Vooreerst kunnen afwijkingen in het transport van calcium aanleiding geven tot een verminderde relaxatie, geassocieerd aan diastolische disfunctie. Het calciumtransport wordt gecontroleerd door inwendige celmechanismen, maar ook door de toevoer van zuurstof via de coronaire arteriën.

Tabel 1: Invloedsfactoren van de diastolische vulling.

Relaxatie
Coronaire bevloeiing van het myocardium
Hartritme
Synchronisatie en uniformiteit van de relaxatie en contractie
Belastingstoestand van het hart
Weerstand van het pericardium
Kamereigenschappen van de LV
LV spiercel eigenschappen
Hormonale invloeden

Een stijging van het hartritme veroorzaakt een waaier compensatie mechanismen om een adequate vulling te verzekeren onder de gewijzigde toestand. Ondermeer een versnelde relaxatie, het verkorten of zelfs verdwijnen van de diastase en een verlagen van de eind-diastolische druk van de LV worden vastgesteld. De synchronisatie en uniformiteit van contractie en relaxatie bewerkstelligen een goede diastolische functie. Een verminderde diastolische functie kan waargenomen worden bij verminderde synchronisatie ten gevolge van LA fibrillatie of niet-uniformiteit ten gevolge van hypertrofie (Lenihan 1995).

Aangezien de vulling rechtstreeks gekoppeld is aan de vullingsdruk, is voorbelasting een belangrijke determinant. Een verminderde vulling, bijvoorbeeld tengevolge van een verminderde relaxatie wordt dikwijls gecompenseerd door een verhoogde vullingsdruk. Studies tonen aan dat de nabelasting eveneens een niet-onbelangrijke invloed uitoefent op de diastolische functie. Zo werd o.a. een verband gelegd tussen het niveau van de nabelasting en de relaxatie (Gillebert and Sys 1994, Leite-Moreira et al. 1999).

Passieve kamereigenschappen hebben een belangrijk aandeel in het behoud van een goede diastolische vulling. De vorm en grootte van de LV zullen in niet onbelangrijke mate het stromingpatroon en bijgevolg de vulling beïnvloeden. Anderzijds zullen ook de eigenschappen van de passieve structuur zoals elasticiteit (verandering van de spiercellengte voor een gegeven

spanningswijziging) en compliantie (verandering van het volume voor een gegeven drukverandering) hun invloed hebben (Lenihan 1995).

Het sympathisch zenuwstelsel tenslotte speelt een belangrijke rol in hartfalen op basis van systolische disfunctie. Ongetwijfeld ondergaat de diastolische functie evenzeer een grote invloed van hormonaal gemedieerde receptorkoppeling. Zo is het reeds uitvoerig aangetoond dat catecholamines zowel de contractiliteit als de relaxatie gunstig beïnvloeden. β-adrenergische stimulatie lijkt eerder de relaxatie dan wel de contractiliteit gunstig te beïnvloeden. Ook het renin-angiotensine systeem kan een rol spelen. Angiotensine-converterende-enzyme (ACE) inhibitoren kunnen onrechtstreeks een verbetering van de diastolische vulling induceren door reductie van de nabelasting. Er zijn aanwijzingen dat ACE-inhibitoren ook een rechtstreeks gunstig effect hebben op de relaxatie (Lenihan 1995).

Externe factoren, o.a. kleplijden, volumebelasting en coronair vaatlijden, kunnen leiden tot een verstoorde diastolische functie. Anderzijds kunnen interne factoren, ziektebeelden eigen aan het myocardium, aan de grondslag van DHF liggen. Voorbeelden zijn hypertrofische cardiomyopathie en restrictieve cardiomyopathie (Price and Wilson 1992). In het geval van hypertrofische cardiomyopathie neemt de diameter van de myocyten toe door productie van nieuwe myofibrillen, waardoor de wanddikte toeneemt en de hartholte sterk gereduceerd wordt. In het geval van restrictieve cardiomyopathie wordt de ventrikelwand abnormaal stijf zonder hypertrofie van de wand.

I.4. Diastologie

I.4.1. INLEIDING

Het kunnen onderscheiden van systolisch en diastolisch hartfalen vormt een essentiële voorwaarde voor een accurate behandeling van congestief hartfalen. De optimale therapie voor één bepaalde toestand kan immers een negatief effect hebben op de andere. In tegenstelling tot systolisch hartfalen, is de definitieve diagnose van diastolisch hartfalen in de klinische praktijk moeilijk te stellen. Diastologie is de wetenschap die zich toelegt op de studie van diastolische disfunctie. Meer dan enkel het achterhalen van de mechanismen aan de grondslag voor diastolisch hartfalen, wordt ook gestreefd naar een integratie van de experimentele resultaten in klinisch bruikbare technieken. De voorbije jaren zijn belangrijke basismechanismen van diastolisch hartfalen bestudeerd. Tezelfdertijd zijn parameters afkomstig van zowel invasieve als niet-invasieve metingen geïntroduceerd als merkers van diastolische disfunctie.

I.4.2. INVASIEVE EVALUATIE MET DRUKMETINGEN

I.4.2.1. Drukverschillen

De onderliggende drijvende kracht van de LV vulling is het drukverschil tussen LA en LV. Met behulp van katheteriseren kunnen drukken in LA en LV rechtstreeks gemeten worden. De drukverschillen tussen LA en LV worden in de klinische praktijk zelden invasief gemeten. Dit is omdat de simultane meting van drukken zowel in het LA als in de LV meestal praktisch onmogelijk is: daar waar katheteriseren toelaat om retrograde metingen uit te voeren in de LV over de aortaklep, is de retrograde meting van LA drukken over de mitraalklep een zeer moeilijke zaak en niet verantwoord voor routine onderzoeken.

Doorgaans wordt de druk in de LV als homogeen verdeeld beschouwd. Nochtans treden er in iedere hartcaviteit ook regionale drukgradiënten op. De aanwezigheid van regionale drukverschillen in de LV (intraventricular pressure gradients, IVPG) zijn voor het eerst gerapporteerd door Ling et al. in 1979 (Ling et al. 1979) en Falsetti et al. in 1980 (Falsetti et al. 1980). Ling observeerde in honden gedurende de diastolische vulling een drukverschil van 2 à 5 mmHg tussen het

midden van de LV en de apex. Ook Falsetti observeerde drukverschillen van 2 mmHg tussen basis en apex.

In 1988 en 1990 bestudeerden Courtois et al. (Courtois et al. 1988, Courtois et al. 1990) de IVPG in detail. Hij kon aantonen dat de IVPG verdwenen gedurende ischemie. Meer nog: het verdwijnen van deze gradiënten blijkt één van de vroegste en meest gevoelige indicatoren voor de aanwezigheid van myocardiale ischemie. Deze observatie bewijst het klinisch belang van de studie en de mogelijk grote diagnostische waarde van deze drukgradiënten.

Hoewel het bestaan van deze IVPG reeds lang bekend is, is de oorsprong en het mechanisme ervan nog een punt van discussie. Nikolic et al. (Nikolic et al. 1995) hebben onderzoek verricht naar de oorsprong van deze drukgradiënten. Hun bevindingen wijzen erop dat de grootte van de drukgradiënten evenredig is met de zogenaamde “zuigkracht” zoals hoger beschreven. Simulaties van Verdonck et al. (Verdonck et al. 1999) in een 1D en Vierendeels et al. (Vierendeels et al. 2000) in een 2D model tonen echter aan dat de aanwezigheid van IVPG op zich geen voldoende bewijs zijn om een “zuigkracht” aan te tonen. De simulaties tonen aan dat ook bij ESV groter dan het evenwichtsvolume IVPG voorkomen, vergelijkbaar met de drukgradiënten zoals opgemeten in de experimentele studies.

I.4.2.2. Relaxatie

De wijze waarop het drukverschil tussen LA en LV tot stand komt wordt grotendeels beïnvloed door de relaxatie van de hartspierwand. Tijdens de relaxatie daalt de LV druk van de eind-systolische druk tot onder het drukniveau in het LA.

De drukdaling gedurende de relaxatie kan gekarakteriseerd worden door de maximale negatieve drukverandering ($-dp/dt_{max}$). Het ogenblik dat deze waarde optreedt valt ongeveer samen met het moment dat de aortaklep sluit (Weisfeldt et al. 1974).

De maximale negatieve drukverandering bepaalt slechts één punt van de drukcurve. Bovendien is de waarde niet onafhankelijk van de maximale ventriculaire druk. Interpretaties betreffende de volledige isovolumetrische relaxatie op basis van dit ene punt dienen dus met de nodige voorzichtigheid te gebeuren. De berekening van een tijdsconstante voor de relaxatie poogt aan dit probleem tegemoet te komen. Hiertoe beschreef Weiss et al. (Weiss et al. 1976)

als eerste de drukval tijdens de isovolumetrische relaxatie als een exponentieel dalende functie. Behoudens een aantal uitzonderingen (Courtois et al. 1997, Senzaki et al. 1999), wordt een mono-exponentiële beschrijving voldoende accuraat geacht. In deel 2, paragraaf 2 wordt dieper ingegaan op de berekening van de tijdsconstante van de isovolumetrische drukval.

I.4.3. Niet-invasieve Evaluatie met Doppler Echocardiografie

I.4.3.1. Inleiding

De rechtstreekse kwantificering van belangrijke determinanten van de diastolische functie zoals voorbelasting, relaxatie en compliantie vereist het meten van drukken en/of volumes. Om kosten, risico en ongemakken gepaard gaande met katheteriseren te vermijden, is men op zoek gegaan naar alternatieven. Sinds haar introductie in het begin van de jaren 1980, is Doppler echocardiografie uitgegroeid tot de methode bij uitstek om op een niet-invasieve manier diastolische functie te evalueren. Hierbij dient wel benadrukt dat met Doppler echocardiografie de vulling gemeten wordt. De afgeleide vullingkarakteristieken geven slechts onrechtstreekse informatie over de onderliggende eigenschappen van de hartspier. Vullingpatronen worden bovendien bepaald door de integraal van alle heersende randvoorwaarden. Karakteristieken, afgeleid uit de stromingspatronen, moeten dan ook in de context van al deze randvoorwaarden geïnterpreteerd worden.

I.4.3.2. Gepulste Doppler Echocardiografie

Wegens de eenvoud in gebruik, de relatief lage economische kost en de superieure tijds- en snelheidsresolutie is de gepulste Doppler techniek (Pulsed wave Doppler, PWD) uitgegroeid tot de “standaard” methode voor de studie van de diastolische vulling.

Transmitraalstroming

Typisch wordt het snelheidspatroon opgemeten met het meetvolume geplaatst tussen de klepbladen van de mitraalklep (Figuur 7, links) (Nishimura and Tajik 1997). Het waargenomen snelheidspatroon is reeds hoger besproken en is schematisch voorgesteld in figuur 7 (rechts).

De acceleratie (a) van de stroming over de mitraalklep gedurende de vroege vullingsfase (E-golf) is een rechtstreeks gevolg van het drukverschil tussen LA en

LV dat op zijn beurt een rechtstreeks gevolg is van de ventriculaire relaxatie. Voor een vaste LV druk is de acceleratie recht evenredig met de LA druk en omgekeerd evenredig met de relaxatieconstante τ (Thomas et al. 1991, Thomas and Weyman 1991). De deceleratietijd (dt) weerspiegelt de stijging van de ventriculaire druk vanaf het moment dat bloed de LV binnen stroomt. De deceleratietijd blijkt sterk afhankelijk te zijn van de relaxatie. Een derde courant gebruikte karakteristiek van dit instroompatroon is de verhouding van de maximale snelheden van de E- en A-golf. In normale omstandigheden is de maximale snelheid van de E-golf groter dan de maximale snelheid van de A-golf. De E over A verhouding is in dat geval groter dan 1.

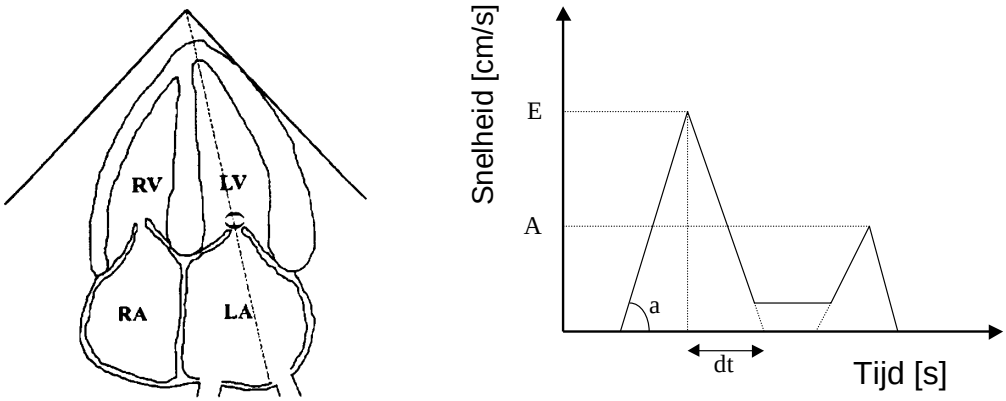

Figuur 7: Plaatsing van het meetvolume en schematische voorstelling van de Doppler snelheid over de mitraalklep.

De ontwikkeling van diastolische disfunctie verloopt over verschillende stadia. Het transmitraal Doppler patroon volgt hierbij een specifiek verloop dat wordt weerspiegeld in de bijhorende afgeleide indices. De verschillende stadia van diastolische disfunctie worden geïllustreerd in figuur 8.

In een eerste stadium van diastolische disfunctie, gekenmerkt door een vertraagde relaxatie, vermindert de snelheid van de E-golf. De LA contractie zal voor de verminderde vulling compenseren waardoor de maximale snelheid van de A-golf toeneemt. De E over A verhouding wordt kleiner dan 1. Typisch voor dit stadium is ook een langere deceleratietijd. In een volgend stadium zal de onder normale drukken verminderde vulling gecompenseerd worden door een stijging van de LA druk. Hierdoor stijgt de maximale E-snelheid opnieuw. De E over A verhouding

wordt opnieuw groter dan 1. Men spreekt van pseudo-normalisatie. Ook de deceleratietijd neemt opnieuw af. Bij verdere terugval van de diastolische functie neemt de E-piek verder toe en de A-piek verder af. Het Doppler patroon evolueert naar een restrictief patroon. In het eindstadium is het restrictief patroon irreversibel.

Door het verplaatsen van de Doppler scanlijn van de tippen van de mitraalklep naar een positie dichter bij de uitstroomzone van de LV pikt men met continue Doppler echocardiografie zowel de instroomsnelheden over de mitraalklep als de uitstroomsnelheden over de aortaklep op. Het einde van de systolische uitstroming komt overeen met het sluiten van de aortaklep. De voet van de E-golf valt samen met het openen van de mitraalklep. De duur van de isovolumetrische relaxatie periode (IVRT) kan dus gemeten worden op dit beeld. De IVRT daalt met afnemende relaxatie. Analoog aan de deceleratietijd en de E/A verhouding evolueert de IVRT echter ook naar een pseudo-normale waarde in het geval van verder afnemende diastolische functie.

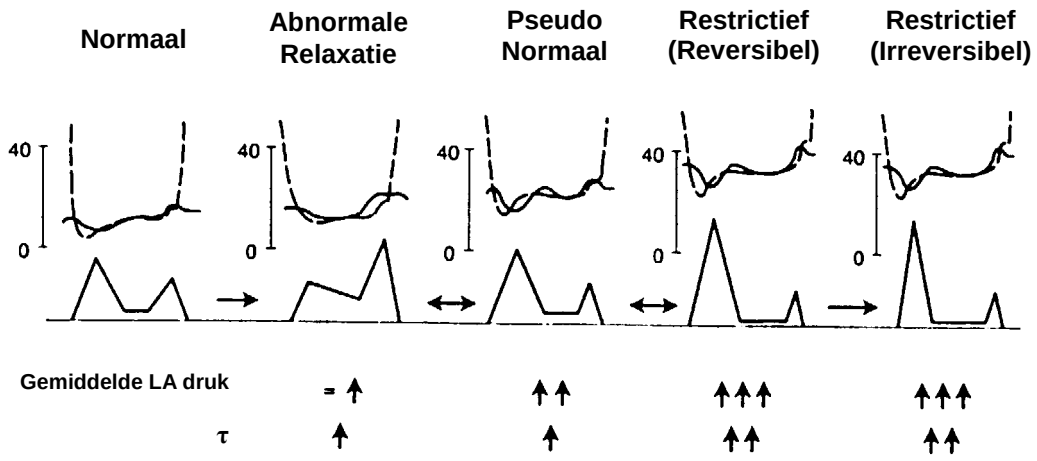

Figuur 8: Evolutie van de E/A verhouding, gemiddelde LA druk en tijdsconstante van LV relaxatie (τ) met toenemende diastolische disfunctie (Nishimura and Tajik 1997).

Alternatieven

In de klinische praktijk is het niet altijd eenvoudig vast te stellen of men met een normaal dan wel een pseudo-normaal snelheidspatroon te maken heeft. Om pseudo-normale beelden te kunnen onderscheiden van normale beelden kan men

gebruik maken van stroming in de pulmonaal venen en weefsel Doppler echocardiografie (Garcia et al. 1998).

De stroming in de longvenen wordt met PWD echocardiografie opgemeten door het meetvolume in een pulmonale vene te positioneren. In tegenstelling tot de normale situatie, contraheert in de pseudo-normale situatie het LA tegen een verhoogde nabelasting ten gevolge van een verhoogde ventriculaire stijfheid. Het bloed wordt bijgevolg preferentieel naar de pulmonaal venen gestuwd. Dit fenomeen maakt het mogelijk normale van pseudo-normale patronen te onderscheiden. Een nadeel van de longvenen stroming is echter dat ze niet altijd visualiseerbaar is met de conventionele transthoracale echocardiografie.

Weefsel Doppler echocardiografie (Tissue Doppler Imaging, TDI) is een recente nieuwe toepassing van Doppler echocardiografie. TDI maakt het mogelijk de snelheid van het myocard te registreren. Hiertoe maakt men gebruik van de klassieke PWD techniek waarbij de hogere frequentiecomponenten, tengevolge van bloedstroming, uitgefilterd worden ten voordele van de lagere frequenties, afkomstig van de wandbeweging. Met het oog op de evaluatie van de diastolische functie wordt voornamelijk de axiale beweging van de LV bestudeerd door het Doppler meetvolume te plaatsen op een basaal segment van het myocard nabij de annulus van de mitraalklep. Een typisch patroon tijdens de diastole vertoont een bifasisch patroon analoog aan de transmitraalstroming met een piek tijdens de vroege vulling (E_m) en een piek tijdens LA contractie (A_m). Normale waarden voor E_m zijn groter dan 10 cm/s voor jonge personen en groter dan 8 cm/s voor ouderen. Bij vertraagde relaxatie daalt E_m onder de 8 cm/s. Omdat ook in het restrictief patroon de E_m waarde onder deze grens blijft, kan TDI als bijkomend hulpmiddel gebruikt worden om normale instroompatronen te onderscheiden van pseudo-normale patronen.

I.4.3.3. Kleuren Doppler echocardiografie

Om de beperkingen van de PWD techniek te overkomen is meer informatie nodig. Met kleuren Doppler echocardiografie wordt een ruimtelijke verdeling van snelheden gemeten. Bij de tweedimensionale kleuren Doppler techniek gaat dit ten koste van de tijdsresolutie. Hierdoor is de 2D kleuren Doppler techniek minder geschikt voor de evaluatie van diastolische functie. De CMD (color M-

mode Doppler, CMD) techniek geeft de ruimtelijke snelheidsverdeling langsheen een vaste scanlijn. De tijdsresolutie evenaart hierbij deze van de PWD techniek (Thomas et al. 1997). De techniek wordt geïllustreerd in figuur 9. Met de scanlijn georiënteerd volgens de centrale instroomas bekomt men snelheidsinformatie in de ruimte en de tijd. Deze driedimensionale informatie is weergegeven in de grafiek aan de rechterzijde van figuur 9. Door de snelheid te coderen in kleur kan men deze informatie in een tweedimensionaal vlak voorstellen. Dit is voorgesteld in het tijd-afstand vlak van de grafiek. De extra informatie in vergelijking met deze bekomen met de PWD techniek kan zowel kwalitatief als kwantitatief geïnterpreteerd worden.

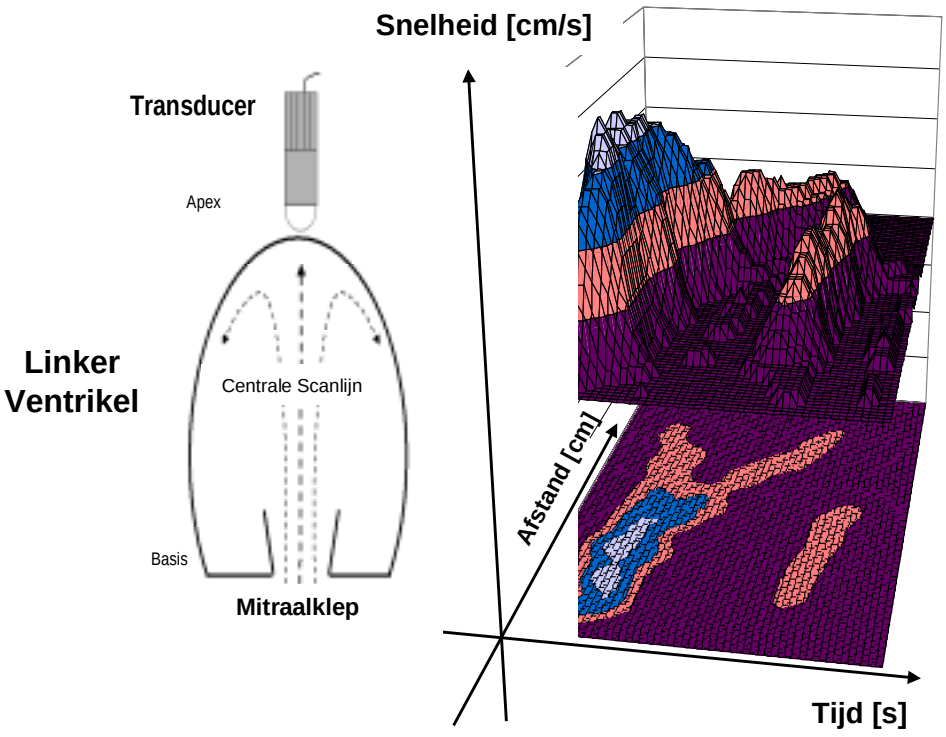

Figuur 9: 3D informatie in een CMD beeld van de LV vulling (**rechts**) voor een apicaal gepositioneerde Doppler probe met de scanlijn gealigneerd met de centrale LV instroming (**links**).

Stromingvoortplantingssnelheid

Een parameter, afgeleid van het CMD beeld en aangewend in de klinische praktijk, is de snelheid waarmee de maximale bloedsnelheid zich voortplant in de LV. Deze snelheid wordt de stromingvoortplantingssnelheid (flow propagation

velocity, v_p) genoemd. De methodes om v_p te bepalen uitgaande van een CMD beeld komen uitvoerig aan bod in paragraaf 3 van deel 2.

Hondenstudies en klinische studies hebben aangetoond dat v_p afneemt in het geval van acute ischemie, veroorzaakt door occlusie van de coronaire bloedvaten. Simultane drukmetingen brachten in deze studies ook een significant vertraagde relaxatie aan het licht (Brun et al. 1992, Stugaard et al. 1994, Stugaard et al. 1993, Takatsuji et al. 1996, Thomas et al. 1997). Recente studies suggereren dat v_p niet gevoelig is aan pseudo-normalisatie. Bij stijgende LA druk zou de afgenomen v_p niet opnieuw toenemen (Garcia et al. 1997, Moller et al. 2000b). Andere studies maken gebruik van CMD beelden om constrictieve pericarditis te onderscheiden van restrictieve cardiomyopathie (Rajagopalan et al. 2001) of voor de kwantificering van klepinsufficiëntie.

Een vulling onder abnormaal hoge LA druk duidt op diastolische disfunctie. Op empirische wijze zijn regels en formules opgesteld om uitgaande van de gemeten Doppler indices de LA druk kwantitatief te schatten. Garcia et al (Garcia et al. 1997) bijvoorbeeld vond dat:

$$LAP = 5.27 \cdot \frac{E}{v_p} + 4.6 \qquad [V.\ 5]$$

Hierin is LAP de LA druk (mmHg), E de snelheid van de E-golf (cm/s) afgeleid van het transmitraal PWD patroon en v_p de stromingvoortplantingssnelheid (cm/s) afgeleid van een CMD beeld. Het is echter duidelijk dat zolang de precieze invloed van de verschillende fysiologische parameters op de respectievelijke Doppler indices niet volledig bekend zijn, men uiterst voorzichtig moet omspringen met dergelijke formules.

Drukgradiënten over Kleppen

De stroming doorheen een opening zoals een hartklep kan beschreven worden met de vergelijking van Bernoulli. In deze vergelijking is de drukval opgebouwd uit drie termen: een convectie term, een niet-permanente term en een weerstandsdeel. In de dagdagelijkse klinische praktijk berekent men de drukval over een hartklep onrechtstreeks met een vereenvoudigde vorm van deze vergelijking:

$$\Delta p = \frac{1}{2}\rho v^2 \qquad [V.\ 6]$$

Waarin Δp de drukval over de klep (mmHg), ρ de massadichtheid van bloed (kg/m^3) en v de maximale proximale snelheid gemeten met PWD echocardiografie is (Hatle and Angelsen 1985). Deze uitdrukking verwaarloost de niet-permanente term, de weerstandsterm en een deel van de convectieve term uit de volledige vergelijking. Daartegenover staat dat deze drukgradiënt heel eenvoudig kan berekend worden aan de hand van één enkele niet-invasieve snelheidsmeting m.b.v. PWD echocardiografie.

Het gebruik van de vereenvoudigde Bernoulli vergelijking levert goede resultaten in bepaalde pathologische omstandigheden, bijvoorbeeld sterke vernauwingen, waar de niet-permanente term effectief verwaarloosbaar is. De beperkingen van PWD en de vereenvoudigde Bernoulli vergelijking voor het schatten van drukgradiënten worden in detail behandeld in paragraaf 5 van deel 2.

De vereenvoudigde vergelijking van Bernoulli, uitgebreid met de niet-permanente term, neemt volgende vorm aan:

$$\Delta p = \frac{1}{2}\rho v^2 + \rho \int_{LA}^{LV} \frac{\partial v[s,t]}{\partial t} ds \qquad [V.\ 7]$$

Men bemerkt dat in de niet-permanente term de snelheid langs een stroomlijn in functie van tijd (t) en afstand (s) voorkomt. Onderstelt men dat de CMD scanlijn centraal door de mitraalklep gaat en dat deze scanlijn samenvalt met een stroomlijn, dan levert het CMD beeld precies de nodige informatie voor het berekenen van drukgradiënt (Greenberg et al. 1996).

Intraventriculaire Drukgradiënten

Als rechtstreekse uitbreiding van de berekening van drukgradiënten over kleppen, opent CMD echocardiografie ook perspectieven om intraventriculaire drukgradiënten (intraventricular pressure gradients, IVPG) niet-invasief, in vivo te bestuderen. De berekening van de IVPG steunt op de ééndimensionale Euler vergelijking:

$$\frac{\partial p}{\partial s} = -\rho\left[\frac{\partial v}{\partial t} + v\frac{\partial v}{\partial s}\right] \qquad [V.\ 8]$$

Opnieuw is het samenvallen van de scanlijn met een stroomlijn een noodzakelijke voorwaarde. Door differentiatie van de snelheidsdistributie verkregen met CMD

echocardiografie, zowel in tijd als ruimte, kan men de distributie van de drukgradiënt in de ruimte berekenen. Integratie van deze verdeling over een bepaalde zone verschaft een ogenblikkelijke regionaal drukverschil (Greenberg et al. 2001).

Deel II
Methodologische Aspecten

II.1. Overzicht

In dit tweede deel komen wetenschappelijke resultaten aan bod die dieper ingaan op enkele methodologische aspecten met betrekking tot de invasieve en niet-invasieve bepaling van diastolische parameters en drukken:

- Bepaling van de relaxatieconstante met invasieve drukmetingen: Mono-exponentieel model met twee of drie parameters?
- Bepaling van de stromingvoortplantingssnelheid van de vroege vullingsgolf: een vergelijking van vier methoden.
- Kwantitatieve verwerking van de informatie in een CMD beeld: Berekening van de longitudinale impedantie.
- Beperkingen van PWD echocardiografie voor de bepaling van drukgradiënten met toepassing op de post-operatieve evaluatie van een aortacoarctatie.

II.2. Bepaling van de Relaxatieconstante met Invasieve Drukmetingen: Mono-exponentieel Model met Twee of Drie Parameters?

II.2.1. INLEIDING

Zowel voor klinische toepassingen als voor onderzoeksdoeleinden is het belangrijk om de relaxatie van de hartspier te kunnen evalueren. Niettegenstaande de vooruitgang in het onderzoek naar niet-invasieve methodes, blijft de analyse van het tijdsverloop van de drukdaling tijdens de isovolumetrische relaxatie de gouden standaard. Behoudens enkele uitzonderingen (Courtois et al. 1997, Senzaki et al. 1999), aanvaardt men algemeen voor de drukval een mono-exponentieel verloop:

$$p(t) = (p_0 - p_\infty) \times e^{-t/\tau} + p_\infty \qquad [V.\ 9]$$

In deze vergelijking is p(t) de druk op het tijdstip t, p_0 de druk op tijdstip 0, τ de relaxatieconstante en p_∞ de drukasymptoot. De tijdsconstante τ karakteriseert de relaxatiesnelheid, heeft de dimensies van tijd en kan geïnterpreteerd worden als de tijd waarop de druk terugvalt tot op 37 procent (1/e) van de beginwaarde (p_0) of ook nog de tijd waarop de druk op nul zou vallen indien de initiële afnamesnelheid aangehouden zou worden.

De berekening van de tijdsconstante τ voor de evaluatie van ventriculaire relaxatie werd voor het eerst beschreven door Weiss et al. in 1976 (Weiss et al. 1976). Hierbij werd om praktische redenen de asymptootwaarde nul ondersteld. Deze aanname laat immers toe om een linearisering van de vergelijking door te voeren Lineaire regressie analyse laat dan toe om de kleinste kwadratenoplossing te bepalen voor τ en p_0.

De beschikbaarheid van niet-lineaire oplossingstechnieken en krachtige rekenapparatuur hebben de noodzaak om te kiezen voor een tweeparameter model (LM_2, met verwaarlozing van de drukasymptoot) omwille van rekentechnische redenen verdrongen. Met behulp van niet-lineaire technieken kan τ berekend worden zonder de aanname van een nulasymptoot. De niet-lineaire Levenburg-Marquardt techniek laat toe naast τ en p_0 ook p_∞ te schatten (LM_3, drieparameter model). De extra vrijheidsgraad in de Levenburg-Marquart techniek resulteert in

een gefitte exponentiële drukcurve die beter aansluit bij de originele curve. Toch is het gebruik van een drieparameter model niet noodzakelijk beter. Immers, door toevoegen van een extra te schatten parameter verbetert weliswaar de overeenkomst tussen gemodelleerde en werkelijke curve, maar verhoogt langs de andere kant ook de variantie op de parameterschattingen. Men schat immers meer parameters met dezelfde informatie.

II.2.2. DOEL

Het doel van dit onderzoek is om meer inzicht te verwerven in de afweging tussen twee- en drieparameter model voor de schatting van de tijdsconstante van de LV relaxatie (τ).

II.2.3. METHODEN

Drukcurves, afkomstig van een experiment in honden, werden geanalyseerd met verschillende methodes. Ter vergelijking werd een referentiekader aangemaakt bestaande uit vergelijkbare gesimuleerde drukcurves (Monte Carlo simulatie).

Het *dierenexperiment* leverde drukcurves op onder verschillende hemodynamische omstandigheden: in rusttoestand, na toediening van isoproterenol (verkort τ) en na toediening van esmolol (verlengt τ). De drukcurves, opgemeten in zes honden, werden digitaal opgeslagen. De nodige analysesoftware werd ontwikkeld in Labview©. τ werd bepaald op basis van een twee- en een drieparameter mono-exponentieel model, telkens met behulp van het niet-lineaire Levenberg-Marquardt algoritme. De resultaten werden vergeleken op overeenkomst tussen gemodelleerde en werkelijke curves enerzijds, en betrouwbaarheidsintervallen op de parameter schattingen anderzijds. De overeenkomst tussen gemodelleerde en werkelijke curve werd gekwantificeerd door berekening van een gemiddelde kwadratische afwijking (MSE, mean squared error). De variantie op de parameterschattingen werd gekarakteriseerd door de bijhorende standaard fout (SE, standard error).

Met behulp van *Monte-Carlo simulatie* werden telkens 100 varianten aangemaakt voor 125 verschillende combinaties van parameterinstellingen voor een exponentiële drukval. De 125 combinaties werden bekomen door p_∞ te variëren van –5 tot +5 mmHg in stappen van 2.5 mmHg, τ te variëren van 40 tot 120 ms in stappen van 20 ms en p_o te variëren van 70 tot 110 mmHg in stappen van 10

mmHg. Voor iedere set van 100 verwante drukcurven werden de parameters opnieuw bepaald met behulp van het twee- en drieparameter mono-exponentieel model. De resultaten werden geanalyseerd in termen van overeenkomst tussen geschatte en oorspronkelijke curve enerzijds en betrouwbaarheid van de parameterschattingen anderzijds.

II.2.4. RESULTATEN

Tabel 2 geeft de gemiddelde waarden van τ, MSE, SE en p_∞, afkomstig van de experimentele metingen in het dierenexperiment voor twee- (LM_2) en drie- (LM_3) parameter mono-exponentieel model onder de verschillende hemodynamische condities.

Tabel 2: gemiddelde waarden van τ, MSE, SE en p_∞ uit het dierenexperiment.

		τ, ms	**SE, ms**	**MSE**	**P_∞, mmHg**
Baseline	LM_2	67.8	0.6	0.9	-
	LM_3	83.5	3.4	0.2	-7.1
Isoproterenol	LM_2	50.4	0.7	0.3	-
	LM_3	48.8	3.8	0.1	0.5
Esmolol	LM_2	113.1	0.9	0.2	-
	LM_3	108.7	4.8	0.1	0.9

Uit tabel 2 blijkt dat kwalitatief gezien voor beide methodes veranderingen in τ voor verschillende hemodynamische condities vergelijkbaar zijn.

Toediening van isoproterenol versnelt de relaxatie (lagere τ), waar toediening van esmolol de relaxatie verlengt (hogere τ). De absolute verschillen zijn echter wel sterk methode afhankelijk. Zoals verwacht is de MSE waarde steeds groter bij een tweeparameter model in vergelijking tot de overeenkomstige resultaten bekomen met een drieparameter model, daar waar de SE steeds groter is bij een drieparameter model in vergelijking met de resultaten bekomen met het tweeparameter model.

Figuur 10 toont resultaten afkomstig van de Monte-Carlo simulatie. De betrouwbaarheid op de schatting van τ voor twee- en drieparameter model voor

verschillende waarden van de drukasymptoot staan tegenover elkaar uitgezet voor een simulaties met een referentie τ van 80ms. Bij een reële nulasymptoot leveren twee- en drieparameter model de zelfde gemiddelde τ-waarde. De betrouwbaarheid van de schatting met behulp van het tweeparameter model is echter groter. Bij een negatieve drukasymptoot behoudt het tweeparameter model haar smaller betrouwbaarheidsinterval in vergelijking met het drieparameter model. Dit gaat evenwel ten koste van een systematische afwijking van de werkelijke τ–waarde, proportioneel met de afnemende drukasymptoot.

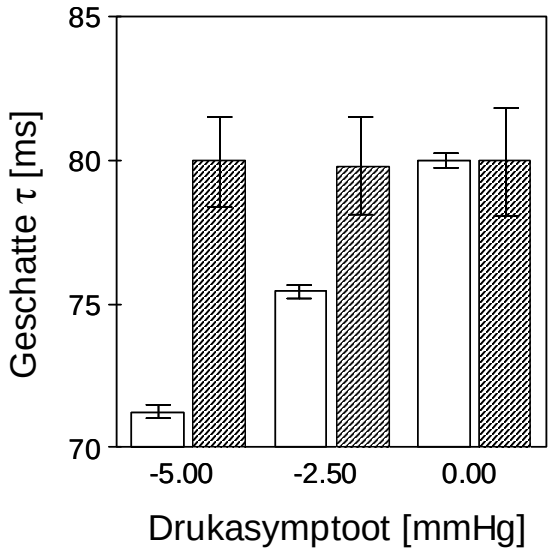

Figuur 10: Monte Carlo simulatie van geschatte τ waarden in functie van de werkelijke drukasymptoot voor een werkelijke τ van 80 ms. Open staven: LM_2, gearceerde staven: LM_3.

II.2.5 DISCUSSIE

Uit de dierenexperimenten blijkt dat bij de keuze tussen twee- en drieparameter mono-exponentieel model, een afweging gemaakt dient te worden tussen MSE- en SE-waarde. Aangezien we uiteindelijk geïnteresseerd zijn in een zo betrouwbaar mogelijke τ waarde dienen we te achterhalen welke invloed de MSE waarde heeft op de schatting van τ. De simulaties leveren ons dit verband. De simulatieresultaten tonen immers aan dat een stijgende MSE waarde samenhangt met een onder- of overschatting van de τ-waarde.

De afweging tussen twee en drieparameter model kan kwantitatief gemaakt worden door de berekening van een relatieve efficiëntie (RE) die de vergelijking maakt tussen de betrouwbaarheid van de schattingen, bekomen met de verschillende methodes, rekening houdend met systematische afwijkingen enerzijds en betrouwbaarheidsintervallen anderzijds. Deze RE is niets anders dan de verhouding tussen de absolute betrouwbaarheid van de schattingen bekomen met respectievelijk het drie- en twee parameter mono-exponentieel model. Figuur 11 toont het verloop van de RE in functie van werkelijke drukasymptoot en werkelijke relaxatieconstante, berekend op basis van de simulaties. Een waarde groter dan 1 duidt op betere resultaten m.b.v. een drieparameter model, een waarde kleiner dan 1 duidt op betere resultaten met het tweeparameter model.

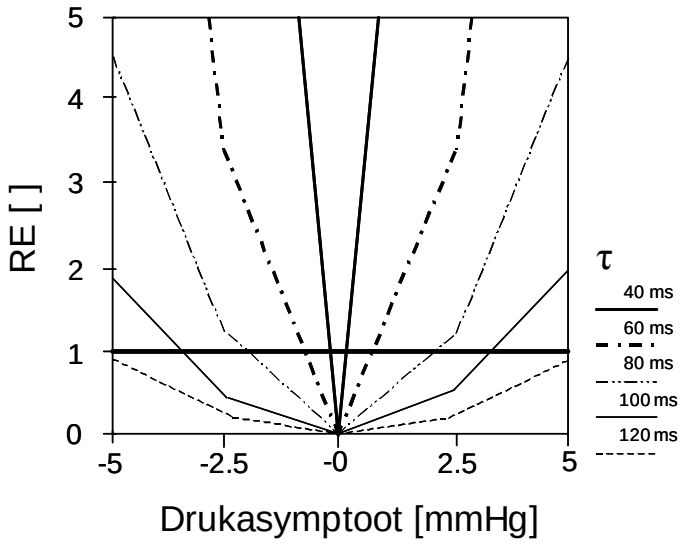

Figuur 11: Relatieve efficiëntie (twee- versus drieparameter model) van τ schattingen in functie van de werkelijke drukasymptoot en τ waarde.

II.2.6 BESLUIT

In deze studie hebben Monte-Carlo simulaties een referentiekader opgeleverd dat toelaat om de verschillende methoden ter berekening van de tijdsconstante van de isovolumetrische relaxatie uitgaande van een mono-exponentieel model te evalueren. De keuze tussen een twee- of drieparameter model kan herleid worden tot de afweging tussen mogelijke systematische onder- of overschatting van τ-waarden in het geval van gebruik van een tweeparameter model t.o.v. de grotere

variantie op de geschatte τ -waarde bij het gebruik van een drieparameter model. Door de berekening van een RE kan deze afweging kwantitatief worden gemaakt.

II.3. Bepaling van de Stromingvoortplantingssnelheid van de Vroege Vullingsgolf m.b.v. CMD Echocardiografie: Een Vergelijking van Vier Methoden

II.3.1. Inleiding en Doelstelling

CMD echocardiografie verschaft de ruimtelijke verdeling van het snelheidsveld langsheen een centrale instroomas van de LV met een hoge tijdsresolutie. De spatiale snelheidsverdeling wordt via een kleurencode afgebeeld in een tijd/afstand assenstelsel (respectievelijk X-as en Y-as) zoals geïllustreerd in figuur 12. Typisch wordt een rode kleur gebruikt voor snelheden naar de transducer toe (positieve snelheden) en blauwe kleuren voor snelheden van de transducer weg (negatieve snelheden). Eigen aan de Doppler techniek is het beperkte meetbereik. Snelheden buiten het meetbereik zijn onderhevig aan aliasing. In de praktijk betekent dit dat bij de overgang naar snelheden, hoger dan het maximale kleurbereik, de kleurencode omslaat van intens rood (maximaal positief) naar intens blauw (maximaal negatief). In figuur 12 zijn in de kern van de vullingsgolven zones met aliasing duidelijk herkenbaar.

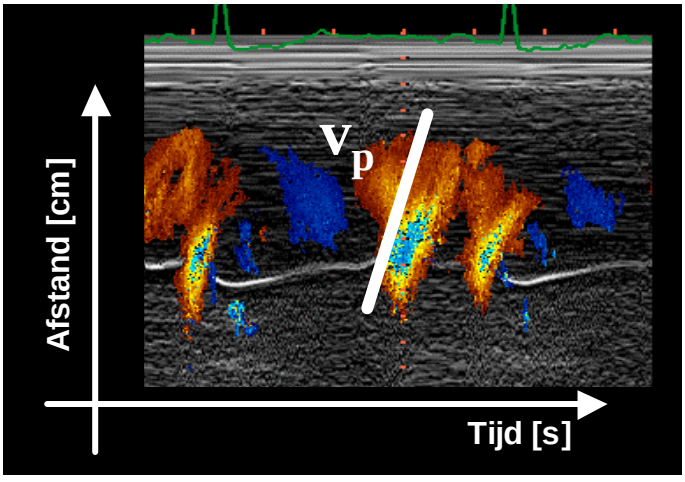

Figuur 12: Kleuren M-mode Doppler beeld van de LV vullingsgolf. De helling van de rechte, geligneerd met het verloop van de snelheden van basis naar apex, is een maat voor v_p.

De voortplantingssnelheid van de stroming in de linker hartkamer (v_p) is een index, afgeleid uit het stromingsveld in de linker hartkamer. v_p is een maat voor

de snelheid waarmee het bloed de LV vult in de richting van de apex. Op een CMD beeld kan v_p afgeleid worden uit de helling van de rechte, geassocieerd met de snelheden van de vroege vullingsgolf. Deze helling heeft de dimensie van snelheid (cm/s). Dit wordt geïllustreerd in figuur 12, waar manueel een rechte geïdentificeerd werd met v_p. Aangezien het bloed met een wervelende beweging de hartkamer vult is v_p kleiner dan de eigenlijke stroomsnelheid van het bloed (Steen and Steen 1994).

Onderzoek naar de invloed van fysiologische parameters op de v_p is volop aan de gang. Zo is reeds aangetoond dat v_p omgekeerd evenredig is met de tijdsconstante van de ventriculaire relaxatie (Brun et al. 1992, Stugaard et al. 1995, Takatsuji et al. 1996). Toch is er nog geen algemene consensus over een gestandaardiseerde methode om v_p te berekenen. Het doel van deze studie is dan ook een vergelijking te maken tussen de verschillende gebruikte methoden om v_p te kwantificeren. De aandacht zal voornamelijk toegespitst worden op verschillen in variabiliteit.

II.3.2. METHODEN

Vier verschillende methodes, in de literatuur voorgesteld om uitgaande van een CMD beeld een karakteristieke waarde voor v_p te bekomen, worden vergeleken. Met het oog op objectieve vergelijking zijn voor elk van deze methodes algoritmes ontwikkeld die toelaten om v_p op een semi- automatische te berekenen. Met behulp van de ontwikkelde software zijn beelden van de LV vulling van 10 patiënten geanalyseerd. De resultaten dienen als een basis voor de discussie.

II.3.2.1. Verschillende Methodes en Ontwikkelde Software.

Figuur 13 illustreert de semi-automatische berekening van v_p volgens de vier methoden met behulp van de geïmplementeerde algoritmen.

Duval-Garcia. Duval-Moulin et al. (Duval-Moulin et al. 1997) en Garcia et al. (Garcia et al. 1998) hebben voorgesteld om een lijn te identificeren met een contour van gelijke snelheden in het CMD beeld. Bij een manuele bepaling wordt heel frequent de visueel goed zichtbare lijn waar de eerste gealiaste snelheden optreden uitgekozen. In een automatisch algoritme kunnen alle snelheden ingesteld worden. Dikwijls wordt ietwat arbitrair de contour met snelheden gelijk aan 50% van de maximale snelheid uitgekozen.

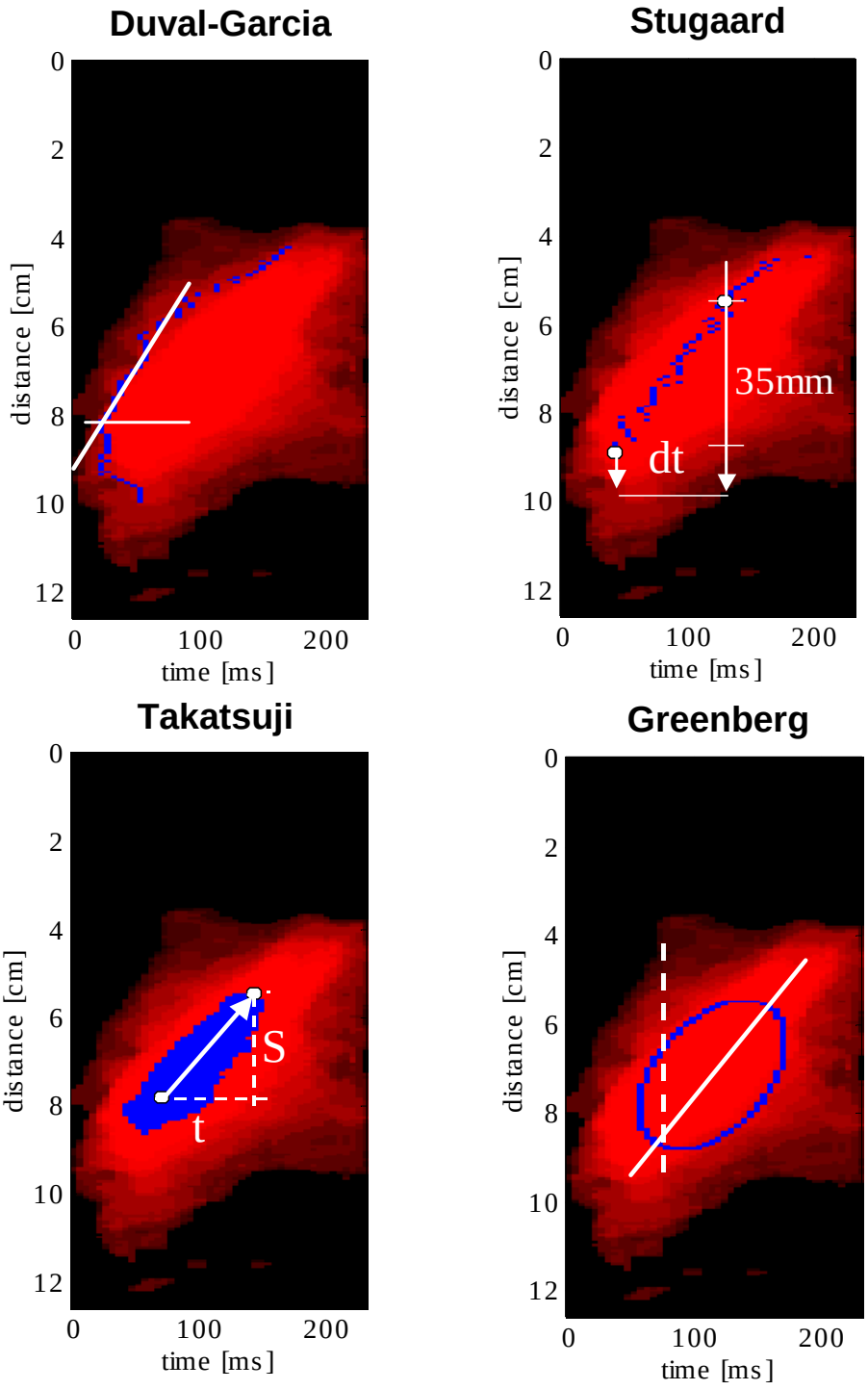

Figuur 13: Automatische bepaling van vp volgens vier methoden. **(A)** Methode 1 (Duval-Garcia): v_p = 51.4 cm/s. **(B)** Methode 2 (Stugaard): TD = 91.7 ms. **(C)** Methode 3 (Takatsuji): v_p = 33.3 cm/s. **(D)** Methode 4 (Greenberg): v_p = -11°.

Takatsuji. Takatsuji et al. (Takatsuji et al. 1996) selecteert in eerste instantie een gebied waar alle snelheden groter zijn dan 70% van de maximale snelheid. Vervolgens wordt een rechte en bijhorende helling gedefinieerd aan de hand van twee punten. Het eerste punt is het punt ter hoogte van de mitraalklep waar de maximale snelheid optreedt. Het tweede punt is het meest apicale punt op de rand van het gebied met snelheden groter dan 70% van de maximale snelheid.

Stugaard. Stugaard et al. (Stugaard et al. 1993) lokaliseren de maximale snelheid op 5 mm intervallen vanaf de tip van de mitraalklepblaadjes tot in de LV apex. Het tijdsverschil in ms tussen de posities van de maximale snelheid aan de mitraalklep en in de LV apex wordt aanzien als een maat voor de v_p.

Greenberg. Greenberg et al. (Stugaard et al. 1997) bepalen met behulp van eigenvectoranalyse een best passende ellips op de vroege vullingsnelheden in het CMD beeld. De hoek van de lange as van de ellips met de verticale is een maat voor v_p.

II.3.2.2. Patiëntenpopulatie en Echocardiografisch Onderzoek

Tien opeenvolgende patiënten, doorverwezen voor een routine onderzoek naar het echocardiografie laboratorium van het universitair ziekenhuis in Gent, werden onderworpen aan een volledig (Doppler) echocardiografisch onderzoek. De gemiddelde leeftijd was 61 ± 20 jaar (bereik 22-78). De groep was samengesteld uit twee vrouwen en acht mannen. Het echocardiografisch onderzoek omvatte M-mode en 2D-echografie, continue en PWD echocardiografie en CMD echocardiografie. Ten behoeve van deze studie werden telkens 5 beelden van de stroming ter plaatste van de mitraalklepblaadjes met PWD en 5 beelden van de centrale instroming langsheen de lange as van de LV met CMD echocardiografie, alternerend opgenomen en digitaal opgeslagen. E en A snelheid werden manueel gemeten. v_p werd op de vier verschillende wijzen gemeten met behulp van de nieuwe software. Als referentie werd v_p ook manueel bepaald m.b.v. de manuele methode van Duval-Garcia. Alle waarnemingen werden door twee waarnemers uitgevoerd. Eén waarnemer herhaalde de metingen éénmaal.

II.3.2.3. Data-analyse en Statistisch Onderzoek

De variabiliteit op herhaalde waarnemingen van één waarnemer (intra-observer variability, VAR_{intra}), op waarnemingen van verschillende waarnemers (inter-

observer variability, VAR_{inter}) en op waarnemingen van opeenvolgende hartslagen (beat-to-beat variability, VAR_{BTB}) zijn berekend als tweemaal de standaardafwijking op de gemiddelde verschillen zoals voorgeschreven door het Britse Instituut voor Standaardisatie (British Standard Institution 1979). Ter vergelijking is ook de correlatiecoëfficiënt tussen overeenkomstige metingen berekend.

II.3.3. RESULTATEN

Een voorbeeld van v_p bepaling volgens de verschillende methoden met de automatische software is weergegeven in figuur 13. De verschillende methoden leveren verschillende v_p waarden op. Tabel 3 vergelijkt VAR_{intra} en VAR_{inter}. Tabel 4 geeft VAR_{BTB}. Op het gebied van VAR_{intra} en VAR_{inter} scoren de automatische methoden duidelijk beter dan de manuele methode. Voor VAR_{BTB} is dit niet meer zo voor de methoden van Stugaard, Takatsuji en Greenberg. De methode van Duval-Garcia blijft wel in de buurt van de manuele methode.

II.3.4 CONCLUSIE

De bepaling van v_p is zeer methode gevoelig. De beste resultaten, rekening houdende met inter-observer en intra-observer (automatische methoden scoren gevoelig beter t.o.v. manuele bepaling) en beat-to-beat variabiliteit (Duval-Garcia methode levert stabielere resultaten dan andere automatische methoden) worden bekomen met een semi-automatische methode op basis van de werkwijze, voorgesteld door Duval et al. en Garcia et al., in het bijzonder wanneer gebruik wordt gemaakt van meerdere operatoren.

Tabel 3: Intra-observer and inter-observer variabiliteit

		Intra-observer variabiliteit			**Inter-observer variabileit**		
		2SD	%	r	2SD	%	r
E	[cm/s]	1.73	2.08	0.996	3.25	3.78	0.992
A	[cm/s]	3.13	3.18	0.998	5.15	5.37	0.996
$v_{p,man}$	[cm/s]	9.92	21.75	0.812	13.97	26.13	0.773
$v_{p,duval\text{-}garcia}$	[cm/s]	5.74	12.92	0.991	6.14	13.76	0.975
$v_{p,stugaard}$	[ms]	3.77	3.45	0.999	5.11	5.96	0.999
$v_{p,takatsuji}$	[cm/s]	3.45	3.86	0.999	4.26	5.16	0.998
$v_{p,greenberg}$	[°]	0.05	4.02	0.999	0.17	15.45	0.988

Tabel 4: Beat-to-Beat variability

		Beat-to-Beat Variabiliteit	
		2SD	%
E	[cm/s]	10.82	14.80
A	[cm/s]	9.02	11.27
$v_{p,man}$	[cm/s]	7.33	20.14
$v_{p,duval\text{-}garcia}$	[cm/s]	9.92	24.28
$v_{p,stugaard}$	[ms]	80.54	89.36
$v_{p,takatsuji}$	[cm/s]	43.76	77.02
$v_{p,greenberg}$	[°]	0.65	58.18

II.4. Kwantitative Verwerking van de Informatie in een CMD Beeld: Berekening van de Longitudinale Impedantie

II.4.1. INLEIDING

Recent werd door Milde et al (Milde et al. 2000) de index "ventriculaire globale diastolische impedantie" (Z) voorgesteld als een parameter voor globale diastolische functie. Z werd gedefinieerd als de verhouding van LV druk (p) over transmitraal debiet Q tijdens de vroege vullingsfase (E-wave). Met behulp van Fourier analyse van het tijdsafhankelijke druk en debietsignaal, kan voor iedere harmonische (ω) de amplitude van deze verhouding berekend worden (vergelijking 10):

$$Z(\omega) = \frac{p(\omega)}{Q(\omega)} \qquad [V.\ 10]$$

Om Z te berekenen in een patiëntenpopulatie en een controlegroep gebruikte Milde et al. signalen afkomstig van de gelijktijdige meting van de snelheid van de vroege vullingsgolf met PWD echocardiografie en van LV drukken met een micromanometer tipcatheter (Millar). De bekomen Z-waarden differentieerden tussen de personen met een normale diastolische disfunctie (n = 9) en normale personen (n = 10).

II.4.2. DOELSTELLING

Het doel van dit onderzoek is om een methode te ontwikkelen om diastolische impedantie op niet-invasieve wijze te bekomen. In dit stadium zal de haalbaarheid en reproduceerbaarheid van de voorgestelde methode getest worden in een hydraulisch model.

II.4.3. METHODEN

II.4.3.1. Niet-invasieve Bepaling van Diastolische Impedantie

De berekening van een impedantie vereist de kennis van drukken en debieten. Aan de hand van snelheidsmetingen kunnen debieten gemakkelijk niet-invasief bekomen worden. Absolute drukmetingen vereisen echter wel een invasieve techniek. Een alternatief is gebruik te maken van drukverschillen. Drukverschillen worden in de klinische praktijk courant benaderd met behulp van de

vereenvoudigde Bernoulli vergelijking (cf. Deel 1, vergelijking 6). Over een niet-pathologische (i.e. niet vernauwde) mitraalklep resulteert de vereenvoudigde Bernoulli vergelijking in onderschatte drukgradiënten aangezien de niet-permanente term, weggelaten in de vereenvoudigde Bernoulli vergelijking, niet verwaarloosbaar is. CMD echocardiografie biedt echter een alternatief om meer accurate drukverschillen over de mitraalklep te berekenen uitgaande van snelheidsmetingen (Greenberg et al. 1996). Hiervoor onderstelt men dat de scanlijn van de CMD meting samenvalt met een stroomlijn in een niet-visceuze stroming. In deze situatie vereenvoudigen de complexe Navier-Stokes vergelijkingen tot de ééndimensionale Euler vergelijking (cf. Deel 1, vergelijking 8). Ook het debiet doorheen de mitraalklep kan niet invasief bekomen worden uitgaande van de snelheid, afgeleid uit de kleurenpixels van het CMD beeld ter hoogte van de mitraalklep, en een oppervlaktebepaling van de mitraalklep met echocardiografie. Door in vergelijking 10 de druk te vervangen door het drukverschil bekomt men een niet-invasieve index voor diastolische impedantie. Deze impedantie, op basis van het drukverschil, wordt in de literatuur ook wel “longitudinale impedantie” genoemd (Nichols and O'Rourke 1990).

II.4.3.2. Beeldverwerking

Beeldverwerkingsalgoritmen zijn ontwikkeld in Matlab 5.3© om drukverschillen over en snelheidsprofielen door de mitraalklep te berekenen op basis van CMD metingen. Met behulp van deze gegevens werd vervolgens het debiet bepaald op basis van snelheidsprofiel en klepdiameter. Tenslotte werden de tien eerste harmonischen van de longitudinale impedantie berekend met Fourier analyse.

II.4.3.3. Hydraulisch Model

De haalbaarheid en reproduceerbaarheid van de niet-invasieve bepaling van Z werd getest in een hydraulisch model van het cardiovasculair systeem (Verdonck et al. 1992). Het model is samengesteld uit een linker hartsimulator, verbonden met een latex model van de arteriële boom. In het model worden LA en LV drukken computergestuurd. Niet-invasieve CMD metingen gebeuren met een Vingmed CFM 800 machine vanuit een apicale positie. In the cardiovasculaire simulator is longitudinale impedantie bepaald bij variërende klepdiameter (13mm en 21mm), veranderlijke hartritmes (45 tot 60 BPM) en oplopende maximale systolische LV drukken (85 tot 125 mmHg). Zowel water als een 40/60 water-

glycerine mengsel zijn als testvloeistof gebruikt. In een multivariaat algemeen lineair model zijn de invloeden van de verschillende variabelen nagegaan.

II.4.4. RESULTATEN

Figuur 14 illustreert de reconstructie van drukgradiënten met behulp van CMD echocardiografie op basis van de Euler vergelijking. Multivariabele regressieanalyse toont aan dat de verschillen in longitudinale impedantie significant waren voor veranderende klepoppervlakte ($p < 0.000$) en testvloeistof ($p < 0.000$). Daarentegen hadden veranderingen in systolische druk noch veranderingen in hartritme een significante invloed op de impedantie.

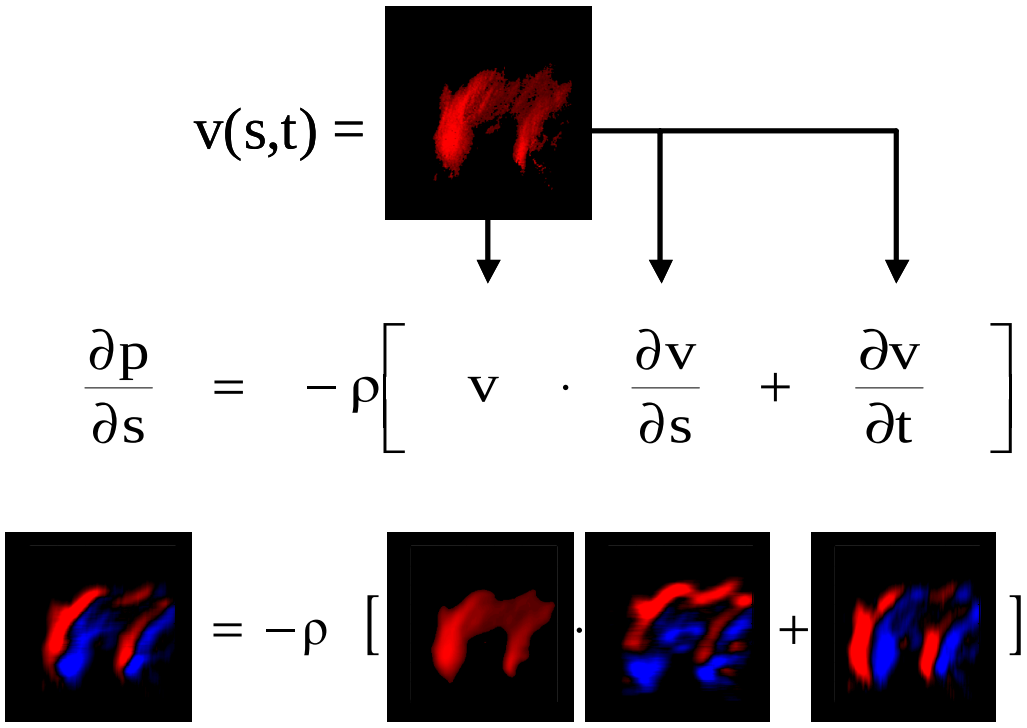

Figure 14: Illustratie van de beeldverwerkingalgoritme voor de berekening van lokale drukgradiënten in de LV met CMD echocardiografie op basis van de Euler vergelijking.

Figuur 15 toont de resultaten van de in vitro testen, gegroepeerd per klepdiameter (13 en 21 mm). Voor alle harmonischen worden significant hogere waarden bekomen in het geval van kleinere diameters.

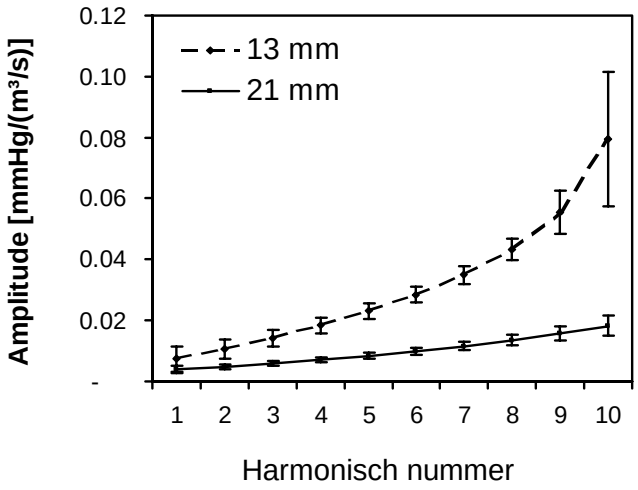

Figure 15: Verschillen in impedantie in het hydraulisch model voor twee verschillende kleppen in mitraalpositie.

II.4.5 CONCLUSIE

Met CMD echocardiografie kan LV longitudinale impedantie niet-invasief bekomen worden. De index is gevoelig voor veranderingen in klepdiameter en testvloeistof, maar niet in systolische druk en hartritme. Het verschaft een kwantitatieve interpretatie van de informatie in een CMD beeld met mogelijks klinisch bruikbare informatie.

II.5. Beperkingen van PWD Echocardiografie voor de Bepaling van Drukgradiënten met Toepassing op de Post-operatieve Evaluatie van een Aortacoarctatie

II.5.1. INLEIDING

Een aortacoarctatie is een aangeboren hartafwijking die bestaat uit een vernauwing van de aorta, de slagader die het bloed in de grote bloedsomloop brengt. De vernauwing vormt een weerstand in de systeemcirculatie welke resulteert in een verhoging van de bloeddruk proximaal van de vernauwing en een lagere bloeddruk distaal van de vernauwing. Vaak wordt de drukgradiënt over de coarctatie als maat voor de ernst van de coarctatie gebruikt. Met behulp van de vereenvoudigde vergelijking van Bernoulli kan men uitgaande van een niet-invasieve snelheidsmeting ter plaatse van de coarctatie de drukgradiënt over de vernauwing berekenen. De snelheidsmeting voert men eenvoudig uit m.b.v. Doppler echocardiografie (Rao 1995).

Ondanks schijnbaar succesvolle ingrepen blijkt het sterftecijfer en de kans op cardiovasculaire aandoeningen toch significant hoger te liggen bij deze patiënten. Een adequate opvolging blijft aldus noodzakelijk. Postoperatieve evaluatie van een aortacoarctatie gebeurt met dezelfde diagnostische methodes als pre-operatief. Bij de postoperatieve evaluatie komt men echter soms tot schijnbaar tegenstrijdige resultaten: ondanks nauwelijks of geen drukverschil tussen rechterarm en been, meet men met Doppler echocardiografie soms abnormaal grote stroomsnelheden tot 4 m/s ter plaatse van de coarctatie die, volgens de vereenvoudigde Bernoulli vergelijking, duiden op een grote drukval (Aldousany et al. 1990, Teien et al. 1993).

II.5.2. DOELSTELLING

Deze studie heeft tot doel de oorzaken van het verschil tussen de drukverschillen, berekend op basis van Doppler snelheidsmetingen, en het arm-been drukverschil bij postoperatieve coarctatie patiënten te onderzoeken. Hierbij wordt van de hypothese uitgegaan dat na operatie stijf littekenweefsel een dynamische obstructie kan veroorzaken. De waarde van een alternatieve uitdrukking (de Seeley vergelijking) voor de schatting van het drukverschil wordt nagegaan.

II.5.3. METHODEN

Als uitgangspunt wordt vertrokken van echocardiografische metingen in postoperatieve patiënten en een controle groep. De overeenkomsten en verschillen op gebied van anatomie, wandeigenschappen en hemodynamica worden nauwkeurig in kaart gebracht. Vervolgens zijn specifieke hypothesen omtrent de stijfheid van de wand en geometrische verschillen uitgewerkt en getoetst in respectievelijk een hydraulisch en een analytisch model. Ook de bruikbaarheid van de Seeley vergelijking als mogelijk alternatief voor de Bernoulli vergelijking is getoetst in een hydraulisch model.

II.5.3.1. Patiënten data

Een groep van 31 postoperatieve coarctatie patiënten (13.0 ± 4.0 jaar) en een controlegroep van 18 gezonde personen (13.9 ± 2.9 jaar) zijn onderzocht met Doppler echocardiografie. Maximale systolische en minimale diastolische diameters en PWD snelheidsprofielen zijn gemeten op 6 verschillende plaatsen langsheen de aorta. Ook het arm-been drukverschil is gemeten. De vernauwinggraad van de aorta is begroot met een coarctatie index (CI), gedefinieerd als de verhouding van de diameter in de vernauwde sectie tot de diameter in een normale sectie. Een dimensieloze stijfheidindex is berekend als:

$$\beta = \frac{\ln(p_s / p_d)}{\left(\frac{D_s - D_d}{D_d}\right)} \qquad \text{[V. 11]}$$

Hierin zijn p_s en p_d respectievelijk de systolische en disatolische druk, en D_s en D_d de overeenkomstige systolische en diastolische diameter (Hirai et al. 1989).

II.5.3.2. Hydraulisch en Analytisch Model

Een vereenvoudigd latex model (figuur 16) van de aorta wordt verbonden met een hartsimulator (Segers et al. 1998, Verdonck et al. 1992). De hartsimulator creëert een pulsatiele stroming doorheen de aorta. Verstijvingen en vernauwingen van de aorta worden gecreëerd met behulp van stijve ringen met diameter gelijk aan of kleiner dan de onbelaste aorta diameter. Na de coarctatie plaats is een bifurcatie voorzien. Dit laat toe om snelheidsmetingen proximaal (p), in situ (s) en distaal (d) van de coarctatie uit te voeren met een perfect gealigneerde Doppler probe.

Het analytisch model gaat uit van de niet-vereenvoudigde Bernoulli vergelijking. Verschillen tussen werkelijke drukverschillen en drukverschillen bekomen met behulp van de vereenvoudigde Bernoulli vergelijking worden bestudeerd voor twee verschillende geometrieën: een puntcoarctatie, gemodelleerd als een diafragma, en een tubulaire hypoplasie, gemodelleerd met een geleidelijke overgang tussen vernauwde en niet-vernauwde secties.

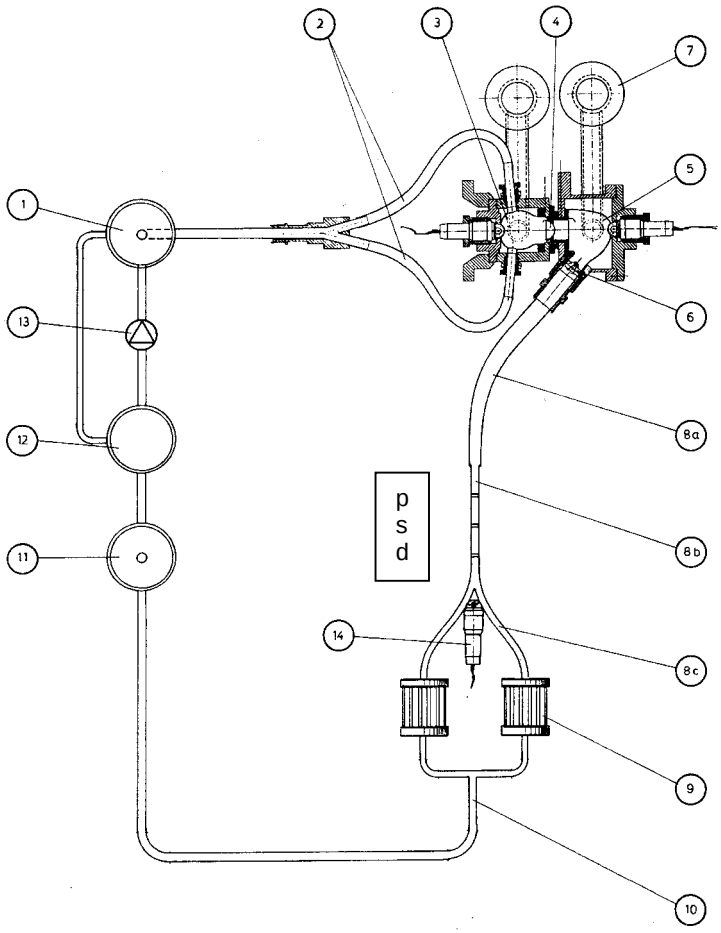

Figure 16: Schema van het hydraulisch model (linker hartsimulator en latex model van de aorta).

II.5.3.3. Hydraulische experimenten: protocol

Twee experimenten worden uitgevoerd. In een eerste experiment wordt de invloed van een loutere verstijving nagegaan. Voor verschillende debieten (1.5 tot 3.0 l/min) worden PWD snelheidsmetingen uitgevoerd in een referentietoestand (niet verstijfde zone) en met een verstijfde zone (diameter gefixeerd op de diameter van

de onbelaste aorta). Snelheidsmetingen worden uitgevoerd voor, ter plaatse en na de verstijfde zone. Met druktransducers wordt simultaan de drukval over de testsectie gemeten.

In een tweede experiment is nagegaan of de Seeley vergelijking een beter alternatief kan zijn voor de Bernoulli vergelijking. De Seeley vergelijking (vergelijking 12) geeft het gemiddelde drukverschil onder de vorm van het dimensieloze Euler getal en is functie van snelheid en geometrie (Seeley and Young 1976):

$$\frac{\Delta p}{\rho v_0^{\,2}} = \frac{K_v}{Re_0} + \frac{K_t}{2}\left[\frac{A_0}{A_1} - 1\right]^2 \qquad \text{[V. 12]}$$

Hierin zijn K_v en K_t coëfficiënten, afhankelijk van de geometrie en bekomen door fitting van experimentele data. v_0 is de snelheid in de onvernauwde sectie en Re_0 is het overeenkomstig Reynoldsgetal. A_0 en A_1 zijn de oppervlaktes van respectievelijk de niet-vernauwde en vernauwde sectie. Het linker lid van vergelijking 12 is niets anders dan het Euler getal. Voor verschillende debieten (0.7 – 1.65 l/min) zijn simultane snelheidsmetingen en drukmetingen over een vernauwde testsectie (CI van 1 to 0.65) uitgevoerd. Gemeten en berekende waarden zijn vergeleken.

II.5.4. RESULTATEN

II.5.4.1. Patiënten Data

Geen klinische symptomen van een residuele coarctatie werden waargenomen in de postoperatieve patiëntengroep. Patiënten en controlegroep vertoonden een overeenkomstig arm-been drukverschil (respectievelijk –10+/-12 en –12+/-10 mmHg). In tegenstelling tot de controlegroep was de gemeten snelheid ter hoogte van het littekenweefsel verhoogd in de patiëntengroep (1.2+/-0.2 versus 2.2+/-0.4 m/s). Niettegenstaande een succesvolle operatieve ingreep blijft de aorta in de patiënten groep een milde vernauwing vertonen (CI = 0.69+/-0.20). Ook de stijfheidindex is significant hoger in vergelijking met de controlegroep en in vergelijking met andere plaatsen langsheen de aorta.

II.5.4.2. Hydraulisch Model

Figuur 17 geeft de resultaten weer van de experimenten in het hydraulisch model. De linkse grafiek van figuur 17 toont berekende en gemeten drukverschillen over vernauwde en niet-vernauwde secties in het model. Berekende Doppler drukgradiënten zijn hoger dan de gemeten instantane drukverschillen. Deze laatste zijn op hun beurt groter dan de piek-tot-piek drukverschillen.

De rechtse grafiek van figuur 17 toont de overeenkomst tussen gemeten en geschatte Euler getal (Seeley vergelijking) in het hydraulisch model. Een vrij goede overeenkomst wordt waargenomen.

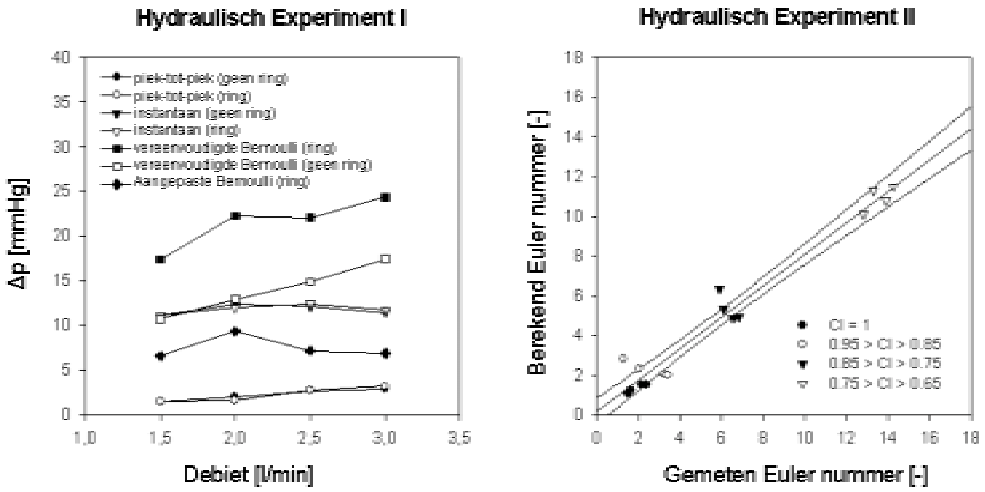

Figure 17: Resultaten van de hydraulische experimenten. Links: gemeten en berekende (Bernoulli vergelijking) drukverschillen. Rechts: overeenkomst tussen gemeten en berekend (Seeley vergelijking) Euler getal.

II.5.4.3. Analytisch model

Figuur 18 vergelijkt gesimuleerde drukgradiënten op basis van respectievelijk de volledige Bernoulli vergelijking en de vereenvoudigde Bernoulli vergelijking voor een puntcoarctatie en een tubulaire hypoplasie. Vooral deze laatste categorie blijkt gevoelig voor overschatting van drukgradiënten op basis van de vereenvoudigde Bernoulli vergelijking.

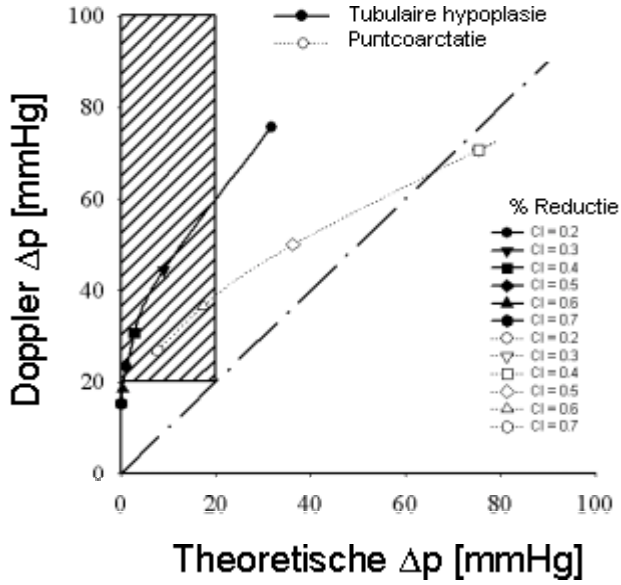

Figure 18: Vergelijking tussen werkelijke drukverschillen en berekende drukverschillen met behulp van de vereenvoudigde Bernoulli vergelijking voor verschillende geometriën en vernauwingsgraden.

II.5.5 CONCLUSIE

De in vitro modellering toont aan dat een loutere afname in compliantie een stijging van de pieksnelheid tot 30% op de plaats van het niet-compliant stuk tegen over staan van de proximale en distale snelheid veroorzaakt, zonder dat daarbij significante drukvallen ontstaan over het niet-compliant stuk. In het geval van tubulaire hypoplasie wordt de drukgradiënt overschat door de vereenvoudigde Bernoulli vergelijking waardoor het gevaar op “valse” gevallen van recoarctatie (d.i. een geschatte drukgradiënt hoger dan 20 mmHg, maar een werkelijke kleiner dan 20 mmHg) niet uitzonderlijk is.

In postoperatieve coarctatie zijn drukschattingen met behulp van de vereenvoudigde Bernoulli vergelijking onbetrouwbaar. De Seeley vergelijking is een mogelijk alternatief dat in het hydraulisch model drukgradiënten oplevert die goed overeenkomen met de werkelijke drukgradiënten.

Deel III

Modelstudies en Klinische Waarnemingen

III.1. Overzicht

In het derde deel komen wetenschappelijke resultaten aan bod die dieper ingaan op de invloeden van fysiologische LV karakteristieken op de hemodynamica van de vulling. Hierbij wordt een arsenaal aan onderzoeksmethoden aangewend: een nieuw hydraulisch model, een gevalideerd numeriek model, experimentele observaties in dierenexperimenten en observaties in de klinische praktijk. De resultaten zijn onder volgende titels ondergebracht:

- Invloed van de determinanten van diastolische functie op de stromingvoortplantingssnelheid: Validatie met een nieuw hydraulisch model.
- De stromingvoortplantingssnelheid in de LV: Overeenkomsten en verschillen tussen een numeriek en hydraulisch model.
- Oorsprong van intraventriculaire drukgradiënten: Inzichten uit een hydraulisch model en dierexperimentele bevindingen.
- Verband tussen inspanningscapaciteit, infarctgrootte en stromingvoortplantingssnelheid in de LV.

III.2. Invloed van de Determinanten van Diastolische Functie op de Stromingvoortplantingssnelheid: Validatie met een Nieuw Hydraulisch Model

III.2.1. INLEIDING EN DOEL VAN DE STUDIE

Interpretatie van hemodynamische karakteristieken, afgeleid uit PWD echocardiografie beelden, moeten geïnterpreteerd rekening houdend met de heersende omgevingsfactoren. O.a. de belastingsafhankelijkheid bemoeilijkt de interpretatie. De stromingvoortplantingssnelheid in de LV (v_p), bepaald m.b.v. CMD echocardiografie, biedt een mogelijke uitweg. Het gedrag van v_p, en in het bijzonder de belastingafhankelijkheid is evenwel onderwerp van discussie. Het doel van deze studie is dan ook om

(A) het bepalen van de individuele bijdrage van relaxatie, compliantie en vullingsdruk in veranderingen van E en v_p met behulp van een hydraulisch model

(B) de studie van E en v_p waarden in verschillende stadia van diastolische disfunctie.

III.2.2. METHODEN

III.2.2.1. Hydraulisch Model

Een nieuw hydraulisch model voor de LV vulling is ontworpen. Het linker hart model (figuur 19) is samengesteld uit een open cilindrisch LA (LA, diameter 30mm), verbonden met een afgeknotte ellipsoïdaal LV (evenwichtsvolume 100ml, base-apex lengte 75mm, korte as 50mm). De LV is vervaardigd uit latexrubber. Om "opblazen" bij hogere drukken te vermijden is de LV omwikkeld met een gaas. Tussen de twee hartkamers is een biologische (xenograft) tricuspide mitralisklep aangebracht. (diameter 21mm, McNeilab Inc., Anaheim, California). De testvloeistof is een water-glycerine mengsel in een 70%-30% verhouding. Met behulp van perslucht kan de LV onder druk gebracht worden en kan een vulling gesimuleerd worden. De relaxatiesnelheid, de vullingsdruk en de compliantie van de LV kunnen ingesteld worden door respectievelijk de perslucht sneller/trager te evacueren uit de perspex kamer rondom de LV, het vloeistofniveau in het LA in te stellen en de dikte van de latex lagen van de LV aan te passen. In onze

experimenten wordt gebruik gemaakt van een compliant en een stijf LV. De compliantie van beide LV's is vooraf gekwantificeerd via hun passief druk-volume verband. In eerste instantie is dit druk-volume verband opgemeten door de LV's te vullen door toevoeging van vloeistof in stappen van 2 ml. De helling van dit verband werd genomen als maat voor compliantie en bedroeg respectievelijk 1.35 ml/mmHg (compliant LV) en 0.45 ml/mmHg (stijf LV).

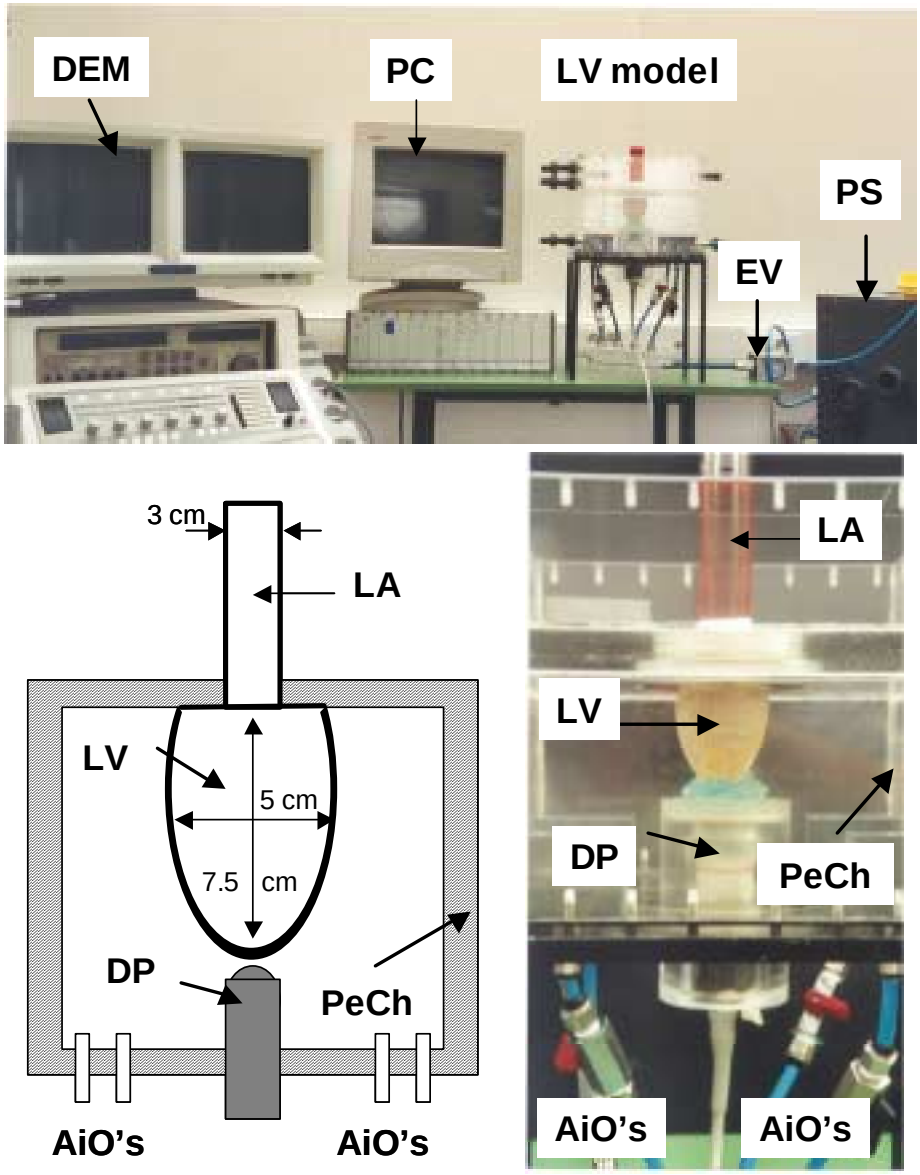

Figuur 19: Hydraulisch LV model. **Boven:** Overzicht van de opstelling; DEM: Doppler-echo machine; PC: PC met meet- en stuurprogramma; EV: Electromagnetische klep; PS: Pneumatisch systeem. **Onder Links:** Schematische tekening van de model LV. **Onder Rechts:** Foto van de model LV. DP: Doppler probe; PeCh: plexi-kamer, AiO's: luchtuitlaten.

III.2.2.2. Instrumentatie en analyse van druk- en snelheidsmetingen

Het model is uitgerust met drukopnemers (Millar, Houston, TX, USA) in LA en LV. Met behulp van een mono-exponentiële functie wordt de tijdsconstante van de isovolumetrische relaxatie (τ) berekend. Een 5.5 Mhz Doppler probe (Vingmed 800 CFM) is geplaatst aan de apicale zijde van de LV. PWD beelden en CMD beelden van de vullingsgolven zijn opgenomen en geanalyseerd off-line op een semi-automatische wijze volgens de methode van Duval-Garcia. Figuur 20 toont een CMD beeld, bekomen in het model. De contour, bestaande uit snelheden gelijk aan 50% van de maximale E-snelheid wordt automatisch gedetecteerd (figuur 20, blauwe pixels) en is dus operator onafhankelijk. Met behulp van een kleinste kwadratenmethode wordt op deze contour de best passende lijn gefit. v_p wordt berekend als de helling van deze lijn. De maximum E-snelheid wordt gemeten met behulp van PWD echocardiografie waarbij het meetvolume één centimeter voorbij de mitraalklep geplaatst wordt.

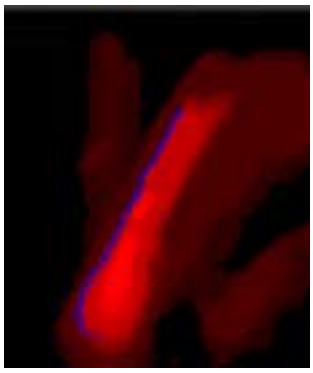

Figuur 20: CMD beeld, opgemeten in het hydraulische model. De contour van gelijke snelheden (50% van de maximale snelheid) wordt automatisch gedetecteerd en weergegeven door de blauwe pixels.

III.2.2.3. Studieprotocol

Op basis van de resultaten van simulaties in het hydraulisch model is een voorspelling gemaakt van E en v_p in vier stadia van diastolische disfunctie.

(I) Experimenteel model: Parameterstudie

Het gedrag van E en v_p zijn bestudeerd in een orthogonale parameterstudie. De metingen worden gedaan voor variërende vullingsdrukken (LAP = 3, 10 and 30

mmHg), relaxatie constanten (τ = 45, 60 and 90ms) en wijzigingen in compliantie (C = 0.45 en 1.35 ml/mmHg). Iedere meting is tweemaal herhaald voor elke combinatie van de parameters.

(II) Voorspelling van E en v_p in verschillende stadia van diastolische disfunctie

Voorspellingen zijn gemaakt van E en v_p met bijhorend 95% betrouwbaarheidsinterval voor verschillende combinaties van waarden van de LV eigenschappen. Elke combinatie stemt overeen met een specifiek stadium van diastolische disfunctie: een referentie situatie (REF), een vertraagde relaxatie (DR), een pseudo-normaal geval (PN) en een restrictieve vulling (RF).

III.2.2.4. Statistiek

Met behulp van een multivariate procedure zijn de invloeden van LV karakteristieken op E en v_p waarden gelijktijdig getest. Uitgaande van het meest volledige model (inclusief alle tweede en derde orde interactietermen) is het definitief model bekomen door stapsgewijze de niet significante termen één na één te elimineren. De parameterschattingen en bijhorende berekende variantie-covariantiematrices zijn gebruikt om voorspellingen te maken van de onafhankelijke variabelen bij nieuwe combinaties van de onafhankelijke variabelen. p waarden, kleiner dan 0.05, worden als statisch significant beschouwd.

III.2.3. RESULTATEN

III.2.3.1. Parameterstudie

E en v_p zijn bepaald in het compliante en stijf LV model, voor vullingsdrukken van 3, 10 en 30 mmHg, en relaxatieconstanten τ van 45, 60 and 90 ms. Tabel 5 toont het multivariaat model voor E en v_p.

Zowel de relaxatie constante als de vullingsdruk alsook de compliantie oefenen een significante invloed uit op E en v_p. Alle interactietermen zijn uit het model verwijderd wegens niet significant ($p > 0.05$). Door het verdwijnen van de interactietermen wordt de interpretatie van de parameterschattingen (β waarden, tabel 5) eenvoudig. De verandering van een onafhankelijke variabele met één eenheid zal een verandering van de afhankelijke variabele veroorzaken met grootte gelijk aan de overeenkomstige β waarde. Aldus blijken E en v_p af te

nemen met toenemende τ (negatieve β waarden). In tegenstelling daarmee nemen E en v_p toe met toenemende vullingsdruk LAP (positieve β waarde). v_p blijkt echter wel minder belastingsafhankelijk in vergelijking met E. Dit kan afgeleid worden uit de significant verschillende β waarden. Compliantie C verandert E en v_p in omgekeerde zin: daar waar een toename in compliantie ook een toename in v_p veroorzaakt (positieve β waarde), veroorzaakt dezelfde stijging in compliantie een afname in E (negatieve β waarde).

Tabel 5: Multivariaat lineair model voor E and vp: parameterschattingen (β), standard errors (SE), t-waarden en significantie (p) voor de onafhankelijke variabelen vullingsdruk (LAP), relaxatieconstante (τ) en compliantie (C).

Afhankelijke variabele		**β**	**SE**	**t-waarde**	**p**
v_p [cm/s]	Constante	42.667	2.047	20.849	.000
	LAP [mmHg]	0.297	0.041	7.157	.000
	τ [ms]	-0.302	0.025	-11.903	.000
	C [ml/mmHg]	7.860	1.053	7.462	.000
E [cm/s]	Constante	99.809	1.277	78.167	.000
	LAP [mmHg]	0.771	0.026	29.822	.000
	τ [ms]	-0.254	0.016	-16.082	.000
	C [ml/mmHg]	-7.078	0.657	-10.770	.000

III.2.3.2. Voorspelling van E en v_p voor Verschillende Stadia van Diastolische Disfunctie

Uitgaande van de hoger bekomen resultaten zijn voorspellingen gemaakt van E en v_p in vier verschillende stadia van diastolische disfunctie. Er is voor gezorgd dat deze waarden binnen het bereik blijven van de waarden, ingesteld in hoger uitgevoerde experimenten. Een referentiestadium (REF) is bekomen door τ in te stellen op 50 ms, LAP op 5 mmHg en C op 1.20 ml/mmHg. Uitgaande van deze referentie situatie is een vertraagde relaxatie (DR) gecreëerd door τ op te voeren tot 75 ms, terwijl alle andere variabelen constant gehouden worden. Het pseudo-normale vullingspatroon (PN) werd dan bekomen door de vullingsdruk te verhogen tot 15 mmHg en de compliantie te verminderen tot 0.90 ml/mmHg. Het restrictieve patroon (RF) werd tenslotte bekomen door een aanvullende

drukstijging tot 25 mmHg, een additionele stijging in τ tot 85 ms en een verdere afname van C tot 0.60 ml/mmHg.

De staafdiagrammen van figuur 21 (gearceerde staven) tonen de voorspelde waarden van E en v_p in de referentie situatie (REF), voor een vertraagde relaxatie (DR), een pseudo-normale vulling (PN) en een restrictieve vulling (RF). De foutmarges stellen het 95% betrouwbaarheidsinterval voor, berekend met de Working-Hotelling procedure. In vergelijking met de referentie situatie (REF) is E significant lager gedurende vertraagde relaxatie (DR) en hoger gedurende pseudo-normalisatie (PN) en restrictieve vulling (RF). De v_p vertoont een analoge daling gedurende de vertraagde relaxatie, maar stijgt niet boven de referentie waarden uit in het geval van pseudo-normalisatie en restrictieve vulling.

III.2.4. Discussie

Onze bevindingen met betrekking tot de invloed van relaxatie (τ), vullingsdruk (LAP) en compliantie (C) op E zijn in overeenstemming met vroegere studies (Appleton 1997, Choong et al. 1988, Solomon et al. 1999, Thomas et al. 1991). E neemt af met een vertraagde relaxatie en toenemende compliantie en neemt toe met stijgende vullingsdruk. Onze bevindingen omtrent v_p zijn overeenkomstig met resultaten die een omgekeerd evenredig verband aantoonden tussen v_p en de relaxatieconstante τ, zowel bij mensen als dieren (Brun et al. 1992, Duval-Moulin et al. 1997, Garcia et al. 2000, Garcia et al. 1998, Stugaard et al. 1995, Takatsuji et al. 1996). In onze experimenten werd een positieve relatie tussen compliantie en v_p waargenomen. Indien men de stroming in de LV voorstelt als de stroming door een cilindrische buis, is dit in tegenspraak met de wetten van de stromingsdynamica. Immers, in een buis geldt de Moens-Korteweg vergelijking die stelt dat de voortplantingssnelheid van een drukgolf omgekeerd evenredig is met de compliantie van de wand. Onze bevindingen kunnen echter verklaard worden door op te merken dat het concept van een cilindrische buis te eenvoudig is om de vulling van de LV te beschrijven, aangezien de LV een afgesloten kamer en geen open buis is. Bovendien is de voortplantingssnelheid, gemeten met CMD echocardiografie een voortplantingssnelheid van de vullingsgolf en niet van de drukgolf. Rekening houdend met deze opmerkingen kan het vastgestelde positieve verband tussen compliantie en voortplantingssnelheid intuïtief verklaard worden door de invloed van een stijver LV dat de instroming meer verhindert dan een

compliant LV. Numeriek simulaties (Vierendeels et al. 2000) en in vivo observaties (Duval-Moulin et al. 1997) bevestigen deze hypothese.

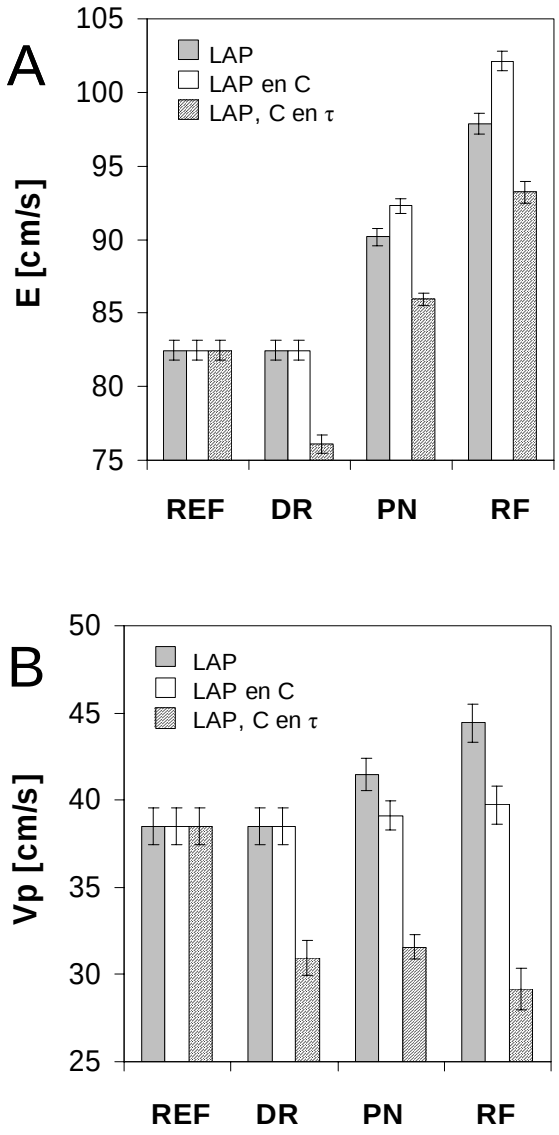

Figuur 21: Voorspelde (**Luik A**) E-snelheid (E) en (**Luik B**) voortplantingssnelheid (v_p) voor verschillende combinaties van LV karakteristieken: een referentie toestand (REF), vertraagde relaxatie (DR), pseudo-normale vulling (PN) en restrictieve vulling (RF). De gearceerde staven tonen de gecombineerde invloed van relaxatie (τ), vullingsdruk (LAP) en compliantie (C). De volle en witte staven tonen de geïsoleerde invloed van respectievelijk vullingsdruk (LAP) en de combinatie vullingsdruk (LAP) / compliantie (C).

Verscheidene studies, zowel in mensen als dieren, hebben aanwijzingen gegeven dat v_p relatief ongevoelig is voor veranderingen in vullingsdruk (Firstenberg et al. 2000a, Garcia et al. 1997, Moller et al. 2000b, Stugaard et al. 1993, Takatsuji et

al. 1996). Onze bevindingen wijzen daarentegen wel in de richting van een belastingsafhankelijkheid. In vergelijking met de E-snelheid, is v_p wel minder gevoelig voor verschillen in vullingsdruk. Bovendien zal in een reële situatie een gevoelige drukstijging samengaan met een daling in compliantie (concaaf druk-volume verband) waardoor het effect van de drukstijging op v_p gecompenseerd wordt door de daling in compliantie.

Beperkingen van het model

Het ontwikkelde hydraulisch model beoogt de simulatie van de complexe interactie tussen cardiovasculaire vloeistofmechanica en diastolische functie van het linkerhart. De combinatie van latex, omringd door een gaas is uiteraard niet in staat om de ingewikkelde fysiologische processen in de (pathologische) hartspierwand op cellulair niveau na te bootsen. Bovendien is het lineaire passieve druk-volume verband een vereenvoudiging t.o.v. de werkelijkheid. In het model werd de mitralisklep vervangen door een tricuspide bioprothese zonder chordae tendinae. Ook de simulatie van de verschillende stadia van diastolische functie is te eenvoudig, vergeleken met de reële situatie, waar o.a. ook inotrope en chronotrope veranderingen hun invloed uitoefenen. Het doel van dit model reikt echter niet tot het nabootsen van gedetailleerde fysiologische processen. Niettegenstaande haar beperkingen, is het model goed in staat om de invloed van belangrijke karakteristieken op de vloeistofdynamische eigenschappen van de vulling zichtbaar te maken en een verklaring te geven aan de fysische betekenis van vp.

III.2.5. CONCLUSIE

In dit onderzoek is een nieuw hydraulisch model voor de LV vulling ontwikkeld. In het model zijn de geïsoleerde invloeden van relaxatie, vullingsdruk en compliantie op veranderingen in E en v_p nagegaan. v_p is niet absoluut ongevoelig voor vullingsdruk. In vivo compenseert een daling in compliantie mogelijks voor een stijging van de vullingsdruk waardoor v_p relatief drukongevoelig lijkt.

III.3. De Stromingvoortplantingssnelheid in de LV: Overeenkomsten en Verschillen tussen een Numeriek en Hydraulisch Model

III.3.1. INLEIDING

In de vorige paragraaf werd een nieuw hydraulisch LV vullingmodel geïntroduceerd. In het model werd de interactie tussen v_p en LV diastolische parameters onderzocht. In deze paragraaf worden de resultaten vergeleken met numeriek simulaties.

III.3.2. NUMERIEK MODEL

Numeriek simulaties worden uitgevoerd met een 2D axisymmetrisch model voor de vulling van de linkerhartkamer. Het model werd ontwikkeld binnen het doctoraatsonderzoek van Jan Vierendeels (Vierendeels 1998). Het model berekent de vloeistofdynamica van de LV vulling, waarbij de vloeistofwand interactie mee in rekening gebracht wordt.

III.3.3. SIMULATIEPROTOCOL

CMD beelden zijn geregistreerd in het hydraulisch model voor een model LV met compliantie 1.35 ml/mmHg onder variërende waarden voor τ (45 tot 90ms) en LA vullingsdruk (3 tot 30 mmHg). Dezelfde metingen zijn herhaald in een model LV met compliantie 0.45 ml/mmHg.

Overeenkomstig met de metingen in het hydraulisch model, zijn de CMD beelden gesimuleerd met het numerieke model voor 12 verschillende combinaties van de parameters: 9 combinaties voor een LV compliantie van 1.35 ml/mmHg met variërende τ (45, 60 en 90ms) en variërende LA vullingsdruk (10, 20 en 30 mmHg), aangevuld met 3 bijkomende simulaties in een LV met compliantie 0.45 ml/mmHg bij een vaste LA vullingsdruk (30 mmHg) en een variërende τ (45, 60 en 90 ms). De nodige randvoorwaarden, in essentie het LV passief druk-volume verband en het snelheidsprofiel ter hoogte van de mitraalklep, werden afgeleid uit de experimenten in het hydraulische model en aangeboden aan het numerieke model.

III.3.4. RESULTATEN

Teneinde visueel de overeenkomst tussen gemeten en gesimuleerde CMD beelden te kunnen nagaan, zijn de gesimuleerde beelden weergegeven in hetzelfde formaat met behulp van een blauw-rode kleurenschaal. Figuur 22 toont voor vier verschillende instellingen de gemeten en berekende CMD beelden. Treffende gelijkenissen op het gebied van penetratie van de hoge snelheden in het LV tussen gemeten en gesimuleerde CMD beelden kunnen worden waargenomen voor de verschillende situaties.

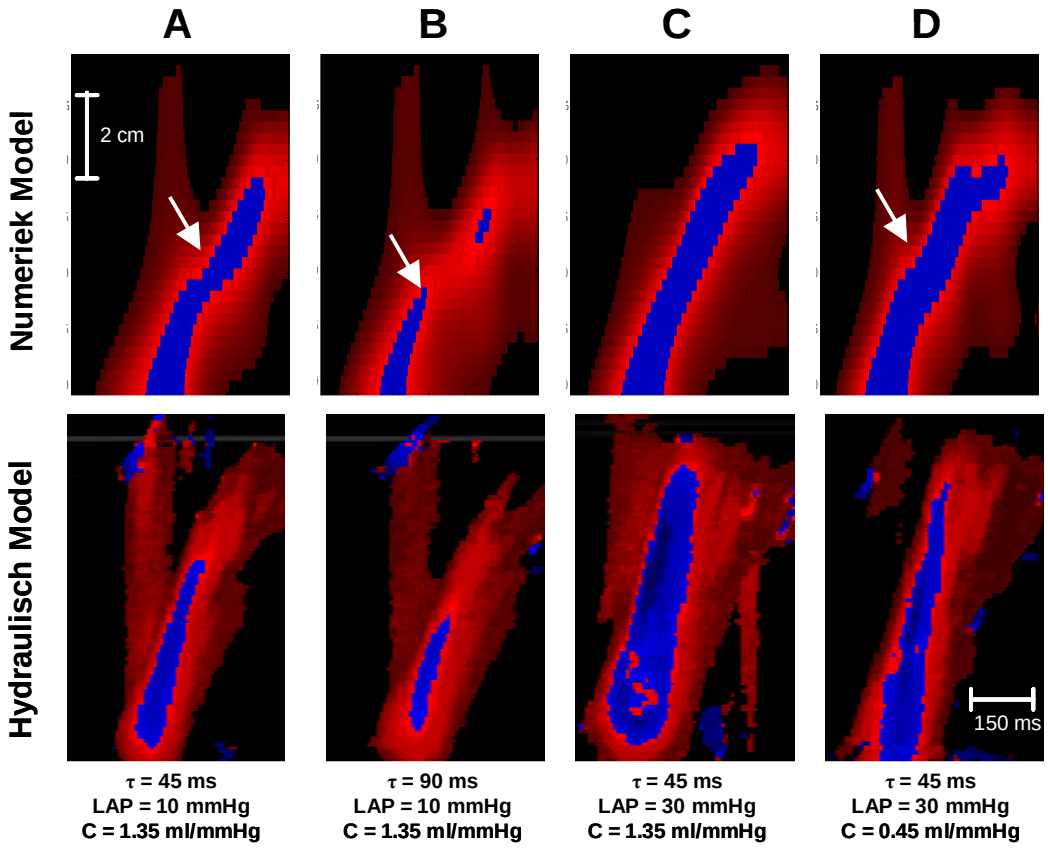

Figuur 22: Gemeten (**onder**) en gesimuleerde (**boven**) CMD beelden van de LV vulling voor variërende instellingen van τ, LA druk en LV compliantie. Pijlen duiden posities aan waar wervels stagneren.

Teneinde de beelden kwantitatief te vergelijken is v_p bepaald met behulp van de Duval-Garcia methode (cf. Deel 2, paragraaf 3). De v_p op basis van gemeten CMD beelden in het hydraulisch model vertoont een matige correlatie met de v_p afkomstig van de gesimuleerde CMD beelden ($r = 0.67$, $p < 0.001$). Gemeten v_p

waarden (hydraulisch model) zijn consistent groter dan de gesimuleerde v_p waarden (numeriek model).

Figuur 23 toont de gesimuleerde v_p in functie van τ voor verschillende LA druk niveaus (links) en verschillende LV compliantie (rechts). Volledig in overeenstemming met de hydraulische experimenten (cf. Deel 2, paragraaf 2) daalt v_p met stijgende τ en dalende LA druk. De invloed van LV compliantie op v_p is niet éénduidig. Voor kleine τ vallen v_p in compliant en stijf model nagenoeg samen. Voor grotere τ resulteert een toename in compliantie in een toename van v_p. Dit laatste is in overeenstemming met de resultaten bekomen in het hydraulische model (cf. Deel 2, paragraaf 2).

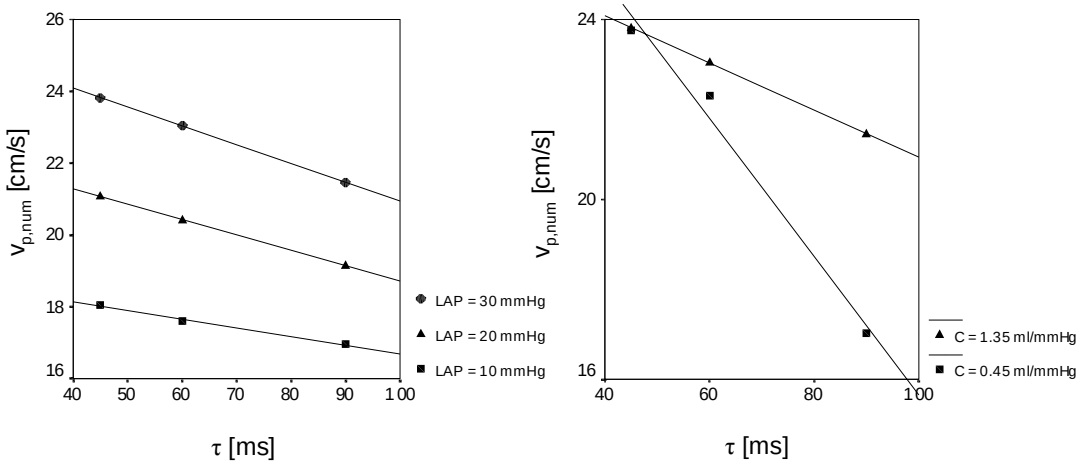

Figuur 23: $v_{p,num}$ in functie van τ voor verschillende niveaus van LA druk (**links**) en verschillende LV compliantie (**rechts**).

III.3.5 DISCUSSIE EN CONCLUSIE

De interactie tussen v_p en LV diastolische variabelen is bestudeerd in een hydraulisch model en vergeleken met bevindingen op basis van een numeriek model. Algemeen wordt een goede overeenkomst tussen hydraulisch en numeriek model vastgesteld. v_p stijgt met afnemende τ en toenemende LA druk.

Het niet-éénduidige gedrag van v_p onder invloed van compliantie kan verklaard worden door het feit dat tengevolge van een stijver LV de v_p lokaal in de omgeving van de LV basis toeneemt, maar desalniettemin globaal afneemt doordat de wervels in het LV veel sneller stagneren in vergelijking met een

complianter LV. Dit laatste kan duidelijk waargenomen worden op figuur 22 (D) (zie pijl). De stijging van v_p in de omgeving van de basis is in overeenstemming met de Moens-Korteweg vergelijking. De globale daling is in overeenstemming met de waarnemingen in het hydraulisch model.

III.4. Oorsprong van Intraventriculaire Drukgradiënten: Inzichten uit een Hydraulisch Model en Dierexperimentele Bevindingen

III.4.1. INLEIDING

Onderzoek naar de oorsprong en invloedfactoren van plaatselijke drukverschillen in de LV (intraventricular pressure gradients, IVPG) is reeds geruime tijd aan de gang. Tot nog toe was dit onderzoek vrij academisch aangezien deze drukverschillen enkel op een omslachtige, invasieve wijze gemeten kunnen worden. Recent onderzoek van Greenberg et al. (Greenberg et al. 2001) heeft echter geleid tot een methode die toelaat om uitgaande van niet-invasieve snelheidsmetingen met CMD echocardiografie deze drukverschillen te reconstrueren. Dit onderzoek opent de deur naar klinische toepassingen in het echolab van ieder ziekenhuis. Om uit IVPG bruikbare informatie te halen dient men alle interfererende factoren te kennen. Tot op heden is vooral veel aandacht besteed aan de invloed van de systolische functie op de IVPG tijdens diastole. Dit onderzoek in soms vrij complexe dierenmodellen duidt “elastic recoil”, het tijdens diastole vrijkomen van elastische energie, opgeslagen in de gecomprimeerde hartwand tijdens systole, als de overheersende factor. Numerieke simulaties wijzen echter uit dat de zogenaamde “elastic recoil” niet noodzakelijk is om de aanwezigheid van IVPG te verklaren.

III.4.2. DOELSTELLING

Dit onderzoek wil de mogelijke invloed van diastolische variabelen op IVPG in kaart brengen. In het bijzonder wordt gewerkt rond de hypothese dat drukgradiënten nauw verbonden zijn met lokale verschillen in de tijdsconstante van de drukval tijdens de isovolumetrische relaxatie (τ).

III.4.3. METHODEN

In eerste instantie wordt het gedrag van τ in een hondenexperiment geobserveerd. Drukmetingen worden hiervoor simultaan uitgevoerd in LA en LV ter hoogte van de basis en de apex in een referentietoestand, tijdens infusie van esmolol en tijdens infusie van isoproterenol. τ waarden worden berekend en de mogelijke

verbanden tussen τ, verschillen in τ en IVPG tijdens de isovolumetrische relaxatie (IVPGivr) en de vroege vulling (IVPGe) worden bestudeerd.

Vervolgens worden analoge metingen uitgevoerd in het zelfde hydraulische model voor de LV vulling als beschreven in paragraaf 2 van dit deel. Opnieuw zal het model toelaten om de geïsoleerde invloed van belangrijke fysiologische parameters na te gaan.

III.4.4. RESULTATEN

Hondenmodel. Figuur 24 (links) toont drukcurves gemeten in het hondenmodel. τ waarden zijn consistent langer ter hoogte van de basis in vergelijking met de apex. Dit verschil in τ (Δτ) neemt af tijdens esmolol infusie (Δτ = 1.4 ± 0.1 %) en neemt toe tijdens isoproterenol (Δτ = 12.1 ± 2.1 %) infusie in vergelijking met de referentie situatie (Δτ = 4.8 ± 0.6 %). IVPG worden in het hondenmodel waargenomen tijdens de isovolumetrische relaxatie (IVPGivr) en tijdens de vroege vulling (IVPGe). IVPGivr en IVPGe nemen toe tijdens de infusie van isoproterenol (2.1 ± 0.2 mmHg en 2.5 ± 0.3 mmHg) en nemen af bij infusie van esmolol (0.5 ± 0.1 mmHg en 1.0 ± 0.1 mmHg) in vergelijking met de referentiesituatie (1.3 ± 0.1 mmHg en 1.7 ± 0.1 mmHg). Een significante correlatie tussen IVPGivr en IVPGe werd vastgesteld ($r = 0.923$, $p < 0.001$). Ook het proportioneel verschil in τ tussen basis en apex (Δτ) en τ zelf waren significant gecorreleerd met IVPGivr ($r = -0.676$, $p < 0.001$ (Figuur 25, links) en $r = -0.520$, $p < 0.001$) en IVPGe ($r = 0.709$, $p < 0.001$ en $r = 0.733$, $p < 0.001$).

Hydraulisch model. Figuur 24 (rechts) toont drukcurves gemeten in het hydraulisch model (rechts). Kwalitatief stelt men een gelijkaardig verloop vast met de curves gemeten in het hondenmodel (Figuur 24, links). Tijdens de isovolumetrische relaxatieperiode en de vroege vulling dalen de drukken sneller en dieper in de LV apex in vergelijking met de LV basis. Aangezien in het hydraulisch model geen LA contractie gemodelleerd is, vertonen de overeenkomstige drukcurves ook geen LA contractiegolven.

De metingen in het hydraulisch model ondersteunen de bevindingen in het dierenexperiment. τ is korter aan de apex en het verschil in τ tussen basis en apex vertoont een verband met de IVPGivr en IVPGe ($r = 0.788$, $p < 0.001$ (figuur 25, rechts)). Er werd geen significante correlatie tussen τ en IVPG gevonden.

In het hydraulisch model zijn metingen uitgevoerd waarbij de LV diastolische variabelen één voor één gewijzigd werden. Een multivariate regressie analyse op de resultaten leert dat bovenop $\Delta\tau$, ook LV compliantie een significante invloed uitoefent op de IVPGivr en IVPGe. LA druk heeft enkel een kleine, doch significante invloed op IVPGe. In het hydraulisch model kon geen significant verband tussen τ en IVPG aangetoond worden.

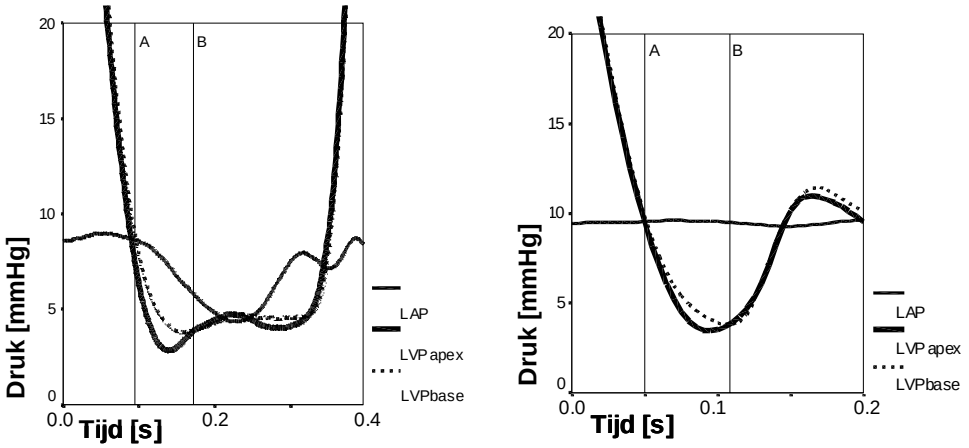

Figuur 24: LA en LV drukken tijdens LV isovolumetrische relaxatie en vulling in het hondenmodel (**links**) en het hydraulisch model (**rechts**).

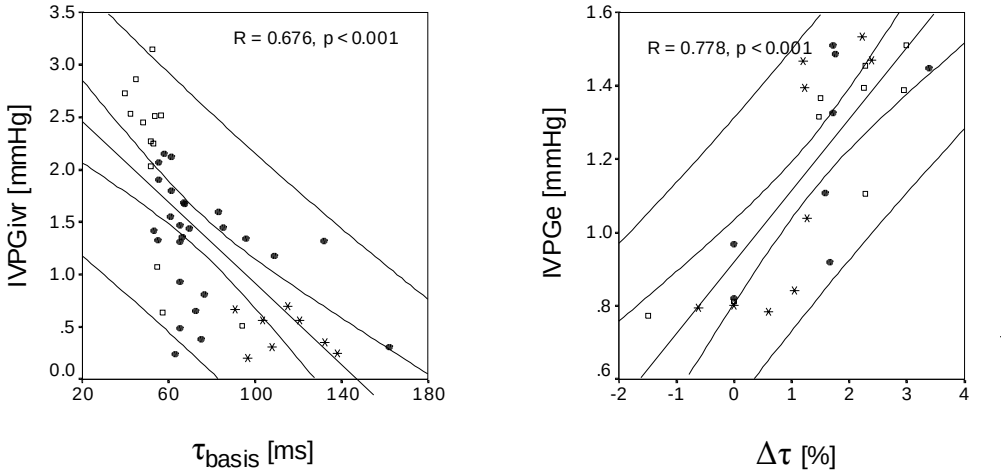

Figuur 24: Regressie tussen IVPGivr en τ in het hondenmodel (**links**) en IVPGe en $\Delta\tau$ in het hydraulisch model (**rechts**).

III.4.5 Discussie en Conclusie

Regionale verschillen in τ en regionale drukverschillen in de LV zijn systematisch bestudeerd in een hondenmodel en een hydraulisch model.

Regionale variabelen

Een regionaal verschil in τ werd zowel in honden- als hydraulisch model vastgesteld. Het significante verband tussen $\Delta\tau$ en IVPG tijdens de isovolumetrische relaxatie, en vooral een gelijkaardige relatie tussen $\Delta\tau$ en IVPG tijdens de vroege vulling suggereert dat reeds tijdens de relaxatiefase de vroege vulling actief voorbereid wordt, met de ontwikkeling van IVPG en eventueel bijhorende redistributie van bloed in de LV. De oorsprong van de $\Delta\tau$ moet gezocht worden in regionale wandbewegingen, op hun beurt een gevolg van één of een combinatie van regionale verschillen in relaxatie of regionale verschillen in zogenaamde “elastic recoil”.

Globale variabelen

De resultaten geven aan dat de grootte van IVPG beïnvloed wordt door globale diastolische variabelen zoals LV compliantie en vullingsdruk. Dat deze variabelen, die een belangrijke invloed uitoefenen op de vulling, ook een niet onbelangrijke invloed hebben op de IVPG hoeft niet te verwonderen aangezien vulling en IVPG intrinsiek verbonden zijn via de stromingsvergelijkingen.

III.5. Verband tussen Inspanningscapaciteit, Infarctgrootte en Stromingvoortplantingssnelheid in de Linker Ventrikel

III.5.1. INLEIDING

Een restrictief vullingspatroon, gekenmerkt door een hoge E-snelheid en een korte deceleratietijd (d_t), voorspelt een slechte LV functie na het doormaken van een hartinfarct. De prognose kan nog verfijnd worden. Moller et al. (Moller et al. 2000a) hebben immers aangetoond dat patiënten met een pseudo-normaal patroon, gekenmerkt door normale waarden voor E en d_t, ook een verhoogd risico hebben op overlijden na een myocard infarct. Met behulp van CMD kan een normaal vullingspatroon onderscheiden worden van een pseudo-normaal (respectievelijk hoge en lage v_p).

In normale patiënten staat de inspanningscapaciteit in een duidelijke relatie met diastolische functie. Na het doormaken van een myocardinfarct is het verband tussen diastolische functie en inspanningscapaciteit minder duidelijk. Mogelijks interfereren factoren zoals infarctgrootte en ejectiefractie (EF) in deze relatie.

III.5.2. DOELSTELLING

Deze studie heeft tot doel om inspanningscapaciteit te vergelijken binnen een groep patiënten met een geschiedenis van myocardinfarct tussen patiënten met een normaal versus abnormaal vullingspatroon. De factoren infarctgrootte en ejectiefractie worden mee in rekening gebracht.

III.5.3. METHODEN

41 patiënten met een minimum 6 weken oud myocardinfarct zijn opgenomen in de studie. Alle patiënten ondergingen binnen een tijdspanne van twee dagen een echocardiografisch onderzoek, een 99Tc-Tetrofosmin gated SPECT onderzoek en een fietsproef inclusief ademhalingsonderzoek met gasanalyse.

Echocardiografisch onderzoek

Met een Hewlett-Packard 2500 Sonos systeem werden de stroompatronen over de mitraalklep met PWD echocardiografie opgemeten. De analyse van de beelden gebeurde off-line door één onderzoeker die geen kennis had van de SPECT en

fietsproef resultaten. De hemodynamische karakteristieken E, A, E/A, d_t en v_p werden berekend als het gemiddelde van drie opeenvolgende waarnemingen. v_p werd bepaald op een semi-automatische wijze volgens de methode van Duval-Garcia, zoals hoger beschreven (zie deel II, paragraaf 3). De patiënten werden onderverdeeld in vier groepen volgens de graad van diastolische disfunctie. De gehanteerde criteria op basis van d_t en v_p zijn overgenomen van Garcia et al. en weergegeven in tabel 6.

Tabel 6: Indelingscriteria voor de stadia van DHF op basis van Doppler metingen.

	Groep I normaal (n = 9)	Groep II Vertraagde relaxatie (n = 12)	Groep III pseudo-normaal (n = 12)	Groep IV restrictief (n = 8)
d_t	150-200ms	>200ms	150-200 ms	<150 ms
v_p	>45 cm/s		<45 cm/s	

SPECT onderzoek

Met behulp van de SPECT metingen zijn LVEF en LV volumes berekend. Bovendien werd de grootte van het infarct gekwantificeerd door de berekening van een infarctscore (IS). De berekening van IS resulteert in een waarde op een schaal van 0 tot 100 waarbij 0 duidt op geen infarct en 100 overeenkomt met een volledig geïnfarcteerde LV. De gemiddelde EF was 48%, de gemiddelde infarctscore 17.

Inspanningsproef

Tenslotte werden de patiënten ook onderworpen aan een fietsproef met analyse van de gasuitwisseling. De patiënten fietsten volgens een standaard protocol waarbij de weerstand met 25 Watt opgevoerd werd iedere twee minuten. Op basis van de fietsproef werden volgende variabelen opgenomen in de studie: totaal gepresteerd aantal Watts, piek zuurstofopname, gedefinieerd als het gemiddelde van de opname gedurende de laatste minuut. Gemiddelde Total Watt was 700 Watt. Gemiddelde VO_2max was 22ml/kg/min.

III.5.4. RESULTATEN

In de totale patiëntenpopulatie werden geen significante correlaties vastgesteld tussen de hemodynamische parameters afgeleid uit PWD beelden (E, A, E/A) enerzijds en LVEF, LV volumes noch IS anderzijds. Enkel een zwakke, doch statistisch significant negatieve relatie tussen d_t en infarctscore werd vastgesteld ($r = -0.374$, $p = 0.02$). v_p vertoonde daarentegen sterkere correlaties met verschillende opgemeten karakteristieken: IS ($r = -0.585$, $p = 0.001$), LVEF bij rust ($r = 0.420$, $p = 0.009$), EDV bij rust ($r = -0.330$, $p = 0.04$) en ESV bij rust ($r = -0.382$, $p = 0.02$).

Na opdeling van de patiënten in vier groepen volgens de graad van diastolische disfunctie, werd vastgesteld dat groepen III en IV een grotere infarctscore en een kleinere LVEF bij rust vertoonden in vergelijking met de patiënten van groepen I en II.

Total Watts noch VO_2max correleerden significant met ook maar één van de diastolische parameters (E, A, E/A, d_t en v_p). Nochtans werd, na opdeling van de patiënten in de vier groepen op basis van d_t en v_p, een duidelijk verschil waargenomen tussen inspanningscapaciteit in de normale groep enerzijds en de vertraagde relaxatie, pseudo-normale en restrictieve groep anderzijds.

III.5.5 DISCUSSIE

Een duidelijke relatie tussen infarctgrootte en v_p werd vastgesteld in dit onderzoek. Deze vaststelling verruimt vroegere bevindingen waar een verband tussen v_p en infarctgrootte op basis van vrijgekomen enzymen werd vastgesteld in de acute fase van het infarct. Deze vaststelling ondersteunt de bevinding dat een lagere v_p geassocieerd is met minder gunstige klinische vooruitzichten na myocard infarct.

Belangrijk bij dit alles is dat men op basis van v_p in staat is ook de groep patiënten met een pseudo-normaal vullingspatroon te isoleren. Er is immers aangetoond dat ook deze groep een verhoogd risico vertoont. Onze resultaten ondersteunen deze bevindingen voor zover dat in de pseudo-normale groep zowel LVEF als IS significant lager zijn in vergelijking met de normale groep.

De relatie tussen inspanningscapaciteit en diastolische functie na myocard infarct is voorwerp van discussie. In onze studie blijkt echter dat enkel in patiënten met

een volledig bewaarde diastolische functie (groep I) ook een bewaarde inspanningscapaciteit vertoonden. Niet alleen de groepen met pseudo-normale en restrictieve vullingpatronen, maar ook de groep met vertraagde relaxatie toonden een duidelijk afgenomen inspanningscapaciteit.

III.5.6. CONCLUSIE

In patiënten met een geschiedenis van myocard infarct is zowel d_t als v_p gerelateerd met IS. Patiënten met een pseudo-normaal of restrictief vullingspatroon vertonen duidelijk lagere LVEF en hogere IS. Niettegenstaande geen rechtstreeks verband tussen inspanningscapaciteit en d_t noch v_p afzonderlijk werd vastgesteld, kon op basis van de combinatie d_t en v_p vastgesteld worden dat in patiënten met een bewaarde diastolische functie inspanningscapaciteit hoger ligt dan in een groep met verminderde diastolische functie.

Besluit
Originele Bijdragen en Toekomstig Onderzoek

Hartfalen is een belangrijke doodsoorzaak in de Westerse maatschappij. Diastolisch hartfalen neemt tot 40% van de gevallen van hartfalen voor haar rekening. Een definitieve diagnose van diastolisch hartfalen is vooralsnog moeilijk te stellen zonder invasieve metingen.

ORIGINELE BIJDRAGEN

Dit proefschrift levert een bijdrage tot de integratie van niet-invasieve technieken, i.h.b. kleuren M-mode Doppler (CMD) echocardiografie, ter bepaling van diastolisch hartfalen in de klinische praktijk. Hiervoor is gebruik gemaakt van vier types onderzoeksmiddelen: hydraulische modellen, numerieke simulaties, dierexperimentele modellen en studies in patiëntenpopulaties. De resultaten situeren zich op twee niveau's.

Enerzijds zijn een aantal *methodologische aspecten* uitgewerkt.

- Aannemend dat de drukval tijdens de isovolumetrische relaxatie priode voldoende nauwkeurig beschreven kan worden door de tijdsconstante van een mono-exponentiële functie, dient een keuze gemaakt tussen vaste (nul) drukasymptoot en vrije drukasymptoot. Met behulp van experimentele data en Monte Carlo simulaties is aangetoont dat deze keuze gelijk staat aan een afweging tussen systematische fout (bij vaste drukasymptoot) en een grotere spreiding op de geschatte waarden (bij vrije drukasymptoot). Via de berekeneing van een relatieve efficiëntie is de keuze kwantitatief gemaakt.

- Vier methodes ter bepaling van de stromingvoortplantingssnelheid (v_p), uitgaande van CMD beelden, zijn geïmplementeerd in semi-automatische computeralgoritmen. Analyse van patiëntendata toont aan dat de geautomatiseerde methode van Duval-Garcia de beste resultaten oplevert inzake reproduceerbaarheid.
- De numerieke informatie in een CMD beeld leent zich tot kwantitatieve verwerking. Een preliminaire studie in een hydraulisch model geeft aan dat longitudinale impedantie, bepaald uit een CMD beeld, een reproduceerbare index is, sensitief voor klepoppervlakte en testvloeistof.
- Een studie in post-operatieve coarctatie patiënten, ondersteund met experimenten in een hydraulisch model, toont de beperkingen van gepulste Doppler echocardiografie en de vereenvoudigde Bernoulli vergelijking aan. Een alternatieve uitdrukking om drukgradiënten te schatten, de Seeley vergelijking, levert veelbelovende resultaten in het hydraulisch model.

Anderzijds is basisonderzoek verricht naar de invloed van *diastolische functie*.

- Een nieuw hydraulisch model voor de studie van de LV vulling is ontwikkeld. In het model zijn significante relaties tussen v_p enerzijds en LV relaxatie, LA vullingsdruk en LV compliantie anderzijds in kaart gebracht. De resultaten laten toe om de evolutie van v_p voor verschillende stadia van diastolische disfunctie te simuleren. Het model is in staat klinisch waargenomen evoluties te verklaren.
- De resultaten van het ontwikkelde hydraulische model zijn getoetst aan berekeningen in een gevalideerd numeriek model. De numerieke resultaten bevestigen de in het hydraulische model waargenomen verbanden tussen diastolische variabelen en v_p, en brengen deze in overeenstemming met de Moens-Korteweg vergelijking voor de golfvoortplantingssnelheid.
- Intraventriculaire drukgradiënten (IVPG) zijn bestudeerd in een dierexperimenteel model, gecombineerd met hydraulische experimenten. Enerzijds is de invloed van globale diastolische karakteristieken op IVPG aangetoond. Anderzijds is een regionaal verschil in LV relaxatie geïdentificeerd als een mechanisme dat tijdens de isovolumetrische relaxatie

periode de actieve vulling voorbereidt en aldus ook rechtstreeks de vroege vullingsfase beïnvloedt.

- Een klinische toepassing sluit dit proefschrift af. In een grondig gedocumenteerde studiegroep van post-infarctpatiënten, wordt met behulp van v_p, diastolische functie in rechtstreeks verband gebracht met infarctgrootte en inspanningscapaciteit.

TOEKOMSTIG ONDERZOEK

In dit onderzoek hebben een aantal modellen meer inzicht verschaft in de stromingskarakteristieken van de LV vulling. Hierbij werden een aantal vereenvoudigingen doorgevoerd. Het introduceren van een beweegelijke mitraalklepring en het modelleren van een lekkende klep zijn voor de hand liggende uitbreidingen die nog meer details van het vullingsproces kunnen onthullen.

De resultaten van dit proefchrift leveren talrijke argumenten op om te streven naar een gestandaardiseerde bepaling van v_p. De geïmplementeerde semi-automatische algoritmen zijn daartoe een eerste aanzet.

In dit proefschrift is aangetoond dat wijzigingen in intraventriculaire drukgradiënten veranderingen in diastolische variabelen weerspiegelen. Het verenigen van deze drukinformatie met snelheidsinformatie biedt perspectieven om nog beter de vullingsstatus te kunnen inschatten.

Aim and Outline of the thesis

Aim

Congestive heart failure is identified as an imporant cause of mortality in the Western community. Basically, two mechanisms are governing heart failure: systolic dysfunction (failing pump function) and diastolic dysfuncion (abnormal filling). Distinguishing diastolic from systolic dysfunction is essential for a proper treatment since the optimal therapy for one condition may aggravate the other. In contrast to systolic dysfunction, diagnosing diastolic dysfunction remains challenging in the clinical setting.

In the past two decades, diastology has emerged as the science that characterizes left ventricular filling and function. Diastology not only investigates the basic mechanisms that are governing diastolic filling, function and their relationship, but also seeks to integrate these concepts into clinical practice.

Invasive pressure measurements allow for a definite diagnosis of diastolic heart failure. However, expenses and risks accompanying catheterization hamper the use of invasive pressure measurements in routine examinations and follow-up studies. Therefore, research is focused on non-invasive assessment of diastolic heart failure. The ability to derive non-invasive information on left ventricular function makes Doppler echocardiography a most attractive tool in clinical practice. However, the complexity of the Doppler approaches are well known. Doppler derived indices provide indirect information about the function of the heart and have to be seen in relation to other factors influencing cardiac function, such as preload and heart rate.

This thesis aims to contribute to the integration of non-invasive techniques for the evaluation of diastolic heart failure, especially color M-mode Doppler echocardiography, in clinical practice. Efforts have been focussed on the interaction between physiological determinants of left ventricular diastolic function and hemodynamics of the cardiovascular system. Research has been conducted using hydraulic and numeric models. Results are compared to measurements in animals and humans.

Outline

The thesis consists of 12 chapters (in English), preceded by a **synthesis in Dutch**, conform the regulation of the Faculty of Applied Sciences of the Ghent University. The synthesis comprises an introduction to diastolic heart failure and an overview of the scientific results. The **12 Chapters in English** are divided into three parts: (1) Introduction, (2) Methodology en (3) Model studies and clinical observations.

PART I: INTRODUCTION

Chapter 1 provides an introduction into the cardiovascular system. Special attention is paid to systolic and diastolic function. Congestive heart failure is introduced and an overview of the difficulties in diagnosing diastolic heart failure in the clinical setting is given. **Chapter 2** offers some technical background concerning cardiac measurement techniques, including invasive pressure measurements, (Doppler) echocardiography and single photon emission computed tomography (SPECT). Finally, chapters 3 and 4 are dealing with methods for the evaluation of diastolic dysfunction: invasive techniques and standard Doppler techniques in **Chapter 3**, next to color M-mode Doppler echocardiography in **Chapter 4**.

PART II: METHODOLOGY

Part two reports results of "methods-oriented" research. **Chapter 5** deals with the calculation of the time constant of pressure decline during left ventricular isovolumic relaxation. **Chapter 6** offers a detailed comparison between four methods for the assessment of flow propagation velocity using semi-automated software. **Chapter 7** describes a preliminary study that explores the quantitative information in a color M-mode Doppler image. Finally, **Chapter 8** investigates the limitations of the standard pulsed Doppler techniques for the assessment of pressure differences using the simplified Bernoulli equation.

PART III: MODEL STUDIES AND CLINICAL OBSERVATIONS

Part three gathers the experimental research and clinical observations on diastolic filling and function. **Chapter 9** describes the development of a new hydraulic LV filling model and subsequent research on the interaction between flow

propagation velocity and diastolic variables. **Chapter 10** confronts the experimental findings of chapter 9 to simulation results in a numerical model. **Chapter 11** revisits the origin of the subtle regional differences in pressures within the left ventricular cavity in a canine model and the hydraulic model during isovolumic relaxation and early filling. **Chapter 12** is a clinical study on diastolic function in remote myocardial infarction. The relationship between exercise capacity, infarct size and flow propagation velocity are analyzed.

In a conclusion chapter, research results are discussed and future prospects are given.

Part I: Introduction

CHAPTER 1

The Cardiovascular System: Systolic and Diastolic (dys)Function

1. Introduction

In this introductory chapter, the anatomy and physiology of the normal heart are introduced, next to some control mechanisms of cardiac function. Also, the mechanisms, prevalence and diagnosis of congestive heart failure in general and diastolic heart failure in particular are explained.

2. Cardiac Anatomy

2.1. The Heart

The human heart is situated in the thoracic cavity in between the lungs. The pericardium, composed of two layers (visceral and parietal pericardium), encloses the heart. A small amount of lubricating fluid separates the two pericardial layers and reduces friction created by the pumping heart. The heart wall itself is composed of three layers: the outer layer or epicardium, the middle, muscular layer or myocardium, and the inner endothelial layer or endocardium.

The human heart is divided into four chambers. The “upper” chambers of the heart, the atria, are anatomically separated from the “lower” chambers or ventricles by a fibrous ring. The four cardiac valves are situated within this ring. From functional point of view, the heart is divided into right- and left-sided pumps, which propel oxygen deficient blood into the pulmonary circulation and oxygenated blood into the systemic circulation, respectively. The direction of blood flow in the circulation is (Figure 1.1): venae cavae, right atrium (RA), right ventricle (RV), pulmonary artery, lungs, pulmonary veins, left atrium (LA), left ventricle (LV), aorta, arteries, arterioles, capillaries, venules, veins, and back to the venae cavae.

2.2. The Left Heart

Left and right sided heart are separated by the septum (Figure 1.2). The left heart is composed of LA and LV. The LA receives oxygenated blood from the lungs via the pulmonary veins. No valves separate the pulmonary veins from the LA. Therefore, alterations in LA pressure are reflected retrograde into the pulmonary vasculature, and acute elevations in LA pressure will cause pulmonary congestion. The LA is a thin-walled, low-pressure chamber. Blood flows from the LA into the LV through the mitral valve. The mitral valve is a bicuspid valve with two valve cusps or leaflets. The leaflets are delicate, yet durable. The cusps of the valve are attached to thin strands of fibrous tissue called chordae tendinae. The chordae tendinae extend to the papillary muscles, which are muscular projections arising from the ventricular wall. The mitral valve assures one-directional blood flow from LA to LV, i.e. the mitral valve prevents backflow from the LV into the LA

during LV contraction and ejection. The thick musculature of the LV facilitates the development of high pressure during ventricular contraction. The LV and the aorta are separated by the aortic valve, consisting of three cuplike cusps, secured to a fibrous ring. The valve prevents backflow from the aorta into the ventricle during LV relaxation and filling.

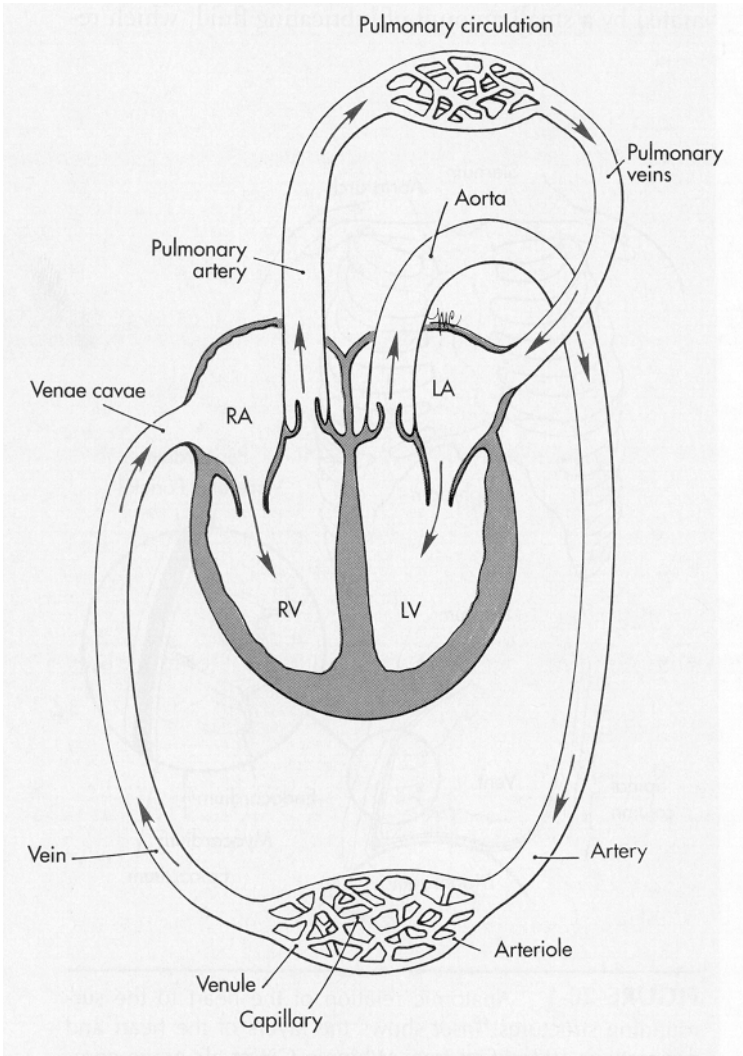

Figure 1.1: The sequence of blood flow in the circulation (Price and Wilson 1992).

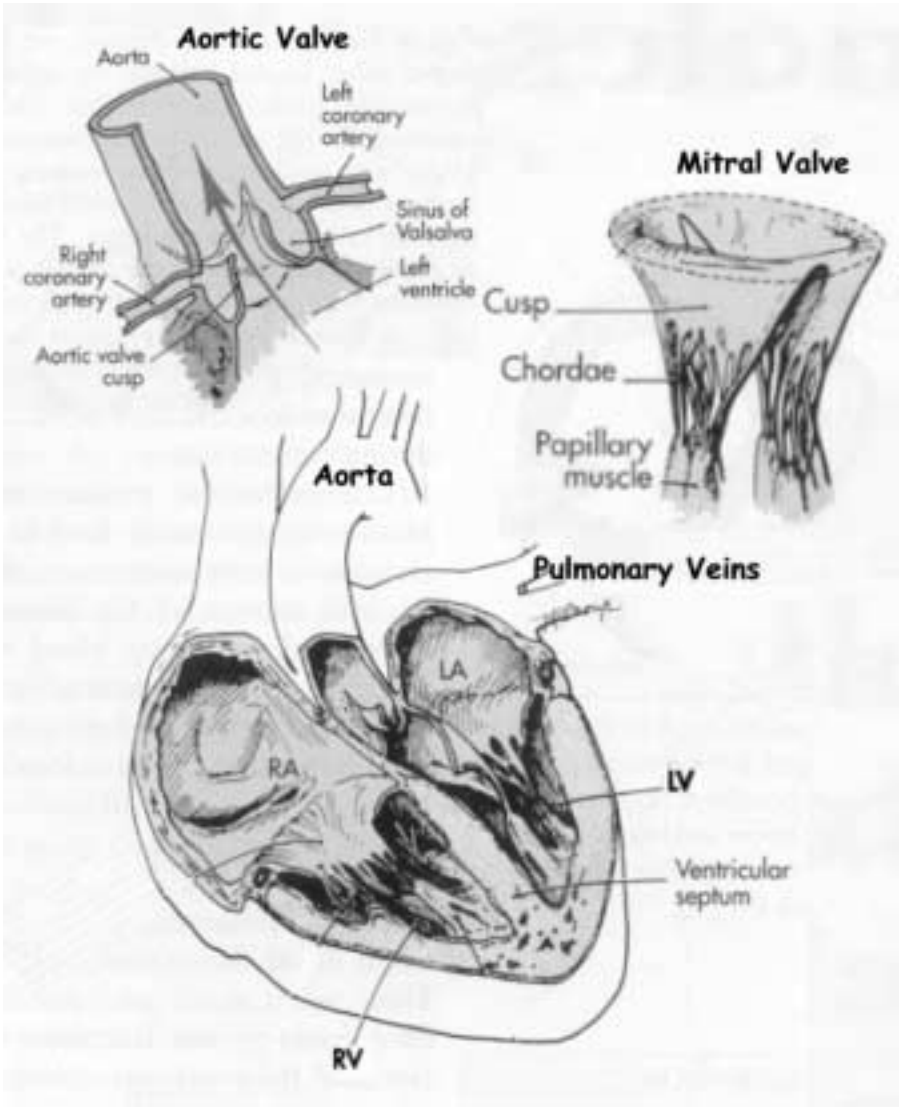

Figure 1.2: Anatomy of the human heart, aortic valve and mitral valve (Price and Wilson 1992).

3. Cardiac Physiology

3.1. Cardiac Contraction and Relaxation: Cellular Mechanism

The myocardium of the heart consists of cardiac muscle cells or myocytes as illustrated in figure 1.3 (A). Ventricular myocytes (100 μm in length, 20 μm in diameter) are composed of myofibrils which in turn are composed of sarcomeres (1.6-2.2 μm in length) as illustrated in figure 1.3 (B). Each sarcomere is composed of several thick myosin filaments, each surrounded by six thin actin filaments. The interaction between these filaments produces force and shortening of the myocardium.

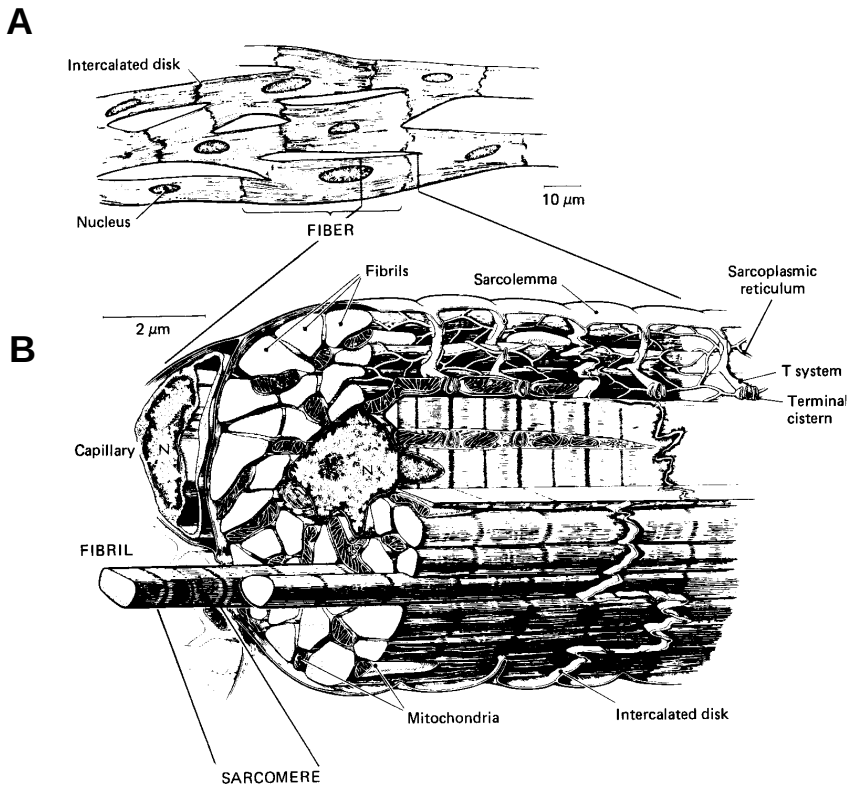

Figure 1.3: Anatomy of the myocardium: **(A)** myocytes; **(B)** myofibrils and sarcomeres (Apstein and Morgan 1994).

The cycle of myocardial contraction and relaxation is directly related to the cytosolic calcium concentration (Figure 1.4). With electrical depolarization of the sarcolemma (surface membrane), calcium enters the myocyte via slow (L-type) calcium channels. This triggers the release of massive amounts of additional

calcium stored in the sarcoplasmic reticulum. The calcium diffuses into the sarcomere, causing a conformational change in the troponin-tropomyosin complex. Troponin and tropomyosin are regulatory proteins that permit myosin to interact with actin and the myocyte to contract. For the myocyte to relax, the process must be quickly reversed. Up to 90% of the calcium is actively removed by the calcium ATPase pump in the sarcoplasmic reticulum and the rest by sodium-calcium exchange and other mechanisms. This is achieved against a 10000-fold concentration gradient and requires a high expenditure of energy. One molecule ATP (adenosine triphosphate) is consumed for every two molecules of calcium removed by the calcium ATPase pump. In the myocyte, ATP is produced in a large number of mitochondria.

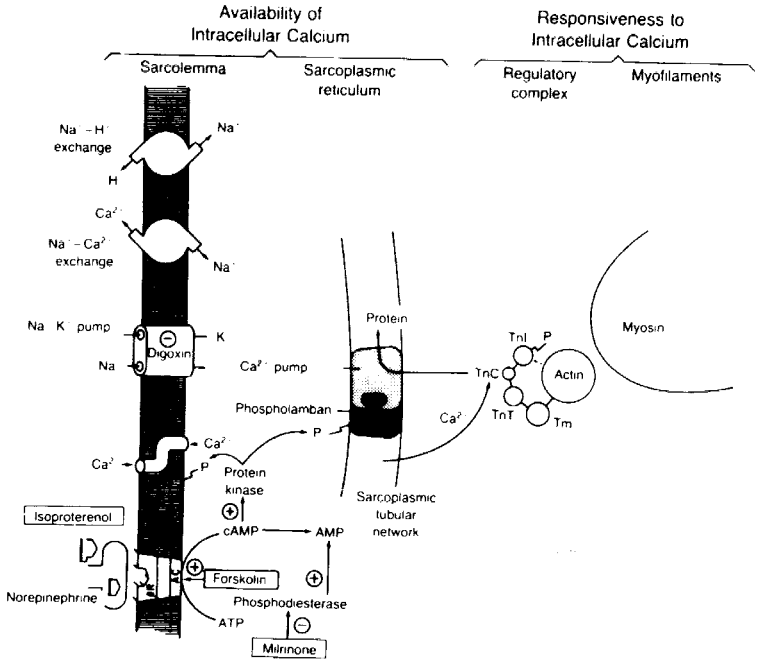

Figure 1.4: Cellular mechanism of contraction and relaxation (Apstein and Morgan 1994).

3.2. . CARDIAC CONTRACTION AND RELAXATION: ELECTRICAL APPROACH

Each cardiac cycle consists of a sequence of interdependent electrical and mechanical events. An electrical excitation wave stimulates the cardiac muscle. This electrical excitation is actually a depolarization wave, triggering the release

of calcium and is followed by electrical recovery or repolarization. The mechanical responses are muscular contraction and muscular relaxation, respectively.

3.2.1. Conduction System

Because the fibrous ring between the atria and ventricles isolate these chambers electrically as well as anatomically, a specialized conduction pathway exists in the myocardium to ensure rhythmic and synchronized excitation and contraction of the heart muscle. Figure 1.5 illustrates the conduction system of the heart. The normal sequence of excitation through the conduction system is as follows: sinoatrial (SA) node, atrial pathways, atrioventricular (AV) node, bundle of His, bundle branches, and Purkinje fibers.

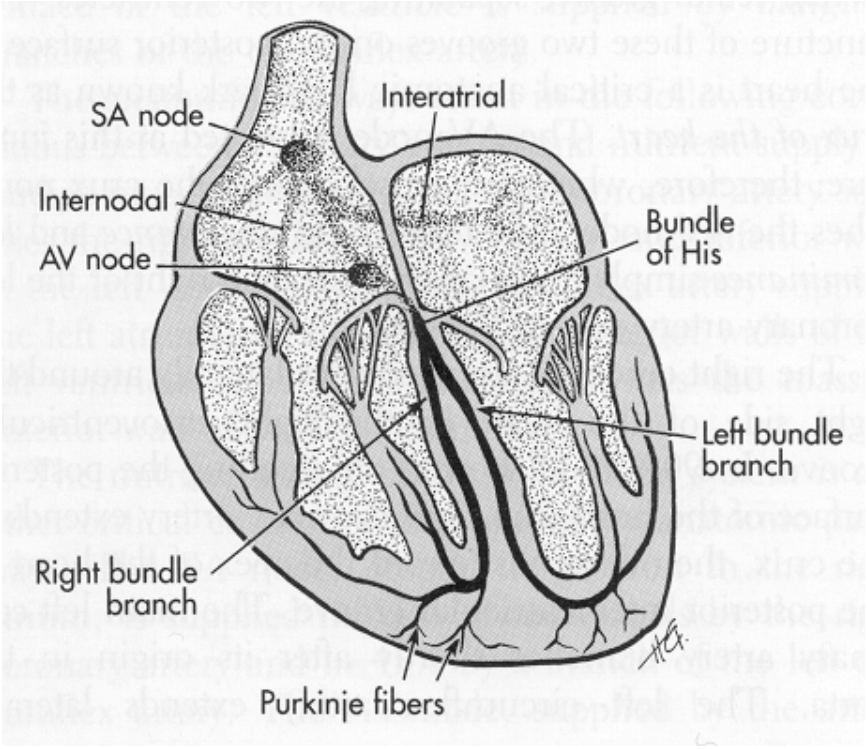

Figure 1.5: Cardiac conduction system for electrical impulses (Price and Wilson 1992).

The SA node acts as a natural pacemaker and is situated in the posterior wall of the right atrium. A cardiac impulse, starting from the SA-node, firstly spreads to the interatrial pathway and provokes contraction of the atria. The electrical impulse than reaches the AV node, which is positioned at the top of the

intraventricular septum. The AV node performs two critical functions: (1) it delays the cardiac impulse for 0.08 to 0.12 seconds and (2) it limits the number of impulses reaching the ventricles. Normally no more than 180 impulses per minute are permitted to reach the ventricles. The wave of electrical excitation spreads from the AV node to the bundle of His, the bundle branches and the Purkinje fibers.

3.2.2. Electrocardiogram

The electrocardiogram (ECG) reflects the summated electrical activity of all the myocardial cells recorded from the body surface (Figure 1.6). Characteristic wave complexes on the ECG are P, QRS, and T-waves. The P-wave corresponds to atrial depolarization, originating from an impulse from the SA node. The QRS complex represents ventricular depolarization. The amplitude of this wave is large as a result of the large muscle mass traversed by the electrical impulse. The PR interval includes the transmission time through the atria and the delay of the impulse at the AV node. Ventricular repolarization generates the T wave.

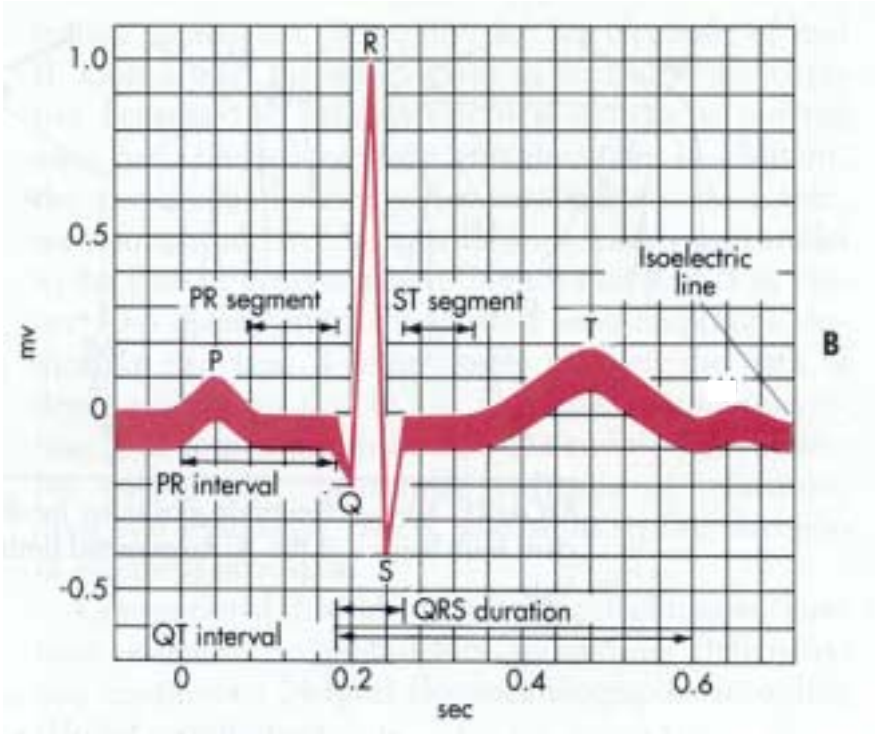

Figure 1.6: Complexes in the electrocardiogram.

3.3. CARDIAC CONTRACTION AND RELAXATION: THE HEART AS A PUMP

3.3.1. Pressure-Volume Loop

In mechanical terms, the ventricular cardiac cycle is best described using a pressure-volume loop as shown in figure 1.7. This representation typically describes the working of the heart as a pump. Point B represents the end of filling where the aortic valve is closed and where the open mitral valve closes. LV pressure increases during isovolumic contraction until the aortic valve opens (C). The ejection phase begins at point C with ventricular volume decreasing until LV pressure falls below aortic pressure. The aortic valve closes at point D and isovolumic relaxation begins. The mitral valve opens at point A when LV pressure falls below LA pressure. Ventricular filling occurs between points A and B and a second cardiac cycle begins with mitral valve closure. Using the pressure volume loop as a reference, systole (ejection) can be defined as the period from B to D, whereas diastole (filling) can be associated with the period from D to B.

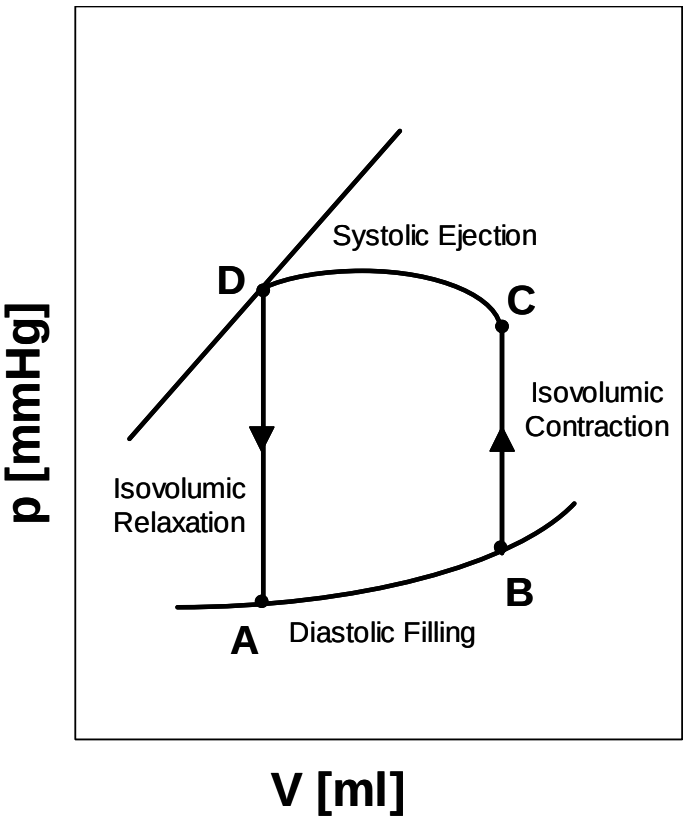

Figure 1.7: The ventricular cardiac cycle represented by its pressure-volume loop; p: LV pressure, V: LV volume.

3.3.2. Systolic and Diastolic Pressure and Flow Events

Figure 1.8 presents pressure and flow events during the cardiac cycle (Yellin 1995). The timing of the events can be situated within the cardiac cycle using the ECG diagram on top of the figure.

Systole

During ventricular systole pressure rises from 0 to 120 mmHg. When LV pressure rises above aortic pressure, the aortic valve opens and blood is ejected from the LV in the arterial system. The volume ejected by each ventricle per minute is the cardiac output (CO). Average cardiac output is 5-6 l/min. However, cardiac output varies to meet the demands of the pheripheral tissues for oxygen and nutrients. Stroke volume (SV) is the volume of blood ejected by each ventricle per beat. Approximately two thirds of the volume of blood in the ventricle at the end of diastole (end-diastolic volume, EDV) is ejected during systole. This portion of ejected blood is known as the ejection fraction (EF; EF = SV/EDV). The residual ventricular volume at the end of systole is referred to as the end-systolic volume (ESV).

Diastole

Based on figure 1.8 , the diastolic portion of the heart cycle can be subdivided into four phases: (1) isovolumic relaxation, (2) rapid or early filling (E-wave), (3) diastasis (L-wave) and (4) atrial contraction (A-wave). In the first phase, between the time of aortic valve closure and mitral valve opening, LV pressure relaxes exponentially from the aortic pressure level to the pressure level existing in the LA. The next phase, i.e. early filling (E-wave), begins when pressure in the LV falls below that in the LA, causing the mitral valve to open and the LV to begin filling. The early filling phase coincides with and is dependent on continued LV relaxation. This phase ends when pressure in the two chambers is equalized. Although this rapid filling comprises only about 30% of diastole, it accounts for up to 80% of LV filling volume. The third phase is the diastasis. Little filling, if any, comes from pulmonary vein flow (L-wave). With increased heart rate this phase shortens more than the other three. The fourth phase, atrial contraction (A-wave), contributes for 15% to 25% of LV filling volume under normal conditions but can contribute as much as 40% if LV relaxation is diminished.

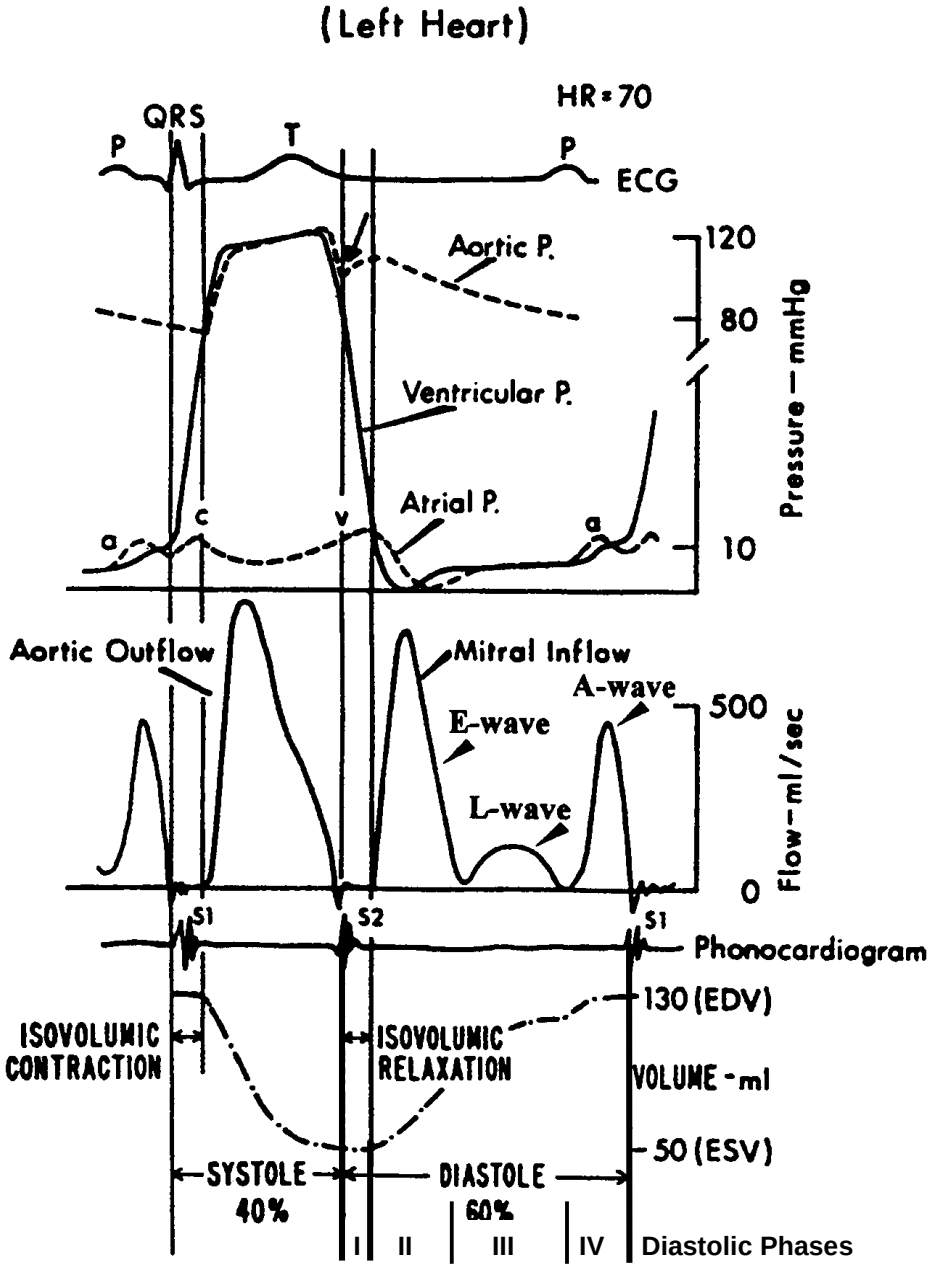

Figure 1.8: Pressure and flow events during the cardiac cycle (Yellin 1995).

Basically because relaxation is an energy consuming and therefore "active" process, commencing during the second half of the ejection phase, sometimes the isovolumic relaxation phase and early filling phase are considered to be the end of systole (Brutsaert et al. 1993, Brutsaert and Sys 1989, Gillebert and Sys 1994). By this definition diastole only comprises diastasis and atrial filling. Consequently, in this definition diastole accounts for about 50% of the cardiac cycle at normal heart

rates, contributing for only 15% to 25% of the LV volume. Although this approach offers some advantages in understanding cellular and mechanical events, it introduces a difficult terminology for the clinician who, based on phenomenological evidence, is convinced that ejection ends with, and diastole commences after aortic valve closure[1].

[1] In this work, unless explicitly stated otherwise, the "clinical" definition of diastole is used, considering LV isovolumic relaxation and the early filling phase as a part of diastole.

4. Systolic and Diastolic Function

4.1. Cardiac Function

The function of the heart is to generate the appropriate cardiac output that meets the needs of the metabolism. Cardiac output depends on the relationship between two variables: heart rate (HR) and stroke volume (SV):

$$CO = HR \times SV \qquad \text{[Eq. 1.1]}$$

Heart rate is largely under the extrinsic control of the autonomic system. Parasympathetic and sympathetic fibers innervate the SA node and the AV node, influencing the rate and speed of impulse conduction. Stroke volume is influenced by both intrinsic and extrinsic control mechanisms.

Because of the pulsatile character of the heart, performance in terms of stroke volume has to be seen as the result of two independent but interrelated functions: filling (diastolic function) and emptying (systolic function) of the heart. The first is defined as the capacity of the LV to contract and eject the stroke volume at the high pressures in the aorta. The second is defined as the capacity of the LV to relax and then to accept the stroke volume at the low pressures existing in LA

4.2. Systolic Function

The stroke volume ejected during systole is mainly dependent on three control mechanisms: (1) preload (Starlings Law), (2) contractility, and (3) afterload.

4.2.1. Preload: Starlings Law of the Heart

The relationship between cardiac output and filling pressure was first recognized by Starling at the beginning of the 20th century and called “the law of the heart”[2]. Starlings law of the heart states that stretching the myocardial fibers during diastole by increasing EDV will increase the force of contraction during systole. Stretching the sarcomere maximizes the number of interaction sites available for actin-myosin linkage by increasing the overlap between the myofilaments (Figure

[2] This mechanism has been discovered, based on results of experiments by O. Frank (Frank, O. 1895) in isometric and isotonic contracting frog hearts, next to experiments by E. Starling (Starling E.H. 1918), focussing on LV volume and EF in dog hearts contracting under different conditions of venous inflow and aortic resistance. Therefore this mechanism is also called the "Frank-Starling" mechanism.

1.9). Consequentially the force of contraction rises. Typically, the sarcomere is stretched to 2.0 μm during diastole.

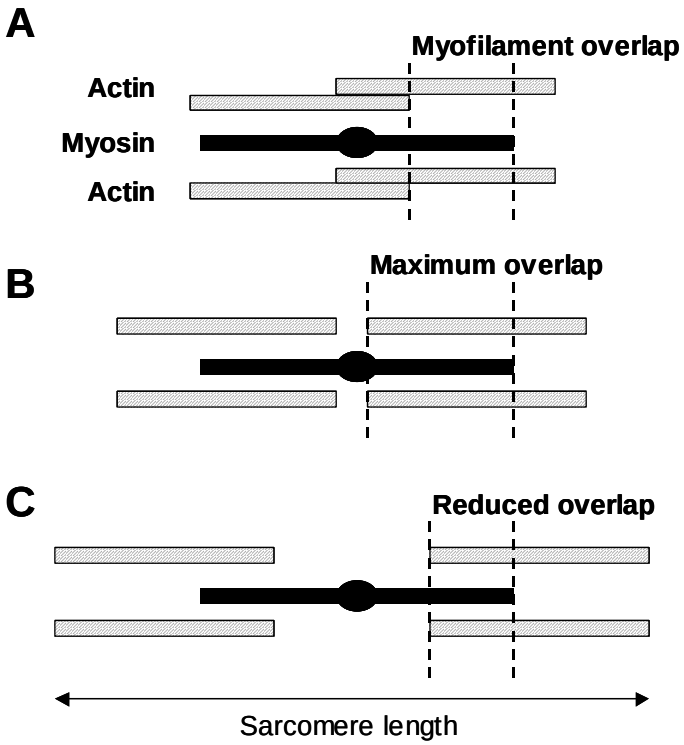

Figure1.9: Effect of sarcomere length on myofilament overlap. **(A)** Usual sarcomere length of 2.0 μm. **(B)** Optimal sarcomere length of 2.2 μm. **(C)** Excessive sarcomere length of 2.5 μm.

The optimal sarcomere length is 2.2 μm. Therefore a reserve in sarcomere length and resultant force of contraction exists. Starlings Law is functional within limits, determined by the myocardial structure. Stretching the sarcomere to more than 2.4 μm reduces the strength of contraction. Fortunately, the sarcomeres are extremely resistant to overstretching.

The relationship between myocardial fiber length and force of contraction is referred to as the ventricular function curve (Figure 1.10). The degree of fiber stretch or preload is determined by the ventricular volume. The volume of blood contained within the ventricles during diastole depends on the amount of venous return. Venous return is influenced primarily by circulating blood volume and the venous tone. Increasing ventricular EDV initially increases force of contraction

and thus SV. The curve shows a plateau, indicating that from a certain point additional increments in EDV will not improve function.

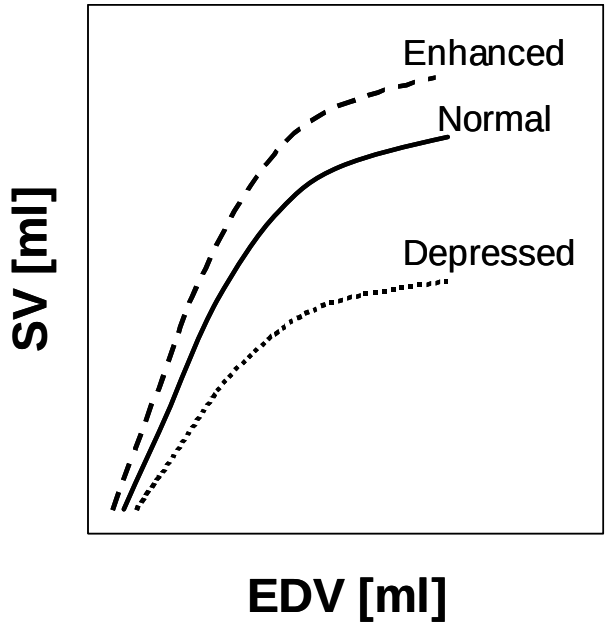

Figure 1.10: Ventricular function curves.

4.2.2. Contractility

Contractility refers to changes in the developed force of contraction that occur independent of changes in myocardial fiber length. Increased contractility is the result of intensification of the interactions at the actin-myosin cross-bridges in the sarcomere. The intensity of these interaction relates to the intracellular concentration of free calcium ions.

Analysis of the mechanical behaviour of the ventricle in general and the contractility of the heart in particular has been using the varying-elastance model, introduced in the 1960s by Beneken and De Wit (Beneken and De Wit 1967), and verified by Suga and Sagawa (Sagawa et al. 1988). The varying-elastance model for the heart consists of a pressure source (venous pressure) emptying into the left ventricle with a time-varying elastance E(t). Originally Suga et al. (Suga 1995) approximated the end-systolic and end-diastolic pressure-volume curves as two straight lines that intersected in a common point on the volume axis. Based on this approach the elastance E as a function of time became:

$$E(t) = \frac{p(t)}{V(t) - V_{\varphi}} \qquad \text{[Eq. 1.2]}$$

where V_{φ} is the unloaded volume defined as the intercept of the end-systolic pressure volume relationship (ESPVR) with the volume axis. The maximum value of E(t), reached in general close to end-systole and called E_{max} has been claimed to represent myocardial contractility, dependent of heart rate but relatively independent of loading conditions (Suga 1995). Figure 1.11 shows the time-varying elasance curve, measured in a dog heart (left panel) and pressure-volume loops under varying preload. The slope of the end-systolic pressure-volume relationship (ESPVR), connecting the end-systolic points of the pressure-volume loops, quantifies contractility.

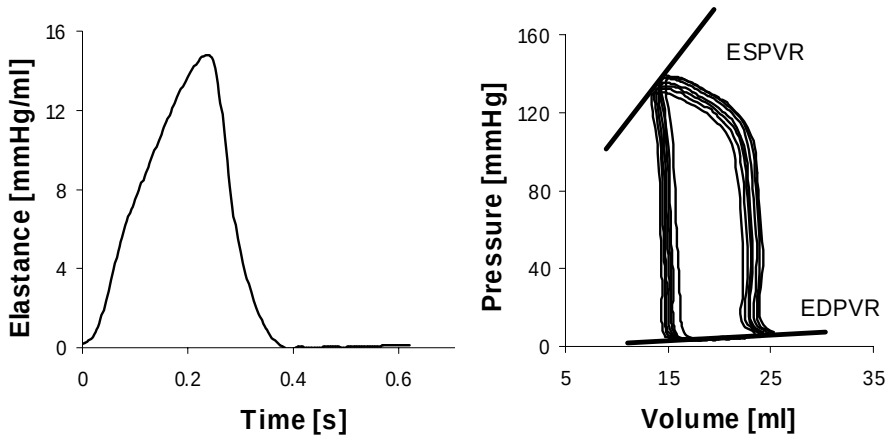

Figure 1.11: Time-varying elastance curve **(Left);** pressure-volume loops in a dog heart varying preload **(right)**. ESPR: end-systolic pressure volume relationship, EDPVR: end-diastolic pressure volume relationship.

4.2.3. Afterload

Afterload can be defined as the stress that the ventricle must develop during systole to open the aortic valve and eject blood. It is a function of intraventricular pressure, intraventricular radius (size) and ventricular wall thickness. Considering the LV as a simple spherical shell the relationship between these variables is expressed by the Laplace[3] law:

[3] Laplace, Pierre-Simon (1749-1827). French mathematician and physicist.

$$\sigma = \frac{p \cdot r}{2h} \qquad \text{[Eq. 1.3]}$$

where p is pressure (in mmHg), r is the radius (in cm) and h is the thickness of the wall (in cm) (Shintani and Glantz 1994). Additional assumptions concerning the visco-elastic properties of the LV wall allow for an extension of this simple model to more complex geometries (Arts et al. 1993).

According to this relationship, wall stress is directly augmented by factors that increase ventricular pressure and volume, and is attenuated when the ventricular wall hypertrophies.

4.3. Diastolic Function

The SV entering the LV during diastole is strongly dependent on (1) preload (LA pressure), (2) the mitral valve, (3) relaxation, and (4) LV compliance.

4.3.1. Preload: Role of Left Atrial Function

Ventricular filling depends significant on the atrial pressure which, in turn, is a function of the chamber properties. LA function can be divided into (1) a reservoir function, (2) a conduit function, and (3) a pump function (Arakawa et al. 1987, Arakawa et al. 1989, Meisner et al. 1985).

The reservoir function refers to the ability of the LA to store blood when the mitral valve is closed, and is important in producing an appropriate driving pressure and in providing an appropriate amount of blood for the following ventricular rapid filling. The LA fills passively with blood from the pulmonary veins during ventricular systole. Initially the volume increases but the pressure decreases (Figure 1.12, 1-2) and then they both increase forming the ascending limb of the V-loop (Figure 1.12, 2-3). In this the LA can be considered as an isolated chamber. In this way, the LA favours the following LV rapid filling by releasing the accumulated blood with the aid of the accumulated driving pressure. The according atrial volume and pressure decrease forms the descending limb of the v-loop (Figure 1.12, 3-4; corresponds to E-wave in figure 1.8).

During the following ventricular slow filling period LA volume and pressure increase. The magnitude of the volume change and pressure change during this period is not wide enough to permit reliable construction of a pressure-volume-

loop (conduit function of LA). During this period LA and LV form a common chamber and the conduit function refers to that portion of the pulmonary vein flow that passes through LA into LV (Figure 1.12, 4-5; see also L-wave in figure 1.8).

Finally, atrial pump function refers to the volume of blood injected into LV by contracting LA (atrial systole) resulting in the a-loop (Figure 1.12, 5-6-1; see also A-wave in figure 1.8).

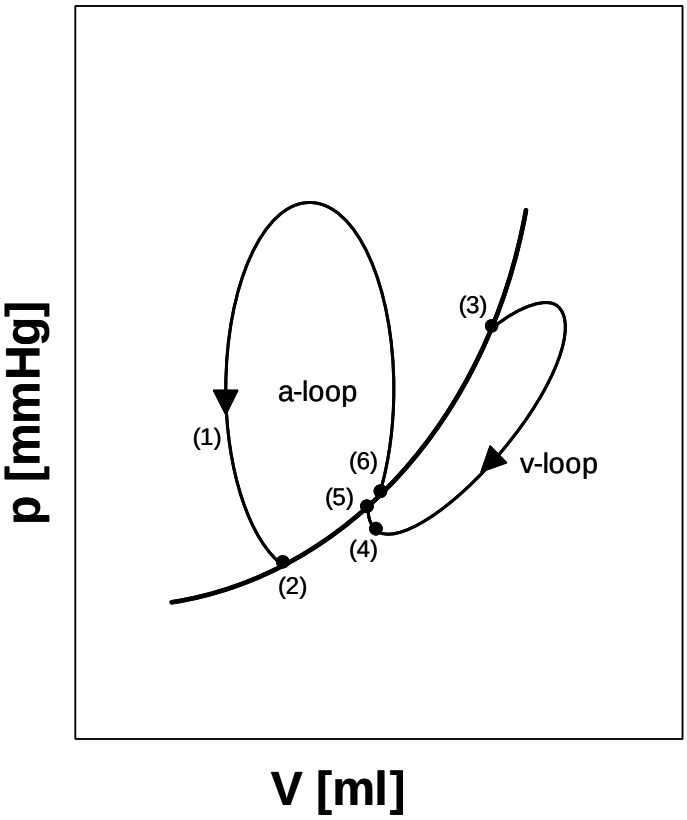

Figure 1.12: LA pressure-volume relationship; p: LA pressure, V: LA volume.

4.3.2. The Mitral Valve

The mitral valve is composed of four primary elements: the valve annulus, the valve leaflets, the papillary muscles, and the chordae tendinae. The valve leaflets, chordae tendinae, and papillary muscles all participate in the normal functioning of the mitral valve, especially during systole (Yoganathan et al. 1995). Salisbury et al. (Salisbury et al. 1963) found that the chordae tendinae tension only paralleled the LV pressure tracings during isovolumic contraction and that the

tracings were divergent during the rest of the cardiac cycle, supporting the hypothesis that under normal conditions the mitral apparatus passively opens and closes under the influences of the flow through the mitral valve. This hypothesis is also supported by numerical models that are able to predict the movements of the mitral valve during diastole, solely based on fluidodynamical modelling (Bellhouse 1972, Lee and Talbot 1979, Segers and Fronteau 1991, Verdonck et al. 1996, Verdonck et al. 1994).

In conclusion, under normal conditions, the resistance of the mitral valve opposing the inflow is basically determined by the geometrical difference between valve and chamber dimensions. Under pathological conditions (e.g. mitral valve stenosis, prolapse or insufficience) this hypothesis does not hold. However, in this work only healthy mitral valves are considered.

4.3.3. Left Ventricular Relaxation

In the normal heart, ventricular relaxation starts during mid-systole and continues throughout the first third of diastolic filling. During relaxation LV pressure falls from end-systolic pressure to below LA pressure. Because filling only starts after this cross-over between ventricular and atrial pressure, the onset, rate, and extent of relaxation are major determinants of diastolic filling and function. Relaxation rate depends on calcium flux. Physiologic determinants of relaxation are heart rate, temperature, and neurohormal stimulation , and to some extent also afterload (Leite-Moreira et al. 1999).

4.3.4. Passive Pressure-Volume Relationship: LV Compliance

The passive diastolic pressure-volume relationship of the LV is determined by the volume of the chamber and the material properties of the wall. An exponential form for the pressure-volume curve during filling is generally accepted and may be represented by the expression

$$p = b \cdot e^{k_c V} \qquad \text{[Eq. 1.4]}$$

where p is LV cavity pressure (in mmHg), V is LV volume (in ml) and b and k_c are curve-fitting parameters (Gaasch 1994). This exponential relation results in a linear relation between instantaneous or operating stiffness and pressure

$$\frac{dp}{dV} = k_c \times b \cdot e^{k_c V} = k_c \times p \qquad \text{[Eq. 1.5]}$$

where the curve-fitting parameter (k_c) represents a simple modulus or index of chamber stiffness. LV compliance (C) is the reciprocal of LV stiffness

$$C = \frac{dV}{dp} \qquad \text{[Eq. 1.6]}$$

Compliance or stiffness characterizes the entire LV. In order to gain insights into functional or structural abnormalities of the myocardium, regional characteristics, such as myocardial stiffness derived from the stress-strain relationship, remain mandatory. Stress-strain relationships can be derived from the LV pressure-volume relationship using for example the Laplace law (cf. supra, equation 1.3)

4.3.5. LV filling: Active or Passive Process?

The concept that LV pressure and volume are determined by the balance between the forces caused by pressures within the ventricular cavity that expand the ventricle and passive forces, caused by elasticity of the myocardium, that resist this expansion remains the centerpiece of the pressure-volume relationship during late diastole. However, besides other variables such as active relaxation, mechanical interaction between the left and right ventricles and the pericardium, the passive LV properties also play an important role during early diastole. Intensive research, going back as early as 1906[4], has integrated the influence of passive LV properties in the concept of the so-called elastic recoil and diastolic suction during early filling.

In the late 1950s, Brecher et al. (Brecher and Kissen 1957) contributed significantly to the clarifying of the concept of elastic recoil. The pressure-volume relationship of figure 1.14, obtained by Brecher et al., was the first to demonstrate the positive and negative portions of the passive pressure-volume relationship of the LV. It was obtained by infusion and aspiration of saline in an arrested canine LV. The volume with according zero transmural pressure was defined as the equilibrium volume (V_0).

[4] Henderson Y, 1906. The volume curve of the ventricles of the mammalian heart, and the significance of this curve in respect to the mechanics of the heart-beat and the filling of the ventricles. Am J Physiol 16:325.

The negative portion provides the physical basis for the so-called concept of diastolic suction. Because it allowed the incorporation of both the positive and negative portion of the LV passive pressure-volume relation, Nikolic et al. (Nikolic et al. 1988) introduced a logarithmic model for the passive LV pressure volume relationship (Equation 1.7).

$$p_p = -S_p \ln\left(\frac{V_{max} - V}{V_{max} - V_0}\right) \qquad \text{[Eq. 1.7]}$$

where V_{max} is the maximum attainable volume of the LV, V_0 is the equilibrium volume, S_p is a material property, and the subscript p refers to the positive portion of the pressure-volume relation.

This model represents a more meaningful conceptualization of the passive pressure-volume relationship, in contrast to the higher described exponential model.

Differentiating yields

$$S_p = \frac{dp_p}{dV \big/ (V_{max} - V)} \qquad \text{[Eq. 1.8]}$$

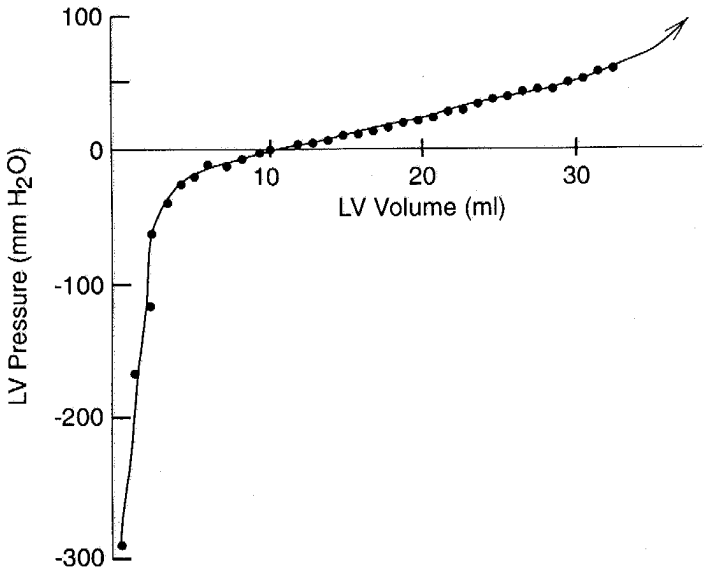

Figure 1.14: Passive LV pressure-volume relationship (Brecher and Kissen 1957).

S_p is a constant, defined as chamber stiffness, normalized by scaling the instantaneous volume to the operating range of the ventricle in the positive plane. Because S_p has the units of pressure, it is reasonable to conclude that it is related to the wall stress modified by a geometric factor. In a similar way the negative portion of the pressure-volume relation can be modeled (Equations 1.9 and 1.10).

$$p_n = -S_n \ln\left(\frac{V - V_{min}}{V_0 - V_{min}}\right) \qquad \text{[Eq. 1.9]}$$

$$S_n = \frac{dp_n}{dV \big/ (V - V_{min})} \qquad \text{[Eq. 1.10]}$$

where the subscript n denotes the negative portion of the pressure-volume relation and V_{min} is the minimum attainable volume of the LV.

Figure 1.14 suggests that an end-systolic volume below equilibrium volume provides the potential for the LV to generate negative pressures if subsequent filling is prevented. However, the aspiration of saline from a passive ventricle is not the same as the contraction of a beating heart below equilibrium volume. Using a technique of end-systolic volume clamping in the intact canine preparation, Yellin and coworkers (Yellin et al. 1986) unmasked this potential in the beating heart. The instrumentation of the experimental model is shown in figure 1.15. Using an occluder in mitral position with remote control mechanism, LV pressure (LVP), LA pressure (LAP), mitral valve flow (MiF) and aortic valve flow (AoF) are measured in filling and non-filling beats.

Figure 1.16 shows the pressure-time relation, obtained in the model from onset of isovolumic relaxation to end relaxation following clamping at end-systolic volume (i.e. in a non-filling beat). The filled circles are the actual data points, t_1 is the time of mitral valve opening. This animal experiment demonstrates that if LV filling is impeded, negative pressures may occur in the LV. This potential is associated with so-called diastolic suction during early filling. The pressure-volume loops of figure 1.17 explain the concept of diastolic suction in more detail (Yellin and Nikolic 1994). Loop A has an end-systolic volume greater than the equilibrium volume, V_0, and can never reach a pressure lower then “a”. Increased

contractility (broken line and dotted loop) can reduce end-systolic volume to below V_0 and lead to diastolic suction. Loop B has the potential ability to relax to "b" and can have the same filling volume as loop A with a lower mean LA pressure.

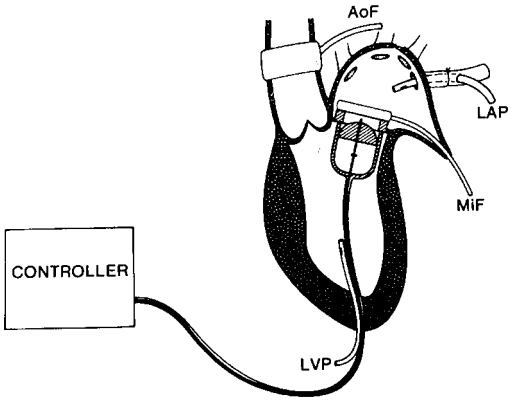

Figure 1.15: Instrumentation of the clamping model of Yellin and coworkers (Yellin et al. 1986). AoF: Aortic valve flow, MiF: Mitral valve flow, LAP: Left atrial pressure, LVP: Left ventricular pressure.

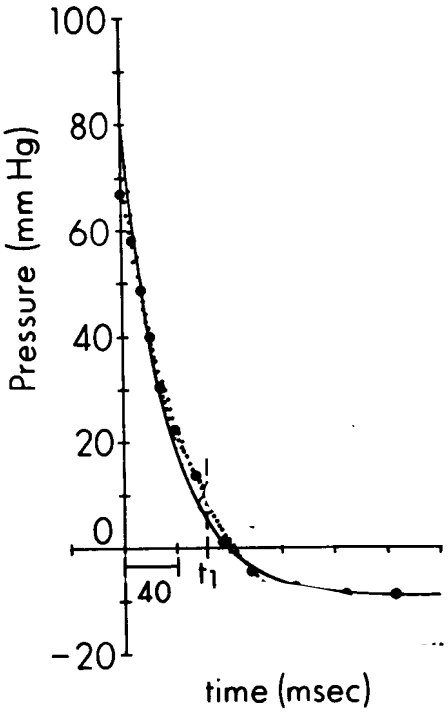

Figure 1.16: Pressure decay in the nonfilling, intact canine heart (Yellin and Nikolic 1994).

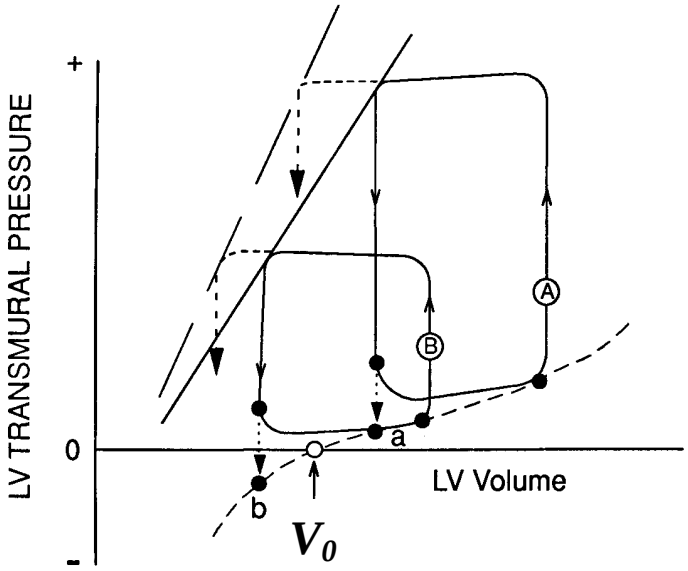

Figure 1.17: Concept of diastolic suction in the filling LV (Yellin and Nikolic 1994).

A more fundamental question is whether the contraction to below the equilibrium is necessary for an efficient filling of the LV or whether this potential help in filling is only of value during more demanding conditions (e.g. during exercise). Recently Verdonck et al. (Verdonck et al. 1999) and Vierendeels et al. (Vierendeels et al. 2000) demonstrated in a 1D and 3D numeric model of LV filling that a contraction to below the equilibrium volume V_0, including subsequent elastic recoil and suction, is not mandatory for obtaining normal LV filling patterns.

5. Congestive Heart Failure

5.1. Definition

Congestive heart failure (CHF), defined[5] as "*a pathophysiological state in which an abnormality of cardiac function is responsible for failure of the heart to pump blood at a rate commensurate with metabolic requirements or to do so only from an elevated filling pressure*" (Braunwald 1992, Coronel et al. 2001), is a chronic and progressive disease that affects millions of people (Mandinov et al. 2000). Its rapidly increasing prevalence is in part due to aging of the population and an improved survival rate in heart disease patients. Patients with a diagnosis of CHF have a grim prognosis. However, the natural history of the disease may be modified if the underlying cause can be determined and treated. The clinical syndrome of CHF occurs when cardiac dysfunction prevents adequate perfusion of peripheral tissue. Inadequate perfusion leads to stimulation of compensatory mechanisms, which are responsible for many of the clinical signs and symptoms of the condition.

5.2. Systolic and Diastolic Heart Failure

Initially the evaluation of myocardial performance and CHF was focused on the detection and evaluation of systolic heart failure (SHF). Systolic function was evaluated based on the assessment of filling pressure as a surrogate for LV volume. However, as early as in 1963, Braunwald and Ross highlighted the limitations of using LV filling pressure as an index of systolic dysfunction and speculated on the possible role of impaired relaxation and diastolic dysfunction (Braunwald and Ross 1963). Braunwald and Ross suggested that diastolic heart failure (DHF), i.e. CHF caused by abnormal diastolic function, may be far more common than previously recognized.

Figure 1.18 illustrates the differences in the pressure-volume loops for systolic and diastolic dysfunction. In systolic dysfunction, LV contractility is decreased and therefore the end-systolic pressure-volume relationship (ESPVR) is displaced

[5] Many attempts have been made to come up with a general set of criteria that describe heart failure. Because of the wide variability of the clinical symptoms and signs, and of their etiology's no general consensus exists. The Braunwald definition is a definition of heart failure from a clinical/pathophysiological viewpoint and is widely used in literature (Coronel et al. 2001).

downward and to the right. There is a diminished capacity to eject blood into a high pressure aorta. In diastolic dysfunction, the diastolic pressure-volume relation is displaced upward and to the left. There is diminished capacity to fill at low diastolic pressures.

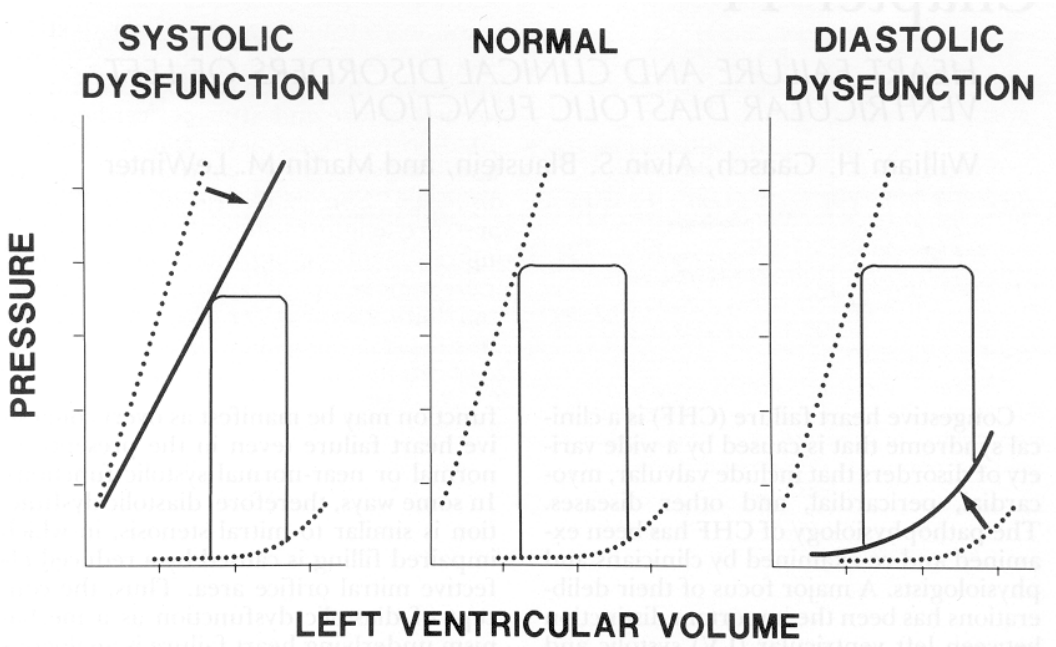

Figure 1.18: Pressure-volume loops; systolic dysfunction (**left**), normal (**middle**) and diastolic dysfunction (**right**) (Gaasch et al. 1994).

Figure 1.19 shows the possible changes in the LV pressure-volume loop caused by DHF in more detail. The diastolic pressure-volume relationship can be altered by an abnormal pressure decay during relaxation, pericardial constraint, increased chamber stiffness or LV dilatation.

5.3. Pathophysiology of Heart Failure

DHF is an insidious disease, accompanied by a series of compensatory changes that are beneficial in the short run but have long-term deleterious effects because long-term activation of the compensatory mechanisms disrupts the normal hemodynamic and neurohumoral balance, resulting in the progressive deterioration of cardiac function. Table 1.1 displays an overview of the most important variables interfering in diastolic function.

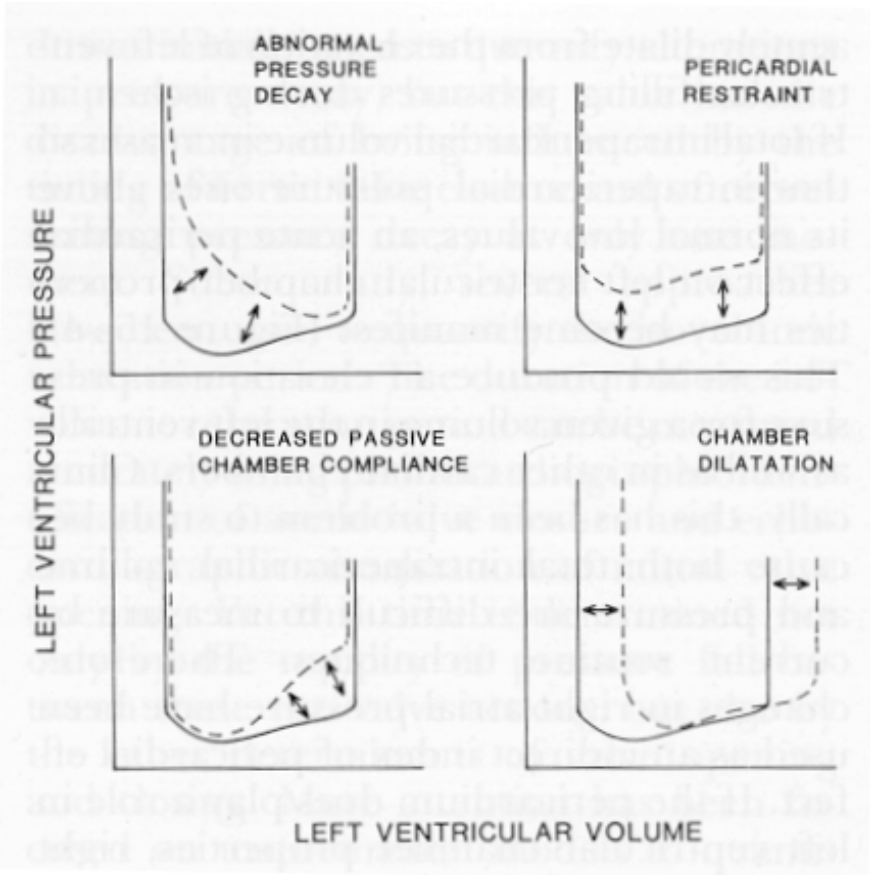

Figure 1.19: Possible changes in the pressure-volume-loop caused by diastolic dysfunction (full line is normal refernce case) (Gaasch et al. 1994).

Table 1.1: Interfering variables in diastolic function

Calcium flux
Heart rate
Asynchronous contraction-relaxation
LV chamber properties
LV muscle properties
Pericardial constraint
Ventricular interdependence
Coronary blood flow
Loading conditions
Hormonal influences

Abnormal calcium flux can cause variations in the onset, rate and extent of myocardial segmental lengthening, effecting ventricular heterogeneity. The rate of cross-bridge inactivation depends on the rate of calcium uptake by the sarcoplasmic reticulum (Apstein and Morgan 1994). This reuptake process is energy dependent and is therefore impaired by a reduction in intracellular ATP. This mechanism is likely to be responsible for delayed relaxation in the setting of myocardial ischemia.

As the heart rate increases, diastasis disappears, and ultimately early and atrial filling are fused. At higher heart rates, relaxation is progressively shortened, contractility improved, and LV end-diastolic pressure decreased (Lenihan 1995).

Normal diastolic filling is dependent on synchronized contraction and relaxation between LA and LV and within the LV itself. With LV hypertrophy loss of atrioventricular synchrony is commonly observed. Regional non-uniformity occurs in hypertrophic or infiltrative cardiomyopathies, or in myocardial infarction with scarring. Impaired ventricular activation, such as seen in patients with a bundle branch block or ventricular pacing, alters relaxation, thereby slowing the rate of early filling (Lenihan 1995).

LV chamber compliance has a major effect on indexes of diastolic filling. Certain passive structural elements such as increased cardiomyocyte size, increased wall thickness and increased collagen content can significantly alter the diastolic pressure-volume relationship. Extrinsic compression of the ventricle is an additional mechanism which results in diastolic dysfunction. Constrictive pericarditis is an encapsulation of the heart by the pericardium that has become fibrous and often calcified. Other external factors include interaction between the ventricles, pulmonary-cardiac contact pressure and engorgement of the coronary vasculature (Lenihan 1995).

Afterload induced changes in myocardial relaxation is a mechanism for diastolic dysfunction (Leite-Moreira et al. 1999).

The sympathetic nervous system plays an important role in modulating LV performance in patients with CHF, both due to systolic and diastolic dysfunction. Catecholamines have been demonstrated to improve contractility and to increase the rate of relaxation. β-adrenergic stimulation appears to improve cardiac

relaxation to a greater extent than it improves contraction. The renin-angiotensin system also plays an important role in diastolic LV filling and heart failure. By reducing afterload and augmenting cardiac output, angiotensin-converting-enzyme inhibitors (ACE) provide greater functional capacity. There is also evidence that local production of angiotensin II in the heart, may play an important role in hypertrophy and DHF (Lenihan 1995).

The underlying causes that lead to DHF can be subdivided into external (mechanical) factors to the myocardium on one hand, and factors intrinsic to the myocardium on the other hand. Insults to the myocardium, cardiomyopathies, involved in diastolic or combined systolic/diastolic dysfunction are (Lenihan 1995, Mandinov et al. 2000, Price and Wilson 1992): (1) congestive (dilated) cardiomyopathy, (2) hypertrophic cardiomyopathy, and (3) restrictive cardiomyopathy. Table 1.2 gives an overview of the corresponding change in cardiovascular characteristics.

Congestive Cardiomyopathy

Congestive cardiomyopathy is characterized by a grossly dilated and hypodynamic ventricle. There may be a lesser degree of myocardial hypertrophy.

Hypertrophic Cardiomyopathy

Hypertrophy is a compensating mechanism in which the diameter of cardiac muscle fibers increase by synthesis of new myofibrils. This process helps to sustain systolic function with pressure volume overload. However, the increase in cardiac mass and wall thickness greatly reduces the size of the LV cavity thereby producing negative effects on diastolic properties and creating ventricular filling impairment. Hypertrophy can be concentric or concentrated towards the upper portion of the intraventricular septum. From histological examination, cardiac myocytes show marked hypertrophy and a loss of the normal parallel arrangement. Interstitial fibrose is also seen with this pattern of fiber disarray.

Restrictive Cardiomyopathy

Restrictive cardiomyopathy usually does not include significant ventricular hypertrophy, but rather an abnormal stiffness of the muscle that impedes relaxation and diastolic filling. An amyloid intracellular infiltrate is the most

common cause of this restriction. The intrinsic myocardial stiffness can be increased by amyloidal infiltration, fibrosis, or myocardial ischemia.

Table 1.2: Cardiomyopathies in diastolic dysfunction

	Congestive	Hypertrophy	Restrictive
h	≈	↑	≈↓
V_{LV}	↑	↓	≈↓
V_{LA}	↑	↑	↑
$LV_{compliance}$	≈	↓	↓↓
$LV_{contractility}$	↓↓	↑	≈

h: LV wall thickness, V_{LV}: LV volume, V_{LA}: LA volume, $LV_{compliance}$: LV compliance, $LV_{contractility}$: LV contractility. ≈: unchanged, ↑ increased, ↓: decreased compared to normal reference case.

5.4. Prevalence of Congestive Heart Failure and Diastolic Heart Failure

Studies, conducted in Europe and the USA between 1953 and 1995, estimate the prevalence of heart failure between 3/1000 and 21/1000 (whole population) and 23/1000 and 130/1000 (persons > 65 years) (Murdoch and McMurray 1998). The National Heart, Lung and Blood Institutes estimates that more than 4.8 million Americans are afflicted with heart failure, with 400,000 new cases and 875,000 hospitalizations occurring each year. There are between 200,000 to 400,000 deaths annually attributed to heart failure (Kannel 1999).

In addition to the cost of human life, heart failure poses a tremendous financial burden on the health care system. In developed countries, total expenditure on CHF ranges between 1% and 2% of the total healthcare budget. Annual cost of CHF per patient is related to the New York Heart Association (NYHA) class of disease severity and the country. In Europe, figures range from 318 € (NYHA class I-II, the Netherlands) up to 24,790 € (NYHA class IV, Belgium) (Berry et al. 2001). In the USA CHF accounted for annual expenditures exceeding $4.7 billion. It has been estimated that by the year 2030, the number of persons over 65 will exceed those under 65 and that 2.6 million people will be treated for heart failure in the USA (Kannel 1999).

Whereas in the past CHF has been almost synonymous with LV systolic heart failure, it has become apparent in the last two decades that in up to 40% of the patients systole is normal and diastole abnormal (Mandinov et al. 2000). In several studies of CHF, the prevalence of isolated diastolic dysfunction ranged from 13% to 75% (Lenihan 1995, MacFadyen et al. 2001, Rusconi et al. 1998, Shintani and Glantz 1994, Vasan et al. 1995, Vasan et al. 1999). The average incidence was 8% for subjects younger than 65 and 32% for those older than 65.

Patients with isolated diastolic heart failure have a fourfold mortality risk compared with control subjects who are free of CHF (Lenihan 1995, Mosterd et al. 1999, Senni et al. 1998, Vasan et al. 1999). Most studies report an annual mortality rate for DHF of about 8%, indicating that DHF is more benign than other forms of CHF with an annual mortality of about 19% (Vasan et al. 1995). In contrast, a study of Senni et al. (Senni et al. 1998) shows SHF and DHF having both a similar prognosis, at least over the first three to four years of follow-up. Because of the aging Western population, the proportion of CHF due to isolated diastolic dysfunction seems destined to increase. Moreover, in patients with chronic heart failure that is a result of systolic dysfunction, it is the increase in LV filling pressure that correlates most closely with the degree of exercise limitation, independently of the severity of systolic dysfunction (Miyashita et al. 2001).

6. Guidelines for the Diagnosis of Primary Diastolic Heart Failure

6.1. Primary Diastolic Heart Failure: A Definition

Numerous clinical trials have examined and defined appropriate therapy for the treatment of SHF. In contrast, the optimal treatment for DHF has not yet been determined because appropriate clinical trials await the development of rigorous and widely acceptable entry criteria to define the study population. In an attempt to point out guidelines for the diagnosis of DHF and to catalyze research on diastolic dysfunction, the European Working Group on Diastolic Heart Failure formulated a definition for DHF (European Study Group on Diastolic Heart Failure 1998). In this definition three obligatory conditions have to be simultaneously fulfilled for a diagnosis of primary DHF:

(1) presence of signs of CHF,

(2) presence of normal or only mildly abnormal LV systolic function,

(3) evidence of abnormal LV relaxation, filling, diastolic distensibility or diastolic stiffness.

Nonetheless important efforts have been made to understand the mechanisms of DHF and several non-invasive methods are proposed for the evaluation of DHF (cf. infra: Chapter 3 and 4), no overall accepted non-invasive univocal criteria are at this time available and integrated in routine clinical practice. Therefore condition (3) hampers the clinical applicability of the definition.

6.2. Classification Based on Diagnostic Certainty

Vasan and Levy (Vasan and Levy 2000) refined the definition of the European working group in their “call for standardized diagnostic criteria”. A cornerstone of their definition includes the principle that the only definitive objective evidence of diastolic dysfunction requires cardiac catheterization, which is not always feasible in all CHF subjects. The noninvasive assessment of diastolic dysfunction was considered being too complex and imprecise.

For the diagnosis and classification of diastolic heart failure, Vasan and Levy turned the three levels as proposed by the European working group into three

hierarchical levels via three tables with hierarchical conditions. The classification is applicable to patients who do not have CHF attributable to valvular heart disease, cor pulmonale, or a primary volume overload state. In order to get more insight into the decision system behind the tables of Vasan and Levy, the according decision three is constructed (Figure 1.20).

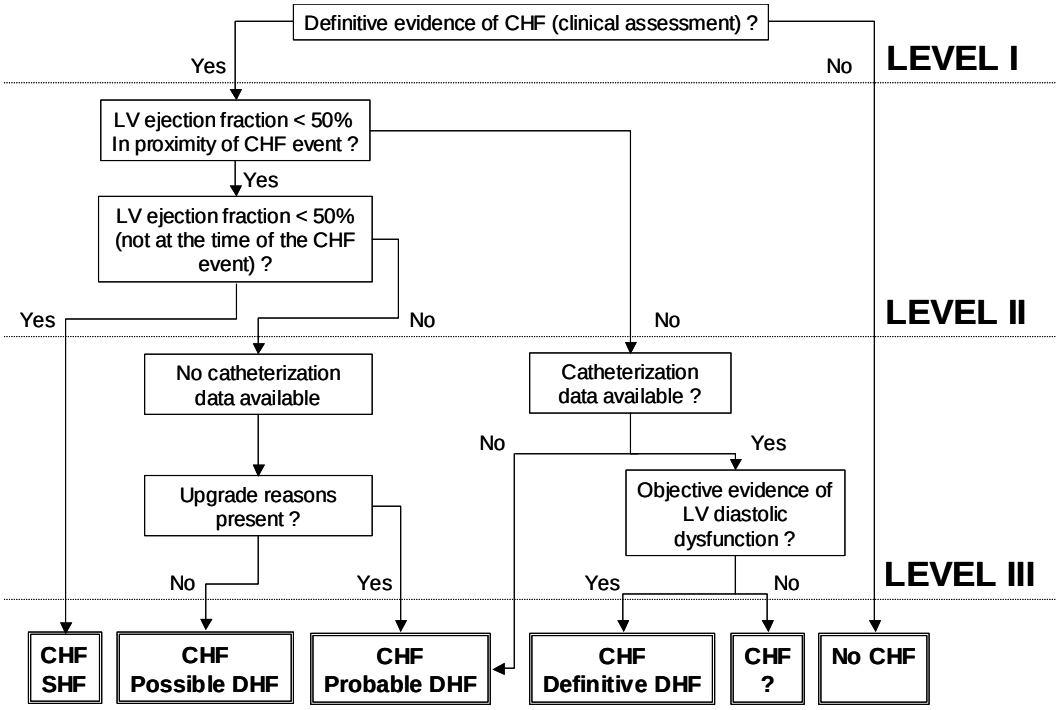

Figure 1.20: Diagnosis of diastolic dysfunction: decision tree

Level One

On the first level the clinical diagnosis of CHF is made. It is emphasized that in this stage, the lack of systolic dysfunction has not to be taken into account for rejecting CHF. It is well established that the signs and symptoms of CHF poorly correlate with LV ejection fraction. Therefore, rejecting CHF on the basis of a normal ejection fraction can result in a significant underestimation of DHF.

Level Two

On a second level the diagnosis of SHF is considered. A cut-off value for the ejection fraction of 50% is considered a limit for SHF. The definitive diagnosis of

SHF is made for patients with non-transient systolic dysfunction, i.e. for patients with an ejection fraction below 50%, not at the time of heart failure.

Level Three

On a third level the diagnosis of DHF is considered. The classification criteria for diastolic dysfunction are based on the degree of diagnostic certainty and result in three categories: possible, probable and definitive DHF. Note that diagnosis of definitive DHF is only possible if cardiac catheterization information is present. Because Vasan and Levy exclude the possibility of disposal of cardiac catheterization information in patients with transient systolic dysfunction, diagnosis of definite DHF in patients with transient systolic dysfunction is not possible. Instead, Vasan and Levy consider patients with transient systolic dysfunction having possible DHF or having probable DHF if some "upgrade" reasons exist. Valid evidence for the upgrading from possible to probable DHF is summarized in table 1.3.

Table 1.3: Reasons to upgrade diagnosis from possible DHF to probable DHF

1. Markedly elevated blood pressure during the episode of HF (SBP > 160 mmHg or DBP > 100 mmHg)
2. Echocardiographic concentric hypertrophy without wall-motion abnormalities
3. A tachyarrhytmia with shortened diastolic filling period
4. Precipitation of event by the infusion of a small amount of intravenous fluid
5. Clinical improvement in response to therapy directed at the cause of diastolic dysfunction (such as lowering blood pressure, reducing heart rate, or restoring the atrial booster mechanism)

For patients with no SHF at the time of the cardiac event, Vasan and Levy did integrate the possibility of having cardiac catheterization information, which allows a diagnosis of definite DHF. Patients with no SHF at the time of the cardiac event, but who did not underwent cardiac catheterization are classified in the category having "probable" DHF.

6.3. DISCUSSION

The decision system as described by Vasan and Levy leaves some openings for discussion.

A situation of combined systolic and diastolic dysfunction is not considered. In the hierarchical decision tree, systolic dysfunction in proximity of the CHF event is always “overruling” diastolic dysfunction. Also, because of the hierarchical structure, a problem arises in the specific situation of definitive evidence of CHF on level I, no systolic dysfunction in proximity of the CHF event on level II, and catheterization results that does not support evidence for DHF on level III (i.e.: after the diagnosis of CHF, objective evidence for systolic and diastolic dysfunction is rejected). In this particular case, either the diagnosis of CHF at the first level should be questioned or some more detailed information (e.g. using echocardiography) should be considered to check the invasive findings.

The Vasan and Levy approach for classification of diastolic dysfunction, because considered too complex and imprecise, does not consider the noninvasive evaluation of diastolic dysfunction using Doppler echocardiography. Neglecting Doppler ultrasound seems fair in large clinical trials because the noninvasive diagnosis of diastolic function using Doppler techniques is not yet integrated in the routine procedures of most echocardiography laboratories. On the other hand, the availability of invasive information is also doubtable. In the long term the integration of noninvasive criteria will be mandatory.

7. Conclusion

In this introductory chapter, the anatomy and physiology of the normal heart are introduced, next to some control mechanisms of cardiac function. The function of the heart is to maintain a cardiac output that meet the needs of the metabolism. In this context, LV performance has to be seen as the result of two independent but interrelated functions: systolic and diastolic function. The first is defined as the capacity of the LV to contract and eject the stroke volume at the high pressures in the aorta. The second is defined as the capacity of the LV to relax and then to accept the stroke volume at the low pressures existing in LA. Intrinsic control mechanisms are interfering in both systolic (e.g. Starlings Law) and diastolic function (e.g. concept of diastolic suction).

Also, the mechanisms, prevalence and diagnosis of congestive heart failure in general and diastolic heart failure in particular are explained. Congestive heart failure is the leading reason for hospitalization in Europe and the US for patients older than 65 years. It is also the most expensive condition to treat. Up to 40% of patients with congestive heart failure have isolated diastolic dysfunction. Patients who meet the definition of CHF are a heterogeneous group and have diverse reasons for the occurrence of elevated filling pressure and/or low cardiac output. Further stratification of CHF subjects into those with LV systolic dysfunction and those with predominantly LV diastolic dysfunction is important because of therapeutic and prognostic differences between the two subsets of CHF patients.

Whereas criteria for systolic function are easily obtained, objective evidence of diastolic dysfunction is more difficult to obtain. The lack of a general accepted adequate diagnostic methodology for qualifying diastolic dysfunction confuses clinicians and feeds the still ongoing controversy about the existence and importance of diastolic dysfunction.

In the long term the integration of non-invasive criteria is mandatory to omit invasive procedures as the definite tool for diagnosis of DHF. Ongoing research has already contributed significantly to development of (non-)invasive diagnostic tools for DHF. The current status of the emerging field of diastologie is reviewed in Chapters 3 and 4. In chapter 2 first the principles and technical aspects of some cardiac measurement techniques are described.

CHAPTER 2

Cardiac Measurements: Principles and Technical Background

1. Introduction

In this chapter the reader is introduced to principles and technical background of three cardiac measurement techniques, appearing in this work: cardiac catheterization for direct invasive pressure measurement and two cardiac imaging techniques, (Doppler) echocardiography and single photon emission computed tomography (SPECT).

2. Cardiac Catheterization

2.1. Catheterization

Cardiac catheterization is the standard technique for direct measurement of filling pressures. Two general approaches to the heart are currently used: right-sided heart catheterization and left-sided heart catheterization. Besides measurement of pressures in chambers and vessels, cardiac catheterization allows for several other examinations and interventions, including sampling of the oxygen content, opafication of the cardiac chambers and/or coronary arteries with contrast material, and determination of cardiac output. Normal pressures, pressure waveforms and oxygen content are illustrated in figure 2.1.

2.2. Left-Sided Heart Catheterization

Left-sided heart catheterization involves the retrograde passage of the catheter through the arterial system to the aorta, across the aortic valve, and into the LV. The catheter is commonly inserted in either the brachial or femoral artery. While retrograde measurements of LV pressure can be made by passing the catheter across the aortic valve, retrograde passage of the catheter across the mitral valve is very difficult. To avoid the risks and difficulties, involved in passing the mitral valve, LA pressure is estimated based on LV pressure tracings. As the ventricles fill during diastole, the atrial and ventricular chambers are in direct communication. At the end of diastole the pressures between these two chambers have equilibrated. Consequently, at the end of diastole atrial pressures are equal to ventricular pressures.

2.3. Right-Sided Heart Catheterization

Pulmonary capillary wedge pressure (PCWP), obtained with right-sided heart catheterization (Figure 2.2), is often taken as a surrogate for LV filling pressure.

PCWP is measured with a ballonn-tipped catheter. Periodically the ballon is inflated. With inflation of the balloon, blood flow propels the catheter distally into the pulmonary vasculature until the tip wedges in a small arterial branch. This wedge position is referred to as the pulmonary capilary position. In this position, the pressure transmitted backward from the left side of the heart through the

pulmonary vasculature is sensed by the catheter tip, neglecting the lung resistance. Therefore, the PCWP reflects LA pressure and, consequently, LVEDP.

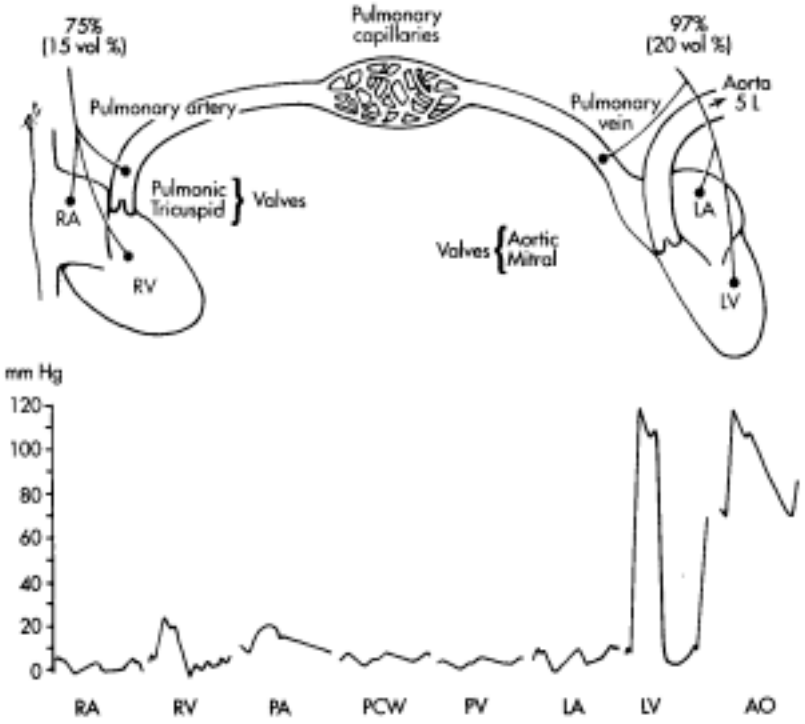

Figure 2.1: Normal pressures, pressure waveforms and oxygen content obtained using catheterization (Price and Wilson 1992).

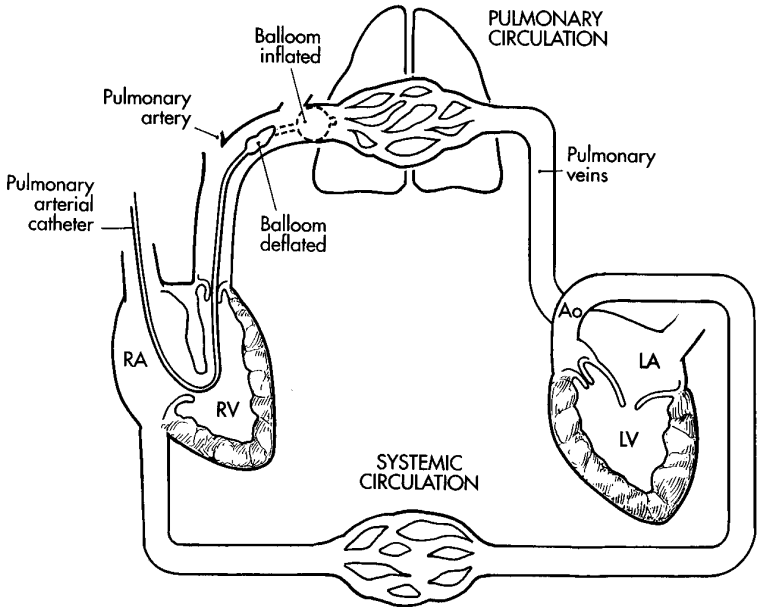

Figure 2.2: Schematic view of right-sided heart catheterization (Price and Wilson 1992).

3. Echocardiography

3.1. INTRODUCTION

The principal aspects of diastolic function, LV stifness and LV relaxation include pressure in their formal definition: stiffness is related to the local slope of the ventricular pressure-volume curve, whereas relaxation is characterized by the exponential time constant τ of the pressure decay during isovolumic relaxation. However, hemodynamic measurements are impractical in most patients and unsuitable for bedside or serial evaluation, and therefore noninvasive methods required development. At first accomplished by radionucleide methods (Udelson and Bonow 1994), the study of LV filling by echo-Doppler technique emerged, in the last 10 years, as the best method for noninvasive evaluation of LV diastolic function in the clinical setting (Thomas 1994). Clinical ultrasound combines structural imaging with blood flow information obtained using the Doppler principle. It provides safe, noninvasive assessment of cardiac structure and function with a portability and cost-effectiveness unrivaled by competing methodologies.

3.2. MEDICAL ULTRASOUND

Ultrasound waves are mechanical waves with frequencies above the audible range, i.e. $f_0 > 20$kHz. In medical ultrasound applications such as imaging and blood flow measurements, the employed frequencies comprise the range from about 1 to 20 Mhz (Evans et al. 1989).

The ultrasound waves originate from a transducer. An ultrasound transducer generates acoustic waves by converting magnetic, thermal, or electrical energy into mechanical energy. The most efficient technique for medical ultrasound uses the piezoelectric effect, which was first demonstrated in 1880 by Jacques and Pierre Curie[6, 7]. They applied a stress to a quartz crystal and detected an electrical potential across opposite faces of the material. The Curies also discovered the inverse piezoelectric effect by applying an electric field across the crystal to

[6] Curie P, Curie J. 1880. Developpement par pression de l'électricité polaire dans les cristeaux hémiédres a faces enclinées. Comp Rend 91 :383.
[7] Curie, Pierre (1859-1906). French physician and Nobel laureate.

induce a mechanical deformation. In this manner, a piezoelectric transducer converts an oscillating electric signal into an acoustic wave, and vice versa.

Doppler and imaging techniques consist of illuminating the objects of interest by a beam of ultrasound and by analyzing the energy received from its interaction, i.e. reflection, absorption, or scattering with these objects. Objects much smaller than a wavelength cause Rayleigh[8] scattering: a portion of the energy is scattered uniformly in all directions. If an object is much larger than a wavelength, it becomes a specular reflector: it acts much like a mirror. Specular reflections that return to the transducer may be a factor of 10^3 below the intensity of the transmitted signal. Backscattered ultrasound on red blood cells (Rayleigh scatter generally much weaker than the specular reflections from adjacent tissue interfaces. Figure 2.3 shows a commercial echocardiography machine (Vingmed 700CFM, General Electric).

3.3. IMAGING PROCEDURES

Ultrasonic waves, applied to the chest wall and directed at the heart, are reflected back to the transducer whenever the beam crosses a boundary between tissues of different densities or acoustic impedances. The mechanical energy from these reflected sound waves, or cardiac “echoes”, is converted to electrical energy by the transducer and displayed in the form of a cardiac image.

Two-dimensional echocardiography generates a cross-sectional image as illustrated shematically in figure 2.4 (left panel). M-mode echocardiography generates lines of information that displays the motion of reflecting objects along a single scanline over time (Figure 2.4 (right panel)). M-mode therefore provides the maximum degree of temporal resolution.

M-mode echocardiography is of particular value for evaluation of regional abnormalities, such as the mitral valve leaflet motion characteristics.

[8] Rayleigh, John William Strutt, 3rd Baron (1842-1919). British mathematician, physicist, and Nobel laureate.

Figure 2.3: Clinical Echocardiography machine.

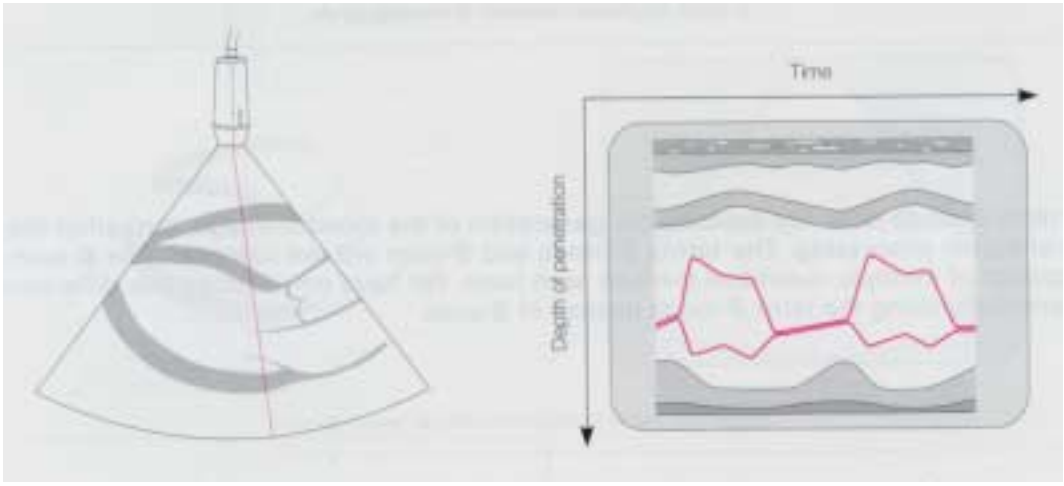

Figure 2.4: 2D echocardiography parasternal longaxis view **(Left panel)** and corresponding M-mode image showing the movement of the mitral leaflets **(Right panel)** (Schmailz and Ormerod 1998).

3.4. DOPPLER ECHOCARDIOGRAPHY

3.4.1. Doppler Principle

The principle that the perceived frequency of a traveling wave is altered by motion of the source, the receiver, or both, was first enunciated by the Austrian mathematician and physicist Christian Johann Doppler (Figure 2.5). The elementary formula for motion of source or observer first appear in his classic article "Über das farbige Licht der Doppelsterne und einiger anderer Gestirne des Himmels", published in 1842[9].

Figure 2.5: Doppler, Johann Christian (1803-1853)
Austrian mathematician and physicist.

Under the assumption of a stationary sound source of frequency f_0, a receiver moving towards the sound source perceives a frequency f_R, which is given by

$$f_R = f_0 + \frac{v}{c} \times f_0 \qquad \text{[Eq. 2.1]}$$

where v denotes the velocity at which the receiver moves and c the speed of sound. If the receiver moves away from the sound source, equation 2.1 still holds, but this motion corresponds to a negative velocity.

On the other hand, if the receiver is stationary and the sound source moves towards the receiver, the latter experiences the frequency

[9] Doppler, J. 1842. Ueber das farbige Licht der Dopplesterne und einiger anderer Gestirne des Himmels. Abhandlungen der Konigl. Bohmischen Gesellschaft der Wissenschaften 2: p. 465.

$$f_R = \frac{c}{c - v} \times f_0 \qquad \text{[Eq. 2.2]}$$

In the case of a sound wave reflected by a moving object, the perceived frequency f_R with respect to the transmitted frequency f_0 is obtained by combining equation 2.1 and equation 2.2, since the reflector acts as both a receiver and a transmitter

$$f_R = \frac{c + v}{c - v} \times f_0 \qquad \text{[Eq. 2.3]}$$

The Doppler frequency f_D is defined as the difference between f_R and f_0. Thus, the Doppler frequency caused by a moving reflector is given by

$$f_D = f_R - f_0 = \frac{2v}{(c - v)} \times f_0 \qquad \text{[Eq. 2.4]}$$

In medical applications, the velocity *v* is much smaller than the sound speed ($|v| \approx$ 0-5 m/s, $c \approx 1540$ m/s) and equation 2.4 simplifies to

$$f_D = \frac{2v}{c} \times f_0 \qquad \text{[Eq. 2.5]}$$

The Doppler frequency is not only proportional to the velocity, but also to the transmitted frequency, i.e., different Doppler frequencies are obtained, when the moving reflector is insonified with different frequencies f_0.

It is also important to note that the receiver experiences only a Doppler frequency shift according to equation 2.5, if the reflector is moving along the transmitted wave direction. For any other angle formed between the transmitter/receiver and the reflector's motion direction, the former perceives only the Doppler frequency shift corresponding to the vector component being parallel to the transmitted wave direction (Figure 2.6). Thus, equation 2.5 must be scaled by $\cos\theta$

$$f_D = \frac{2v}{c} \cos\theta \times f_0 \qquad \text{[Eq. 2.6]}$$

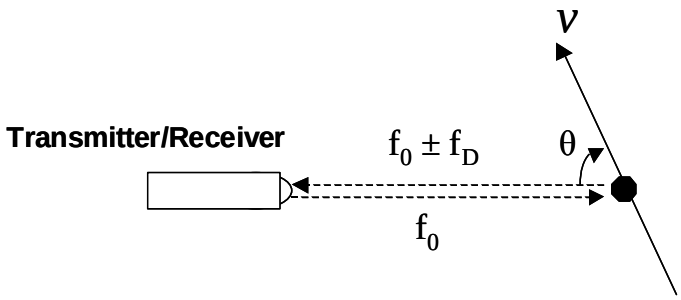

Figure 2.6: The Doppler frequency shift is proportional to the reflector's velocity component that is parallel to the transmitted wave direction.

3.4.2. Doppler Signal

Johann Christian Doppler correctly suggested that his principle would apply to any wave motion including light. Doppler-shifted frequencies originating from backscattered ultrasound on red blood cells are only a small component of the total ultrasonic energy returning to the transducer. Research of McLeod (McLeod 1974) resulted in equation 2.7 for the signal-to-noise ratio of the Doppler signal

$$\frac{S}{N} \propto \frac{V_v}{V_b} \cdot \frac{\theta \times e^{-2\alpha r}}{r^2 \times n} \cdot \frac{P_a}{BW} \qquad \text{[Eq. 2.7]}$$

where V_v/V_b is the ratio of the volume of the vessel lumen (V_v) or flow stream falling within the sample volume to the total sample volume (V_b), θ is the scattering cross section, e is Euler's[10] constant of exponential growth or decay (e = 2.7183), α is the tissue absorption coefficient, r is the range from the target to the transducer, n is the electronic device noise, BW is the system bandwidth, and P_a is the average emission power.

From equation 2.7 it can be noticed that several factors have an influence on the strength of the signal. V_v/V_b can be interpreted as the ratio of the signal-producing volume to the beam sample volume. The negative exponential term in the numerator is the signal attenuation term. This term consists of a tissue absorption coefficient (α) and the range (r), doubled to reflect the round trip, direct line

[10] Euler, Leonhard (1707-1783). Swiss mathematician.

passage of the sound wave from the transducer to the target. Other terms that influence the signal strength are the scattering cross section (θ) and the average input power (P_a). The noise terms in the denominator of equation 2.7 represent the factors that decrease the ability to recognize the Doppler-shifted frequencies either by introducing extraneous frequencies or by decreasing the strength of the reflected signal that actually reaches the transducer. The squared range (r^2) reflects the hemispheric reflective pattern of the scattered energy. The electronic noise (n) is inherent to all high gain amplifiers. The last noise term is signal bandwidth (BW). Because frequency resolution is related to bandwidth, any increase in bandwidth is effectively an increase in noise.

3.4.3. Doppler Modes

Introduction

The use of the Doppler frequency shift of backscattered ultrasound as a non-invasive means to evaluate blood flow was for the first time described in the late 1950's (Satomora 1959). Applications were introduced in clinical practice during the next decade. In this period the continuous and pulsed wave Doppler systems were developed, allowing the quantitative and qualitative examination of valvular stenosis and regurgitation. Later, the pulsed Doppler system is extended to obtain velocity estimates at multiple range gates, resulting in color Doppler echocardiography that provides a spatial map of the blood velocity component towards the transducer along a sector of scanlines (Hatle and Angelsen 1985, Weymann 1994).

Figure 2.7 illustrates the different Doppler modes. With Continuous wave Doppler (CWD), the velocity is measured from the complete ultrasound beam with no spatial resolution. Velocity data can be obtained from a single chosen sample depth with the pulsed wave Doppler mode (PWD). In the color M-mode Doppler mode (CMD), the PWD mode is extended to several locations along the ultrasound beam. Finally, by sweeping the beam, the velocity can be measured over a complete sector (2D).

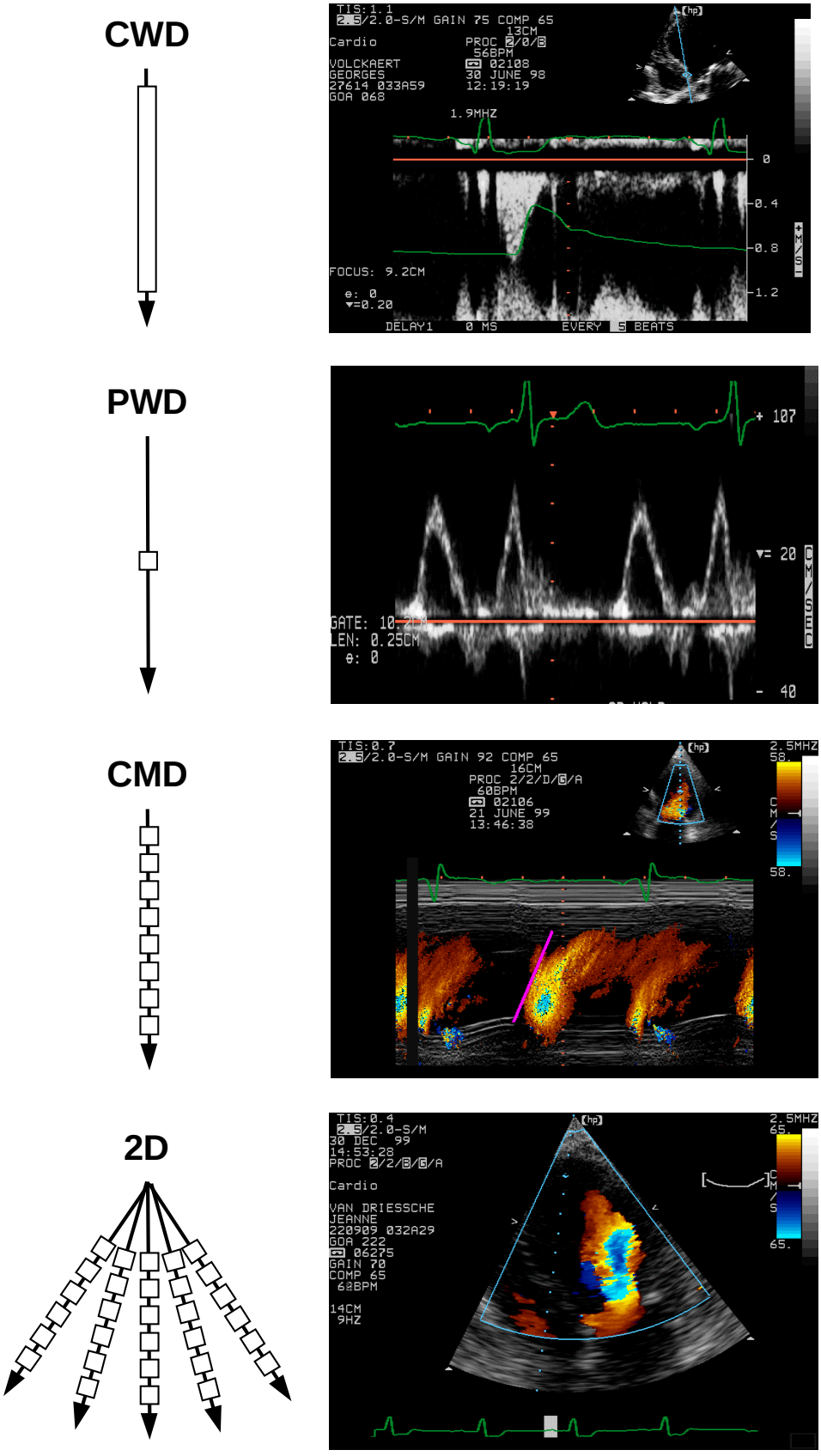

Figure 2.7: Doppler echocardiographic modes. **Left side:** position of the sample volume(s); Continuous wave Doppler **(CWD)** of aortic valve flow, Pulsed wave Doppler **(PWD)** of mitral valve flow, Color M-mode Doppler **(CMD)** of LV filling, and Two-dimensional color Doppler **(2D)** of LV filling. **Right side:** Resulting images. CWD and PWD: time variation of velocitys in one sample volume. CMD and 2D: spatial distribution and time variation of velocities encoded in colors.

Continuous Wave Doppler

Continuous wave Doppler systems utilize a pair of piezoelectric elements to transmit and receive ultrasonic energy waves simultaneously. The transmitting transducer is continuously excited by the transmitting amplifier, which operates at a constant carrier-frequency f_0. The receiving transducer captures the echoes from stationary, quasi-stationary, and moving objects. According to equation 2.4, the desired Doppler information must be extracted from the received signal. The most common technique to achieve this is to pass the received signal through an IQ (in-phase and quadrature-phase) detector, as shown in figure 2.8.

This demodulating scheme consists of multiplying the received echo $x(t) = \cos(\omega_0 + \omega_d)t$ by a pair of sinusoids at the transmit frequency (ω_0) that are 90 degrees out of phase with each other ($\cos \omega_0 t$ and $\sin \omega_0 t$). The resulting signals are low-pass filtered to obtain $I(t) = \cos \omega_d t$ and $Q(t) = \sin \omega_d t$. The magnitude and the phase of the Doppler shift can be determined from the quadrature components, I(t) and Q(t). The demodulated components can be combined to form a complex Doppler signal Z as shown in equation 2.8

$$Z(t) = I(t) + jQ(t) \qquad \text{[Eq. 2.8]}$$

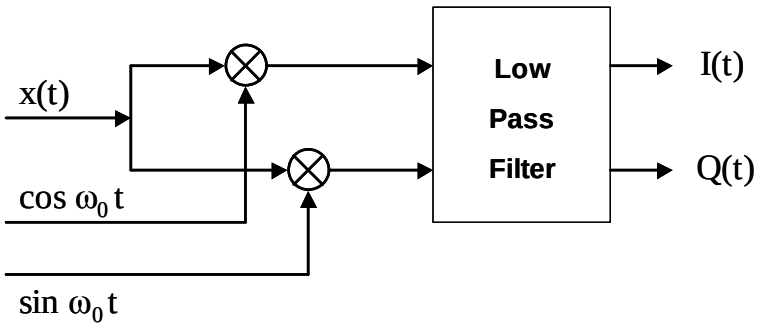

Figure 2.8: Quadrature demodulation diagram.

A time-frequency analysis of the complex Doppler signal is performed to examine changes in the flow velocity as a function of time. A short-time Fourier transform (STFT) is generally employed to create a spectral Doppler image. The STFT first divides the signal into overlapping segments and performs a Fourier transform of

each segment. The frequency (or velocity) and temporal resolution are controlled by the choice of the segment length and the overlap between the segments.

Doppler-shifted frequencies obtained from moving blood cells occur in the audible range. Normal blood flows causes Doppler frequencies in the 0-5 kHz range, whereas jets in stenotic vessel segments or from malfunctioning heart valves may cover the 5-20 kHz range. The result, however, does not only contain the desired Doppler information from blood, but also those from heart and vessel wall movements, typically in the 0-1200 Hz range. Those frequencies must be filtered out by a tunable high-pass filter, the so-called “Wall Motion Filter”, since their amplitudes are typically 40-100 dB higher than those from blood cells (Garcia et al. 1998, Isaaz et al. 1989).

Pulsed Wave Doppler

While continuous wave Doppler has several strenghts, including the ability to examine high velocity flows and determine the maximum velocity along the ultrasonic beam, its major weakness is the inability to localise velocities along this same path. This weakness can be partially overcome by pulsed-wave systems as introduced in the late 1960s by Peronneau, Wells, and Baker (Baker 1978, Peronneau 1970, Wells 1977). Transmission of a series of ultrasonic pulses, as opposed to a continuous wave, allow the user to define a range or depth of interrogation. The range specification allows the system to calculate the time required for each pulse to reach the desired depth and the reflected signal to return to the receiver. Analysis of the phase shift between transmitted and time-gated received signal, due to the movement of the ultrasound scatters, such as red blood cells, allows the estimation of blood velocity.

Ultrasound bursts are transmitted repeatedly with a pulse repetition frequency PRF. The maximum PRF is limited by the range of the target, r, and the speed of sound, c, as shown in equation 2.9

$$PRF_{max} = \frac{c}{2r} \qquad \text{[Eq. 2.9]}$$

For example, the examination of a target at 10 cm requires a time-of-flight equal to 2r/c, or approximately 130 μs. The number of pulses that can be transmitted to make a velocity estimate from a single sample volume, or range gate, is limited by

the duration in which the flow through the sample volume is considered stationary.

The time of flight for a burst to travel in parallel to the ultrasound beam towards a sample volume at distance x and back to the transducer is given by

$$t_f = \frac{2x}{c} \qquad \text{[Eq. 2.10]}$$

Thus, the phase difference between the transmitted wave (reference wave) and the received echo is given by

$$\phi = 2\pi \cdot f_0 \cdot t_f = 2\pi \cdot f_0 \cdot \frac{2x}{c} \qquad \text{[Eq. 2.11]}$$

By definition, the frequency of a signal is the derivation of its phase with respect to time

$$\frac{1}{2\pi} \cdot \frac{d\phi}{dt} = 2 \cdot f_0 \cdot \frac{1}{c} \cdot \frac{dx}{dt} \qquad \text{[Eq. 2.12]}$$

Since dx/dt corresponds to the projected velocity $v \cdot \cos\theta$, equation 2.12 represents the Doppler frequency or

$$f_D = 2 \cdot f_0 \cdot \frac{v}{c} \cdot \cos\theta \qquad \text{[Eq. 2.13]}$$

From this equation it can be noticed that, although generally called a Doppler system, the pulsed wave system does not measure a frequency shift. The system detects the displacement in the reflected signal that is acquired for a set of transmitted pulses.

The returning echo, or backscattered signal, is analysed for a specific interval following the time-of-flight for each pulse. The finite duration of the pulse, typically three to six cycles of the transmit frequency, results in a measurement derived from a range interval as opposed to an idealized point location. The duration of a three cycle pulse at f_0 = 2 MHz is 1.5 μs which corresponds to an axial measurement length of approximately 1.2 mm.

The tradeoff between temporal and velocity resolution is similar to the case for continuous wave Doppler analysis. Continuing the earlier example of velocity estimation at 10 cm, a series of 64 pulses can be transmitted and received in

approximately 8.8 ms. This results in a temporal resolution of aproximately 10 ms and a frequency resolution of aproximately 120 Hz. This frequency resolution is equivalent to a velocity resolution of approximately 4.7 cm/s. The temporal resolution can be increased to approximately 5 ms using a series of 32 pulses, however, the velocity resolution decreases to approximately 9.4 cm/s.

The gating of the echoes at a fixed time after the burst is transmitted implies the sampling of the received signal. Therefore, from Shannon's sampling theorem, the PRF must be twice as much as the maximum frequency shift to be detected. Hence, the maximum unambiguously measurable velocity, the so-called Nyquist velocity, yields

$$v_{max} = v_{Nyq} = \frac{c}{2 \cdot f_0 \cdot \cos\theta} \cdot \frac{PRF}{2} \qquad \text{[Eq. 2.14]}$$

As the velocity exceeds the interval [$-v_{Nyq}$, v_{Nyq}], the Doppler frequency wraps around and becomes ambiguous. Filling in equation 2.9 in equation 2.14 reveals an additional tradeoff between velocity and spatial resolution imposed by the pulsed-wave system.

Tissue Doppler echocardiography

Pulsed Doppler echocardiography has been traditionally applied for the measurement of red blood cells velocities across intravascular structures. However, the acquisition of tissue velocities only requires two relatively simple alterations in the standard pulsed Doppler signal processing: bypassing of the high pass filter and lowering of the gain amplification to eliminate the weaker intensity blood flow signals (Isaaz et al. 1989).

Color Doppler Echocardiography

Color Doppler echocardiography provides a spatial map of the blood velocity component directed towards the transducer throughout a region of interrogation within the heart or blood vessels. The ability to measure multiple velocities along the ultrasound beam path is possible if the PRF is set for the maximum depth desired and the reflected echo signal is gated into multiple intervals representing a set of spatial locations. The extension of this approach to estimate a two dimensional velocity maps requires repositioning of the ultrasound beam and repeated interrogation along adjacent paths (N) through the region of interest. The

additional desire to display this velocity map as a function of time requires repetition of the entire process to achieve an acceptable temporal resolution. The temporal resolution (*T*) is generally described as the number of 2D velocity maps, or frames that are displayed per second (F). The tradeoff in the allocation of pulses (k) is shown in equation 2.15

$$k \cdot N \cdot F = \frac{1}{T} = PRF \qquad \text{[Eq. 2.15]}$$

The total number of pulses available, the PRF, can be divided among the frame rate (F), the number of scan lines (N), and the number of pulses per scanline (k). Each of the variables in equation 2.15 effect the temporal, spatial, and velocity resolution. From the previous example with a maximum range of 10 cm, the 7700 pulses per second can theoretically be allocated to obtain a sector map using 64 scanlines per frame (N) and a packet size of 8 pulses per scanline (k). This would permit the interrogation of 15 frames per second (F).

With only eight samples, the classical Fourier approach used in pulsed Doppler and continuous Doppler result in a poor estimate of the mean velocity. Various techniques have been investigated to provide more accurate velocity estimates. The autocorrelation method is the commonly used method in which each echo is correlated with the corresponding one from a previous pulse. This determines the motion that has occurred during each pulse period. The autocorrelation algorithm is a frequency domain estimation approach and was implemented for cardiac application by Kasai et al. in 1985 (Kasai 1985). The technique was used as early as 1965 in other fields and identified as the optimal unbiased estimator for meteorological radar applications. The estimated mean velocity is proportional to the mean frequency of the Doppler signal.

While tradeoffs of velocity and spatial resolution are similar to pulsed Doppler interrogation, color Doppler mapping is further complicated by the desire for resolution in both spatial directions as well as in time.

Color M-mode Doppler Echocardiography

M-mode echocardiography allows visualization of cardiac structures along a selected scanline. The combination of this imaging modality and Doppler processing was introduced in 1981 by Eyer (Eyer et al. 1981). The temporal

resolution of velocity estimates can be greatly increased to 150 samples per second when the scan line is fixed (N = 1). An additional increase in the packet size (k), or number of pulses per sample, is also possible from approximately 8 to greater than 50, significantly increasing velocity resolution.

4. Single Photon Emission Computed Tomography

4.1. Introduction

Single-photon emission computed tomography (SPECT) acquires information on the concentration of radionuclides introduced into the patient's body. SPECT dates from the early 1960's, when the idea of emission traverse section tomography was introduced by D.E. Kuhl and R.Q. Edwards prior to either positron emission tomography (PET), X-ray computed tomography (X-ray CT), or magnetic resonance imaging (MRI) (Price and Wilson 1992, Tsui).

4.2. Theory and Instrumentation

As in X-ray CT, SPECT imaging involves the rotation of a photon detector array around the body to acquire data from multiple angles. Using this technique, the position and concentration of radionuclide distribution is analysed. Because the emission sources (injected radionuclides) are inside the body cavity, this task is far more difficult than for X-ray CT, where the source position and strength (outside the body) are known at all times. That is, in X-ray CT the attenuation is measured, not the transmission source. To compensate for the attenuation experienced by emission photons from injected tracers in the body, contemporary SPECT machines use mathmatical reconstruction algorithms to increase resolution.

Different radionuclides are used for SPECT imaging that emit a single photon (usually about 140keV), rather than positron emission (resulting in two high energy 511 keV photons) as in PET. Because only a single photon is emitted from the radionuclides used for SPECT, a special lens known as a collimator is used to acquire the image data from multiple views around the body. The use of a collimator results in a tremendous decrease in detection efficiency as compared to PET. For positron emission tomographs, collimation is achieved naturally by the fact that a pair of detected photons (gamma rays) can be traced back to their origin since they travel along the same line after being produced. In PET, there might be as many as 500 detectors that could "see" a PET isotope at any time where as in SPECT, there may be only 1 or 3 collimators. Figure 2.9 shows a triple headed gamma camera (Marconi, Inc).

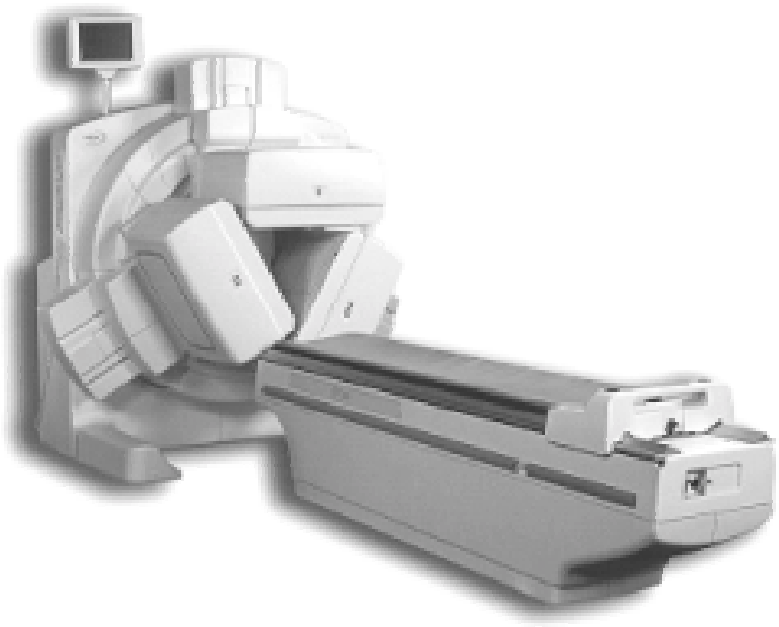

Figure 2.9: IRIX gamma camera (3 heads).

4.3. CARDIOVASCULAR APPLICATIONS

The currently two most frequently used radionuclide techniques are: (1) myocardial imaging with Thallium or a Tc-labeled perfusion agent to evaluate myocardial perfusion, and (2) blood pool scanning with a Tc-labeled tracer to evaluate ventricular function.

4.3.1. Myocardial Perfusion Imaging

Myocardial imaging with Thallium-201 or a Tc-labeled perfusion agent is useful in the evaluation of ischemia in coronary artery disease because distribution of the tracer within the myocardium primary depends on blood flow. The tracer concentrates in normally perfused myocardial cells. Consequentally tracer uptake will be diminished or absent in regions of ischemia or infarction. These regions of poor tracer uptake will appear as defects or “cold spots” on the recorded image. This is illustrated in figure 2.11, showing two short axis views of the LV. An area of reduced tracer uptake in the inferior region (arrow) indicates damaged myocardium.

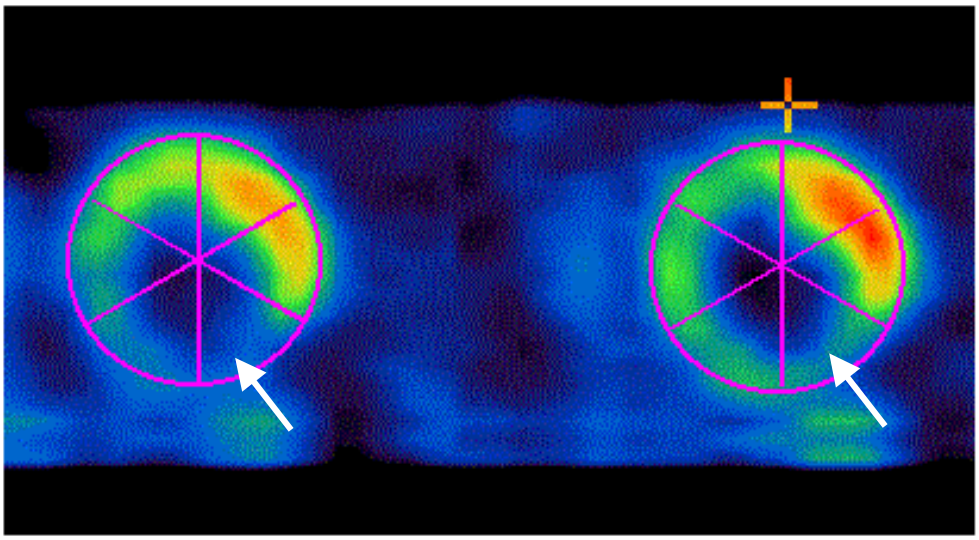

Figure 2.10: Short axis scans of the LV with SPECT. In the inferior region (arrow) damaged myocardium appears as an area of reduced tracer uptake.

Ischemia can be distinguished from infarction analysing subsequent scans. A persistent defect suggests infarction. A disappearance of the defect suggests ischemia. Perfusion imaging is usually performed in combination with exercise testing. Serial images are recorded in multiple projections during exercise and at rest because perfusion abnormalities may not be apparent at rest.

4.3.2. Blood pool scanning

This technique involves labeling red blood cells or albumin with Technetium so that the blood volume or blood pool can be visualized as outlined by the cardiac chambers and vessels. First pass blood pool scanning is used to record the initial passage of the radioactive tracer through the heart. Equilibrium imaging involves recording multiple images after distribution of the radioactive tracer has equilibrated. This technique is referred to as multiple gated blood pool scan. With this method of scanning, images are recorded over multiple cardiac cycles and then summated or superimposed to improve resolution of the nuclear image. To accurately synchronize the camera with the cardiac cycle, the camera is gated or triggered by the ECG. The gated blood pool scan permits noninvasive determination of ejection fraction, ventricular volumes, and regional patterns of wall motion.

5. Conclusion

In this chapter principles and technical background concerning cardiac measurement techniques are introduced. Especially aspects important for the research presented in this thesis are treated.

Cardiac catheterization is still the reference for cardiac pressure measurements. Two approaches are used: left- and right heart catheterization.

Doppler echocardiography has emerged, in the last 10 years, as the best method for noninvasive evaluation of LV diastolic function in the clinical setting. Several modes, including continuous wave, pulsed wave, 2D color Doppler and color M-mode are addressed.

Finally single photon emission computed tomography (SPECT) is introduced. Using different tracers cavity sizes and ejection fractions, but also perfusion defects can be quantified.

CHAPTER 3

Diastology: Integration of Diastolic Concepts in Clinical Practice

1. Introduction

Distinguishing diastolic from systolic dysfunction is essential for a proper treatment of CHF since the optimal therapy for one condition may aggravate the other. For example: inotropic agents may be beneficial in CHF due to systolic dysfunction, in case of isolated DHF they are ineffective or even deleterious (Rusconi et al. 1998).

At the bedside, diastolic dysfunction is difficult to diagnose and to differentiate from systolic dysfunction on the base of medical history, physical examination, electrocardiography and chest radiography. An increase in filling pressure or a reduction in stroke volume may be either caused by LV systolic or diastolic dysfunction. Symptoms of pulmonary venous congestion, although typical of diastolic dysfunction, are also present in CHF because of systolic dysfunction. On the other hand, signs of subnormal cardiac output, although typical of systolic dysfunction are also exhibited during exercise by patients with LV diastolic dysfunction (Rusconi et al. 1998).

Methods that can distinguish SHF and DHF need to be developed. In the past two decades, diastology has emerged as the science that characterizes LV filling and function. Diastology not only searches for the basic mechanisms that are governing diastolic filling, function and their relationship, but also seek to integrate these concepts into clinical practice. In this section, the progress made in diastology, both in the fundamental understanding of the mechanisms of diastolic dysfunction and the integration into clinical practice, is addressed.

2. Invasive Assessment Using Pressure Measurements

2.1. PRESSURE WAVEFORM

Normal diastolic filling is dependent on synchronized contraction and relaxation between the LA and the LV and within the LV itself. Changes in the normal course of contraction and relaxation will be reflected in the LV pressure waveforms. This is illustrated in figure 3.1, showing pressure waveforms in normal and abnormal LV diastolic filling.

In case of pericardial constriction, typically a “dip-and-plateau” pattern results from rapid early filling that is prematurely halted because of maximal volume restriction by the pericardium. With impaired relaxation, the pressure decline is not as rapid, and LV pressure decline occurs later in diastole. In case of a decreased compliance, LV pressure significantly rises during filling and atrial contraction, compared to the normal pressure waveform.

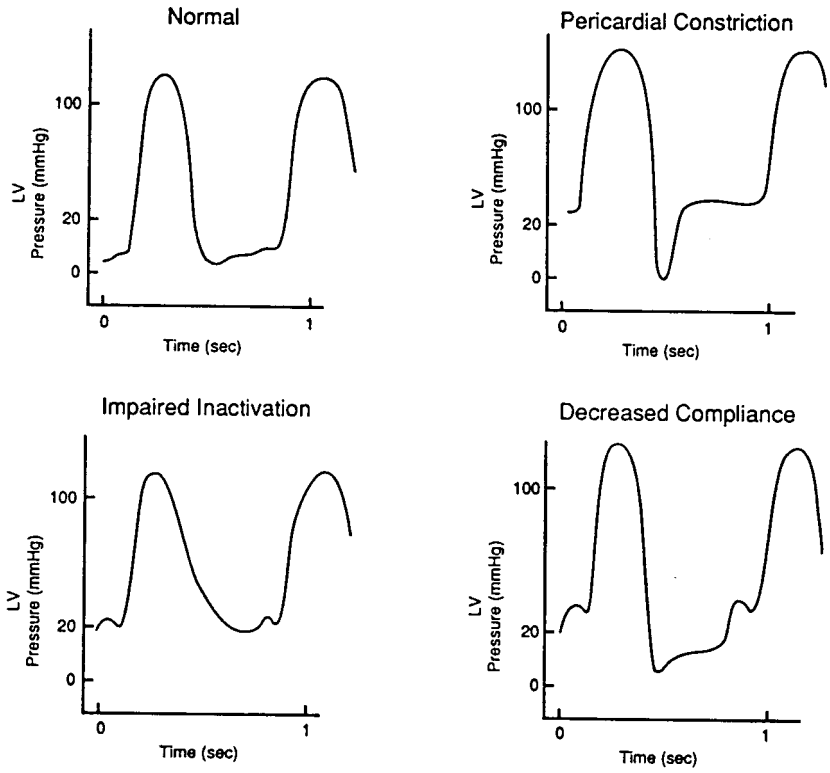

Figure 3.1: LV pressure waveforms in the normal and diseased LV (Lenihan 1995)

2.2. LV ISOVOLUMIC RELAXATION CONSTANT

Because the rate of isovolumic LV pressure fall is intimately coupled to LV relaxation, several indices derived from the pressure tracings during isovolumic relaxation are proposed as markers for LV relaxation.

Peak Negative Rate of Pressure Change

Peak negative rate of LV pressure change (LV dp/dt_{min}) occurs at aproximately the time of aortic valve closure and a value lower then 1100 $mmHg \cdot s^{-1}$ is considered indicative of slow isovolumic LV relaxation in man (Hirota 1980, Weisfeldt et al. 1974). The normal control value is 1864 ± 390 $mmHg \cdot s^{-1}$. Significantly lower values are reported in hypertrophic and congestive cardiomyopathy, but not in coronary artery or hypertensive disease. Because the value of maximum pressure change occurs at a single point in time, it can not represent the entire relaxation period.

Time Constant of Isovolumic Relaxation

The time constant of LV pressure decay (τ), obtained via an exponential curve fit, was first described by Weiss in 1976 (Weiss et al. 1976) as a global measure of LV relaxation. In an isolated canine heart preparation Weiss and coworkers demonstrated that the time-course of isovolumic pressure fall subsequent to maximum negative dp/dt is exponential, independent of systolic stress and end-systolic fiber length, and dependent on heart rate. He concluded that τ might be an index of the activity of the active cardiac relaxing system and might be dependent on systolic fiber shortening.

Weiss et al. modeled the LV pressure decay using an exponential function as shown in equation 3.1:

$$p(t) = (p_0 - p_\infty) \times e^{-t/\tau} + p_\infty \qquad \text{[Eq. 3.1]}$$

where p(t) is LV pressure as a function of time (in mmHg), t is time (in ms), p_∞ is the asymptote to which LV pressure declines (in mmHg), and p_0 is LV pressure (in mmHg) at peak negative dp/dt (where t = 0 ms). τ equals the time period needed for the pressure to fall to 37% (1/e) of its starting value. It is also the time period needed for the pressure to reach the zero level, assuming the initial rate of decline does not change.

Measured pressure data during isovolumic pressure decay were fitted to this model to obtain an estimation of τ (in ms). The pressure asymptote p_∞ was assumed being zero. The portion of the LV pressure curve used in the estimation of τ is important. The region used usually begins at the moment of peak negative dp/dt. In contrast, the end point for curve fitting varies. Weiss et al. (Weiss et al. 1976) used the pressure level, 5 mmHg above end-diastolic pressure to define the extent of the pressure curve used for the estimation of τ. Other investigators have used the LA to LV pressure cross-over to define the time period.

While a monoexponential form of pressure decay is generally accepted as an accuarate model, the techniques for calculation of τ vary; several approaches are suggested: linear vs. non-linear and zero pressure asymptote vs. non-zero asymptote (Gillebert et al. 1997, Mirsky and Pasipoularides 1990). In specific conditions more complex functions are proposed for modeling the isovolumic pressure decay. The methodology for assessing the time constant of isovolumic relaxation τ will be discussed in more detail in chapter 5.

Today, the time constant of isovolumic relaxation τ is the most widely used index of isovolumic LV relaxation kinetics. In man, normal values of τ, calculated with a zero-pressure asymptote vary from 33 ± 8 ms to 36 ± 6 ms, independent of age. A significant prolongation of τ has been reported in many clinical conditions (Paulus et al. 1992).

2.3. Intraventricular Pressure Gradients

While regional pressure differences between the left ventricle and the aorta during ejection have been recognized for some time, the presence of diastolic intraventricular pressure differences (IVPG) was first reported by Ling et al. in 1979 (Ling et al. 1979) and Falsetti et al. in 1980 (Falsetti et al. 1980).

Figure 3.2 (Courtois et al. 1988) illustrates IVPG obtained in dogs from simultaneous LV pressure recordings with a dual micromanometer catheter with 3 cm spacing between the sensors. Maximum early diastolic pressure is reached first near the apex, as indicated by the peak of the F wave recorded from a transducer located 2 cm from the apex (F_{2cm}), then begins to decay (single arrow). At the same time as pressure near the apex (2 cm) is falling, pressure measured by a transducer located 5 cm from the apex indicates that pressure is stil increasing

(double arrow), resulting in a substantially delayed F wave (F_{5cm}). During the atrial filling phase, pressure in the base (A-wave) rises well before the apical wave A-wave.

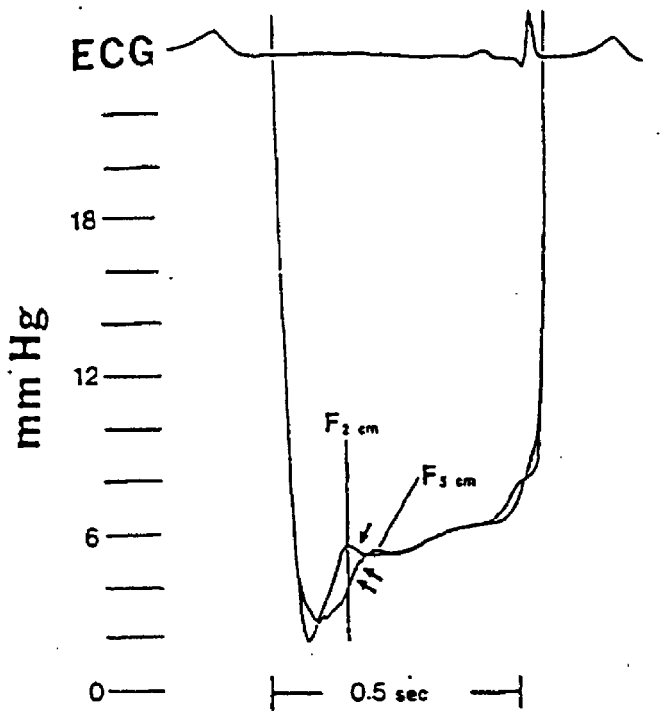

Figure 3.2: simultaneous LV pressure recordings (Courtois et al. 1988)

Ling observed a 2-5 mmHg pressure difference during early diastolic filling between the mid ventricular level and the apex in a series of chronically instrumented animal experiments. Falsetti also found a 2.1 mmHg base-to-apex peak pressure difference between the ventricular apex and base during early filling under baseline conditions. In addition, Falsetti also examined the magnitude of the peak IVPG under various hemodynamic conditions using isoproterenol and propanol, two pharmacologic agents that increase and decrease ventricular contractility, respectively. Falsetti observed increases to 4.9, 7.7 and 15.7 mmHg with graded infusions of isoproterenol at 4, 10 and 20 microg/min and a decrease in the magnitude of the intraventricular pressure difference with propanol.

In 1988, Courtois et al. (Courtois et al. 1988) systematically studied the regional diastolic pressure differences during left ventricular filling in a canine model and

demonstrated a 3.1 mmHg difference between the apex and a ventricular location 6 cm away. Courtois used simultaneous pulsed Doppler echocardiographic velocity measurements to show basic pressure-velocity relationships characterized by timing differences between the pressure crossovers and peak early filling velocity. In a subsequent investigation, Courtois and coworkers (Courtois et al. 1990) found that these IVPG disappeared rapidly during ischemia induced by coronary occlusion, suggesting that quantitation of these gradients might be useful in the diagnosis of coronary artery didease in patients. Courtois et al. speculated that the presence of IVPG might be evidence for diastolic suction (cf. Chapter 1, 5.2.3).

Nikolic et al. (Nikolic et al. 1995) have examined the origin of regional pressure gradients in the LV during early diastole. In an animal model where controlled ventricular filling was achieved by a mitral valve occluder (cf. Chapter 1, Figure 1.15), they observed diastolic intraventricular pressure differences in both filling and nonfilling beats. Ultrasonic crystal measurements of lateral and longitudinal ventricular dimensions also demonstrated no significant difference in ventricular geometry between filling and nonfilling beats. Their results support a hypothesis that intraventricular pressure gradients are increasing with increasing elastic recoil (i.e. with ESV below the equilibrium volume).

In 1998, Smiseth et al. (Smiseth et al. 1998) investigated mechanisms of LV intracavitary flow during early filling in humans and animals. Simultaneously LV apical and outflow tract pressures, next to clor M-mode Doppler velocities were measured. In this study the arrival of the early LV filling wave at the apex was associated with a substantial pressure gradient between apex and outflow tract. The pressure gradient was sensitive to changes in preload and correlated strongly with peak early transmitral flow.

Recently, Firstenberg et al. (Firstenberg et al. 2001) reported improvements simultaneous increase of LV function and intraventricular pressure gradients in humans. The changes in intraventricular pressure gradients correlated directly with improvements in τ and ESV.

Intraventricular pressure gradients are potentially usefull for clinical diagnosis. However, the origin of changes in intraventricular pressure gradients under

different physiogical conditions is still a matther of debath. Verdonck et al. (Verdonck et al. 1999) in a 1D and Vierendeels et al. in a 3D (Vierendeels et al. 2000) numerical model of LV filling observed intraventricular pressure gradients comparable to those observed by Courtois et al. (Courtois et al. 1988) and Ling et al. (Ling et al. 1979). In both models however, LV end-systolic volume was greater than the equilibrium volume V_0, indicating that the observation of intraventricular pressure gradients in a beating heart provides no definite proof for the presence of the so-called elastic recoil.

3. Non-Invasive Assessment Using Doppler Echocardiography

3.1. TRANSMITRAL FLOW PROFILE

The standard approach for the noninvasive evaluation of diastolic filling uses pulsed Doppler echocardiography with the Doppler sample volume positioned within the mitral inflow tract between the tips of the mitral leaflet tips (figure 3.3). The assessment is done in the apical 4 chamber view. The recorded velocity profile of left ventricular inflow shows a biphasic pattern with an early filling wave (E-wave) and a late filling wave during atrial contraction (A-wave).

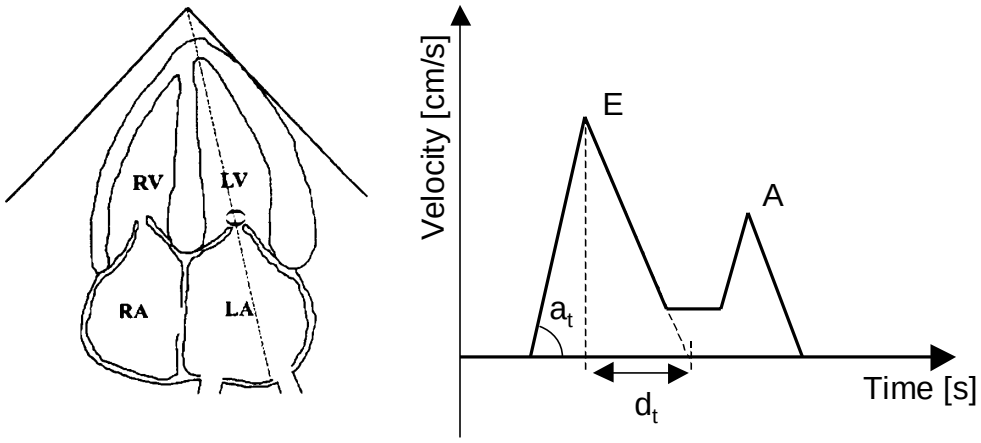

Figure 3.3: Transmitral velocity profile obtaned using Doppler Echocardiography. Placing of the Doppler Sample volume **(left)** and typical inflow profile showing an E- and A-wave **(right)**.

The LV fills under the action of the atrio-ventricular pressure gradient as illustrated in figure 3.4. For a given mitral valve geometry the determinants of ventricular filling indices are related to the factors that determine this pressure gradient. Intensive research in numerical and hydraulic models, next to experimental research in animals (Appleton 1988, Choong et al. 1988, Flachskampf et al. 1993, Flachskampf et al. 1992, McQueen et al. 1982, Solomon et al. 1999, Thomas 1994, Thomas et al. 1991, Thomas and Weyman 1989, Thomas and Weyman 1991, Yellin et al. 1994) have clearly isolated the role of several physical and physiological determinants of the indices derived from the transmitral flow pattern. For example: for a fixed LV pressure, acceleration (a) is

linearly related to LA pressure and inversely related to the LV relaxation constant; deceleration time (d_t) reflects the LV pressure rise as a consequence of LV filling and is demonstrated being strongly dependent on LV relaxation.

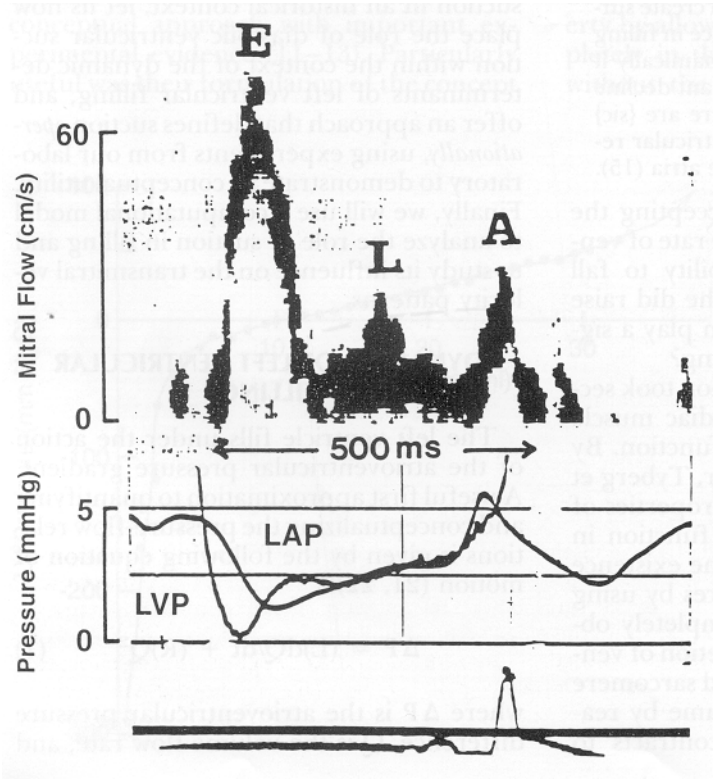

Figure 3.4: Simultaneous recordings of transmitral velocity, LV pressure and LA pressure during LV filling (Yellin and Nicolic 1994).

The Doppler derived indices from the transmitral velocity pattern are related to numerous LV functional characteristics, including dp/dt, relaxation and stiffness (Garcia et al. 2001, Nakatani et al. 1999, Scalia et al. 1997). Also, Kovacs and coworkers have designed a formal method, the so-called PDF[11] formalism (Kovacs et al. 1987), for the qualitative and quantitative interpretation of global ventricular diastolic behavior.

As a consequence, several empiric indices have been proposed as markers for ventricular diastolic function, including the peak and integrated velocities of the E- and A-waves, their ratio's, and the acceleration (a) and deceleration times (d_t) of the early filling wave (Briguori et al. 1998, Cohen et al. 1996, De Maria et al.

1991, Nishimura and Tajik 1997, Rusconi et al. 1998, Taylor and Waggoner 1992, Thomas et al. 1991, Vitarelli and Gheorghiade 1998).

Despite the significant progress in understanding the nature of the transmitral flow pattern, the clinical applicability remains limited because a single transmitral velocity pattern may result from a multitude of different combinations of the underlying determinants. In other words: the inverse problem of translating transmitral filling characteristics to LV function characteristics has no uniquely determined solution.

Especially in the evaluation of diastolic function, the problem of the non-unique solution is limiting the clinical use of the standard pulsed Doppler approach. This is illustrated in figure 3.5, displaying LA and LV pressures, next to transmitral filling patterns for different stages of diastolic (dys)function.

The most commonly used characteristic of this velocity profile is the ratio of the maximal E-wave velocity over the maximal A-wave velocity or the E/A ratio. Figure 3.6 displays the variation in the E/A ratio during the course of worsening diastolic function.

Under normal conditions the maximal E-wave velocity is higher than the maximal A-wave velocity with an E/A ratio more than 1. The initial stage of diastolic dysfunction with delayed LV relaxation causes a decreased E-wave velocity, a compensatory increase in A-wave velocity and a reversal of the E/A ratio, becoming less than 1. Further deterioration of LV diastolic function with increasing LA pressure will cause an increase in E-wave velocities and pseudo-normalization of the E/A ratio, becoming again more than 1. In severe diastolic dysfunction with a stiff left ventricle and elevated filling pressures the E-wave velocities further increase with a short deceleration time and a very small or absent A-wave causing a further increase of the E/A ratio. However, a similar large E-wave with a high E/A ratio is also seen in young people with normal or hyper dynamic left ventricular diastolic function. Therefore, in clinical practice it is not always easy to decide whether a particular patient is on the left side or on the right side of the U-shaped graph of figure 3.6. Also the deceleration time (d_t) suffers from this ambiguity. Normal values are smaller than 220 ms, whereas with

[11] PDF: “Parametrized Diastolic Filling formalism”

delayed relaxation d_t increases above 220 ms. However, with pseudo-normal filling, d_t normalizes to a value in the range of 150 to 200 ms. This value further decreases to below 150 ms with restrictive filling.

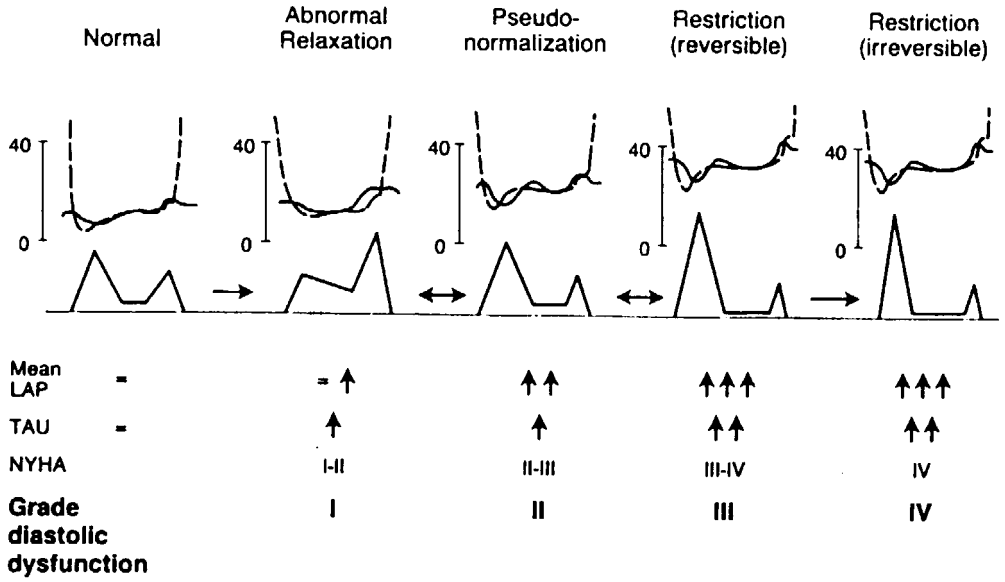

Figure 3.5: LA and LV pressures, and transmitral velocity profiles for different stages of diastolic dysfunction (NYHA: New York Heart Association class of disease severity) (Nishimura and Tajik 1997).

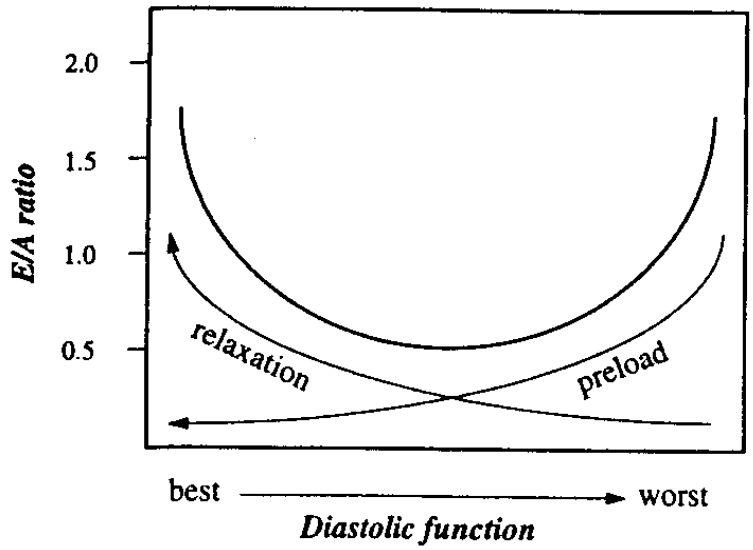

Figure 3.6: Ambiguity of Doppler derived indices (Garcia et al. 1998).

3.2. COMPLEMENTARY INFORMATION USING PWD ECHOCARDIOGRAPHY

Several other types of data can be used clinically in conjunction with that from mitral flow velocity curves to better define the state of diastolic dysfunction (Garcia et al. 1998, Nishimura and Tajik 1997, Rusconi et al. 1998).

3.2.1. Combined Transmitral and Aortic Valve Flow

Isovolumic relaxation time (IVRT) is measured from the apical 5 chamber view. This is done by aligning the Doppler beam between the mitral and aortic valves (figure 3.7). Either pulsed wave or continuous wave Doppler may be used. The time from aortic valve closure to mitral valve opening is defined as the IVRT.

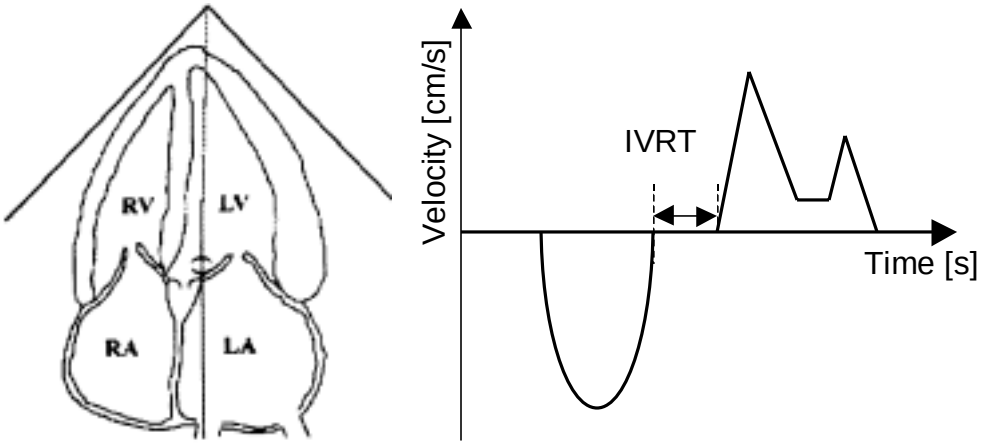

Figure 3.7: Assessment of isovolumic relaxation time (IVRT) using pulsed Doppler echocardiography. Placing of the Doppler Sample volume in the apical 5 chamber view **(left)** and typical flow profile showing aortic and mitral flow **(right)**.

Normal values are smaller than 100 ms, whereas with delayed relaxation IVRT increases to above 100 ms. However, with pseudo-normal filling, IVRT normalizes to a value in the range of 60 to 100 ms. This value further decreases to below 60 ms with restrictive filling.

3.2.2. Pulmonary Vein Flow

Another source of additional information are the pulmonary vein velocity curves, obtained from the apical 4 chamber view by placing a pulsed wave sample volume in the pulmonary veins where they enter the left atrium (Appleton 1997, Rusconi et al. 1998) (Figure 3.8). A normal pulmonary vein velocity curve consists of

systolic forward flow (S_1 and S_2), diastolic forward flow (D), and a reversal of velocity at atrial contraction (AR).

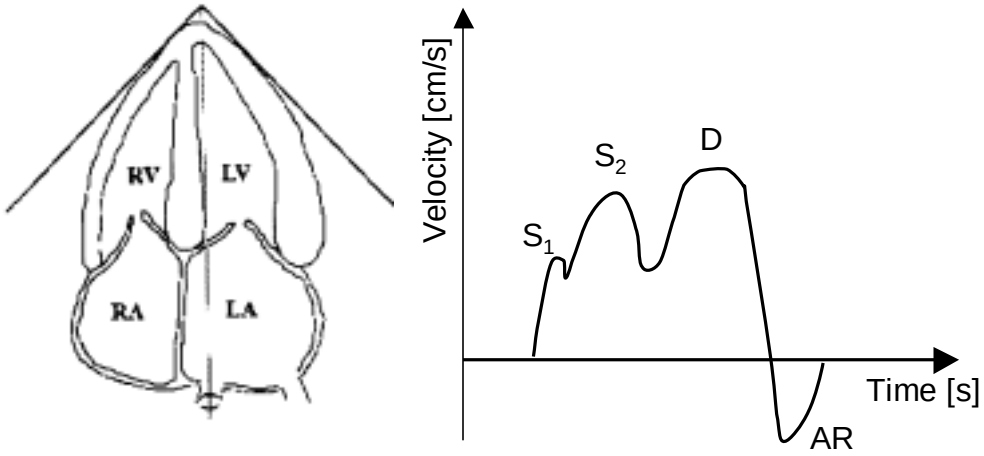

Figure 3.8: Assessment of pulmonary vein flow using pulsed Doppler echocardiography. Placing of the Doppler Sample volume **(left)** and typical flow profile showing systolic waves (S_1 and S_2), diastolic wave (D) and atrial reversal wave (AR) **(right)**.

Systolic forward flow is influenced by several factors, including LA compliance, atrial relaxation, mean LA pressure, descent of the annulus toward the LV apex, RV contraction. In patients with high LA pressures and poor LV systolic function, the velocity of systolic forward flow is decreased. Diastolic forward flow occurs at the time when there is an open conduit between the pulmonary veins, LA and LV. Thus, the contour of diastolic flow velocity is similar to that of the early part of the mitral flow velocity curve and is dependent on the same factors that influence the early mitral velocity curve. Isolated relaxation abnormalities cause a higher systolic/diastolic velocity ratio on the pulmonary velocity curves. Restriction to filling with a high LA pressure produces a low systolic/diastolic velocity ratio.

The reversal of velocity at atrial contraction in the pulmonary vein curves provides clinically relevant information that supplements that obtained from mitral flow velocity curves. At the time of atrial contraction, there continues to be an open conduit between pulmonary vein, LA and LV. There is forward flow into the LV, with blood also going retrogradely into the pulmonary veins. As the left ventricular filling pressure increases and LV compliance decreases, a higher

resistance to forward flow occurs during atrial contraction. This results in less forward flow into the LV and reflux of a greater volume of blood into the pulmonary vein during atrial contraction. Conversely, with low filling pressures and normal compliance of the LV, there will be more forward flow into the LV and reflux of a smaller volume of blood into the pulmonary vein during atrial contraction. Because ventricular relaxation usually is completed by the time of atrial contraction, the ratio between forward flow velocity into the LV and retrograde flow into the pulmonary vein is an indirect indicator of ventricular compliance.

The clinical use of pulmonary vein flow is hampered by difficulties in obtaining an accurate Doppler signal in up to 50% of the patients.

3.2.3. Tissue Doppler echocardiography

Tissue Doppler provides additional clinical useful information about diastolic function. (Garcia et al. 1998, Gorcsan et al. 1996, Gulati et al. 1996, Nagueh et al. 1997)

To display Tissue Doppler velocities, a pulsed Doppler sample volume of 1 cm is placed at the mitral valve annulus in either an apical 2 (anterior or inferior annulus) or 4 (lateral or medial annulus) chamber view (Figure 3.9).

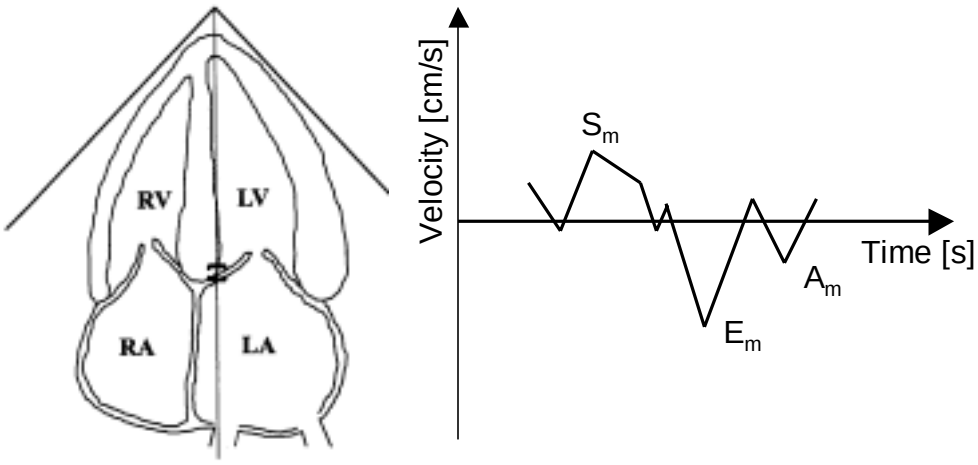

Figure 3.9: Tissue Doppler echocardiography. Placing of the Doppler Sample volume at the medial annulus **(left)** and typical velocity profile showing systolic (S_m) and diastolic (E_m and A_m) waves **(right)**.

In a typical velocity profile, a velocity signal directed towards the LV centroid during systole (S_m) and two distinct signals directed away from the centroid during early (E_m) and late (A_m) diastole can be observed.

In healthy normal subjects, the motion of the myocardium during diastole in either the circumferential or the axial plane appears as a mirror image of the mitral inflow velocity patterns. A fall in the ratio of the myocardial E_m velocity to A_m velocity with age is noted, as it has been previously well described in the LV filling curves. Because of their relative preload independence, diastolic myocardial velocities may be used to differentiate normal from pseudonormal filling patterns. Patients with advanced diastolic dysfunction and pseudonormal filling have lower E_m compared to those with normal filling .

3.2.4. Overview

Table 3.2 summarizes the cut-off values for the several degrees of diastolic dysfunction, obtained using several PWD approaches.

Tabel 3.2: Doppler indices for the assessment of diastolic function

		Normal (Young)	**Normal (Old)**	**Delayed Relaxation**	**Pseudo-Normal**	**Restrictive Filling**
E/A	[cm/s]	>1	>1	<1	1-2	>2
DT	[ms]	<220	<220	>220	150-200	<150
IVRT	[ms]	<100	<100	>100	60-100	<60
S/D	[-]	<1	≥1	≥1	<1	<1
AR	[cm/s]	<35	<35	<35	≥35	≥25
Em	[cm/s]	>10	>8	<8	<8	<8

3.3. COLOR DOPPLER ECHOCARDIOGRAPHY

3.3.1. 2D Color Doppler Echocardiography

In contrast to pulsed Doppler echocardiography, 2D color Doppler echocardiography provides velocity information in a two dimensional spatial map. The clinical use of 2D color Doppler echocardiography for the evaluation of diastolic filling is limited because of the low temporal resolution.

3.3.2. Color M-mode Doppler Echocardiography

In contrast to 2D color Doppler echocardiography, color M-mode Doppler (CMD) echocardiography has a temporal resolution that equals the resolution of the pulsed Doppler mode (200 Hz). CMD echocardiography provides velocity information along a single scanline with a spatial resolution of 0.3mm. Nonetheless having a dimension less information compared to 2D color Doppler echocardiography, CMD echocardiography provides a dimension more information compared to the standard pulsed Doppler technique (Thomas et al. 1997). CMD echocardiography is an important emerging technique in the area of Doppler echocardiography. The blood velocity information in a CMD image allows for the reconstruction of accurate pressure gradients (Greenberg et al. 2001, Greenberg et al. 1995, Greenberg et al. 1996, Vandervoort et al. 1993). Moreover, the analysis of the intraventricular flow field features provides additional information about diastolic filling and function (Brun et al. 1992, De Mey et al. 1998, Garcia et al. 1998, Stugaard et al. 1993, Takatsuji et al. 1996).

Various methodologies for analyzing CMD images qualitatively and quantitatively are discussed in chapter 4.

3.3.3. Strain and strain-rate imaging

Analogue to the pulsed Doppler mode, color Doppler echocardiography can be used for measuring both blood flow velocities (Thomas et al. 1997) and tissue velocities (Gorcsan et al. 1996, Miyatake et al. 1995). Recently, the calculation of strain and strain rate, based on the tissue velocity information in a color Doppler image, the so-called strain-rate imaging technique, is introduced (D'hooge et al. 2000, Urheim et al. 2000).

4. Conclusion

Evidence of diastolic dysfunction can be derived using invasive and non-invasive measurements. The invasive measurement of an elevated filling pressure or impaired relaxation is considered the golden standard. However, routine use of cardiac catheterization is not feasible nor desirable. Therefore, non-invasive techniques are developed. Principally Doppler studies of mitral inflow are used to verify LV diastolic function in the echolab.

The pulsed Doppler approach is difficult because results must be interpreted in the context of loading conditions, heart rate and systolic function. It has to be emphasized that these non-invasive criteria do not provided equivocal evidence for diastolic dysfunction as values suffer from pseudo-normalization.

Color M-mode Doppler echocardiography is a technique that might provide potential valuable information about diastolic function. The role and relevancy of CMD echocardiography of LV filling in the assessment of diastolic function is addressed in more detail in chapter 4.

CHAPTER 4

Diastolic Filling and Pressure Imaging: Taking Advantage of the Information in a Color M-mode Doppler Image †

† The content of this chapter has been accepted for publication in Eur J Echo (December 2001):
Diastolic Filling and Pressure Imaging:
Taking Advantage of the Information in a Color M-mode Doppler Image
S. De Mey, J De Sutter, J Vierendeels, P Verdonck.

Abstract

The ability to derive non-invasively information on LV diastolic function on one hand and pressure gradients on the other hand, makes Doppler ultrasound a very attractive tool in clinical practise. However, the limitations of the standard Doppler approaches in differentiating between normal and pseudonormal filling patterns, next to the limitations of the simplified Bernoulli equation for assessing pressure gradients, are well described. In this manuscript the role of color M-mode Doppler echocardiography as a tool that can overcome these limitations is discussed. Relevant key concepts of the hemodynamics of LV filling and its relationship with CMD echocardiography are introduced.

1. Introduction

1.1. BACKGROUND

The potential ability to derive non-invasively information on LV diastolic function, makes Doppler ultrasound a very attractive tool in clinical practice. The traditional approach to evaluate LV diastolic function non-invasively uses pulsed wave Doppler echocardiography (PWD) with the sample volume positioned at the level of the mitral valve leaflet tips. The recorded velocity profile of LV inflow shows an early filling wave (E-wave) and a late filling wave during atrial contraction (A-wave). A multitude of indices such as peak E and A velocity, their ratio, and acceleration and deceleration times are derived from this velocity pattern and proposed as markers for diastolic function (Cohen et al. 1996, De Maria et al. 1991, Nishimura and Tajik 1997, Taylor and Waggoner 1992, Vitarelli and Gheorghiade 1998). Intensive research, using numerical (Flachskampf et al. 1992, McQueen et al. 1982, Meisner 1986, Thomas et al. 1991) and in vitro (Flachskampf et al. 1993) models, next to observations in animals and humans (Appleton 1988, Appleton et al. 1997, Briguori et al. 1998, Choong et al. 1988, Ishida et al. 1986, Meisner 1986, Yellin et al. 1994), have clearly elucidated the physical and physiological determinants of the transmitral velocity pattern. Although it provided us with many clinical useful insights, this research revealed also the limitations of PWD echocardiography in clinical practice for assessing diastolic function.

Another widely used application of Doppler echocardiography is the assessment of pressure drops across orifices: e.g. using the simplified Bernoulli equation pressure drops across the mitral valve are estimated based on PWD derived velocities (Hatle and Angelsen 1985). However, the limitations for assessing pressure gradients using the simplified Bernoulli equation are largely demonstrated (Baumgartner et al. 1999, De Mey et al. 2001b, Nakatani et al. 2000, Verhaaren et al. 2001).

To overcome the limitations of standard PWD echocardiography, additional techniques remain necessary. Analysis of the pulmonary venous flow patterns (Appleton 1997), and more recently the use of tissue Doppler imaging (TDI) (Gorcsan et al. 1996, Gulati et al. 1996, Miyatake et al. 1995, Nagueh et al. 1997,

Zamorano et al. 1997), strain (Urheim et al. 2000) and strain rate imaging (D'hooge et al. 2000), and color M-mode Doppler (CMD) echocardiography (Garcia et al. 1998) have been suggested as promising new tools in the evaluation of left ventricular diastolic function using ultrasound based technology. In this review we will focus on CMD echocardiography.

1.2. COLOR M-MODE DOPPLER ECHOCARDIOGRAPHY OF LV FILLING

Whereas PWD velocity measurements represent a temporal velocity variation throughout the cardiac cycle obtained at a single point in space, CMD echocardiography interrogates all the velocities along a scan line and provides a spatio-temporal velocity map with a temporal resolution of 5 ms, a spatial resolution of approximately 0.3 mm and a velocity resolution of typically 3 cm/s (Thomas et al. 1997). Figure 4.1 (left panel) shows the orientation of the scan line, captured from an apical window. The scan line is parallel to the inflow track of LV filling. The right panel (top) shows a three-dimensional graph containing the spatial and temporal distributed velocity information. A CMD image provides the same three-dimensional information in a two dimensional plane with the velocity encoded in colors (figure 4.1, right panel, bottom).

Two distinct approaches are used to cope with the velocity information in a CMD image. On one hand, qualitative properties of the flow field within the LV cavity are analysed. This approach has led to the concept of flow propagation velocity (v_p). On the other hand, efforts are made towards the development of ‘pressure imaging’ techniques, i.e. visualising and calculating pressure differences, hereby fully exploiting quantitatively the numerical velocity information, stored in a CMD image. In this manuscript the progress in both approaches will be reviewed and discussed.

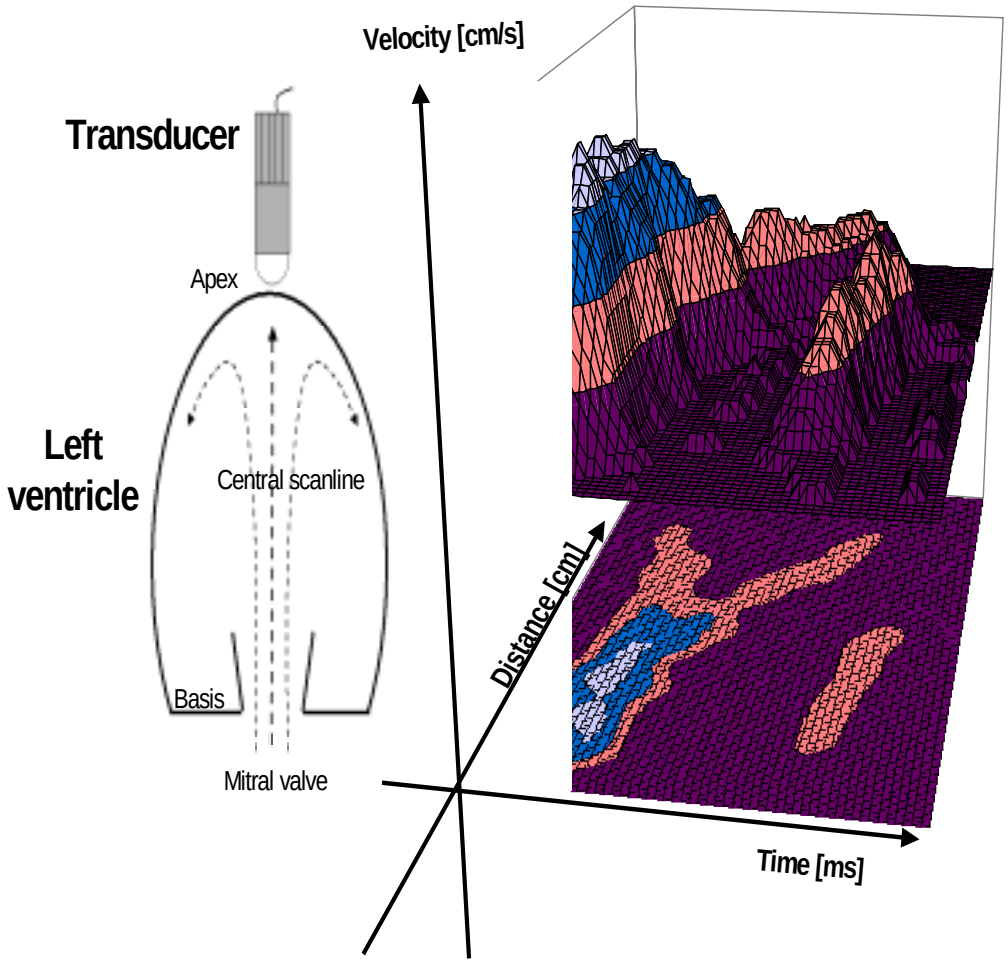

Figure 4.1: Left panel: Schematic representation of the recording of a CMD image of LV filling with the scanline aligned with the central inflow tract. **Right Panel:** Spatiotemporal velocity information, obtained using CMD echocardiography, represented in a three-dimensional graph (top) and in a two-dimensional plane with the velocity encoded in colors (bottom).

2. Hemodynamics of LV Filling and CMD Echocardiography

2.1. Hemodynamics of LV Filling

CMD echocardiography of LV filling provides velocities along one scan line in a three-dimensional flow field. Therefore, to understand the hemodynamics of the velocity information in the CMD image, the entire flow field within the LV cavity has to be considered. From the early seventies to the late nineties, several research groups have focussed their efforts on understanding the intraventricular flow field. Although those studies were conducted with different objectives, it provided us with many useful insights concerning the filling mechanisms of the LV and confirmed that vortex formation is a crucial phenomenon in the mechanism of LV filling.

Vorticity at a point in a fluid is related to the angular velocity of an infinitesimal fluid mass that is instantaneously occupying a point in space (Batchelor 1967). The injection of fluid through an orifice is a mechanism that generates vorticity, resulting in a smoke ring like vortex (Figure 4.2, left panel). Therefore, because LV filling is basically the filling of a cavity through an orifice, LV filling generates smoke ring like vortices in the LV cavity (Figure 2, right panel). The diameter of the core of the ring (a) and the diameter of the annulus around the core (b) characterise the vortex ring as shown in Figure 4.2. The fluid particles trapped within the annulus around the core are travelling with the vortex ring at a propagation speed v_p. This propagation speed does not equal the velocity of an individual fluid particle (v) because individual fluid particles are rotating within the travelling vortex ring (Batchelor 1967, Lamb 1932).

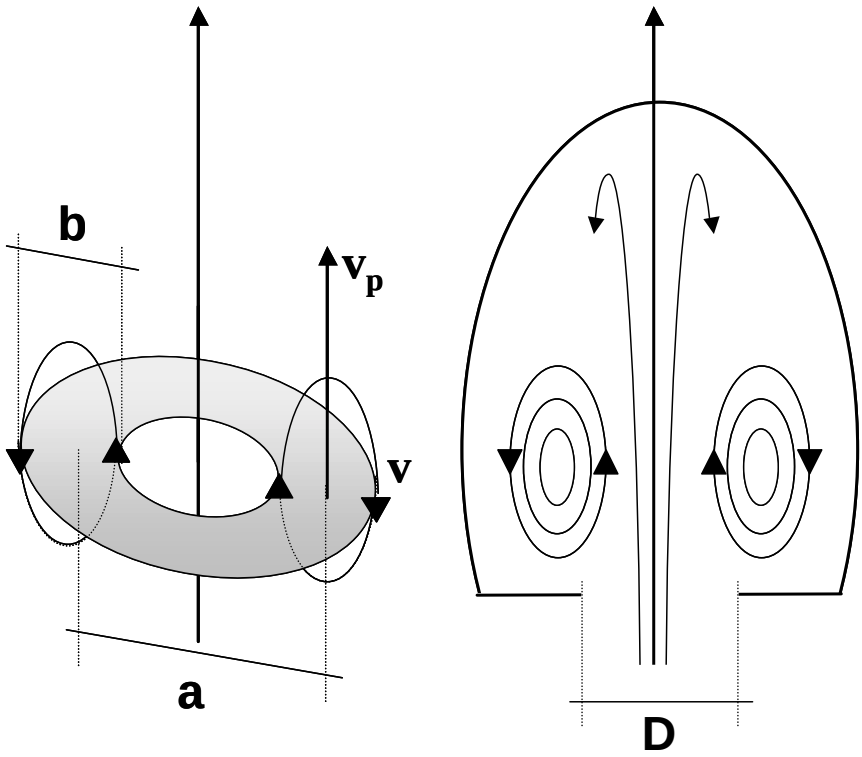

Figure 4.2: Principle of vortex formation during LV filling. A smoke ring like vortex (**left panel**) with a the diameter of the core and b the diameter of the annulus of the core is formed in a LV (mitral valve diameter D, **right panel**). The vortex is propagating with a propagation speed v_p in the direction of the apex. Individual fluid particles are rotating within the vortex ring and have a velocity v.

The generation and travelling of vortices in the LV is confirmed in several studies. In the seventies, studies were initiated to investigate the influence of the flow field on valvular mechanics. Lee et al. (Lee and Talbot 1979) with the use of a numerical model, and Bellhouse et al. (Bellhouse 1972) with the use of an in vitro model described vortex formation during LV filling. According to Bellhouse et al. (Bellhouse 1972), the presence of a vortex ring provides a mechanism for valve closure at the end of diastole. In the late eighties and early nineties several clinical studies have examined the spatial dependent differences of the intraventricular flow in the diseased LV during the cardiac cycle (Beppu et al. 1988, Delemarre et al. 1990, Van Dantzig et al. 1995). Simultaneously, numerical and in vitro

simulations provided a theoretical framework, explaining the observations (Bot 1989, Bot et al. 1990). From this research (Beppu et al. 1988, Delemarre et al. 1990, Van Dantzig et al. 1995) it was concluded that travelling vortices especially are a feature of LV's that have become pathologically dilated. Also, a positive relationship between the presence of vortex rings and a risk for thrombus formation was suggested. However, the use of 2D color Doppler (which has a poor time resolution) and PWD echocardiography (which only provides information at one location) for observing the subtle spatial differences during diastolic filling is a limitation in these studies. In contrast with those studies, recently Rodevand et al. (Rodevand et al. 1999) described the presence of vortices in normal human LV's during diastolic filling using CMD echocardiography, which has a superior time resolution, compared to 2D echocardiography.

In the nineties, in vitro and numerical studies of the flow in a skeletal muscle LV were very elusive in explaining the mechanism of vortex formation and travelling in a cavity (Henry et al. 1997, Iudicello et al. 1997, Shortland 1996). In the in vitro experiments, detailed information about the formation and travelling of vortices during filling was obtained with the use of a helium-neon laser that illuminated planar sections of the model ventricles. Influences of geometrical properties, including cavity volume, valve size, ejection fraction, and inclination of the mitral valve plane on vortex formation and travelling were investigated.

2.2. Travelling Vortices and CMD Echocardiography of LV Filling

In the higher mentioned experimental work (Henry et al. 1997, Iudicello et al. 1997, Shortland 1996), the positive relationship between the position of the vortex ring in the cavity and the position of the maximal blood velocity in the LV along the base-apex axis, i.e. the fact that propagation speed of the vortex ring equals the propagation speed of the maximum velocity, was a key observation. Steen et al. (Steen and Steen 1994), using a hydraulic model, were however the first to realise that the travelling speed of a vortex ring in the LV could therefore be associated with the vp, obtained from a CMD image. This concept is illustrated in figure 4.3, showing two snapshots of the filling of a model LV next to a drawing of a corresponding CMD image. Simultaneously with the propagation of the vortex ring from base (at time t_1) towards the apex (at time t_2), the maximum velocity is

shifting upwards in the CMD image. Therefore, the propagation speed of the ring vortex vp can be derived from the slope in the CMD image:

$$v_p = \frac{s_2 - s_1}{t_2 - t_1} \qquad \text{[Eq. 4.1]}$$

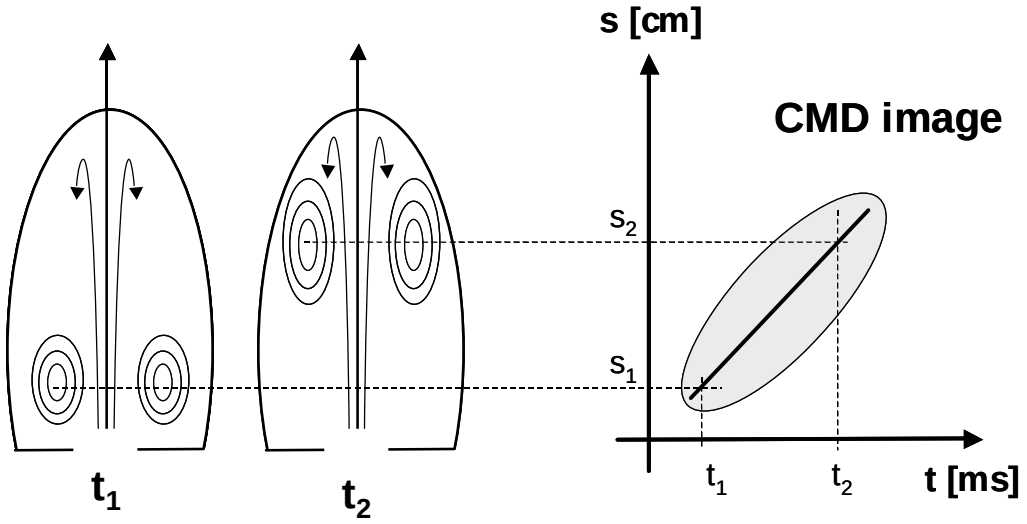

Figure 4.3: Physical interpretation of the flow propagation velocity as derived from a CMD image. The position of the vortex ring at different moments in time in the LV (**left panel**) correspond to the position of the maximal velocity along the base-apex axis, as obtained with CMD echocardiography (**right panel**). Therefore the propagation speed of the vortex ring corresponds to the flow propagation velocity (v_p), obtained from a color Doppler M-mode image.

Vierendeels et al. (Vierendeels et al. 2000), using a numerical model, confirmed this close relationship between the position of the vortex core and the position of the maximum velocities along the base-apex axis.

In case of vortex formation during LV filling, peak E-velocity should always exceed v_p because of the hydrodynamic principle that, due to the intrinsic circular motion of the particles in the ring vortex, the velocity of particles (E) in a vortex ring exceeds the velocity at which the whole ring travels (v_p). The higher peak E-velocity, compared to v_p, is observed in vitro and in numero (Henry et al. 1997, Iudicello et al. 1997, Shortland 1996, Steen and Steen 1994, Vierendeels et al. 2000), and in vivo (Brun et al. 1992, Garcia et al. 1997, Stugaard et al. 1993).

2.3. BIPHASIC FILLING PATTERN

As higher described, vortex formation is a crucial phenomenon in de filling process. However, during the initial flow phase, before the vortex ring has fully developed, blood moves almost simultaneously in the whole ventricle. Therefore, in a CMD image of the early filling wave, very often a biphasic-filling pattern is observed. This is illustrated in figure 4.4 that shows a CMD image of LV filling obtained in a normal subject. Phase I is straight upward and can be associated with the initial motion of the blood column in the LV due to the passing pressure wave. Phase II is the propagation of the maximum velocity that can be associated with the propagation of a vortex ring as described before. The biphasic filling pattern is observed in vitro (Steen and Steen 1994), in numero (Vierendeels et al. 2000) and in vivo (Garcia et al. 1998, Rajagopalan et al. 2001, Rodevand et al. 1999, Stugaard et al. 1993).

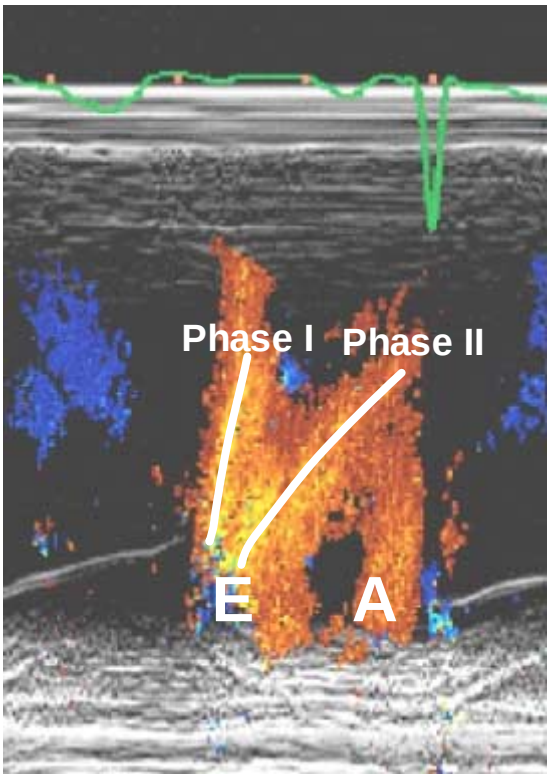

Figure 4.4: Biphasic early filling wave obtained in a patient using CMD echocardiography. Phase I is the instantaneous motion of the fluid due to the passing pressure wave, phase II corresponds to the formation and travelling of a vortex ring.

3. Assessment of Flow Propagation Velocity using CMD Echocardiography

3.1. QUANTIFYING V_P FROM A CMD IMAGE

An adequate recording of a CMD image of LV filling starts with placing the M-mode line parallel with the direction of flow observed by two-dimensional color Doppler echocardiography in an apical four-chamber view. Basically five different approaches are used for identifying v_p of LV filling using CMD echocardiography manually or in a (semi-) automated way. Differences between methods are mainly related to the amount of velocity information and/or the specific part of the CMD image that is considered for identifying a line segment.

Method 1: Brun. Brun et al. (Brun et al. 1992) defined vp as the slope (in m/s) of the line segment identifying the black-to-color transition of the early filling wave. The segment begins with the onset of flow in the LV inlet and ends as far as possible in the left ventricular chamber. The line segment has to be reasonably linear (Figure 4.5 (A)).

Method 2: Duval-Garcia. Because the black-to-color transition, as defined by Brun et al., is not always clearly visible, Duval-Moulin et al. (Duval-Moulin et al. 1997) and Garcia et al. (Garcia et al. 1998) have modified this method by considering boundaries of equal velocities, so-called isovelocity boundaries instead of black-to-color transitions (Figure 4.5 (B)). Typically the isovelocity contour of the first aliasing velocities (in case of manual analysis) or the isovelocity contour of 50% of the maximum velocity (in case of semi-automatic analysis) is addressed, starting at the position of the mitral valve, going typically four cm into the LV.

Method 3: Stugaard. Stugaard et al. (Stugaard et al. 1993) measured the occurrence of the maximal velocities at several positions on the left ventricular base-apex axis. The time-delay (TD, in ms) between occurrence of maximal velocity at the mitral leaflet tips and the maximal velocity further in the LV (typically 35mm away from the leaflet tips) is proposed as a characteristic for flow propagation (Figure 4.5 (C)). The ratio TD and the spatial distance (S, in cm) between the first and last position is proposed as a normalised characteristic for

v_p. The dimension of this normalised characteristic is the reciprocal of a velocity (ms/cm).

Method 4: Takatsuji. Takatsuji et al. (Takatsuji et al. 1996) determined the v_p using the baseline shift, displaying the flow velocities higher than the aliasing velocities in blue within the red filling flow signals. First the point of maximal velocity around the mitral orifice in early diastole was located. Next, the first aliasing limit was changed to 70% of the maximal velocity. The nearest point to the apex on the aliasing boundary (typically occurring at the level of the mid ventricle) was then located. The ratio (in cm/s) of the distance difference (S, in cm) and the time delay (T, in s) between the maximal velocity at the mitral valve leaflets and the most apical point of the aliasing boundary corresponding to 70% of the peak E-wave velocity was proposed as a characteristic for v_p (Figure 4.5 (D)). Note the similarity between the Takatsuji and the Duval-Garcia method in using a contour of equal velocities somewhere between zero and maximum velocity. There is, however, an important difference because the Duval-Garcia method tracks the front part of the contour to identify a line, whereas Takatsuji et al. only uses one point of the contour (typically at the top), next to the point where the maximum velocity occurs, typically in the centre of the area enclosed by the contour.

Method 5: Greenberg. Greenberg et al. (Stugaard et al. 1997) determined vp by eigenvector analysis of the E-wave in the CMD image. This method calculates the principal components of the E-wave as an elliptical representation. Basically the algorithm is taking into account all velocities in a selected region of interest of the CMD image and fits an elliptical geometry on it. The angle of rotation of the long axis of the ellipse is used as a parameter for v_p. This angle is expressed in degrees and negative angles are measured clockwise (Figure 4.3 (E)).

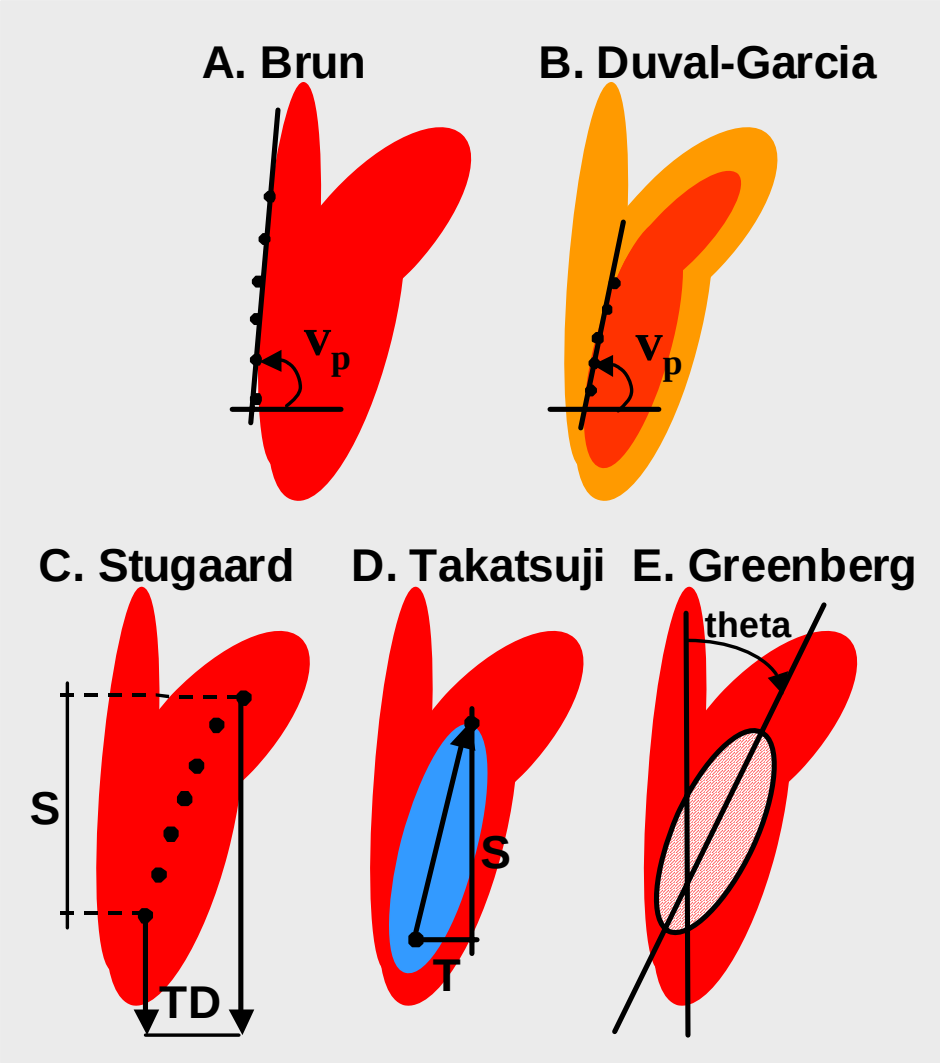

Figure 4.5: Schematic representation of five different methods for quantifying flow propagation proposed by Brun et al. **(A)**, Duval et al. and Garcia et al. **(B)**, Stugaard et al. **(C)**, Takatsuji et al. **(D)** and Greenberg et al. **(E)**.

3.2. REPRODUCIBILITY

From a theoretical viewpoint, keeping in mind the higher explained relationship between travelling speed of vortices and the position of the maximum velocity along the LV base-apex axis, the approach of Stugaard et al. (Stugaard et al. 1997) seems the most straightforward. However, from a practical point of view, other approaches might be preferred for reasons of reproducibility.

Table 4.1 shows inter- and intra-observer variability's for the different approaches as reported in literature. Because of difficulties for some images in determining the black-to-color transition, the method of Brun has a high variability. Also the

approach of Stugaard suffers from large variability's because the method determines the time difference in a semi-automated way, based on only two pixels. Nonetheless the automated algorithm provides more observer independent determinations, minor noise in an image can strongly influence the determination of vp, yielding large beat-to-beat variability's.

Table 4.1: inter and intra-observer variability

Method	Inter-observer variability		Intra-observer variability		Reference
	% (†)	cm/s (‡)	% (†)	cm/s (‡)	
Brun	18 ± 18	-1.6 ± 18	20 ± 9	2.7 ± 10	(Nagueh et al. 1996)
Duval-Garcia	8 ± 6	1.3 ± 4.5	6 ± 6	2.1 ± 3.7	(Gonzalez-Vilchez et al. 1999)
Brun	9 ± 19	NA	1 ± 7	NA	(Mego et al. 1998)
Duval-Garcia	4 ± 18	NA	2 ± 16	NA	(Garcia et al. 1997)
Duval-Garcia	11	NA	9	NA	(Garcia et al. 1999)
Duval-Garcia	12	NA	8	NA	(Garcia et al. 2000)
Duval-Garcia	7.6 ± 3.8	NA	8.3 ± 6.4	NA	(Moller et al. 2000c)
Duval-Garcia	8 ± 6	NA	7 ± 5	NA	(Moller et al. 2000a)
Brun	> 20	NA	> 20	NA	(Duval-Moulin et al. 1997)
Brun	50	NA	NA	NA	(Steen et al. 1994)
Stugaard	20	NA	NA	NA	(Steen et al. 1994)
Takatsuji	NA	-1.0 ± 6.2	NA	1.0 ± 3.4	(Takatsuji et al. 1996)

(†) Mean percent error ± SD; (‡) Mean difference ± SD; NA: not available

The strict procedure as proposed by Takatsuji et al. (Takatsuji et al. 1996) has, in case of manual execution, the advantage of filtering out variability. However, analogue to the method of Stugaard, this method finally calculates vp using only two selected pixels, yielding potential sensitivity to noise in an automated procedure, yielding high beat-to-beat variability's. The values in table 4.1 indicate that the Duval-Garcia approach has a reproducibility that meets values of standard Doppler indices (Galderisi et al. 1992). This justifies the fact that in most of the recent work this approach is used for quantifying v_p. This method uses more velocity information (all pixels along an isovelocity line) compared to the

approaches of Stugaard and Takatsuji and is therefore less noise-sensitive. Moreover, linear regression techniques can easily be used for identifying a line with the isovelocity contour, allowing a semi-automated determination of v_p. The method of Greenberg is a fully automated procedure, taking into account all the velocity information in the selected part of the image. The manual selection of the region of interest remains the only possible source of inter-observer and intra-observer variability. Because it integrates all velocity information, the Greenberg method is also almost insensitive to noise in the image. On the other hand, when using the Greenberg method, it is hard to unravel whether changes in vp are due to changes in the first or second phase of the ventricular early filling pattern.

3.3. STANDARDISATION

Regardless of the approach used, v_p is identified with a slope in the spatiotemporal CMD image. However, the quantification of v_p is not standardised. Brun et al. and Takatsuji et al. quantify vp using the tangent of a line, respectively expressed in m/s and cm/s. In contrast, Stugaard et al. prefers reporting a time delay (TD in ms) or a normalised time delay (TD/S in ms/cm). Greenberg et al. quantifies vp as an angle (in °). Because each approach quantifies a slope, transformation of values to on standard quantification is feasible (De Mey et al. 1998). Because vp represents the propagation speed of a vortex ring, the reporting of vp as a velocity seems at first sight the most appropriate. However, to improve accuracy when analysing steep slopes, a transformation to an angle (in °) or a log transformation might be better. This transformation solves the inaccuracy in case of steep slopes and brings data nearer to homoscedasticity (De Mey et al. 1998, Steen et al. 1994).

3.4. PHYSIOLOGICAL DETERMINANTS OF VP AND E/VP

Age dependency

Table 4.2 shows literature data on normal v_p values for different methods. v_p is decreasing with age. Age-dependency is also observed by Brun et al. (Brun et al. 1992) and Mego et al. (Mego et al. 1998), reporting correlation coefficients of r = -0.61 and r = -0.59 respectively.

Left ventricular relaxation

Studies (Table 4.3) in both animals and humans during coronary angioplasty-induced ischemia (Duval-Moulin et al. 1997, Stugaard et al. 1994, Stugaard et al.

1993), during intracoronary dobutamine infusion (Brun et al. 1992), before and during cardiopulmonary bypass (Garcia et al. 2000), in a mixed patient population (Takatsuji et al. 1996) and in patients with HCM (Nishihara et al. 2000) describe a univariate correlation of the constant of isovolumic relaxation (τ) with vp as obtained from the CMD images. In both animals and humans, Garcia et co-workers (Garcia et al. 2000) found that LV relaxation is a major determinant of v_p, best described using a power function $\tau = 592.21\ v_p^{-0.6838}$ ($r = -0.78$, $p<0.001$).

Tabel 4.2: normal values of v_p

Method	Age	N	v_p	Reference
Brun	39 ± 13	29	84 ± 11	(Brun et al. 1992)
Brun	21-35	21	77 ± 25	(Mego et al. 1998)
Brun	36-50	16	70 ± 23	(Mego et al. 1998)
Brun	51-60	13	53 ± 15	(Mego et al. 1998)
Brun	>65	14	43 ± 11	(Mego et al. 1998)
Duval-Garcia	63 ± 11	30	76 ± 16	(Moller et al. 2000c)
Duval-Garcia	60 ± 11	38	74 ± 19	(Moller et al. 2000a)
Duval-Garcia	37.2 ± 8.9	7	54 ± 9	(Firstenberg et al. 2000a)
Takatsuji	58.2 ± 13	29	74 ± 17	(Takatsuji et al. 1996)
Takatsuji	56 ± 10	26	73 ± 19	(Nishihara et al. 2000)
Stugaard	20-70	54	43 ± 27 (†)	(Stugaard 1994)

Age: mean ± SD; N = number of studies; v_p = flow propagation velocity (mean ± SD) in cm/s; (†) Time Delay (TD) in ms

Filling pressure

A study of Duval-moulin et al. (Duval-Moulin et al. 1997) concludes that during ischemia, the premature cessation of late filling is associated with increased diastolic pressures. Also, in a univariate analysis, several investigators found a significant correlation between left atrial pressure, left ventricular minimal pressure or left ventricular end-diastolic pressure on one hand and v_p on the other hand (Brun et al. 1992, Garcia et al. 1997, Garcia et al. 2000, Gonzalez-Vilchez et al. 1999, Stugaard et al. 1994, Stugaard et al. 1993, Takatsuji et al. 1996). In

contrast, in multivariate analysis, most studies were not able to demonstrate a significant load dependency of vp. Only in a study of Brun et al. (Brun et al. 1992), in a multivariate model, both the relaxation constant and the difference between LV pressure at mitral valve opening and minimal LV pressure remained simultaneously significant variables for determining v_p. Moreover, several experimental studies (De Mey et al. 1999, Firstenberg et al. 2000a, Garcia et al. 1999, Garcia et al. 2000, Moller et al. 2000b, Stugaard et al. 1995) reported no significant change in vp for altering loading conditions including volume loading, caval constriction, Trendelburg's position, inverse Trendelberg's position, after inhalation of amyl nitride and during lower body negative pressure.

Table 4.3: Relaxation constant and filling pressure as physiological determinants of v_p

	Method	r- τ (†)	r-p (‡)	Reference
Animals	Duval-Garcia	-0.65	-0.65	(Garcia et al. 2000)
	Stugaard	0.81	0.78	(Stugaard et al. 1993)
	Stugaard	0.89	0.91	(Stugaard et al. 1994)
Humans	Brun	-0.73	-0.69	(Brun et al. 1992)
	Takatsuji	-0.82	-0.61	(Takatsuji et al. 1996)
	Duval-Garcia	-0.53	NA	(Duval-Moulin et al. 1997)
	Takatsuji	-0.76	NA	(Nishihara et al. 2000)
	Duval-Garcia	-0.75	NA	(Garcia et al. 2000)
	Duval-Garcia	NA	-0.45	(Gonzalez-Vilchez et al. 1999)
	Duval-Garcia	NA	-0.34	(Garcia et al. 1997)
	Brun	NA	NS	(Nagueh et al. 1996)
	Duval-Garcia	NA	NS	(Firstenberg et al. 2000a)

(†) correlation coefficient of the univariate regression between v_p (or TD) and the constant of isovolumic relaxation (τ); (‡) correlation coefficient of the univariate regression between v_p (or TD) and filling pressure; NA: not available; NS: not significant

Clinical Implications

In case of diastolic dysfunction, standard PWD derived indices such as the ratio of peak early filling (E) velocity to peak late filling (A) velocity are sensitive for pseudonormalisation. In contrast, Takatsuji et al. (Takatsuji et al. 1996) conclude

that the spatial and temporal analysis of v_p by CMD echocardiography was free of pseudo-normalisation in evaluating left ventricular diastolic dysfunction. This is illustrated in figure 4.6, showing three CMD images for a normal (Normal, left panel), delayed relaxation (DR, middle panel) and pseudo-normal (PN, right panel) filling pattern, next to the corresponding pulsed Doppler tracings of mitral flow. Whereas the E/A ratio can not distinct the normal and the pseudo-normal case, the v_p value remains delayed in case of pseudo-normal filling, compared to the normal v_p value.

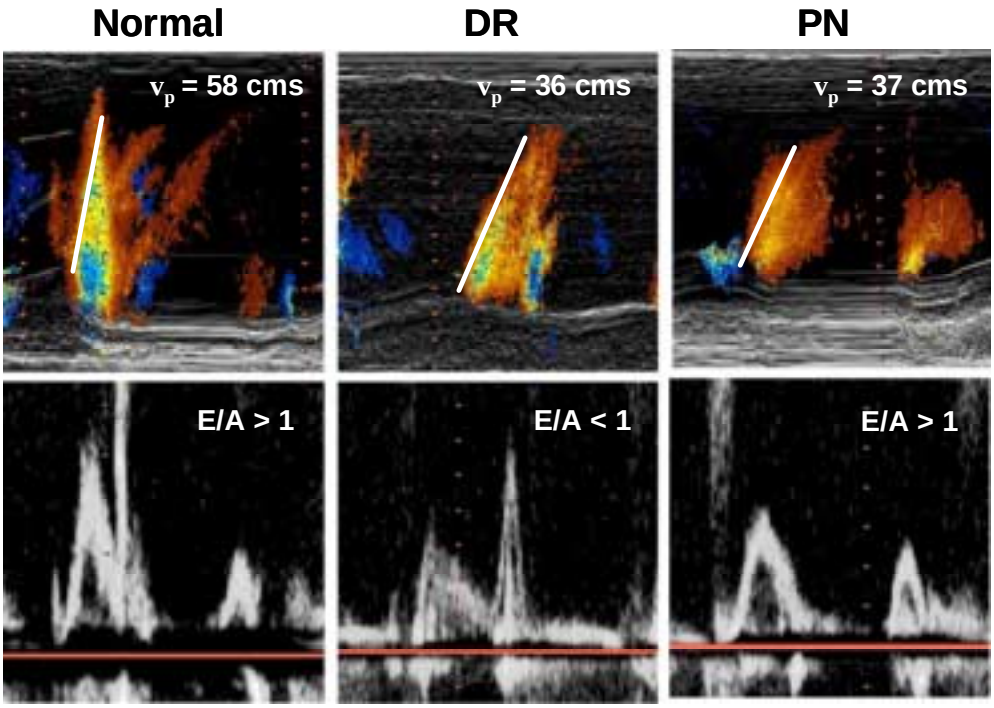

Figure 4.6: CMD and PWD images of left ventricular filling. **Left panel**: Normal filling pattern (v_p = 58cm/s, E/A > 1). **Middle panel**: Delayed relaxation filling pattern (v_p = 37cm/s, E/A < 1). **Right panel**: Pseudo-normal filling pattern (v_p = 36cm/s, E/A > 1).

Steine et al (Steine et al. 1998) demonstrated slowing of vp in patients with acute myocardial infarction. Infarct size was a determinant of slowing v_p. In a serial echocardiographic study in patients after a first myocardial infarction, Moller et al. (Moller et al. 2000a) concluded that pseudonormal or restrictive filling patterns, detected using CMD, are related to progressive LV dilation and predict cardiac death.

Rajagopalan et al. (Rajagopalan et al. 2001) used CMD to differentiate between constrictive pericardial heart disease and restrictive cardiomyopathy. Their results, obtained using the Duval-Garcia method, indicated a progressively slower v_p in patients with restrictive cardiomyopathy, compared with patients with constrictive pericarditis. Accordingly the observed time delay, obtained using the approach of Stugaard, was longer in patients with restrictive cardiomyopathy. In contrast, the slope of the black-to-color transition, as proposed by Brun et al. (46), was not significantly different between the two groups.

As the main determinants of PWD peak E-velocity are left atrial pressure (LAP) and LV relaxation, several authors propose the ratio of E and v_p as an index of left atrial pressure (LAP), LV end-diastolic pressure or pulmonary capillary wedge pressure (PCWP) (Firstenberg et al. 2000a, Garcia et al. 1997, Gonzalez-Vilchez et al. 1999, Nagueh et al. 1996, Nagueh et al. 1999). Hereby, v_p is believed to correct for the load-dependency of E. All studies propose a linear relationship of the form:

$$p = \alpha \cdot \frac{E}{v_p} + \beta \qquad \text{[Eq. 4.2]}$$

where p is filling pressure and α and β are fitting constants. Table 4.4 summarises these findings. Overall a moderate to excellent correlation is reported (r = 0.67-0.87).

Table 4.4: Non-invasive estimation of filling pressure using E/v_p

Population	Method	α	β	r	Reference
Atrial fibrilation	Brun	NA	NA	0.65	(Nagueh et al. 1996)
MI	Duval-Garcia	5.27	4.6	0.80	(Garcia et al. 1997)
HCM	Brun	5.28	4.5	0.67	(Nagueh et al. 1999)
miscellaneous	Duval-Garcia	NA	NA	0.62	(Gonzalez-Vilchez et al. 1999)
healthy volunteers	Duval-Garcia	0.039	1.02	0.81	(Firstenberg et al. 2000a)

α, β: linear regression model parameters; r: correlation coefficient; MI: myocardial infarction; HCM: hypertrophic cardiomyopathy; NA: not available

Firstenberg et al. (Firstenberg et al. 2000a) reported a relationship between load and E/v_p in a population of healthy volunteers. In contrast, Garcia et al. (Garcia et al. 1997) has studied a heterogeneous population of patients. For those two populations, the slope of the relationship between load and E/v_p differs significantly. This is an indication that, besides filling pressure, also other covarying LV properties such as relaxation and compliance may interfere in the relationship between load and the E/v_p ratio (De Mey et al. 2000a).

4. Pressure Imaging

4.1. Background

The Navier-Stokes equations are a complex set of coupled differential equations, dictated by the principles of conservation of mass and momentum, and are governing flow velocities. In the situation of the analysis of a central inflow streamline of LV filling, the Navier-Stokes equations can be simplified considerably to the 1D Euler equation (Vandervoort et al. 1993):

$$\frac{\partial p}{\partial s} = -\rho\left[\frac{\partial v}{\partial t} + v \cdot \frac{\partial v}{\partial s}\right] \qquad \text{[Eq. 4.3]}$$

where v(s,t) is velocity at time t and distance s along the streamline, p is local pressure, and ρ is blood density. Thus local pressure gradients, $\partial p/\partial s$, can be calculated directly from velocities along a streamline. The calculation of the partial derivatives of Equation 4.3 can be visualised and schematically represented (Greenberg et al. 1995). Figure 4.7 shows this representation for a CMD image of LV filling. The representation for $\partial v/\partial t$ (time dependent variation of v for all positions along s) shows first an acceleration (in red), followed by a deceleration (in blue). In the spatial direction ($\partial v/\partial s$) acceleration is positive in the region of the mitral valve (bottom of the image, blue color) and deceleration is observed in the upper part of the LV.

4.2. Transvalvular Pressure Gradients

In daily clinical practice, for most stenotic and regurgitant orifices, the simplified Bernoulli equation is commonly used to estimate a pressure difference from measured velocities (Hatle and Angelsen 1985):

$$\Delta p = \frac{1}{2}\rho \cdot v^2 \qquad \text{[Eq. 4.4]}$$

where p is pressure (in Pa), ρ density (in kg/m³) of blood and v velocity (in m/s). In this equation, the unsteady flow component, the energy losses by turbulence and friction, and the gravitational component are neglected, only retaining the steady component. Filling in the value of the density of blood at 37° (1060 kg/m³) and converting pressure from Pa to mmHg (0.133 Pa = 1 mmHg) results in the

equation $\Delta p=4.v^2$. When flow through a normal mitral valve is considered, the assumptions, needed for application of the simplified Bernoulli equation, are not met because of the larger amount of fluid passing through the orifice, yielding a contribution of the unsteady component equalling the steady component. Several authors have addressed the importance of the unsteady component and the according limitations of the simplified Bernoulli equation using in vitro, numerical and experimental studies (Baumgartner et al. 1999, De Mey et al. 2001b, Nakatani et al. 2000, Pasipoularides et al. 1987, Verhaaren et al. 2001).

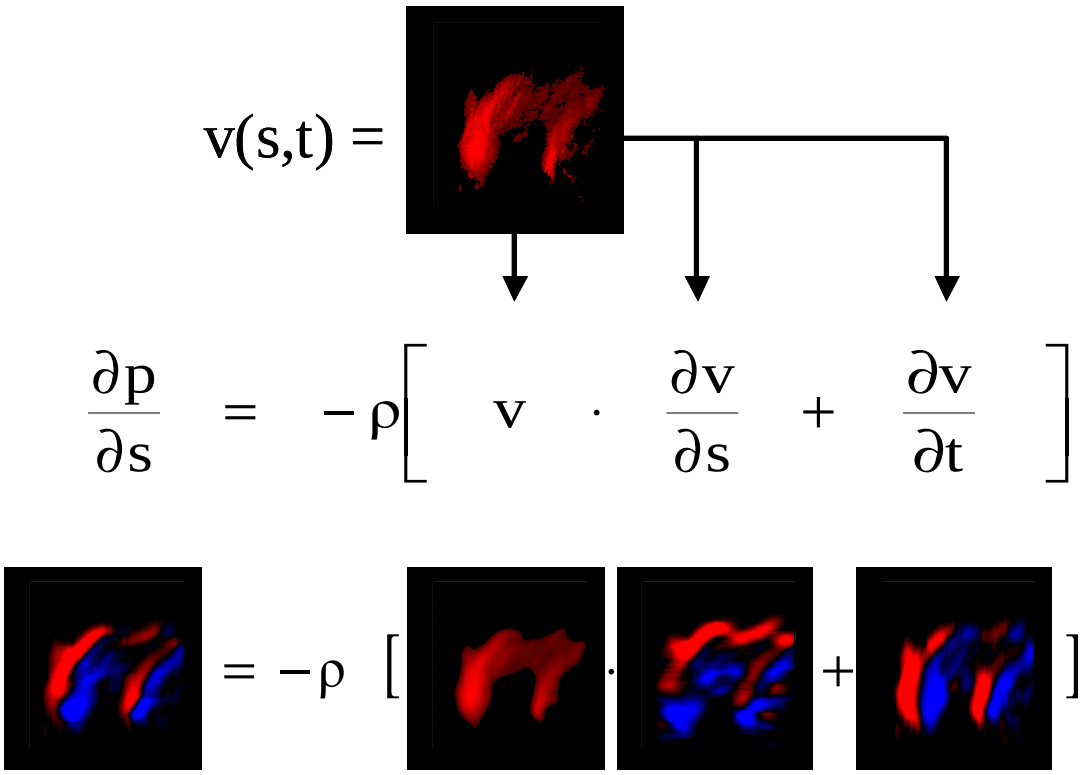

Figure 4.7: Visual representation of the principles of the pressure imaging technique. Using the spatiotemporal velocity image v(s,t) as an input, spatial (∂v/∂s) and temporal (∂v/∂t) partial derivatives are calculated and the time dependent pressure gradients (∂p/∂s) along the base-apex axis of the LV is reconstructed.

Using CMD echocardiography, by integrating the Euler equation (Eq. 4.3) the unsteady component of the pressure drop can be included:

$$\Delta p = \frac{1}{2}\rho \cdot (v_{LA}{}^2 - v_{LV}{}^2) + \rho \int_{LA}^{LV} \frac{\partial v}{\partial t} ds \qquad \text{[Eq. 4.5]}$$

The use of CMD echocardiography for the estimation of pressure gradients across non-restrictive valves by integrating the Euler equation (unsteady Bernoulli equation, equation 4.5) is validated in our laboratory in a hydraulic model of the left heart, consisting of two elastic chambers separated by a prosthetic biological mitral valve. Simultaneously, high-fidelity LA and LV pressure tracings and Doppler measurements were performed. Water-glycerine mixtures, equalling the viscosity of blood, were used as a testfluid. Pressure drops across the mitral valve were calculated using both the simplified Bernoulli equation and the unsteady Bernoulli equation. Results are illustrated in figure 4.8, confirming that the incorporation of the unsteady flow component using CMD echocardiography, yields a more accurate estimation of the transvalvular pressure gradient, compared to the simplified Bernoulli equation.

Recently, the feasibility of including the unsteady component in the calculation of pressure drops over non-restricted orifices using CMD echocardiography is demonstrated in dogs (Greenberg et al. 1996) and humans (Firstenberg et al. 2000b, Isaaz 2000).

4.3. Intraventricular Pressure Gradients

The pressure imaging technique can be extended from transvalvular pressure gradients to intraventricular pressure gradients. Intraventricular pressure gradients during relaxation and filling of the LV were first described by Ling et al. (Ling et al. 1979). Courtois et al. (Courtois et al. 1988) observed a significant subbasal-apical early diastolic pressure gradient along the LV inflow tract with minimum pressure in the apex speculating suction of the blood toward the LV apex. In contrast, using a 1D numerical model, Verdonck et al. (Verdonck et al. 1999), and using an axisymmetric 3D model, Vierendeels et al. (Vierendeels et al. 2000) demonstrated that such pressure gradients are not a rigorous proof of elastic recoil.

Intraventricular pressure gradients yield potential important clinical usefull information. In a study of Courtois et al. (Courtois et al. 1988), during acute ischemia, pressure gradients diminished, making it a possible marker for ischemia in clinical practice. Recently, Firstenberg et al. demonstrated abrupt improvements in diastolic intraventricular gradients following myocardial revascularization (Firstenberg et al. 2001).

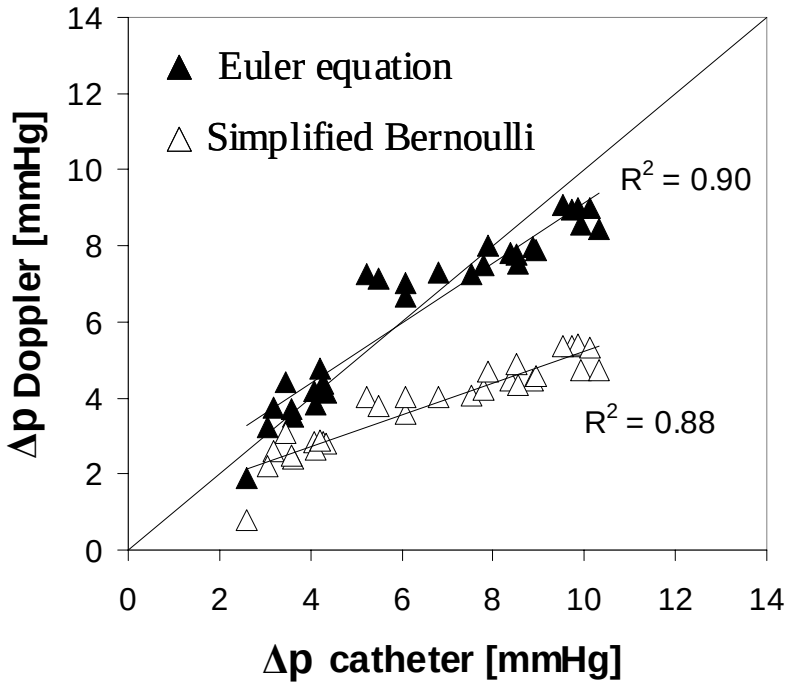

Figure 4.8: Validation of CMD derived pressure drops in a hydraulic model of the left heart. Invasive measured pressure drops (x-axis, mmHg) versus Doppler derived pressure gradients calculated using the simplified Bernoulli equation (open triangles) and integration of the Euler equation (unsteady Bernoulli equation, closed triangles).

5. Future Research

5.1. Future Research in Flow Propagation Velocity

Nonetheless much basic research is already performed, the influences of LV properties on the LV filling pattern remains a matter of debate. In the last two decades, numerical and hydraulic models have proven to be very helpful in understanding the detailed physiological underpinnings of the transmitral filling pattern as recorded using PWD echocardiography. Analogue, the development of new or the refinement of existing numerical and hydraulic models that can isolate the influence on the LV filling pattern of individual changes in LV properties can be very useful in unravelling the individual contributions of relaxation, compliance and filling pressure in changes of v_p and the E/v_p ratio. Preliminary steps in this direction are already undertaken. (De Mey et al. 2000b).

Whereas in an experimental setting vp measurements are used by several research groups, the daily application in a clinical setting remains difficult, mainly because of a lack in standardization and automation, yielding large operator dependent variability's. However, the incorporation of standardized and automated algorithms in the analysis tools, provided with the contemporary sonographers, could reduce operator dependent variability and catalyze the introduction of this diagnostic tool in clinical practice.

5.2. Future Research in Pressure Imaging

Intensive research on LV filling using transmitral flow profiles has resulted in several non-invasive approaches for the quantification of LV properties including relaxation and compliance, relying on approximations of the unsteady component of the pressure drop (Garcia et al. 2001, Scalia et al. 1997). The incorporation of the unsteady pressure component can only contribute to an improvement of those methods.

Recently Milde et al (Milde et al. 2000) introduced the ventricular diastolic impedance Z as an index of global diastolic function. Global diastolic impedance was defined as LV pressure over transmitral flow (Q) during early-rapid filling (E-wave). Simultaneous Doppler E-wave images and micromanometric ventricular pressures were used for calculation of diastolic impedance Z. The

index Z differentiated between "impedance-matched" (normal diastolic function) and "impedance-mismatched" (abnormal diastolic function) subjects in 19 subjects (10 normal, 9 abnormal). Theoretically, longitudinal impedance of left ventricular inflow can be derived non-invasively from color Doppler M-mode images. Although the feasibility of this technique in a hydraulic model is already demonstrated (De Mey et al. 2000b), continuous research remains necessary to unravel the physiological determinants of this index.

The investigation of intraventricular pressure gradients is very complicated because it requires complex instrumentation of models, e.g. using multiple high fidelity pressure transducers. This complex setting also limits the application in clinical practice. Recently, however, Greenberg et al. (Greenberg et al. 2001) validated the ability of CMD to quantify these very small pressure gradients and demonstrated their change induced by β-adrenergic stimulation. The possibility of non-invasively determining intraventricular pressure gradients will enhance research possibilities in this field and opens a track for applications in clinical practice.

6. Conclusion

CMD echocardiography has been shown to be a clinical valuable tool for assessing diastolic function, especially in making a distinction between normal and pseudonormal filling patterns as well as in the assessment of left atrial pressure. Moreover the CMD technique has a high potential for new applications in the field of pressure imaging. In both fields, the use of automated software is mandatory. With the ever increasing capacity of computer power, the incorporation of user friendly analysis software on the commercial available sonographers should become reality.

Acknowledgements

S De Mey is a recepient of grant IWT-971096 of the Flemish institute for the promotion of scientific-technological research in industry.

Part II: Methodology

CHAPTER 5

Assessment of the Time Constant of Relaxation: Insights from Simulations and Hemodynamic Measurements †

† The content of this chapter has been published in Am J Physiol (2001);280:2936-2944:
Assessment of the time constant of relaxation: insights from simulations and hemodynamic measurements.
S. De Mey, JD Thomas, NL Greenberg, PM Vandervoort, PR Verdonck.

Abstract

The objective of this study was to use high-fidelity animal data and numerical simulations to gain more insight into the reliability of the estimated relaxation constant, derived from left ventricular pressure decays, assuming a monoexponential model with either a fixed zero or free moving pressure asymptote. Comparison of the experimental data with the results of the simulations demonstrated a trade off between the fixed zero and the free moving asymptote approach. The latter method more closely fits the pressure curves and has the advantage of producing an extra coefficient with potential diagnostic information. On the other hand, this method suffers from larger standard errors on the estimated coefficients. The method with fixed zero asymptote produces values of the time constant of isovolumic relaxation (τ) within a narrow confidence interval. However, if the pressure curve is actually decaying to a nonzero pressure asymptote, this method results in an inferior fit of the pressure curve and a biased estimation of τ.

1. Introduction

The ability to quantify left ventricular (LV) relaxation rate in normal and pathological conditions is important in investigating myocardial pump function. Despite advances in the noninvasive assessment of relaxation (Nagueh et al. 1997), invasive measurement of the ventricular relaxation rate during isovolumic relaxation remains the “gold standard”. Such invasive parameters include the first derivative of LV pressure with respect to time during isovolumic relaxation (dP/dt) and the time constant of isovolumic relaxation (τ).

The time course of the fall in LV pressure during isovolumic relaxation has been modeled using a monoexponential function with three parameters, described in equation. 5.1 as follows:

$$p(t) = (p_0 - p_\infty) \times e^{-t/\tau} + p_\infty \qquad \text{[Eq. 5.1]}$$

where p(t) is LV pressure as a function of time (in mmHg), t is time (in ms), p_∞ is the asymptote to which LV pressure declines (in mmHg), and p_0 is LV pressure (in mmHg) at peak negative dp/dt (where t = 0 ms). Measured pressure data during isovolumic pressure decay is fitted to this model to obtain an estimation of τ (in ms).

Initially, equation 5.1 was linearized to avoid difficult calculation. Weiss et al (Bernardi et al. 1985, Weiss et al. 1976) further simplified the situation by assuming a zero asymptote, yielding the reduction of a three-parameter monoexponential model to a two-parameter model

$$p(t) = p_0 \times e^{-t/\tau} \qquad \text{[Eq. 5.2]}$$

The assumption of a zero asymptote allows linearization by taking the natural logarithm of both sides of equation 5.2, from which linear regression analysis can be used to determine the least mean squared error (MSE) solution for τ and P_0. Although useful physiological insight has been gained from this approach, a disadvantage of the logarithmic transformation is to give undue weighting to data points (and noise) at low pressures.

A refinement of Weiss' log transformation approach is to substitute the differentiated monoexponential function back into equation 5.1, which allows linearization without the assumption of a zero asymptote (Raff and Glantz 1981). Again, linear regression analysis can be used to obtain an estimate of τ but the differentiation process is very sensitive to noise in the signal.

The improved performance of contemporary computer hardware and software allows direct solution of equation 5.1 using nonlinear least squares parameter estimation techniques, most commonly the Levenberg-Marquardt method. The nonlinear technique allows for an accurate estimation of p_0 and τ both with and without the assumption of a zero asymptote. The use of this nonlinear technique for calculation of τ was initially validated by Bernardi et al (Bernardi et al. 1985).

With nonlinear techniques widely available, they have largely superceded both the log transform and differentiation methods for solving equation 5.1. Nevertheless, the issue of choosing a two- or three-parameter model is still an open question because conflicting results have been reported when using the three-parameter model (free moving asymptote) versus the two-parameter model (zero pressure asymptote assumed) for calculation of τ. A key issue is the trade off between accuracy of fit to the observed data (which should be better with three parameters) and the confidence intervals of the derived parameters (which may worsen with three parameters if there is significant collinearity between them). The objective of this study, therefore, was to use high-fidelity animal data and numerical simulations to gain more insight into the reliability of the estimated relaxation constant when assuming either a zero or free moving pressure asymptote.

2. Methods

LV pressure decay data obtained from both an animal experiment and Monte Carlo simulations were analyzed. τ was determined using the nonlinear Levenberg-Marquardt technique both with (two-parameter exponential model; LM_2) and without (three-parameter exponential model; LM_3) the assumption of a zero pressure asymptote. The differences between the two approaches were then compared for goodness of fit to the pressure curves and the confidence intervals of the estimated τ.

2.1. Animal Experiment.

The investigation conformed to the Guide for the Care and Use of Laboratory Animals (NIH Publication 1996) published by the US National Institutes of Health and was approved by the Animal Research Committee of The Cleveland Clinic Foundation. Eight healthy adult mongrel dogs of either sex weighting 29.7 ± 7.4 kg were studied. The dogs were anesthetized with 25 $mg \cdot kg^{-1}$ intravenous pentobarbital sodium, and anesthesia was maintained throughout the experiments with additional aliquots of pentobarbital sodium. After the dogs underwent tracheal intubation, positive pressure mechanical ventilation was instituted using room air. A micromanometer catheter (Millar, Houston, TX) was introduced into the left atrium (LA) through the LA appendage and positioned across the mitral valve with the pressure sensor in the LV. LA pressure was recorded by an additional single sensor catheter. Pressure and electrocardiogram signals were digitally acquired with 1-ms/12-bit resolution using a multifunction input-output board (AT-MIO-16, National Instruments, Austin, TX) interfaced with a computer workstation (Intel 80486 PC) using customized software developed using LabView version 5.0 (National Instruments). Data acquisition was performed at baseline (for each dog experiment), during isoproterenol infusion (for 6 dog experiments), and during esmolol infusion (for 3 dog experiments). Baseline runs were initiated after allowing sufficient time for hemodynamics to stabilise before starting the experiment. Esmolol or isoproterenol medication runs were initiated after completion of a satisfactory number of baseline acquisition runs. Isoproterenol was infused at 0.025-0.4 $\mu g \cdot kg^{-1} \cdot min^{-1}$ intravenously, and data acquisition runs were initiated after sufficient washin time for an appropriate heart

rate response and hemodynamics to stabilize. Similarly, esmolol was infused at 0.2-0.3 $mg \cdot kg^{-1} \cdot min^{-1}$ intravenously, with data acquisition after hemodynamic stabilization. For the eight dogs, 45 recordings during baseline, 12 recordings during isoproterenol infusion, and 8 recordings during esmolol infusion are registered, with each recording containing ~7 consecutive heartbeats. We thus captured 340, 94 and 56 pressure decays at baseline and during isoproterenol and esmolol infusion, respectively. Post acquisition numerical analysis of raw pressure data was performed using another custom numerical analysis program developed in LabView. In this study, dp/dt was calculated to define the period of isovolumic relaxation as the time period between maximum negative pressure change and the first LA to LV pressure crossover. τ was determined from the pressure curves with the use of the nonlinear Levenburg-Marquardt technique both with and without the assumption of a zero pressure asymptote. With each derivation of the coefficients a MSE value was calculated as a measure of goodness-of-fit of the specific model to the pressure data (Equation 5.3) as follows

$$MSE = \frac{1}{N} \cdot \sum_{i=0}^{N-1} \left(\frac{y_i - f(x_i; a_1 ... a_M)}{\sigma_i} \right)^2 \qquad \text{[Eq. 5.3]}$$

In this equation, (x_i,y_i) are the input data points, $f(x_i;a_1...a_M) = f(X,A)$ is the nonlinear function (where $a_1...a_M$ are coefficients), N the number of input data points, and σ_i the variance. To analyze the efficiency of the different models in estimating τ, the accompanying standard error for each derivation of τ was calculated. Method dependent differences were analyzed.

2.2. Monte Carlo Simulation

One hundred instances of 125 different diastolic pressure curves were created with the use of Monte Carlo simulation in the following manner. First, an exact monoexponential curve was constructed using equation 5.1 with the coefficients p_0 = 70 mmHg, τ = 60 ms and p_∞ = 0 mmHg. By adding Gaussian noise (mean value 0 mmHg and standard deviation 0.4 mmHg) randomly, 100 “data curves” were created from this exact monoexponential pressure decay. The simulation of one pressure curve is illustrated in figure 5.1, showing the exact monoexponential curve (A), the Gaussian noise (B), and the simulated curve (C). From each of the 100 data sets, τ and P_0 were estimated using LM_2, and τ, P_0 and P_∞ were estimated

using LM_3. With each derivation of the coefficients, the MSE value (Equation 5.3) was calculated as a measure of goodness-of-fit of the specific model to the simulated pressure data. The estimated coefficients from the 100 data curves with accompanying standard error were compared with the actual coefficients that produced the original pressure curve. To analyze a range of parameter values, the simulation was repeated with p_0 varying from 70 mmHg to 110 mmHg in steps of 10 mmHg, τ varying from 40 ms to 120 ms in steps of 20 ms and p_∞ varying from -5 mmHg to +5 mmHg in steps of 2.5 mmHg. Thus a total of $5 \times 5 \times 5 = 125$ combinations of the coefficients are simulated, yielding the analysis of 12,500 pressure curves. The results were compared with the findings of the dog experiment.

2.3. STATISTICS

All statistics were performed using SPSS version 9.0 (Chicago, Illinois). Values are means ± standard deviation. Normally distributed variables, calculated using the different models, were compared using repeated-measures ANOVA. Post hoc testing was performed using either a Bonferroni t-test (equal variances assumed) or a Dunnett's t-test (equal variances not assumed). Nonnormally distributed variables were compared using the nonparametric Friedman test for related variables. The level of significance was set at a P value of 0.05.

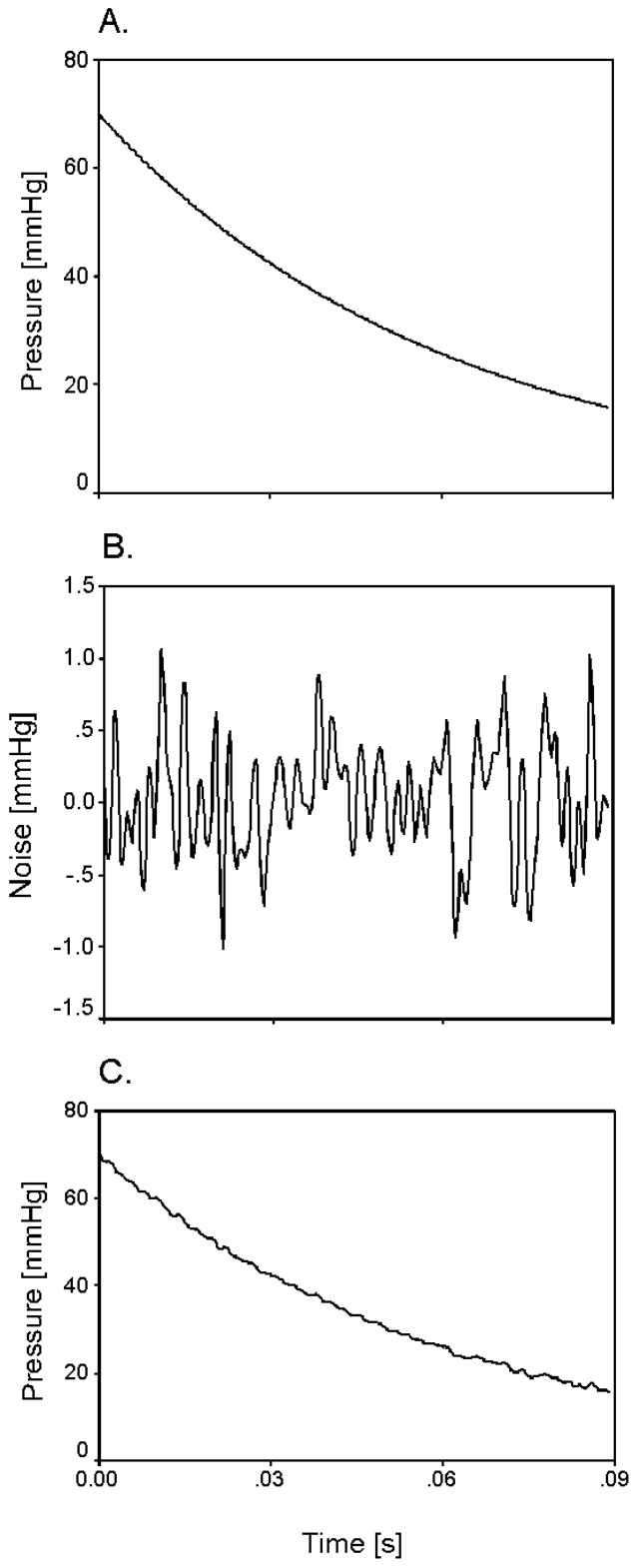

Figuur 5.1: Monte Carlo simulation of a pressure curve: exact monoexponential curve (**A**), Gaussian noise (**B**), and simulated monoexponential curve containing noise (**C**).

3. Results

3.1. ANIMAL EXPERIMENT.

Table 5.1 summarizes the results of the determinations of τ in the dog experiment using the nonlinear Levenburg-Marquardt method with a zero pressure asymptote (two parameter model, LM_2) and a nonzero moving asymptote (LM_3) for the baseline measurements and during infusion of isoproterenol and esmolol.

Table 5.1: Estimation of τ using a fixed zero asymptote monoexponential model (LM_2) and a free moving monoexponential model (LM_3) under baseline conditions, during isoproterenol infusion and during esmolol infusion.

			τ	**SE**	**τ_{min}**	**τ_{max}**	**Range**	**MSE**	**p_∞**
			[ms]	**[ms]**	**[ms]**	**[ms]**	**[ms]**	**[-]**	**[mmHg]**
Baseline	LM_2	mean	67.8	0.6	53.2	132.4	79.2	0.90	-
		stdev	15.5	0.3	-	-	-	0.75	-
	LM_3	mean	83.5*	3.4*	59.2	110.6	51.4	0.17*	-7.1
		stdev	11.4	1.9	-	-	-	0.33	4.8
Isopril	LM_2	mean	50.4‡	0.7	39.7	57.3	17.5	0.27	-
		stdev	5.6	0.4	-	-	-	0.33	-
	LM_3	mean	48.8‡	3.8*	37.0	67.1	30.1	0.09†	0.5‡
		stdev	9.6	3.3	-	-	-	0.09	4.1
Esmolol	LM_2	mean	113.1‡	0.93	90.7	138.1	47.4	0.18	-
		stdev	16.7	0.3	-	-	-	0.12	-
	LM_3	mean	108.7‡	4.8*	77.5	142.0	64.6	0.11†	0.9‡
		stdev	21.7	1.7	-	-	-	0.07	4.6

τ, time constant of isovolumic relaxation; SE, standard error; τ_{min} and τ_{max}, minimum and maximum τ, respectively; MSE, mean squared error; p_∞, asymptote to which left ventricular pressure declines; Levenberg-Marquardt model with 2 and 3 parameters, respectively; SD, standard deviation. * $p < 0.001$ vs. LM_2, † $p < 0.05$ vs. LM_2, ‡ $p < 0.001$ vs. baseline.

The mean values for τ are the result of averaging the calculated τ values, obtained from LV pressure recordings using LM_2 and LM_3. Method-dependent differences were observed. At baseline, τ values obtained with LM_2 were consistently shorter than the values obtained with LM_3 ($p < 0.001$), whereas during either isoproterenol or esmolol infusion, τ values obtained with LM_2 were consistently higher than the values obtained with LM_3. LM_3 most closely fits the pressure

decays, as reflected by the significant difference in MSE between original and fitted pressure decays at baseline and during isoproterenol and esmolol infusion ($p < 0.001$). In contrast, however, the standard error of the estimate was significantly higher when τ is calculated using LM_3 compared with LM_2 at baseline as well as during isoproterenol and esmolol infusion ($p < 0.001$).

LM_3 showed that p_∞ significantly increased with isoproterenol and esmolol infusion compared with baseline values. For both LM_2 and LM_3, τ decreased with isoproterenol and increased with esmolol infusion ($p < 0.001$). However, the relative change compared with baseline values for both isoproterenol and esmolol infusion was different when using LM_2 compared with LM_3. For LM_2, the infusion of isoproterenol resulted in a decrease of τ of 26%, whereas for LM_3 the decrease of τ was 42%. With the use of LM_2, the infusion of esmolol resulted in an increase of τ of 67%, whereas LM_3 resulted in an increase of τ of 30%.

3.2. MONTE CARLO SIMULATION

Table 5.2 shows the results from a representative 2 of the 125 pressure simulations (τ = 60 ms, p_0 = 70 mmHg, and p_∞ = 0 mmHg, and τ = 60 ms, p_0 = 70 mmHg, and p_∞ = -2.5 mmHg). In these and all other simulations, the standard error of the τ estimates were significantly smaller for the zero asymptote model (LM_2) compared with the moving asymptote model (LM_3) ($p < 0.001$).

First, τ, p_0 and p_∞ were determined from 100 pressure decays created with Monte-Carlo simulation starting from a monoexponential curve using the Levenburg-Marquardt technique with a fixed zero asymptote (LM_2) and a free moving asymptote (LM_3). The results are shown in Table 5.2. Both methods had a comparable MSE. For each method, the mean values of the calculated coefficients were a good approximation of the exact coefficients. However, the estimate of τ calculated using LM_3 had a larger standard error ($p < 0.001$). Figure 5.2A shows the regression between the calculated τ and the calculated p_0 for both LM_2 and LM_3. From this graph, it is obvious that, for this particular simulation, the nonlinear method with fixed zero asymptote (LM_2) approach is the better one because this approach provides the smallest confidence interval on the estimated coefficients.

Table 5.2: Monte Carlo simulation of the estimation of τ from pressure curves with coefficients τ = 60 ms, p_0 = 70mmHg and p_∞ = 0 mmHg and τ = 60 ms, p_0 = 70mmHg and p_∞ = -2.5 mmHg.

		LM_2		LM_3	
		mean	SE	mean	SE
p_∞ = 0mmHg	p_0 [mmHg]	70.00	0.28	69.93	1.14*
	τ [ms]	60.00	0.44	59.89	2.20*
	p_∞ [mmHg]	-	-	0.06	1.32
	mse [-]	0.15	0.02	0.15	0.02
p_∞ = -2.5mmHg	p_0 [mmHg]	70.43†	0.28	69.99*	1.14*
	τ [ms]	56.08†	0.41	60.05*	2.14*
	p_∞ [mmHg]	-	-	-2.53†	1.33
	mse [-]	0.20†	0.03	0.15*	0.02

* $p<0.001$ LM_3 vs LM_2; † $p<0.001$ p_∞ = -2.5mmHg vs p_∞ = 0mmHg

A second Monte Carlo simulation was done starting from a monoexponential curve with a negative pressure asymptote (p_∞ = -2.5 mmHg). Again τ, p_0 and p_∞ were estimated using LM_2 and LM_3 (cf. Table 5.2). In this second simulation, LM_3 had the smallest MSE ($p < 0.001$). Moreover, the mean values of the calculated coefficients, estimated using LM_3, were good approximations of the exact coefficients. The standard error on the estimated values was comparable to the standard error accompanying this method in the first simulation. By analogy with the first simulation, using LM_2 resulted in a significantly lower standard error for τ. However, LM_2 significantly underestimated the exact values of τ, as illustrated in Figure 6.2B, which shows the regression between the calculated τ and the calculated p_0 for both LM_2 and LM_3. Simulation of pressure curves with a positive instead of a negative pressure asymptote revealed an overestimation instead of an underestimation of τ when using the fixed zero asymptote approach.

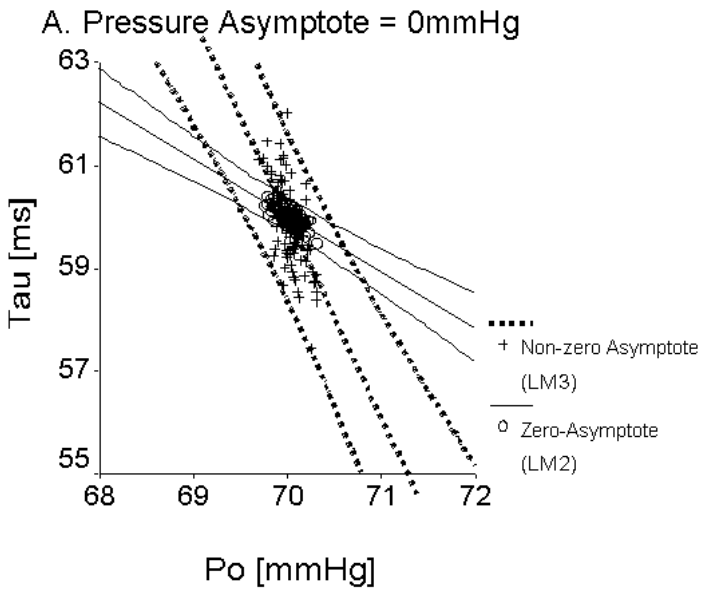

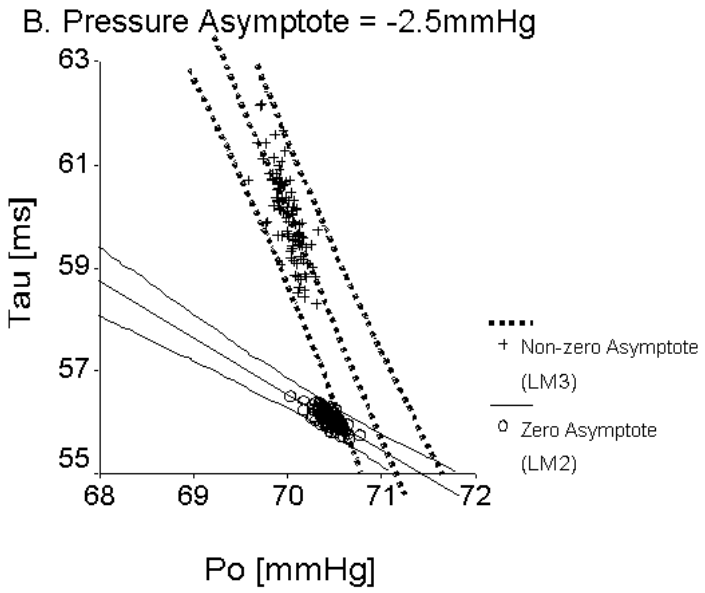

Figure 5.2: Regression of left ventricular (LV) pressure at peak negative first derivative of LV pressure with respect to time during isovolumic relaxation (p_0) and the time constant of isovolumic relaxation (τ) obtained from the analysis of 100 Monte Carlo simulations of an exponential pressure decay with coefficients τ = 60 ms, p_0 = 70 mmHg, and the asymptote at which LV pressure declines (p_∞) = 0 mmHg (**A**) and τ = 60 ms, p_0 = 70 mmHg and p_∞ = -2.5 mmHg (**B**). The analysis was performed using a monoexponential model with two parameters (LM_2 open circles, regression line and 99% prediction interval on the estimates in full lines) and LM_3 (crosses, regression line and 99% prediction interval in dashed lines).

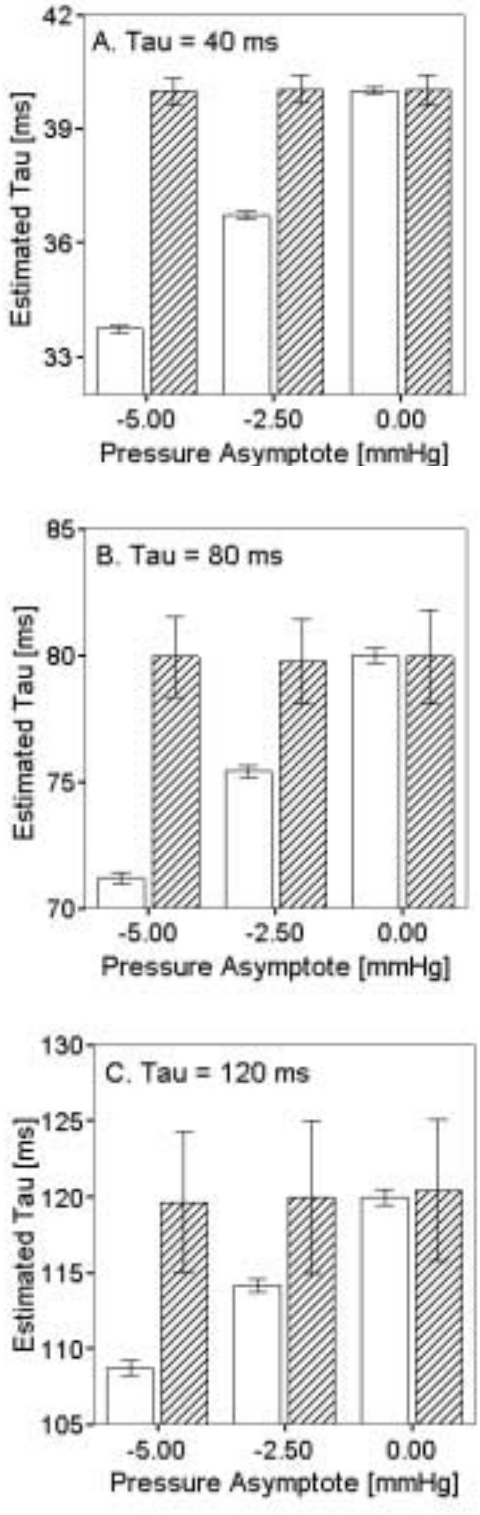

Figure 5.3: Monte Carlo simulation of the influence of the magnitude of the actual pressure asymptote on the estimation of τ using the fixed zero asymptote approach (LM_2) and the free moving asymptote method (LM_3). The estimated values (± SD) of τ using LM_2 (open bars) and LM_3 (hatched bars) for values of the pressure asymptote = 0, -2.5, and -5 mmHg are plotted for reference values of τ = 40 ms (**A**), 80 ms (**B**), and 120 ms (**C**).

The trade off between the magnitude of the variance on the estimated coefficients versus under/overestimation of the exact values is demonstrated in Figure 5.3 at p_0 = 70 mmHg and reference values for τ of 40 ms (A), 80 ms (B), and 120 ms (C). The plots are illustrating the method-dependent sensitivity of the estimates ($\tau \pm$ standard deviation) for variations in p_∞ between 0 and -5 mmHg. In the case of a zero asymptote, both methods estimate τ well because τ do not significantly differ from the reference values ($P > 0.05$). LM_2 has the smallest standard deviation compared with LM_3 ($p < 0.001$). However, with increasing absolute values of the pressure asymptote, the values obtained using LM_2 were moving away from the exact values. Independent of the magnitude of the pressure asymptote, LM_2 kept the smallest confidence interval ($p < 0.001$).

To evaluate the efficiency of the two different estimators of τ, on the basis of LM_2 and LM_3, respectively, a MSE value was calculated as $\mathrm{MSE} = (\mathrm{Variance} + \mathrm{Bias}^2)$ for each estimator (Wonnacot and Wonnacot 2000). This MSE was similar to the variance on an estimated coefficient except that it was measured around the true target rather than around the (possibly biased) mean of the estimator. Formally, we can compare two estimators by calculating the relative efficiency (RE) as the proportion of the two MSE values. The RE values comparing LM_2 and LM_3 for estimating τ are plotted in figure 5.4 for pressure asymptotes varying from -5 mmHg up to + 5mmHg and τ values ranging from 40 ms to 120 ms. Values for RE > 1 indicated a superior estimate of τ when using LM_3. Thus, in case of a zero pressure asymptote, LM_2 is always closer at estimating τ. However, with increasing positive or negative pressure asymptote and decreasing τ, LM_3 becomes superior.

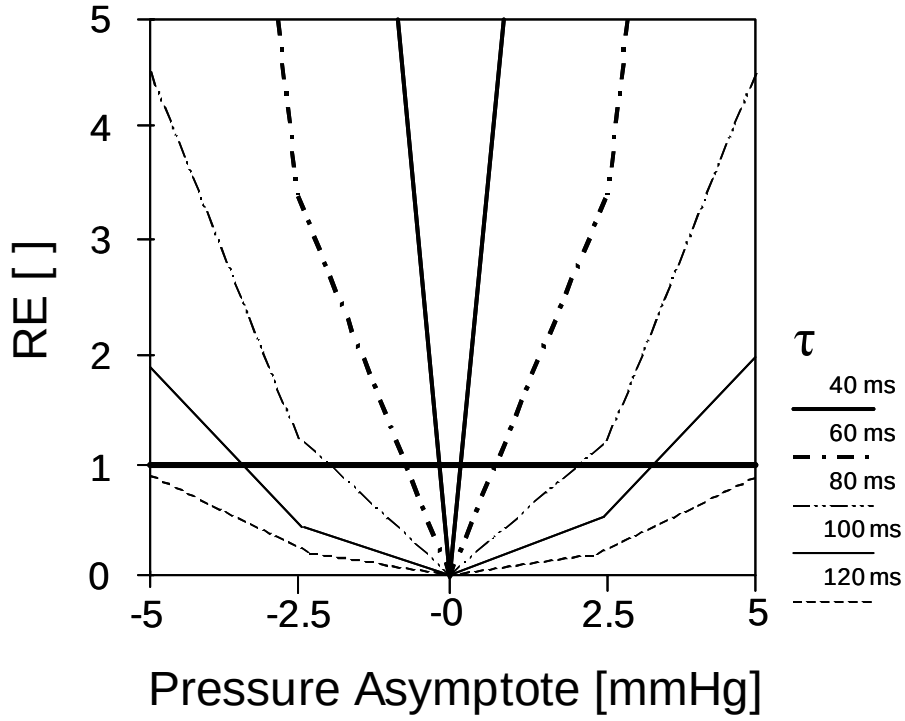

Figure 5.4: Monte Carlo simulation of the relative efficiency (RE, y-axis) of the estimators of τ using LM_2 and LM_3 for p_0 = 70 mmHg, P_∞ varying from -5 up +5 mmHg (x-axis), and τ varying from 40 to 120 ms. Values for RE > 1 are an indication for a superior estimate of τ when using LM_3.

4. Discussion

In this study we exclusively used nonlinear techniques for estimation of τ from pressure decays using a monoexponential model: 1) the nonlinear Levenberg-Marquardt method with a fixed zero pressure asymptote (LM_2), and 2) the Levenberg-Marquardt method with a variable pressure asymptote (LM_3). The two methods were chosen to observe for any divergence in the resultant τ.

Overall, both methods determined comparable values of τ for the data collected. The average values of the MSE when using LM_3 were smaller compared with the values obtained when using LM_2. The smaller MSE reflects a superior goodness-of-fit of LM_3 of modelling the experimental data compared with LM_2. The inferior fitting when assuming a fixed zero pressure asymptote not only provokes a larger MSE but also has an important consequence on the estimated τ values: whereas LM_3 always provides an unbiased estimation of τ, LM_2 results in a biased estimation of τ when analysing pressure decays with a nonzero pressure asymptote. The Monte Carlo simulation showed that in case of a negative (positive) pressure asymptote, using LM_2 leads to a significant underestimation (overestimation) of the exact coefficients. In the animal experiment, under baseline conditions, the τ values obtained with LM_2 were smaller compared with the values obtained using LM_3. In contrast, during either isoproterenol or esmolol infusion, τ values obtained with LM_3 were smaller compared with the values obtained using LM_2. According to the Monte Carlo simulations, this suggests a negative pressure asymptote and a significant underestimation of τ with LM_2 for baseline conditions and a positive pressure asymptote and a significant overestimation of τ for isoproterenol and esmolol. This was indeed confirmed by the values of the calculated pressure asymptotes using LM_3 (cf. table 5.1). Figure 5.5 shows the relationship between actual pressure asymptote and under/overestimation of the τ values using LM_2 in more detail. An excellent correlation (r^2=0.92, $p < 0.001$) was observed between the difference in τ calculated with LM_2 and LM_3 and the pressure asymptote as calculated using LM_3 for the animal data under baseline, and during isoproterenol and esmolol infusion. This correlation explains the differences in relative change of τ during drug infusion when using LM_2 compared with LM_3.

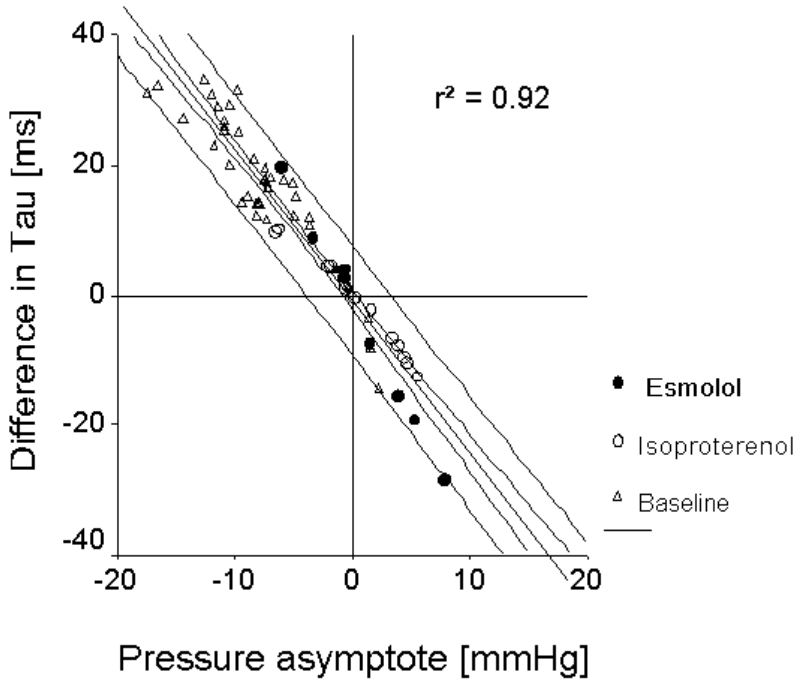

Figure 5.5: Regression between the method-dependent difference in τ and the pressure asymptote in the animal study.

In contrast to the superior MSE and the unbiased estimation of τ, a drawback of LM_3 is the larger standard error on the estimated coefficients. This is primarily the consequence of the increased degree of freedom and error propagation in the algorithm for determining τ when using a free moving asymptote. The trade off between the magnitude of the standard error on the estimates (smaller when using LM_2) and the closer fit that guarantees an unbiased estimation (when using LM_3) can be evaluated quantitatively by calculation of a MSE that combines the bias and standard error on the estimates. This calculation demonstrates for the simulated data that, in the case of a zero pressure asymptote, LM_2 always has a closer estimate of τ. However, with an increasing positive or negative pressure asymptote and decreasing τ, LM_3 becomes superior. This is also observed in the animal data. During drug infusion, the pressure asymptotes are small and, consequently, the bias on the estimates is small. The τ values obtained using either LM_2 or LM_3 did not significantly differ. In contrast, the standard error of the estimates was significantly smaller when using LM_2. At baseline, a significant

negative pressure asymptote was found and, as expected, the bias on the estimates was large. τ values obtained using either LM_2 or LM_3 were significantly different. The standard error of the estimates remained higher when using LM_3 compared with LM_2. With the use of the results of Table 5.1, we calculated the mean relative efficiency for the different groups. For the baseline data, the relative efficiency was 20.70, indicating that LM_3 provides the most reliable estimate. During isoproterenol infusion and esmolol infusion the mean relative efficiency became 0.22 and 0.85, which indicates that LM_2 provides the most reliable estimate.

The problem of choosing a two (fixed zero pressure asymptote assumed)- or three (free moving asymptote assumed)-parameter model is still a matter of debate because conflicting results are reported. Several authors (Bernardi et al. 1985, Martin et al. 1984, Takeuchi et al. 1985, Thompson et al. 1983) have demonstrated the use of a variable asymptote to be a more rigorous and physiologically rational method of modeling LV pressure decline during the isovolumic relaxation period. Bernardi and associates (Bernardi et al. 1985) demonstrated that the Levenberg-Marquardt algorithm with a variable asymptote is a most accurate method for modeling LV pressure decline during the isovolumic relaxation periods. Martin and colleagues (Martin et al. 1984) demonstrated that a variable asymptote method of determining τ was more sensitive to β-adrenergic blockade or stimulation than to drugs that altered cardiac loading conditions.

On the other hand, Yellin and colleagues (Yellin et al. 1986) demonstrated that τ determined from an exponential model using a fixed asymptote method is comparable with τ determined from an exponential model using a measured or best-fit asymptote. Yellin and colleagues (Yellin et al. 1986) further concluded that as long as it is consistently used in the same study, τ resulting from any method provides useful information related to diastolic function. Also, Kettunen and colleagues (Kettunen et al. 1986) advocate the use of a fixed zero asymptote method for practical, clinical use to determine τ. This recommendation is based on their observation that τ determined using a fixed asymptote method is comparable with τ determined using a variable asymptote method with the exception of conditions of β-adrenergic blockade or stimulation. The zero asymptote method

was advocated on the basis of a less complicated mathematical algorithm for most practical clinical purposes. Yamakado et al. (Yamakado et al. 1997) calculated τ with and without a pressure asymptote to investigate the influence of age on ventricular relaxation. No significant differences between the different approaches were observed. In contrast, Davis et al. (Davis et al. 1999) obtained opposite conclusions when analyzing ventricular relaxation rate using the zero or nonzero asymptote model.

Despite closer fitting of the pressure curves when using LM_3 and despite the bias accompanying LM_2, τ estimates with LM_2 may show better correlation with other physiological parameters than LM_3. This is demonstrated for the baseline animal data in figure 5.6, showing the regression between maximum negative dP/dt and τ when using LM_2 (A) and LM_3 (B). Although LM_3 better fit the pressure decays, the better correlation was obtained using LM_2 ($r^2 = 0.51$ vs. $r^2 = 0.45$). We speculate that this phenomenon is due to the biased estimates of τ with LM_2 for the analysis of nonzero asymptote pressure decays. This leads to over- or underestimation of τ and thus to a broader range of τ values, automatically enhancing the correlation.

In previous studies, linear methods were used to determine τ. We also calculated τ values under baseline conditions with linear regression, assuming a fixed zero pressure asymptote as proposed by Weiss et al. (Nagueh et al. 1997, Weiss et al. 1976). The results were compared with the results obtained using the Levenburg-Marquardt technique with zero pressure asymptote (LM_2). The τ values obtained using LM_2 were slightly, although significantly, larger (63.85 ± 17.12 ms vs. 67.83 ± 15.47 ms, $p < 0.001$) compared with the linear method. LM_2 also provided closer fits to the pressure decays, as reflected by the smaller MSE (2.59 ± 2.06 vs. 0.90 ± 0.75, $p < 0.001$).

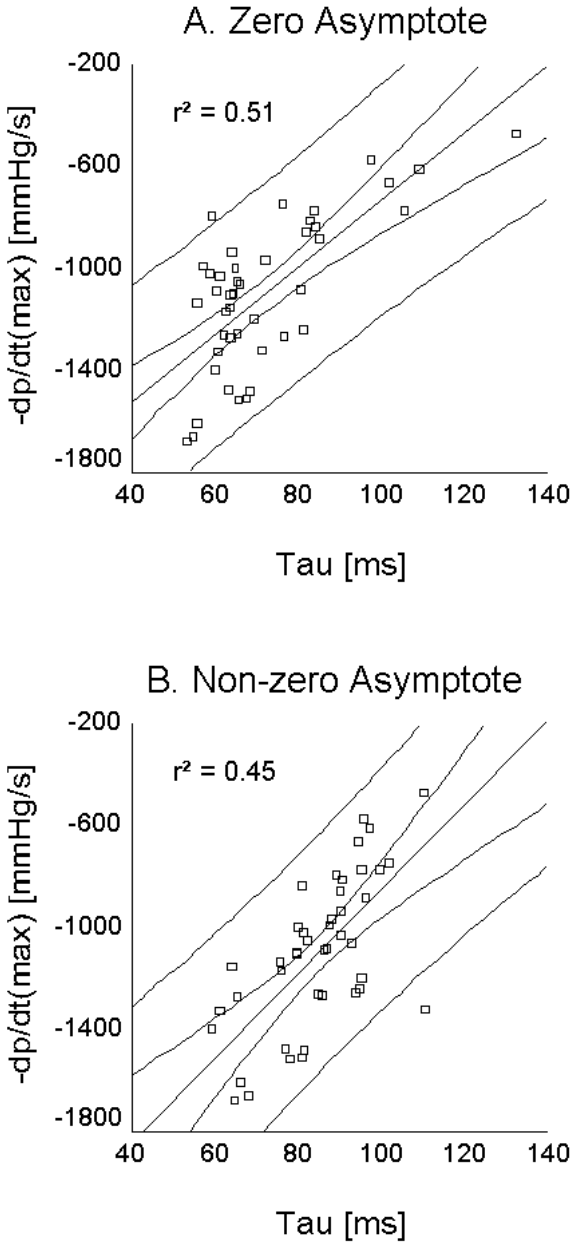

Figure 5.6: Regression between τ and maximum negative LV pressure change (dP/dt_{max}). τ was determined using LM_2 (**A**) and LM_3 (**B**).

It is generally accepted that the isovolumic relaxation period of the LV pressure curve is well approximated by a monoexponential decay model described by Eq. (1) (Bernardi et al. 1985, Davis et al. 1999, Kettunen et al. 1986, Martin et al. 1984, Raff and Glantz 1981, Takeuchi et al. 1985, Thompson et al. 1983, Weiss et al. 1976, Yamakado et al. 1997, Yellin et al. 1986) except in case of a

postextrasystolic LV isovolumic pressure decay (Courtois et al. 1997) and dilated cardiomyopathy (Senzaki et al. 1999). Alternative models have been proposed for fitting the isovolumic pressure decay (Matsubara et al. 1995, Senzaki et al. 1999). Recently Senzaki et al. (Senzaki et al. 1999) reported an improvement of quantitative analyses when using the following more complex hybrid logistic model of equation 5.4

$$p(t) = \frac{2 \times (p_0 - p_\infty)}{1 + e^{t/\tau}} + p_\infty \qquad \text{[Eq. 5.4]}$$

The hybrid logistic model provided more consistent data fits, especially in dilated cardiomyopathy, when a nonlinear relationship between dp/dt and p was observed. We also fitted this model to the pressure decays of the animal study. In accordance with the results reported by Senzaki et al. (Senzaki et al. 1999), the τ values obtained using this model (44.29 ± 5.38 ms) were significantly smaller compared with the values obtained with the other methods. Also, the mean pressure asymptote remained positive (1.82 ± 2.79 mmHg). Assuming an exponential model, the physical meaning of the τ value is the time needed for the pressure to decrease to 37% of its initial value. In contrast, when assuming a hybrid logistic model, the physical meaning of τ is the time needed for the pressure to decrease to 54% of its initial value. Therefore, the hybrid logistic function provides τ values of another magnitude compared with the monoexponential function. Thus comparing values obtained using the different models is difficult. The MSE (0.45 ± 0.35) was significantly ($p < 0.001$) larger compared with the values obtained using LM_3 (0.17 ± 0.33). Thus, in this animal experiment, the monoexponential model provides the closer fit. The standard error of the estimated τ (1.58 ± 1.60 ms) was, however, smaller ($p < 0.001$) compared with the standard error when using LM_3 (3.44 ± 1.85 ms). Therefore, the hybrid logistic method might be a valuable alternative for LM_3, especially for pressure decays with a nonlinear relationship between dp/dt and p.

In conclusion, in this study, Monte Carlo simulations of monoexponential pressure decays have provided a reference, allowing an objective comparison of different methods for estimation of the relaxation constant τ of LV pressure fall. Comparison of the experimental data with the results of the Monte Carlo

simulations demonstrated a trade off between the nonlinear Levenburg-Marquardt fixed zero approach on one hand and the nonlinear Levenburg-Marquardt method with a free moving asymptote on the other hand. The latter method closer fits the pressure curve and has the advantage of producing an extra coefficient (p_∞) with potential diagnostic information. On the other hand, this method suffers from larger standard errors on the estimated coefficients. The nonlinear Levenburg-Marquardt method with fixed zero asymptote produces values of τ within a narrow confidence interval. However, in case of a nonzero negative (positive) pressure asymptote, this method significantly underestimates (overestimates) the real values. Quantitative evaluation of the trade off between bias (when using LM_2) and the magnitude of the standard error on the estimates (larger when using LM_3) demonstrates that, in case of a zero pressure asymptote, LM_2 always has a closer estimate of τ. However, LM_3 becomes superior with an increasing pressure asymptote (both positive or negative) and decreasing τ.

Acknowledgements

We thank P. Segers for critically reviewing the manuscript. S. De Mey was a recipient of grant IWT-971096 from the Flemish Institute for the Promotion of Scientific-Technological Research in the Industry. This study was also supported in part by National Aeronautics and Space Administration grant NCC 9-60 (to J. D. Thomas), and by National Heart, Lung and Blood Institute grant R01-HL56688-01A1(to J. D. Thomas).

CHAPTER 6

How to Assess Left Ventricular Filling Flow Propagation Velocity: A Comparison of Four Different Methods[†]

[†] The content of this chapter has been submitted for publication to J Am Soc Echo:
How to Assess Left Ventricular Filling Flow Propagation Velocity: A Comparison of Four Different Methods.
S. De Mey, J De Sutter, NL Greenberg, JD Thomas, PR Verdonck.

Abstract

Introduction. Although the understanding of the different shapes of the early filling wave as represented in a color M-mode Doppler (CMD) image is still under discussion and subject of continuing research, several manual and (semi-) automated methods have been suggested for the quantification of the flow propagation velocity (v_p) of the early filling wave from a CMD image.

Aim. This study aims to analyse the differences between the several methods for quantifying v_p in more detail. Especially the differences in intra-observer, inter-observer and beat-to-beat variability are investigated.

Methods. Software for the automated analysis of v_p using four different methods (Duval-Garcia, Stugaard, Takatsuji and Greenberg) is developped. A group of ten consecutive patients is enrolled and pulsed wave Doppler (PWD) and CMD images are captured. Inter-observer, intra-observer, and beat-to-beat variabilities are analysed.

Results. Variabilities on PWD derived variables are lower compared to CMD derived variables (e.g. minimum intra-observer variability 1.73% (E), 21.75% (manual v_p), 3.45% (automated v_p, Stugaard)). Automated determination of v_p reduces intra-observer and inter-observer variabilities from respectively 22% and 26% for the manual measurement to a maximum of respectively 13% and 14% for the Duval-Garcia method. However, automated v_p determinations suffer from a high beat-to-beat variability to as much of 89% (Stugaard method), compared to 20% for the manual v_p determination.

Conclusion. Automated analysis allows a more objective assessment of v_p, especially for different observators. Taking observer variabilities and beat-to-beat variabilities into consideration, our results indicate that the method of Duval-Garcia results in determinations of v_p whith a higher degree of repeatability, compared to either manual or other automated methods..

1. Introduction

The traditional non-invasive approach to evaluate LV diastolic function uses pulsed wave Doppler (PWD) echocardiography with the sample volume positioned at the level of the mitral valve leaflet tips. PWD velocity measurements represent a temporal velocity variation throughout the cardiac cycle obtained at a single point in space. Velocity information more proximal or distal from the sampling point is not available. The limitations of the PWD transmitral velocity in making distinction between normal and pseudo-normal filling patterns are well known: in the pseudonormal stage an initial decrease in early filling (E) velocity is counterbalanced by an increased filling pressure provoking a normalisation of the E-velocity (Nishimura and Tajik 1997).

Color M-mode Doppler (CMD) echocardiography is introduced as a promising new technique that can differentiate between normal and pseudo-normal filling (Garcia et al. 1998). CMD echocardiography interrogates all the velocities along a scanline and provides a spatiotemporal velocity map with a temporal resolution of 5 ms, a spatial resolution of typical 0.3 mm and a velocity resolution of typically 3 cm/s (Thomas et al. 1997). Figure 6.1 shows a CMD image of LV filling, captured from an apical window with the scanline aligned with the central inflow in the LV.

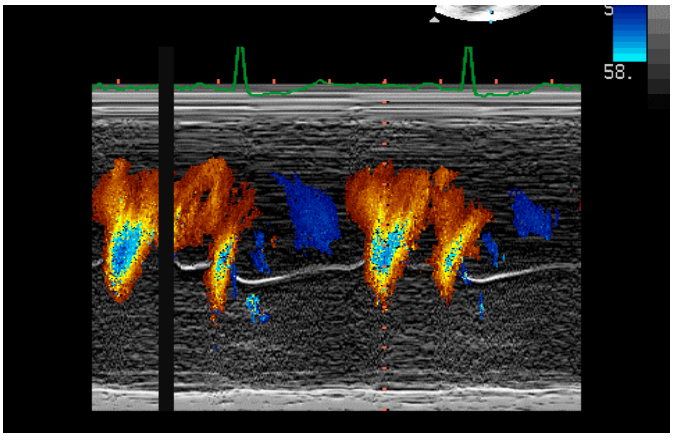

Figure 6.1: Color M-mode Image of LV filling

The shape of the filling waves in the spatiotemporal CMD images contains direct information about the filling mechanics of the left ventricle and thus indirect information about left ventricular function. From this shape the flow propagation velocity (v_p) is obtained and proposed as a marker for diastolic function. v_p is the speed by which the early filling wave travels from base to apex and can be associated with the slope of the E-wave in the CMD image. v_p has been show to be inversely related with the relaxation time constant in humans and animals (Garcia et al. 2000) and with LV stiffness in a numeric model (Vierendeels et al. 2000).

Although the understanding of the different shapes of the early filling wave as represented in a CMD image is still under discussion and subject of continuing research (for a detailed review see (De Mey et al. 2001a)), manual and several (semi-) automated methods have been suggested for the quantification of v_p of the early filling wave from a CMD image. This study therefore aims to analyse the differences between the different methods in more detail. Especially differences in intra-observer, inter-observer and beat-to-beat variabilities are investigated.

2. Methods

Software for the automated quantification of the v_p from a CMD image, based on different previous published methods is developed. This tool is used for the analysis of CMD images of patients admitted to the echocardiography laboratory of the Ghent University Hospital. The results are compared and used as a basis for further discussion.

2.1. Software Implementation of Different Methods

Software developed in Mathlab© (The mathworks, TX) was used to read and process digitally stored CMD images. The processing includes the removing of markers, replacement of aliased velocities and filtering of the images, next to the derivation of v_p in four different ways. Each approach is based on a previously published method as illustrated in figure 6.2.

Method 1. Originally, Brun et al. (Brun et al. 1992) defined v_p as the slope (in m/s) of the line segment identifying the black-to-color transition of the early filling wave. The segment begins with the onset of flow in the LV inlet and ends as far as possible in the left ventricular chamber. The line segment has to be reasonably linear. Because the black-to-color transition is not always clearly visible, Duval-Moulin et al. and Garcia et al. have modified this method by considering boundaries of equal velocities, so called isovelocity boundaries instead of black-to-color transitions (Figure 6.2 (A)). Typically the isovelocity contour of the first aliasing velocities (in case of manual analysis) or the isovelocity contour of 50% of the maximum velocity (in case of semi-automatic analysis) is addressed, starting at the position of the mitral valve, going typically four cm into the LV.

In this study, manual analysis of v_p is performed as described in this section and is referred to as $v_{p,manual}$. Also, in this study an automated Duval-Garcia method is implemented, considering the isovelocity contour of 50% of the maximum velocity that starts at the level of the mitral valve leaflets and goes up to 3.5 cm into the LV and referred to as $v_{p,Duval\text{-}Garcia}$.

Method 2. Stugaard et al. (Stugaard et al. 1993) measured the occurrence of the maximal velocities at several positions on the left ventricular base-apex axis. The

time-delay (TD, in ms) between occurrence of maximal velocity at the mitral leaflet tips and the maximal velocity further in the LV (typically 35mm away from the leaflet tips) is proposed as a characteristic for flow propagation (Figure 6.2 (B)). The ratio of the time delay (TD, in ms) and the spatial distance (S, in cm) between the first and last position is proposed as a normalised characteristic for v_p. The dimension of this normalised characteristic is the reciprocal of a velocity (ms/cm). Our automated algoritm determines the time delay between the maximal velocities occuring at the mitral valve leaflet tips and a position, 3.5 cm further in the LV.

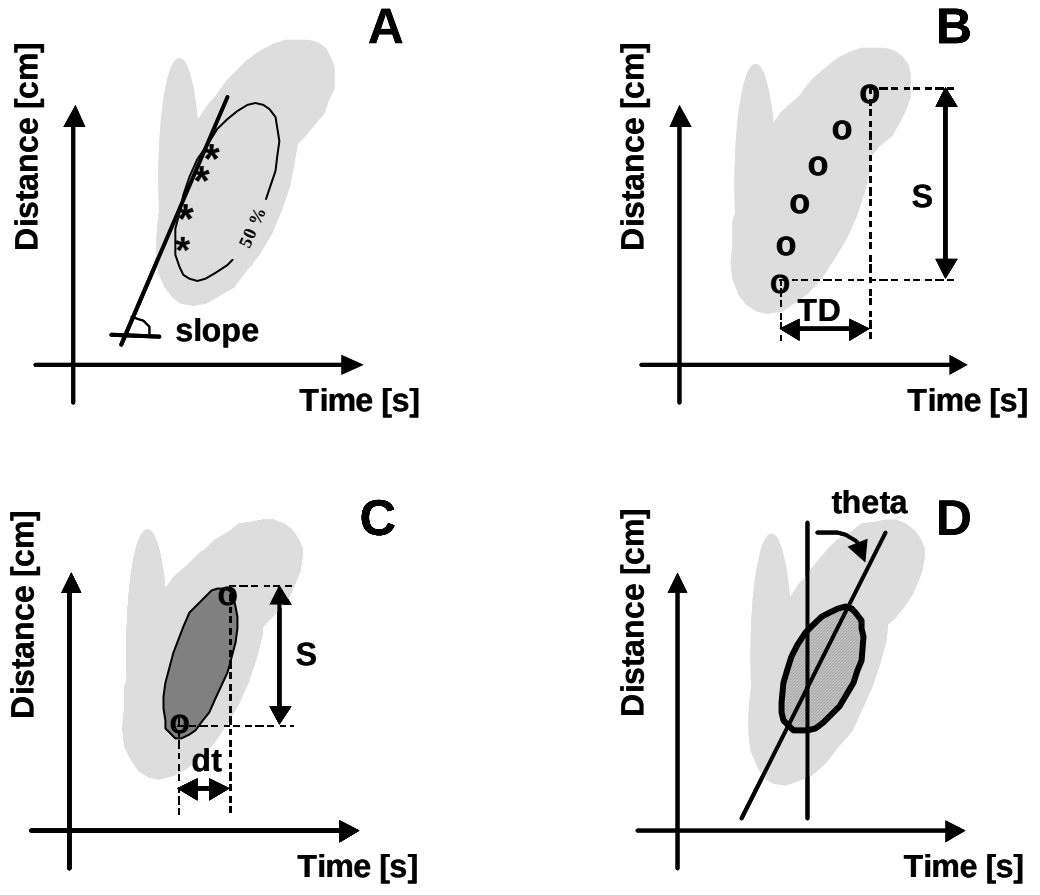

Figure 6.2: Four different methods for the quantification of flow propagation velocity. **(A)** Duval-Garcia. **(B)** Stugaard. **(C)** Takatsuji. **(D)** Greenberg.

Method 3. Takatsuji et al. (Takatsuji et al. 1996) determined the v_p using the baseline shift, displaying the flow velocities higher than the aliasing velocities in

blue within the red filling flow signals. First the point of maximal velocity around the mitral orifice in early diastole was located. Next, the first aliasing limit was changed to 70% of the maximal velocity. The nearest point to the apex on the aliasing boundary (typically occurring at the level of the mid ventricle) was then located. The ratio (in cm/s) of the distance difference (S, in cm) and the time delay (dt, in s) between the maximal velocity at the mitral valve leaflets and the most apical point of the aliasing boundary corresponding to 70% of the peak E-wave velocity was proposed as a characteristic for v_p (Figure 6.2 (C)). Our algorithm, after selection of a region of interest, automatically searches for the maximum velocity occuring in the neighbourhood of the mitral valve leaflet tips and the most apical point that reaches a velocity corresponding to 70% of this maximum.

Method 4. Greenberg et al. (Stugaard et al. 1997) determined v_p by eigenvector analysis of the E-wave in the CMD image. This method calculates the principal components of the E-wave as an elliptical representation. Basically the algorithm is taking into account velocities in a selected region of interest of the CMD image and fits an elliptical geometry on it. The angle of rotation of the long axis of the ellipse is used as a parameter for v_p. This angle is expressed in degrees and negative angles are measured clockwise (Figure 6.2 (D)). In our algorithm all velocities occuring in the selected region of interest are entered for the calculation of the principal components of the corresponding ellips.

2.2. Study Population and Echocardiographic Examination

A group of ten consecutive patients (61.1 ± 20.2 years (mean ± SD), 22 – 78 (range), 8 male / 2 female)), admitted to the echocardiography laboratory of the Ghent University Hospital for a routine examination, is enrolled. All patients underwent a complete two-dimensional (2D) and Doppler echocardiographic study with a 2.0 to 2.5 MHz transducer. PWD images and CMD images were digitally stored on a 5.25-in. optical disks, using a Hewlett Packard Sonos 2500 system. PWD images were captured from an apical transducer position with the sample volume positioned at the mitral leaflet tips. CMD images of LV diastolic filling were recorded with the scanline aligned along the central inflow track. Five PWD images of transmitral flow and five CMD images of LV filling were alternated captured.

2.3. DATA ANALYSIS AND STATISTICS

The PWD images were analysed using a commercially available analysis package (EnConcert©, Agilent Technologies). Maximum velocities of the early filling wave (E-wave velocity) and the wave during atrial contraction (A-wave velocity) were measured.

As a reference, v_p is first determined using the EnConcert© package by tracing manually the slope of the line segment that can be identified with the first aliasing isovelocity contour of the early filling wave (Garcia et al. 1997). Then, the CMD images are analysed using the automated software in four different ways. All measurements, both manual and automated, are performed by two different observers blinded to each others results. One observer has repeated the measurements two days after the first analysis.

Intra-observer and inter-observer variabilities are assessed by calculation of a correlation coefficient on one hand and a repeatability coefficient as defined by the British Standards Institution (British Standard Institution 1979) on the other hand. The repeatability coefficient is defined as twice the standard deviation on the calculated mean difference between the different measurements. 95% of differences are expected to be less then two SD. Equation 6.1 defines the inter-observer variability (VAR_{inter}), based on this repeatability coefficient:

$$VAR_{inter} = 2 \cdot \sqrt{\frac{\sum_{i=1}^{n} \left[\left(\bar{x}_{iA} - \bar{x}_{iB} \right) - \left(\bar{x}_{A} - \bar{x}_{B} \right) \right]^2}{n}} \qquad \text{[Eq. 6.1]}$$

where n is the number of patients, $\bar{x}_{iA}$ ($\bar{x}_{iB}$) are mean values of readings from consecutive images of patient i observed by observer A (B) and $\bar{x}_{A}$ ($\bar{x}_{B}$) is the mean measured value for all patients and images obtained by observer A (B). The definition of the intra-observer variability (VAR_{intra}) for repeated observations by one observer (A and A') is analogue to the definition of the inter-observer variability:

$$VAR_{intra} = 2 \cdot \sqrt{\frac{\sum_{i=1}^{n} \left[\left(\bar{x}_{iA} - \bar{x}_{iA'} \right) - \left(\bar{x}_{A} - \bar{x}_{A'} \right) \right]^2}{n}} \qquad \text{[Eq. 6.2]}$$

Beat-to-beat variability (VAR_{BTB}) is assessed from the measurements of a single observer in an analogue way as follows (equation 6.3). Firstly, the mean values

($\bar{x}_i$) are calculated for the m consecutive images of each patient i (i = 1 to n). Then, again for each patient, the standard deviation on the difference between the calculated mean value $\bar{x}_i$ and each individual value x_{ij} (j = 1 to m) is calculated. Finally, the beat-to-beat variability is calculated as twice the mean standard deviation for all patients:

$$VAR_{BTB} = 2 \cdot \frac{\sum_{i=1}^{n} \sqrt{\frac{\sum_{j=1}^{m} \left(\bar{x}_i - x_{ij}\right)^2}{m}}}{n} \qquad \text{[Eq. 6.3]}$$

Variabilities are reported in both absolute values and as a percentage of the mean observed values. Note that the used repeatability coefficient of the British Institute of Standards corresponds to the “limits of agreement” as defined by Bland-Altman in their plots for comparing two measurements techniques (Bland and Altman 1986). $p < 0.05$ is considered statistically significant.

3. Results

3.1. Automated Quantification of v_p

Figure 6.3 illustrates the automated processing of a digital CMD image. First a region of interest, containing the early filling wave, is selected (left panel). In this region of interest, markers are removed, aliased velocities replaced and a 5 x 5 median filter is applied (right panel). This filter removes noise by replacing pixel values with the median value of the surrounding 5 x 5 matrix of pixels.

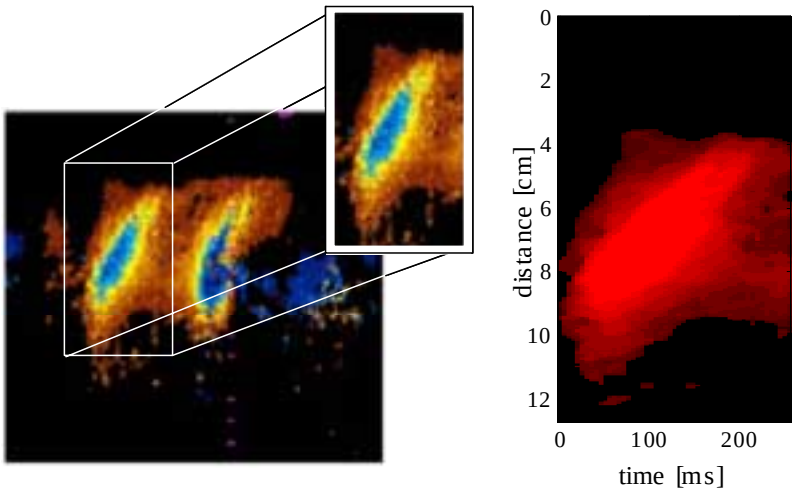

Figure 6.3: Selection of the region of interest (left panel) and dealiasing and filtering (right panel).

Figure 6.4 illustrates the automated quantification of v_p in four different ways. For the same input image, each method results in a different v_p value: 51.4 cm/s (Duval-Garcia), 91.7 ms (Stugaard), 33.3 cm/s (Takatsuji), and -1.1° (Greenberg).

3.2. Intra-Observer and Inter-Observer Variability

Table 6.1 shows the intra-observer and inter-observer variabilities accompanying E and A velocities, next to the variabilities on manual and automated determinations of v_p. Except for the manual tracings of v_p, for each method the correlation coefficient between different readings of the same observer (intra-observer) and different observers (inter-observer) is excellent ($r > 0.975$). The according repeatability coefficients (2SD) however reveal more detailed information concerning differences in repeatability. Compared to the indexes

derived from the PWD images (E and A velocities) the manual determined v_p shows higher values of the repeatability coefficients. The automated determinations of v_p show higher compared to PWD indexes. Compared to the manual determination of v_p, all automated methods have a lower repeatability coefficient.

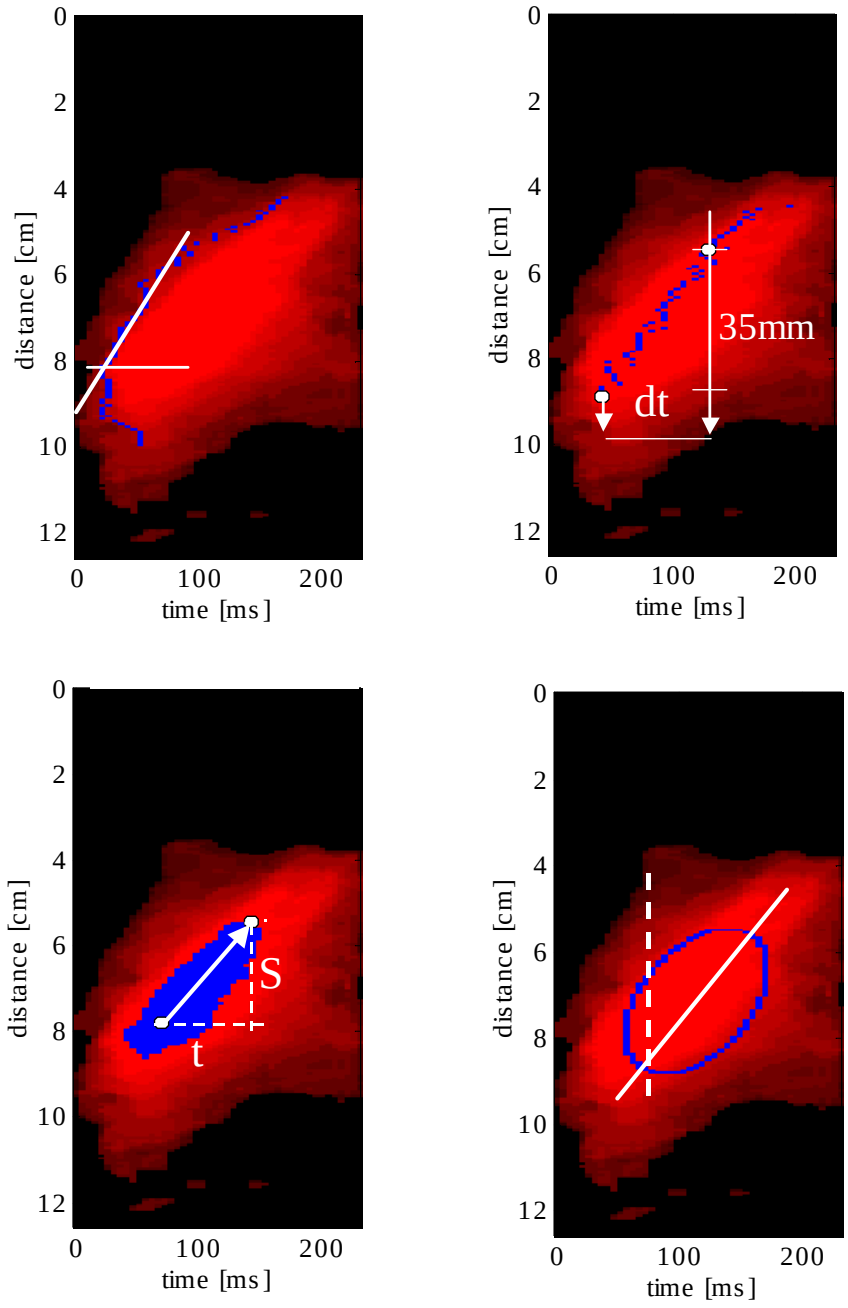

Figure 6.4: Automated quantification of flow propagation velocity in four different ways. **(A)** Method 1 (Duval-Garcia): v_p = 51.4 cm/s. **(B)** Method 2 (Stugaard): TD = 91.7 ms. **(C)** Method 3 (Takatsuji): v_p = 33.3 cm/s. **(D)** Method 4 (Greenberg): v_p = -1.1°.

Table 6.1: Intra-observer and inter-observer variability

		Intra-observer variability			Inter-observer variability		
		2SD	%	r	2SD	%	r
E	[cm/s]	1.73	2.08	0.996	3.25	3.78	0.992
A	[cm/s]	3.13	3.18	0.998	5.15	5.37	0.996
$v_{p,man}$	[cm/s]	9.92	21.75	0.812	13.97	26.13	0.773
$v_{p,duval\text{-}garcia}$	[cm/s]	5.74	12.92	0.991	6.14	13.76	0.975
$v_{p,stugaard}$	[ms]	3.77	3.45	0.999	5.11	5.96	0.999
$v_{p,takatsuji}$	[cm/s]	3.45	3.86	0.999	4.26	5.16	0.998
$v_{p,greenberg}$	[°]	0.05	4.02	0.999	0.17	15.45	0.988

3.3. BEAT-TO-BEAT VARIABILITY

Table 6.2 displays the beat-to-beat variabilities. For all variables, beat-to-beat variabilities are higher compared to variabilities introduced by the observers. The PWD derived E and A velocities show the lowest beat-to-beat variabilities (<15%), whereas the manual traced and automated determined v_p values using the approach of Duval-Garcia results in higher beat-to-beat variabilities (20.14% and 24.28% respectively). Beat-to-beat variabilities on all three other automated determinations of v_p are much higher (>50%).

Table 6.2: Beat-to-Beat variability

		Beat-to-Beat Variability	
		2SD	%
E	[cm/s]	10.82	14.80
A	[cm/s]	9.02	11.27
$v_{p,man}$	[cm/s]	7.33	20.14
$v_{p,duval\text{-}garcia}$	[cm/s]	9.92	24.28
$v_{p,stugaard}$	[ms]	80.54	89.36
$v_{p,takatsuji}$	[cm/s]	43.76	77.02
$v_{p,greenberg}$	[°]	0.65	58.18

Table 6.3 compares mean v_p values, observed by one observer. Depending on the method used, v_p is expressed with different units. The methods of Brun et al, Takatsuji et al and Greenberg et al quantify v_p as a slope or an angle of a line segment. In contrast, Stugaard et al quantifies v_p as the time delay between the appearance of the maximal velocity at two locations, the mitral valve level and the apex. However, in case of a constant distance between the points at mitral valve and apical level, the time delay uniquely corresponds to an angle. In case of alternating distances in the different subjects of a study population, a normalisation is proposed by dividing the time difference by the distance. The normalised time difference with units ms/cm, again, corresponds to an angle. Because basically each method identifies a slope, transformation to one standard unit is feasible. To facilitate comparison between methods, all the values of table 6 3 are also transformed to cm/s.

Table 6.3: Method dependent differences in mean v_p values

	Mean of the readings of observer I	
	Original Units	Transformed units
$v_{p,man}$	36.38 ± 7.13 cm/s	36.38 ± 7.13 cm/s
$v_{p,duval\text{-}garcia}$	45.32 ± 17.44 cm/s	45.32 ± 17.44 cm/s
$v_{p,stugaard}$	105.32 ± 71.53 ms	33.23 ± 48.93 cm/s
$v_{p,takatsuji}$	76.63 ± 45.2 cm/s	76.63 ± 45.20 cm/s
$v_{p,Greenberg}$	1.13 ± 0.72°	41.09 ± 24.69 cm/s

4. Discussion

In this study new automated software is developped to analyse CMD images and to derive $v_{p,}$ based on four different and previously published methods. Using the new software CMD images of ten patients are analysed, allowing a systematic and objective comparison of all methods in a single study. As a reference PWD variables are simultaneously measured and analysed.

4.1. Hydrodynamical Basis

In order to understand the differences between the methods, the hydrodynamical principles of LV filling have to be taken into consideration. Vortex formation is a crucial phenomenon in the filling process. However, during the initial flow phase, before the vortex ring has fully developed, blood moves almost simultaneously in the whole ventricle. Therefore, in a CMD image of the early filling wave, very often a biphasic-filling pattern is observed (Steen and Steen 1994, Vierendeels et al. 2000). A first phase is straight upward and can be associated with the initial motion of the blood column in the LV due to the passing pressure wave. A second phase is the propagation of the maximum velocity that can be associated with the propagation of a vortex ring. The position of the maximum velocities in the second phase of the early filling wave in a CMD image corresponds with the instantaneous position of the travelling vortex (Steen and Steen 1994, Vierendeels et al. 2000).

4.2 Repeatability

From a hydrodynamical viewpoint, keeping in mind the relationship between travelling speed of vortices and the position of the maximum velocity along the LV base-apex axis, the approach of Stugaard et al. seems the most straightforward. However, from a practical point of view, other approaches might be preferred for reasons of repeatability.

Compared to the manual derivation of v_p, the automated methods allow for a more objective and operator independent assessment of v_p as demonstrated by the lower inter-observer variabilities. Four different automated approaches are compared. Differences between methods are mainly related to the amount of velocity

information and/or the specific part of the CMD image that is considered for identifying a line segment.

The methods of Stugaard and Takatsuji determine v_p basically using only two points. Therefore, despite the automated algorithm keeps detecting the same two points in a same input image resulting in low inter- and intra-observer variabilities, slight beat-to-beat differences in images due to noise may introduce considerable beat-to-beat variability in v_p values.

The Duval-Garcia approach uses more velocity information (all pixels along the front of an isovelocity line) compared to the approaches of Stugaard and Takatsuji and is therefore less sensitive to beat-to-beat differences. Because of the semi-automated procedure (manual selection of the linear part of the automated detected contour) intra-observer and inter-observer variabilities are higher compared with the other (full) automated procedures. Nevertheless, compared to the manual tracings of v_p, the interobserver variability remains lower when using the Duval-Garcia approach.

Because the method of Greenberg takes all velocities into account, this method is sensitive to different amounts of velocity information, entered when selecting different region of interests. On the other hand, because it takes all velocities into account, a single pixel containing noise does not influence the result.

Regardless the approach used, a biphasic filling pattern is a potential source for beat-to-beat variability as the automated algorithm may catch different phases of the filling wave in different beats.

Taking both observer variabilities and beat-to-beat variabilities into consideration, tables 6.1 and 6.2 indicate that the method of Duval-Garcia results in determinations of v_p whith a higher degree of repeatability, compared to either manual or other automated methods.

4.3. METHOD DEPENDEND DIFFERENCES

Different units are used. Transformation is feasible because each method basically quantifies a slope. A transformation to cm/s seems the most appropriate because the units become the units of a velocity. However, the expression of an angle as its tangent introduces an inaccuracy in case of steep slopes which does not occur

when expressing the angle in degrees as the arctan operation brings the data nearer to homoscedasticity.

Comparison of the results, transformed to the same units, reveals important method dependent differences in terms of absolute values. Therefore the results of different methods are not interchangable and for follow-up the same method has to be used.

All methods quantify the velocity propagation from base to apex in the LV. The derived v_p value is influenced by LV characteristics, including filling pressure, relaxation, and compliance. However, because each method focusses on different parts of the velocity information in a CMD image, v_p values obtained using different approaches might be influenced by the governing LV characteristics in a different degree. Hereby, consideration of the biphasic filling pattern is crucial. For example, recently Rajagopolan et al. (Rajagopalan et al. 2001) reported significant method-differences in the behaviour of v_p in restrictive versus constrictive cardiomyopathy. Differences were atributed to the different phases in the E-filling wave pattern.

The observed difference between the different approaches in absolute values are important for the quantitative interpretation of v_p values. Garcia et al. for example use a v_p value of 45 cm/s to distinguish normal from pseudo-normal patterns (Garcia et al. 1998). However, as different methods result in different absolute v_p values, this value only holds for v_p values obtained with the approach of Duval-Garcia.

Also several studies propose the ratio of E velocity to v_p to estimate left atrial pressure (Garcia et al. 1997, Gonzalez-Vilchez et al. 1999, Nagueh et al. 1996, Nagueh et al. 1999) using an equation of the form:

$$p = \alpha \cdot \frac{E}{v_p} + \beta \qquad \text{[Eq. 6.4]}$$

where p is pressure and α and β are coefficients. Again, these equations only hold as far as v_p is assessed using the corresponding methods used in the different studies.

5. Conclusion

We have automated the quantitative study of CMD images and the assessment of the v_p of the left ventricular early filling shape in four different ways. All four currently proposed methods to analyse the CMD velocities of left ventricular inflow describe different characteristics of the left ventricular filling wave.

Automation of algorithms reduces operator dependency. However, results of automated determinations of v_p should always be interpreted with care. In the situation of a biphasic early filling wave, results obtained in an automated way should be interpreted with caution. From a practical point of view, the automated Duval-Garcia approach shows the highest degree of repeatability, especially when working with different observers. More work is necessary to investigate the basic relation between v_p, obtained in different ways, and LV characteristics including relaxation, compliance and filling pressure.

CHAPTER 7

Non-invasive Assessment of LV Longitudinal Impedance Using Color M-Mode Doppler Echocardiography †

† The content of this chaper has been published in Computers in Cardiology (2000); 34:17-20:
Non-invasive Assessment of Left Ventricular Longitudinal Impedance Using Color M-Mode Doppler Echocardiography
S De Mey, K Dumont, J Geeraerts, PM Vandervoort, PR Verdonck.

Abstract

We hypothesised that a color Doppler M-mode image of left ventricular inflow provides sufficient information for the non-invasive estimation of the longitudinal impedance of left ventricular filling. The aim of this study was therefore (1) to implement the algorithms for calculation of longitudinal impedance from a color Doppler M-mode image and (2) to study the feasibility and reproducibility of the calculation of longitudinal impedance in an in vitro experiment .In a cardiovascular simulator existing of a pulse duplicator system connected to a model of the arterial tree, color M-mode images of left ventricular inflow were captured. Pressure gradients are calculated by implementing the Euler equation. Velocity at the level of the mitral valve is used for the calculation of flow. Pressure gradients and flow are used for calculation of the longitudinal impedance. Under fixed conditions, no significant beat-to-beat variability in the amplitude of the calculated impedance was observed ($p>0.05$). However, the calculated impedance was significantly higher for the smaller valve ($p<0.05$). In conclusion: longitudinal impedance of left ventricular inflow can be derived non-invasively from color Doppler M-mode images and provides a quantitative interpretation of the numerical velocity information in a color Doppler M-mode image with potential clinical useful information

1.Introduction

Diastolic dysfunction is a condition in which filling of the left ventricle is impeded, resulting in unacceptable symptoms of either low cardiac output, elevated filling pressures, or both (Thomas 1994). Left ventricular diastolic dysfunction is an important cause of cardiac morbidity (Davie et al. 1997). Direct evaluation of diastolic dysfunction requires the measurement of intracardiac pressures. Efforts are made to derive information on diastolic function from non-invasive measurements. Because of its ease of use, Doppler echocardiography has emerged as a preferred method to connect left ventricular filling velocities with diastolic function. Numerous empiric indices have been derived from the mitral inflow pattern, captured at the level of the mitral leaflet tips with pulsed Doppler echocardiography. This inflow pattern is typically composed of two components (Figure 7.1): the E-wave arising from rapid filling and the A-wave arising from atrial contraction.

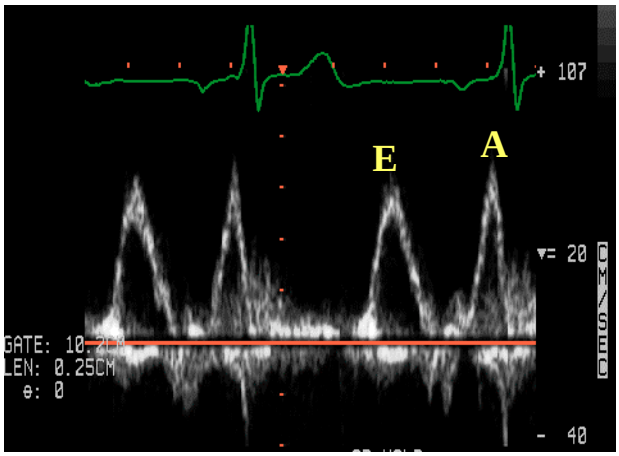

Figure 7.1.: Pulsed Doppler image of ventricular inflow velocities.

However, indices derived from this velocity profile fail to make distinction between normal and pseudo-normal filling pattern (Nishimura and Tajik 1997). To overcome this problem, other echocardiographic approaches are used, such as pulsed Doppler velocities of the pulmonary veins, tissue Doppler echocardiography and color Doppler M-mode echocardiography (Garcia et al. 1998). Color Doppler M-mode echocardiography provides velocity information

along a scanline with both high temporal (200Hz) and spatial (2 mm) resolution. Nonetheless the considerable amount of numerical information in a color Doppler M-mode image, compared to pulsed Doppler echocardiography, the clinical use is limited, as quantitative interpretation remains difficult.

Recently Milde et al (Milde et al. 2000) introduced the ventricular diastolic impedance Z as an index of global diastolic function. Global diastolic impedance was defined as left ventricular pressure P over transmitral flow Q during early-rapid filling (E-wave). Fourier analysis of pressure and flow allows the calculation of the ratio of the amplitudes of each harmonic (equation 7.1):

$$Z(\omega) = \frac{P(\omega)}{Q(\omega)} \qquad \text{[Eq. 7.1]}$$

Simultaneous Doppler E-wave images and micromanometric (Millar) ventricular pressures were used for calculation of diastolic impedance Z (Nichols and O'Rourke 1990). The index Z differentiated between "impedance-matched" (normal diastolic function) and "impedance-mismatched" (abnormal diastolic function) subjects in 19 subjects (10 normal, 9 abnormal).

2. Aim

The aim of this study was:

(1) To implement algorithms for the calculation of ventricular impedance using non-invasive measurements.

(2) To study the feasibility and reproducibility of the non-invasive assessment of ventricular impedance in an in vitro experiment.

3. Methods

3.1. NON-INVASIVE ASSESSMENT OF LEFT VENTRICULAR IMPEDANCE

Simultaneously invasive pressure measurements and flow measurements are required for the calculation of the ventricular impedance as defined in equation 7.1. Pressure measurements are not feasible non-invasively, however pressure differences are routinely assessed non-invasively using the simplified Bernoulli equation (equation 7.2):

$$\Delta P = 4 \cdot v^2 \qquad \text{[Eq. 7.2]}$$

where v is the maximum velocity at the level of the mitral leaflet tips, measured with Doppler echocardiography.

The use of color M-mode echocardiography allows for a more accurate estimation of intracardiac pressure gradients (Greenberg et al. 1996) as for inviscid flow along a streamline, the complex Navier-Stokes equations reduce to the Euler equation (equation 7.3):

$$\frac{\partial \mathrm{p}}{\partial \mathrm{s}} = -\rho\left(\mathrm{v} \cdot \frac{\partial \mathrm{v}}{\partial \mathrm{s}} + \frac{\partial \mathrm{v}}{\partial \mathrm{t}} \right) \qquad \text{[Eq. 7.3]}$$

where v is the local velocity, p is the local pressure, s is the distance along the streamline, t is time, and ρ is blood density. All information needed for the calculation of pressure gradients using equation 7.3 is incorporated in a color M-mode image of ventricular inflow.

The flow through the mitral valve can also be obtained from a color M-mode image from ventricular inflow using equation 7.4:

$$Q = \frac{\pi \cdot D^2}{4} \cdot v \qquad \text{[Eq. 7.4]}$$

where v is the velocity information from the colored pixels at the level of the mitral valve leaflet tips and D is the diameter of the mitral valve.

As we propose the use of pressure gradients for the calculation of ventricular impedance, equation 1 becomes:

$$Z(\omega) = \frac{\Delta p(\omega)}{Q(\omega)} \qquad \text{[Eq. 7.5]}$$

In literature the impedance, defined as in equation 5, is called the 'longitudinal' impedance (Nichols and O'Rourke 1990).

3.2. IMAGE PROCESSING

Image processing algorithms were implemented in the matlab 5.3 environment (The Mathwork, inc.) to extract pressure differences and flow from color Doppler M-mode images. Intracardiac pressure gradients are calculated by implementing the one dimensional Euler equation (Equation 7.3). Flow is calculated by multiplying the velocity information extracted at the level of the mitral valve with valve area (Equation 7.4). From reconstructed pressure and flow curves the 10 first harmonics of the longitudinal impedance (Equation 7.5) are calculated.

3.3. HYDRAULIC MODEL

The feasibility of the non-invasive assessment of ventricular impedance was studied in an in vitro experiment using a hydraulic model of the left heart (Verdonck et al. 1992). The hydraulic model exists of a pulse duplicator system, connected to a model of the arterial tree (Figure 7.2).

From the lung reservoir (1), the test fluid is guided via the pulmonary veins (2) into the left atrium (3) and through the mitral valve (4) into the left ventricle (5). It is then pumped through the aortic valve(6), into the aorta (8a) and further down to the aorta-iliac bifurcation (8c). The fluid then passes the resistance peripheral model (9) and is guided to the (rigid) veins (10). The conduit ends into an overflow (11), from where the fluid flows into a buffering reservoir (12) out of which it is pumped (13) back into the lung reservoir (1). Atrial and ventricular pressure are computer controlled using pressurized air (7). The flow field through the mitral valve can be visualised by color echo-Doppler (Vingmed CFM 800) from an apical or transoesophageal window.

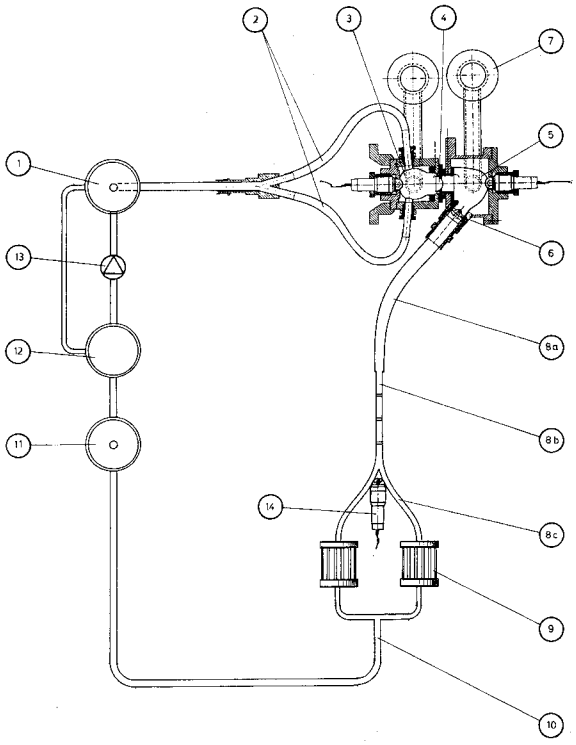

Figure 7.2: Cardiovascular simulator (Verdonck et al. 1992) composed of a model of the arterial tree, connected to a model of the left heart.

3.4. PARAMETER STUDY

In the cardiovascular simulator color M-mode images of left ventricular inflow were captured from an apical window for two different sizes of bioprostheses (13mm and 21mm orifice diameter) mounted in mitral position under varying conditions. Heart rate varied from 45 to 60 beats per minute (BPM) and maximum systolic ventricular pressure varied from 85, 95, 105, 115 to 125 mmHg. Water and a 40/60 water-glycerine mixture were used as testfluid.

3.5. STATISTICS

The influences of mitral valve size, test liquid and heart rate on calculated ventricular impedance were analysed using a multivariate general linear model in SPSS 9.0 (SPSS, inc.). Statistical significance was set at a P-value of 0.05.

4. Results

4.1. IMAGE PROCESSING

Figure 7.3 shows an example of a color M-mode image, captured from an apical window in the hydraulic model and imported in the matlab environment.

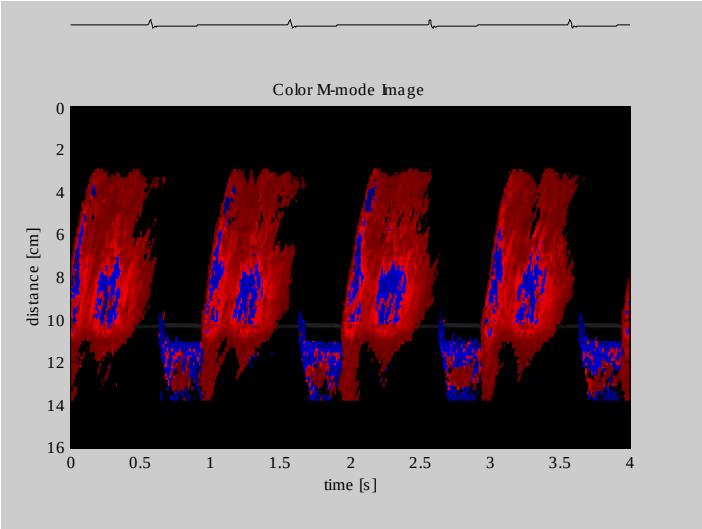

Figure 7.3: Color M-mode image, captured from an apical window in the hydraulic model (x-axis: time in s, y-axis: distance in cm, velocity encoded in color).

Figure 7.4 illustrates the derivation of spatial and temporal derivatives of the color M-mode image, needed for the reconstruction of the pressure gradients using the Euler equation. From the reconstructed pressure gradients and flow curves the 10 first harmonics of the impedance are calculated using Fourier analysis.

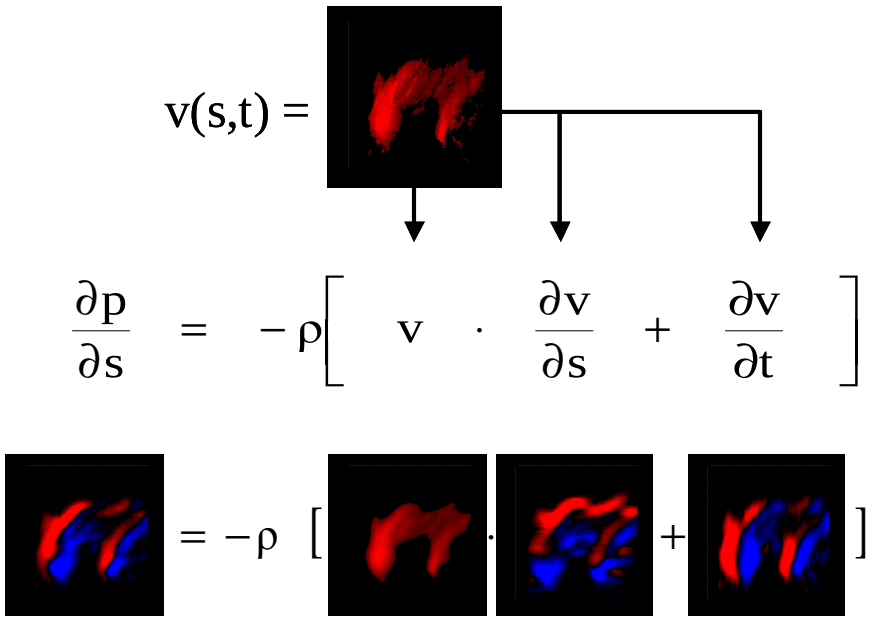

Figure 7.4: Image processing of a color M-mode image. Spatial and temporal derivatives of the spatiotemporal velocity information of the color M-mode are used for reconstruction of the local pressure gradients (Euler equation).

4.2. PARAMETER STUDY

Color M-mode images are captured for two different sizes of mitral valve, two different heart rates, two different test liquids and five different levels of maximum ventricular systolic pressure yielding 2 x 2 x 2 x 5 = 40 experiments. Differences in ventricular impedance's for different valve areas, test fluids and heart rates are shown in figure 7.5.

The differences are statistically analysed using a multivariate general linear model (GLM). The GLM multivariate procedure provides regression analysis and analysis of variance for multiple dependent variables (the impedance for different harmonic numbers) by several factor variables (heart rate, test fluid, valve area and systolic pressure).

Using the Wilks lambda multivariate F-tests, differences in impedance were significant for valve area ($p < 0.000$) and test fluid ($p < 0.000$), whereas differences in impedance were not significant for pressure ($p = 0.138$) and heart rate ($p = 0.495$).

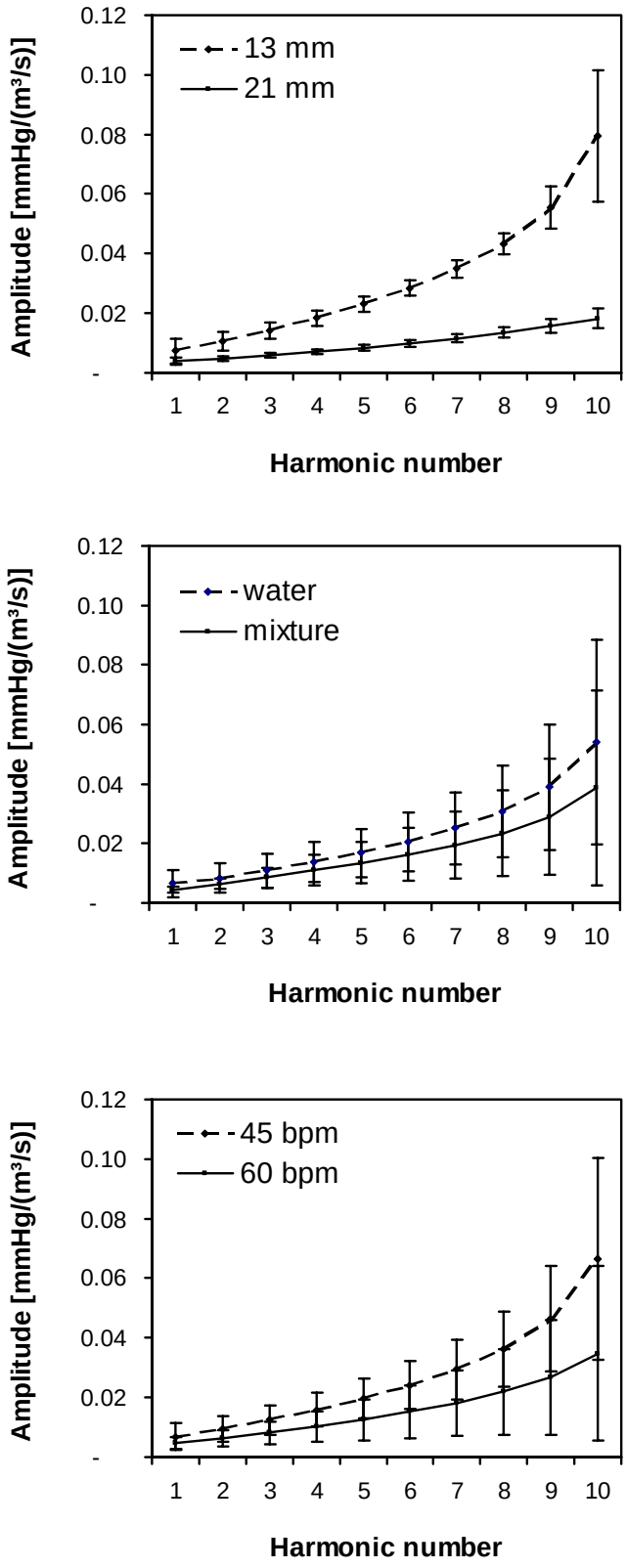

Figure 5: Differences in diastolic impedance for different valve area **(top)**, test liquid **(middle)** and heart rate **(bottom)**

5. Conclusion

Longitudinal impedance of left ventricular inflow can be derived non-invasively from color Doppler M-mode images and provides a quantitative interpretation of the numerical velocity information in a color Doppler M-mode image with potential clinical useful information.

Acknowledgements

The first author is a recipient of a grant from the Flemish Institute for the Promotion of the Scientific-Technological Research in Industry (IWT971096).

CHAPTER 8

Limitations of Doppler Echocardiography for the Post-Operative Evaluation of Aortic Coarctation †

† The content of this chaper has been published in J Biomechanics (2001); 34(7):951-960:
Limitations of Doppler echocardiography for the post-operative evaluation of aortic coarctation
De Mey S, Segers P, Coomans I, Verhaaren H, Verdonck P.

Abstract

Doppler blood flow measurements and derived pressure differences, through the Bernoulli equation, are used in the diagnosis of aortic coarctation, a congenital stenosis distal to the left subclavian artery. Doppler velocities remain elevated at the coarctation site after successful repair of coarctation, leading to high Doppler derived pressure differences without significant arm-leg pressure differences. We studied this apparent contradiction of two diagnostic methods, in vivo using patient and control data, and in vitro using a hydraulic model. Clinical and echocardiographic data from 31 patients, aged 13.0±4.0, 10.5±4.7 years after coarctectomy by end-to-end anastomosis, and 18 age-matched healthy subjects were reviewed. Doppler peak velocities at the aortic isthmus were elevated in patients (2.2±0.4 vs. 1.2±0.2 m/s, P<.001), corresponding to significant Doppler differences (20±7 mmHg), however without significant arm-leg pressure differences. In all patients, a mild anatomic stenosis could still be observed. Local stiffness was increased. The hypothesis that the less distensible surgical scar in post-coarctectomy patients leads to a significant dynamic obstruction in systole was validated in a latex model of the aorta. Rigid rings (0.5 - 1.5 cm), matching the unloaded aortic diameter, were mounted around the aorta. Under loading conditions, Doppler peak velocities increased by 40±7%, yielding Doppler differences of 21±3 mmHg, without a significant pressure drop. An alternative expression to calculate pressure differences, using both velocity and geometric information, was validated in the model. In conclusion, post-operatively, Doppler velocities remain elevated due to a mild anatomical and significant dynamic narrowing, but the specific geometry, resembling a tubular hypoplasia rather than an abrupt stenosis, permits an almost complete pressure recovery explaining the occurrence of Doppler differences in disagreement with the negligible arm-leg pressure difference.

1. Introduction

Aortic coarctation is a congenital heart disease characterised by a narrowing of the isthmus zone, i.e., the section of the descending aorta distal to the left subclavian artery (location 4, figure 1). Aortic coarctation is encountered in approximately 0.1% of newborns (Bergsma 1974) and is the third most prevailing defect in infants and children (5 to 8% of all congenital heart disorders) (Rao 1995). Aortic coarctation often occurs in combination with other congenital cardiovascular defects such as ventricular septum defect or abnormal valves. In 98% of all cases, the coarctation is an isolated narrowing at the ligamentum arteriosum, the remains of the ductus Botalli (Edwards and Davidson 1995). Treatment of aortic coarctation consists of surgical removal or balloon dilatation of the stenosis.

Aortic coarctation is a stenosis in the descending aorta and results in an increased blood pressure in the vessels proximal to the stenosis, while blood pressure is lower in vessels distal to the coarctation. This leads to significant pressure differences between the (right) arm and leg, a standard indication of aortic coarctation (pressure drop, $\Delta p > 20$ mmHg). Though the arm-leg pressure difference seems the most obvious indication of aortic coarctation, its (non-invasive) diagnosis is mainly based on the echo-Doppler technique. The functional severity of the stenosis is often assessed by use of the simplified Bernoulli equation, relating maximal Doppler velocities (v, m/s) to a pressure difference (ΔP, mmHg): $\Delta P = 4.v^2$. Pre-operatively Doppler-derived pressure differences correlate well with arm-leg pressure differences (Park et al. 1993, Robinson et al. 1984).

Post-operatively, after removal of the stenosis, both indices often yield contradictory results: in spite of negligible arm-leg pressure differences, elevated Doppler velocities (2 to 4 m/s) yield high Doppler-derived pressure differences (Aldousany et al. 1990, Carvalho et al. 1990, Chan et al. 1992, Kappetein et al. 1993, Muhler et al. 1993, Teien et al. 1993, Teien et al. 1991, Wendel et al. 1992, Wyse et al. 1984). Marx and Allen (Marx and Allen 1986) reported that inclusion of the proximal Doppler velocity (v_{prox}) within the Bernoulli equation ($\Delta P=4.(v^2-v_{prox}^2)$) corrects for the difference though other sources report that the corrected formula still overestimates the pressure difference (Aldousany et al. 1990).

The aim of this work is to clarify the apparent contradiction between the measured arm-leg and the calculated Doppler-derived pressure difference in post-operative coarctation patients. We therefore first review data from post-operative coarctation patients to evaluate the local geometry and mechanical characteristics of the proximal aorta and the isthmus zone. These data also allow to compare calculated Doppler-derived to measured arm-leg pressure differences. We further use a hydraulic pulsatile model to study whether the presence of a local stiff section in a compliant tube, mimicking scar-tissue in the post-operation coarctation patient, can explain the discrepancy between measured and Doppler-derived pressure differences. We also studied (both in patients and in the hydraulic model) whether an alternative expression for the pressure difference, incorporating the effect of geometry, provides a more reliable method to assess pressure differences in a non-invasive way. The role of ‘pressure recovery’ is explored by examining the full Bernoulli equation.

2. Methods

2.1. ESTIMATING PRESSURE DIFFERENCES FROM MEASURED VELOCITIES

The simplified Bernoulli equation. In clinical practice the simplified Bernoulli equation is commonly used to estimate the pressure difference over a stenosis from measured flow velocities:

$$\Delta p = \frac{1}{2}\rho \cdot v^2 \qquad \text{[Eq. 8.1]}$$

where p is pressure (in Pa), ρ density (in kg/m³) of blood and v velocity (in m/s) at the coarctation site. In this equation, the unsteady flow component and the energy losses by turbulence and friction are neglected. Filling in the value of the density of blood at 37° (1060 kg/m³) and converting pressure from Pa to mmHg (0.133 Pa = 1 mmHg) results in the simplified Bernoulli equation $\Delta p=4.v^2$.

The modified Bernoulli equation. In a less simplified form, the velocity proximal to the coarctation (v_{prox}) is incorporated in the formula, giving:

$$\Delta p=4.(v^2-v_{prox}^2) \qquad \text{[Eq. 8.2]}$$

For both the simplified and modified Bernoulli equation, peak velocities are used. The calculated pressure difference therefore corresponds to the maximum of the instantaneous pressure difference, measured between two locations.

The Seeley equation. The average of the instantaneous pressure difference between two locations can be calculated with an alternative expression that accounts for geometric influences, as proposed by Seeley et al. and given in equation 8.3 (Seeley and Young 1976):

$$\frac{\Delta p}{\rho v_0^{\,2}} = \frac{K_v}{Re_0} + \frac{K_t}{2}\left[\frac{A_0}{A_1} - 1\right]^2 \qquad \text{[Eq. 8.3]}$$

where Δp is the measured, mean instantaneous pressure drop due to the stenosis, ρ the fluid density, v_0 the mean velocity in the unobstructed tube, Re_0 the according Reynolds number in the unobstructed section, A_0 the unobstructed lumen area and A_1 the area in the constriction. U_0 is calculated from the flow measurements for a cross sectional area A_0. In this equation, the pressure drop across the coarctation

is evaluated in terms of dimensionless values (Euler number). The first term at the right side of equation 8.3 accounts for the viscous effects, whereas the second term accounts for the losses due to turbulence (mainly due to a sudden expansion). K_v and K_t are experimentally derived coefficients. Seeley et al. found for K_t a value of 1.52 (independent of the geometry) and for K_v a geometry dependent variable that can be calculated using the equation 8.4:

$$K_v = 32\frac{L_a}{D_0}\left(\frac{A_0}{A_1}\right)^2 \qquad \text{[Eq. 8.4]}$$

where $L_a = 0.83L + 1.64D_1$, with L the length over which the pressure drop is measured, D_0 the diameter of the unobstructed lumen, and D_1 the diameter of the narrowed section.

2.2. POST-OPERATION COARCTATION PATIENT DATA

31 patients, aged 13.0 ± 4.0, 10.5 ± 4.7 years after coarctectomy, with a body surface area (BSA) of 1.4 ± 0.4 m² are studied as well as control population consisting of 18 healthy children with ages matched to our patient population (age: 13.9 ± 2.9 years, BSA: 1.6 ± 0.3 m²). All patients had surgical repair by resection and end-to-end anastomosis. After obtaining parental authorisation and with personal consent of the children, a full clinical and echocardiographic study is performed using a commercially available echo-sonographer (Vingmed CFM 800). All patients were in supine position. Pulsed Wave Doppler (PW) measurements are done at six different locations along the aortic arch (figure 8.1). Additional Continuous Wave Doppler (CW) measurements in the descending aorta are recorded for comparison. Maximal systolic (D_s) and minimal diastolic (D_d) internal diameter of the aorta are measured at the same locations using 2D-echocardiography. Basic anthropometry and systolic (p_s) and diastolic (p_d) blood pressure measurements in both arms and in one of the legs are obtained in all children.

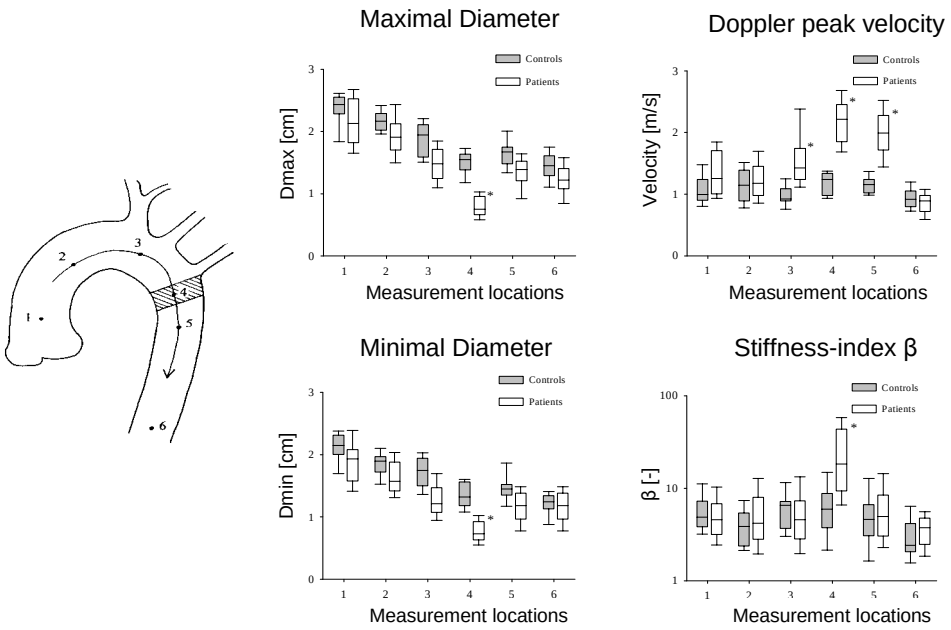

Figure 8.1: Schematic representation of measurement locations along the aortic arch (left side): aortic root (1), ascending aorta (2), descending aorta between the truncus brachiocephalica and the arteria carotis sinistra (3), isthmus zone (4), 2 cm distal to isthmus (5), abdominal aorta at the level of the diaphragm (6). Echocardiographically measured maximal (**left panel, top**) and minimal (**left panel, bottom**) diameter along the aortic arch, Doppler peak velocities (**right panel, top**) and stiffness-index b (**right panel, bottom**) for controls (n=18) and patients (n=31). *: $p < 0.001$ patients versus controls.

The degree of narrowing is quantified by the coarctation index (CI), defined as the ratio of the diameter at the site of the stenosis over the diameter of the normal flow section in the descending aorta. The lower the CI, the higher the severity of the residual stenosis. An index of 0.5 (area reduction of 75%) indicates a severe narrowing and requires surgical intervention. An index of 0.65 (area reduction of 55%) indicates a mild coarctation and does not necessitate an intervention (Carvalho et al. 1990). To assess local arterial distensibility, the dimensionless β stiffness-index (Hirai et al. 1989) is calculated as

$$\beta = \frac{\ln(p_s / p_d)}{\left(\frac{D_s - D_d}{D_d}\right)} \qquad \text{[Eq. 8.5]}$$

Maximal instantaneous pressure differences are estimated using both the simplified (Equation 8.1) and the corrected Bernoulli equation (Equation 8.2), while average instantaneous pressure differences, expressed in a dimensionless form, are estimated using the Seeley equation (Equations 8.3 and 8.4, taking L = 8 cm).

Measurements in patients and controls are averaged per subject group and per location. Data are analysed using 2-way repeated analysis of variance (anova). When the significance level reaches $p < 0.05$, further testing is performed with repeated anova and Bonferroni t-tests to evaluate differences between measuring locations, and with Mann-Whitney U-test for comparison of patients and controls (Sigmastat 2.0, Jandel Scientific). When appropriate, data are presented as Box-Whiskers plots, with the box representing the interquartile range (middle 50% of values) and the whiskers the lines showing the highest and lowest values. The line across the box indicates the median.

2.3. IN VITRO MODEL OF THE AORTA AND POST-OPERATION ISTHMUS

We used a simplified latex model of the aorta to investigate whether the local presence of less distensible scar tissue in post-coarctectomy patients explains the discrepancy between measured and estimated Doppler-derived pressure difference over the isthmus zone (experiment I). In a second series of experiments (experiment II), we focussed on the validation of the Seeley equation (Equation 8.3).

Model description. The model consists of the thoracic and abdominal aorta and is connected to an existing pulse duplicator system (Segers et al. 1998, Verdonck et al. 1992) (Figure 8.2). Pulse duplicator system and aorta are separated by a prosthetic aortic valve. The pulse duplicator consists of two elastic chambers, separated by a mitral valve. The contraction of the elastic chambers is realized by means of pressurized air. The electronic steering allows the independent regulation and monitoring of left atrial and ventricular pressures and volumes. The ascending aorta and aortic arch are modelled as a proximal latex tube (8a) (length: 30 cm, diameter: 2 cm). The descending aorta and isthmus are modelled as a distal latex tube (8b) (length: 25 cm, diameter: 1.2 cm). The abdominal aorta ends with the iliac bifurcation, with both iliac arteries (8c) having a length of 25 cm and a

diameter of 0.7 cm. Each of the iliac arteries is connected to a peripheral resistance (9) and further to a rigid tube (10) (the venous circuit) ending into an overflow (11) to create a constant but adjustable venous pressure. From the overflow, the test fluid (water) flows in a reservoir (12) and is pumped back (13) into the lung reservoir (1) to close the loop.

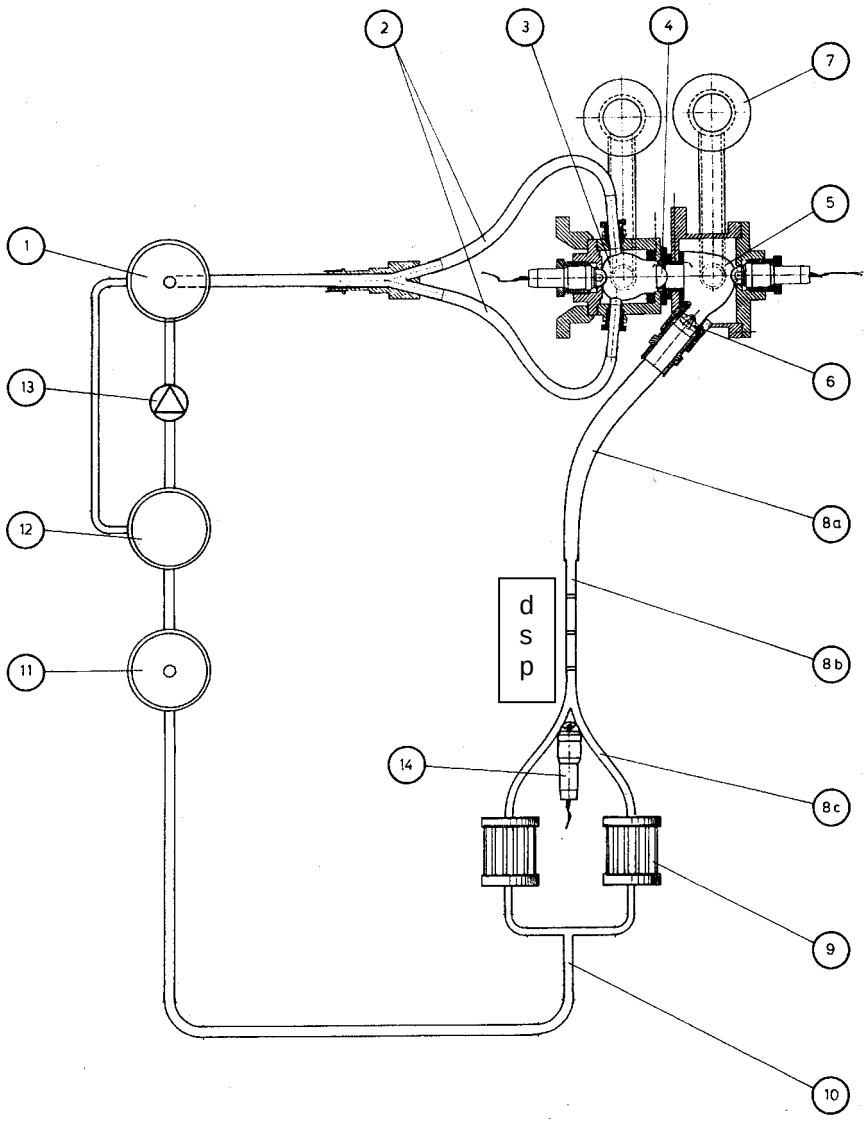

Figure 8.2: Schematic drawing of the hydraulic model: pulse duplicator system and latex model of the aorta and an arterial bifurcation (numbers are explained in text). Measurements are done at locations indicated by p (proximal), s (in situ) and d (distal). The Doppler probe (14) is placed in de aorta-iliac bifurcation for optimal flow measurement.

Experiment I. The effect of scar tissue on pressure and flow in post-coarctectomy patients was investigated in the latex model of the aorta. Measurements are performed at baseline (no obstruction or stiff section) and with rigid PVC rings with internal diameter equal to the external diameter of the descending aorta (1.2 cm) mounted 8 cm proximal to the bifurcation to simulate the rigid local scar tissue (figure 8.2, s). Tests are performed for ring lengths of 0.5, 1 and 1.5 cm. The distal location of the coarctation site is chosen for measuring accuracy: the Doppler probe can be placed between the iliac arteries, allowing a perfect alignment of the Doppler beam to the flow direction in the sample volume, avoiding the need for angle correction. Aortic velocities are measured 4 cm proximal (Figure 8.2, p), at the coarctation (Figure 8.2, s) and 4 cm distal to it (Figure 8.2, d) with pulsed Doppler echocardiography (Vingmed CFM 800). High fidelity pressure tip transducers (Millar, Houston, Texas, USA) measure pressure continuously 8 cm proximal and 8 cm distal to the isthmus zone. The sampling rate (computer A/D card, National Instruments, Texas, USA) is 200 Hz. Measured instantaneous and peak-to-peak pressure differences are averaged over 4 consecutive heartbeats. An electronic flow meter (Endress & Hauser, Reinach, Switzerland) is fixed on the venous circuit for cardiac output measurement. Flow rate is varied from 1.5 to 3.0 l/min while the heart rate is kept at 60 bpm. Doppler measurements are averaged over 3 to 4 consecutive heart periods in steady state, and are presented as mean ± standard deviation.

Experiments are performed with three different models, having different elasticity levels determined with a static pressure-volume curve. The pressure-volume relationships of the three models were linear within the pressure ranges applied during the experiments. The slope of the pressure-volume curve, i.e. compliance, was 0.14, 0.24 and 0.64 ml/mmHg, respectively. For each measurement, maximal instantaneous pressure differences estimated with the simplified and modified Bernoulli equation (equations 8.1 and 8.2) are compared to the actually measured maximal pressure difference, calculated as (i) the difference between maximal pressures proximal and distal to the isthmus zone (peak-to-peak) or (ii) the maximum of the instantaneous difference between proximal and distal pressure (instantaneous).

Experiment II. With this additional series of experiments, we wish to investigate whether the Seeley equation (equation 8.3) allows an accurate estimate of the (average instantaneous) pressure difference. Measurements were done for the most compliant model (0.64 ml/mmHg). Rigid PVC rings with internal diameter equal and less than the external diameter of the aorta (1.2, 1.1 cm and 0.9 cm) are mounted 8 cm proximal to the bifurcation to simulate a residual stiffening and/or narrowing of the aortic arch. High fidelity pressure tip transducers (Millar, Houston, Texas, USA) measure pressure continuously 4 cm proximal, and 4 cm distal to the isthmus zone. Flow rate is varied from 0.7 to 1.65 l/min while the heart rate is kept at 60 bpm. The measured average instantaneous pressure difference over the coarctation is compared to an estimated pressure difference using the Seeley equation (equation 8.3) for values of the CI ranging from 1 (unobstructed tube) to 0.65 (mildly narrowed tube).

3. Results

3.1. PATIENT DATA

None of the patients shows clinical signs of residual coarctation: the arterial pulses are equally palpable in arms and right leg, blood pressure in the right arm is normal and the arm-leg pressure difference (difference between systolic pressures) is in favour of a good repair with the leg pressure slightly higher than the arm pressure (Table 8.1). No signs of left ventricular hypertrophy are found echocardiographically. Notwithstanding successful repair of coarctation, a mild narrowing is still observed in most patients as indicated by the echocardiographically measured maximal and minimal diameters along the aortic arch (Figure 8.1, left panels). The diameter at the coarctation site (measurement location 4) is smaller in patients compared to controls ($p < 0.001$). Within the patient group, the diameter of the isthmus zone is also significantly smaller compared to the adjacent locations ($P<0.001$). The CI is 0.64 ± 0.17, based on dimensions in systole and 0.69 ± 0.20 based on diastolic dimensions. The right panel (bottom) of figure 8.1 shows the variation of the stiffness-index β along the aorta. β is significantly higher in patients at the operation site, compared to controls ($p < 0.001$) and, within the patient group, higher at the operation site than at adjacent measuring locations ($p < 0.001$).

Table 8.1: Mean values ± standard deviations for the non-invasive blood pressure (BP) measurements in patients and controls, systolic blood pressure (SBP), diastolic blood pressure (DBP). All values are in mmHg.

Non-invasive BP	Patients (n=18)		Controls (n=31)	
	SBP (mmHg)	DBP (mmHg)	SBP (mmHg)	DBP (mmHg)
Right arm	115 ± 11	61 ± 8	116 ± 12	65 ± 9
Left arm	109 ± 15	57 ± 12	118 ± 11	70 ± 11
Leg	125 ± 16	55 ± 11	130 ± 14	59 ± 8
Right arm-leg difference	-10 ±12		-12 ± 10	

Doppler peak velocities are given in figure 8.1 (right panel, top). Peak velocity at the aortic isthmus in patients is 2.2 ± 0.4 m/s, corresponding to a Doppler difference of 20 ± 7 mmHg (simplified equation) or 8 ± 9 mmHg (modified equation). The arm-leg pressure difference however is negative (table 8.1). In controls, the peak Doppler velocity at the same measuring location is only 1.2 ± 0.2 m/s, corresponding with a Doppler difference of 5 ± 2 mmHg (simplified equation) or 1 ± 2 mmHg (corrected equation). Average (dimensionless) pressure differences were calculated using the Seeley equation. Results can not be compared to directly measured instantaneous pressure differences (non-invasive pressure recording only yields systolic and diastolic values), but results are expressed as a function of coartcation index (left panel of figure 8.3).

3.2. HYDRAULIC MODEL: EXPERIMENT I.

Using a non-distensible ring with a diameter equal to the external aortic diameter, a length of 0.5 cm, and an overall compliance of the latex model of 0.24 ml/mmHg, Doppler peak velocities at the level of the ring increase with 40 ± 7%, averaged over the different flow rates. For a flow rate of 2 l/min, peak velocity increases from 1.52 ± 0.02 m/s to 2.36 ± 0.05 m/s. Figure 8.4 (left panel) shows for different flow rates the measured peak-to-peak and instantaneous pressure differences, and Doppler derived (simplified and modified Bernoulli) pressure differences, at baseline conditions (no rigid ring, open markers) and measured in presence of the rigid ring (ring, closed markers). The pressure gradients, calculated using the modified Bernoulli equation at baseline conditions, are not entered in the figure as they equal zero for all flow rates. Overall, instantaneous pressure differences are higher than peak-to-peak pressure differences. Doppler derived pressure differences (simplified Bernoulli) are higher than instantaneous pressure differences. Doppler derived pressure differences (modified Bernoulli) are in between instantaneous and peak-to-peak pressure differences. We found no statistically significant difference between data at baseline and with the rigid ring for the instantaneous ($p = 0.716$) and peak-to-peak ($p = 0.955$) pressure difference. In contrast, Doppler derived velocities are significantly influenced by the application of the stiff ring, suggesting pressure differences higher than 20 mmHg in case of the simplified Bernoulli. Consequently, Doppler-derived differences are significantly different between baseline and with the presence of

the rigid ring ($p < 0.001$). Analog results are found for larger rings and for the models with compliances 0.14 and 0.64 ml/mmHg.

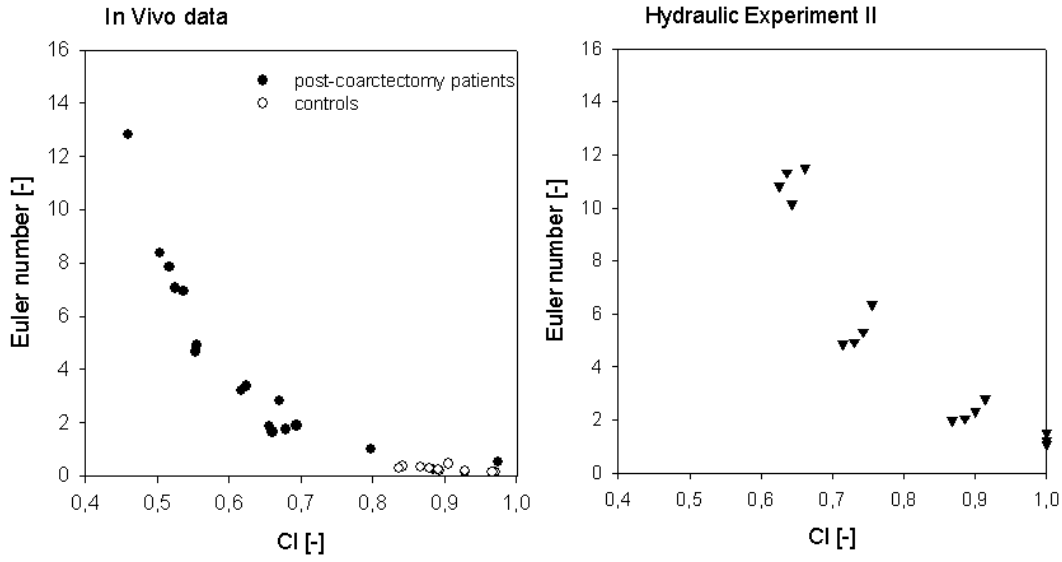

Figure 8.3. Left panel: estimated Euler number as a function of CI for patients and controls. **Right panel:** estimated Euler number as a function of CI for the hydraulic model (experiment II).

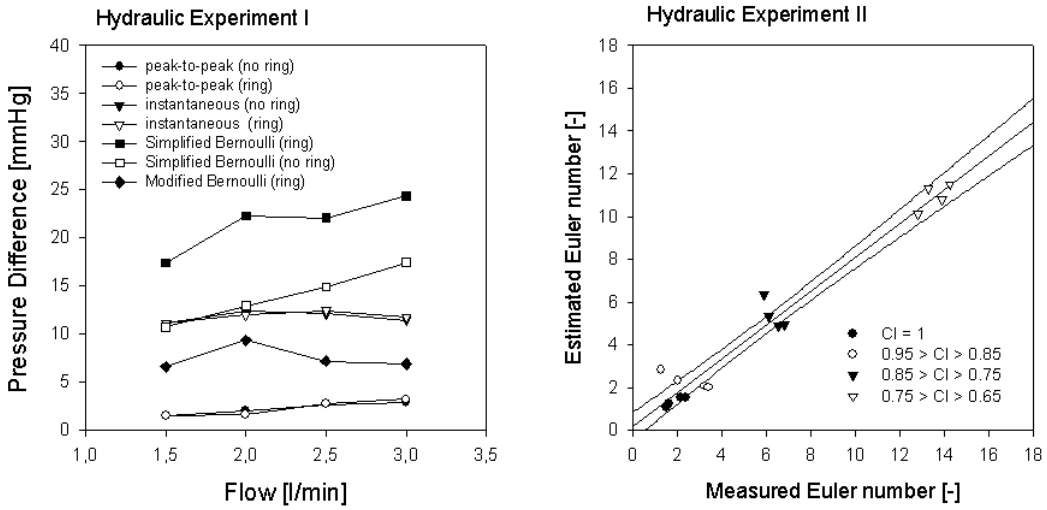

Figure 8.4. Left panel: measured peak-to-peak, maximal instantaneous pressure differences and Doppler derived (Bernoulli) pressure differences, at baseline conditions (no ring, open markers) and with a stiff ring around the aorta (ring, closed markers) for different flow rates. Overall, Doppler derived pressure differences (Bernoulli) are higher than instantaneous pressure differences, which are higher than peak-to-peak pressure differences. **Right panel:** Measured and estimated Euler number in the hydraulic model for CI ranging from 1 to 0.65.

3.3. HYDRAULIC MODEL: EXPERIMENT II.

In this second experiment, measurements are performed for a CI ranging from 1 to 0.65, and flows ranging from 0.7 to 1.65 l/min. For all the experiments, the averaged maximum instantaneous pressure difference was 5.32 +/- 1.5 mmHg, whereas the averaged mean instantaneous pressure difference was 0.40 +/- 0.33 mmHg. In figure 8.4 (right panel), the measured Euler number, derived using the measured mean instantaneous pressure difference is plotted against the calculated mean pressure drop (using equation 8.3) for different values of CI. We found reasonable agreement between predicted and measured values ($r^2 = 0.84$, $p < 0.001$). The mean instantaneous pressure differences are increasing with increasing CI. We found no significant difference between measured pressure differences for the experiments without a ring (CI = 1), and with a ring of a diameter equal to the diameter of the aorta ($0.85 < CI < 0.95$).

4. Discussion

The main results of the reviewed patient data are that (1) in spite of a successful repair, Doppler derived differences still remain elevated, even after incorporation of the proximal velocity, and (2) a non-significant arm-leg pressure difference is measured in all patients. The echocardiographic evaluation reveals a mild anatomical stenosis. Further, at the operation zone, scar tissue increases local stiffness, as revealed by the stiffness-index b. In systole, the stiffer section extends less than the surrounding tissue, resulting in a dynamic or functional obstruction. This is confirmed by the significant difference ($p < 0.005$) in CI as derived from the diameters measured during systole vs. diastole.

The issue whether the local stiffening of the isthmus zone can provoke a significant elevation of the corresponding velocities was addressed in a hydraulic model. Using rigid rings of the same diameter as the latex tube, the velocities at the level of the ring increase by about 40%, resulting in significantly elevated Doppler differences. The velocity shift is comparable to the difference in velocity of 45% at the isthmus site between controls and patients. Due to the local increase of velocity, potential (pressure) energy is partly converted into kinetic (velocity) energy and pressure will be lower at the (non-compliant) isthmus zone. However, we found no clinical important pressure drop over the non-compliant segment. This means that distal to the stiff section, velocities decrease and most of the kinetic energy is again restored into potential energy. This is a well known hydraulic phenomenon, called ‘pressure recovery’.

Pressure recovery is closely related to the geometry of the obstruction. The conversion of kinetic into potential energy implies that little energy is lost due to turbulence. To illustrate this point in more detail, we analytically analysed the full Bernoulli equation. Details are given in appendix. Two different geometry's simulate a pre- and post operation coarctation zone, modelled as a local sharp stenosis (pre-operation; figure 8.1a, appendix) and as a smoothly varying mild stenosis (tubular hypoplasia; post-operation; figure 8.1b, appendix). In the sharp stenosis model, energy (pressure) is lost due to turbulence and the pressure distal to the stenosis is markedly lower than proximal to the stenosis. Here, Doppler differences will be in good agreement with arm-leg pressure differences. In the

tubular hypoplasia, there are small energy losses due to turbulence, and pressure is built up distal to the stenosis where the streamlines smoothly diverge. In this case, pressure recovery is found and the agreement between Doppler difference and arm-leg pressure difference is lost. This corresponds well with the clinical practice where, mainly in the post-operative case (predominance of tubular hypoplasia), the use of the Doppler technique leads to false positive diagnoses of recoarctation, while in the pre-operative case the problem seldom occurs. The mathematical computations (Figure 8.2, appendix) demonstrate that post-operatively, in case of a tubular hypoplasia, a Doppler derived difference of 60 mmHg can accompany an arm-leg pressure difference of less then 20 mmHg which is a clinical criteria for recoarctation. Incorporation of the proximal velocity in the Bernoulli equation augments the reliability of the Doppler differences but still yields false positive diagnoses.

As pressure recovery is strongly related to the morphology of the stenosis, literature data on post-operative evaluation after coarctectomy should be interpreted with care. The post-operative geometry of the isthmus zone is dependent on the surgical technique and the age of the patient at the time of operation. Study populations are often heterogeneous, including patients operated by different techniques or data from patients operated at early age pooled with those operated at older age (Aldousany et al. 1990, Teien et al. 1991, Wendel et al. 1992, Wyse et al. 1984). There is a larger anatomical difference in post-coarctation sites repaired by the subclavian flap technique or by resection and end-to-end anastomosis.

Echocardiography is the traditional way to assess the morphology of the stenosis for the diagnosis of an aortic coarctation. However, the coarctation index alone does not determine the functional severity of a stenosis. The blood flow and the pressure proximal and distal to the stenosis are also important factors and pressure differences are considered as an important diagnostic criterion. The issue is how to obtain a reliable estimate of the pressure difference in a non-invasive way. A traditional marker is the arm-leg pressure difference. In fact, the in vivo measured arm-leg pressure difference is a peak-to-peak pressure difference of the systolic pressures at the arm and leg. Our hydraulic experiments revealed important differences between peak-to-peak and instantaneous pressure differences (Figure

8.4, left panel), with the instantaneous pressure differences higher than the peak-to-peak pressure differences. Thus, the arm-leg pressure difference might be an underestimation of the actual pressure difference over the coarctation. Another disturbing fact is the long distance between the two measuring sites. The arterial wave shape (and systolic and diastolic pressure) changes continuously throughout the arterial bed due to a finite wave propagation velocity and wave reflection in the arteries. In normal conditions, the systolic pressure increases from the proximal aorta towards the periphery (Milnor 1989). This phenomenon explains the negative arm-leg pressure differences in both patients and controls.

As it is difficult to measure the pressure differences directly, people have tried to use the easily available velocity information to estimate the pressure difference. Most often, this resulted in the use of the simplified or modified Bernoulli equation, providing an estimate of the maximal instantaneous pressure difference. Our data, in agreement with others, illustrate that these expressions are unreliable in the post-operation coarctation patients.

The simplified or modified Bernoulli equation does not account for the influence of the geometry. The expression as proposed by Seeley et al. provides a potential alternative. It allows to calculate the mean instantaneous pressure difference over a distance, taking into account the local geometry via dimensionless coefficients, experimentally derived and validated by Seeley et al. for $CI < 0.6$. We applied equation 8.3 for $0.6 < CI < 1$, and our data suggest that these coefficients may be used with reasonable accuracy for this range of coarctation indices. We also applied the Seeley equation to the in vivo data of patients and controls. Figure 8.3 (left panel) shows the calculated Euler number for post-coarctectomy patients and controls as a function of CI. The right panel shows the corresponding graph with data obtained in the hydraulic model (experiment II). There is a qualitative agreement between both graphs. However, quantitatively, the graph of the hydraulic experiment is shifted upward, compared to the in vivo data. This may indicate that the coefficients, as derived by Seeley et al. for his hydraulic experiments, should be optimised for the clinical data. Other problems arise from the tapering character of the aorta and of the inclusion of velocity U_0 in equation 8.3, which is the velocity in an unobstructed section of the tube. In the arterial tree, however, branches divide the flow, and it is difficult to measure velocities in

a section of the aorta without branches and hence constant flow. Though the Seeley equation is promising and an improvement over the Bernoulli equation, it requires a validation study in vivo with high fidelity invasive in vivo pressure measurements, so as to compare estimated pressure differences to the average instantaneous pressure difference.

5. Conclusion

We conclude that in the post-operation coarctation patients, Doppler derived pressure differences based on the Bernoulli equation are unreliable. The expression proposed by Seeley et al. for the average instantaneous pressure drop potentially provides an alternative method for an accurate estimate of pressure differences using non-invasive measurements for both pre- and post operation coarctation patients.

Acknowledgements

This study was supported by a grant of the Flemish Institute for the Promotion of Scientific-technological Research in Industry (IWT-971096) and the Belgian National Bank. Patrick Segers is a post-doctoral fellow sponsored by the Fund for Scientific Research - Flanders (FWO-Vlaanderen). Special regards to Sara De Troeyer for executing part of the experiments.

Appendix: Analysis using the complete Bernoulli equation

The influence of stenosis geometry is studied using a mathematical model. Pressure and velocity are computed for steady flow in a rigid tube model, based on the laws of conservation of mass (Equ!ation. 8.1A) and energy (Bernoulli equation ,equation 8.2A):

$$A_1 \cdot v_1 = A_2 \cdot v_2 \qquad \text{[Eq. 8.1A]}$$

$$\overset{1}{\underset{2}{\Delta}}\left[z + \frac{p}{\rho g} + \frac{v^2}{2g} + F \right] = 0 \qquad \text{[Eq. 8.2A]}$$

where A_i is area of the flow section (in m²), z altitude (in m), p pressure (in Pa), ρ density (in kg/m³), g gravity constant (in m/s²), v velocity (in m/s) and F the energy losses due to turbulence and friction (in m), $_1$ and $_2$ indicating two different flow sections.

The energy losses (due to turbulence) are calculated as in equation 8.3A, with ξ a coefficient depending on the geometry of the stenosis:

$$F = \xi \frac{v^2}{2g} \qquad \text{[Eq. 8.3A]}$$

Values are found in Idelchik, 1994. The energy losses due to friction are neglected. Computations are done for a tubular hypoplasia (a gradual narrowing, mainly observed post-operatively, figure 8.5 (a)) and a local stenosis (mainly observed pre-operatively, figure appendix 8.5 (b)) for a flow rate of 2 l/min and a coarctation index ranging from 0.2 to 0.7. The computed pressure gradients are compared to the Doppler derived gradients, calculated using the simplified Bernoulli equation and the computed velocity.

Figure 8.5 shows the calculated pressures for both the tubular hypoplasia (Figure 8.5 (c)) and the local stenosis (Figure 8.5 (d)), a CI = 0.5 and a flow rate of 2 l/min. An almost complete pressure recovery is observed in the case of tubular hypoplasia and this in contrast to a local stenosis where the pressure is only partly restored to its original value (Figure 8.5 (d)).

Figure 8.6 compares the computed pressure differences to the Doppler derived differences for a flow rate of 2 l/min and a CI ranging from 0.2 to 0.7. The Doppler derived differences overestimate the theoretically derived pressure differences. Taking a pressure drop of 20 mmHg as a criterion for a significant (re)coarctation, the marked area represents cases of calculated Doppler derived differences which would lead to false diagnoses. Especially the tubular hypoplasia geometry is sensitive to this phenomenon.

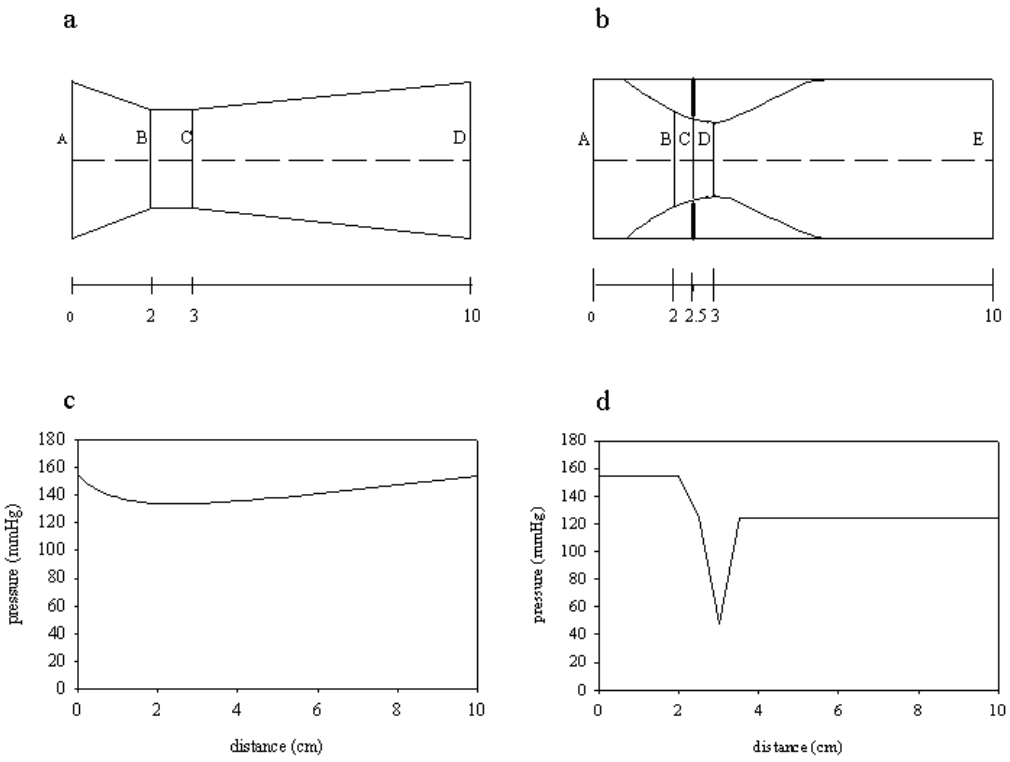

Figure 8.5. (a) Model of a tubular hypoplasia: the diameter varies linearly between maximal and minimal values. **(b)** Model of a local stenosis: straight tube with a diaphragm. Both models have circular flow sections with a non-constricted diameter of 1.2 cm. **(c)** and **(d)** show the calculated pressure along the flow tube for a flow rate of 2 l/min and a coarctation index of 0.5.

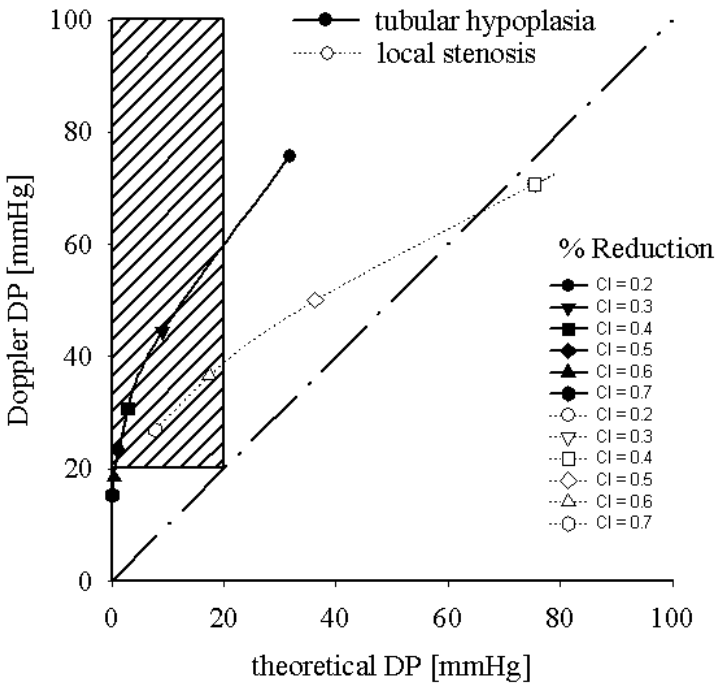

Figure 8.6: Comparison of estimated Doppler-derived pressure differences and theoretically calculated arm-leg pressure differences for a tubular hypoplasia and a local stenosis (models of figure 5) for a flow rate of 2 l/min and a coarctation index (CI) of 0.2 to 0.7. The marked area encloses the “false” Doppler pressure differences.

Part III: Experimental Research and Clinical Observations

CHAPTER 9

Assessment of LV Diastolic Filling Using Color M-mode Doppler Echocardiography: Validation in a New Hydraulic Model †

† The content of this chaper has been submitted for publication in Am J Physiol:
Assessment of LV diastolic filling using color M-mode Doppler echocardiography: validation in a new hydraulic model.
S. De Mey, J De Sutter, P Vandervoort, M De Buyzere, P Verdonck.

Abstract

Objective. To explore in a new hydraulic model the individual contributions of LV relaxation, filling pressure and compliance in changes of E, v_p and E/v_p for different stages of diastolic function.

Background. The effect of LV properties on v_p and the E/v_p ratio remains a matter of debate.

Methods. A new hydraulic model, consisting of an open cylindrical LA connected to an ellipsoidal LV, is designed. E and v_p are measured for varying values of τ (45-60-90ms), LV compliance (0.45-1.35 ml/mmHg) and filling pressure (3-10-30mmHg). The results are used for predicting the evolution of E, v_p and E/v_p during different stages of diastolic function.

Results. An increase in compliance decreases E, whereas it augments v_p. v_p is less load dependent, compared to E. E is decreasing with delayed relaxation, increasing in case of pseudonormalization and becoming higher than the reference values during restrictive filling. The v_p value is lower in case of delayed relaxation, compared to the reference situation. Nonetheless the higher value compared to the delayed relaxation value, v_p remains lower than the reference value during pseudonormalization. v_p is further decreasing during restrictive filling.

Conclusion. The effect of simultaneous changes in compliance and loading are counterbalancing changes in v_p. Therefore, under normal physiologic conditions where load and compliance are coupled, v_p is apparently load insensitive and E/v_p is increasing with increasing filling pressure. Moreover, in the different stages of diastolic dysfunction , due to the interference of the co-varying relaxation, the increase in E/v_p is more pronounced.

1. Introduction

The potential ability to derive information on left ventricular (LV) chamber properties such as LV relaxation or LV compliance from the transmitral velocity profile made Doppler ultrasound a very attractive tool to study LV diastolic filling. Although a few disease-specific inflow velocity patterns have been described, it should be realized that load-dependency of most Doppler derived indexes remains a problem in differentiating between filling patterns (Cohen et al. 1996, Garcia et al. 1998, Nishimura and Tajik 1997). Particularly the distinction between a normal and the so-called pseudonormal filling state (normalized because of an increased filling pressure) is difficult.

In the search to unravel load-dependency, the LV intracavitary flow field has been proposed as a possible source of additional information, helpful in differentiating between normal and pseudonormal filling patterns (Garcia et al. 1998). Intracavitary flow patterns can be studied using color Doppler M-mode echocardiography (CMD) which captures velocity profiles at several locations along a scanline simultaneously (Garcia et al. 1998). From the intracavitary velocity field, the speed at which the blood is propagating towards the apex (the flow propagation velocity, v_p) can be derived (Brun et al. 1992, Stugaard et al. 1993, Takatsuji et al. 1996). v_p has been shown to be inversely related with the time constant of LV relaxation (Brun et al. 1992, Duval-Moulin et al. 1997, Steine et al. 1998, Stugaard et al. 1994, Takatsuji et al. 1996). As the main determinants of PWD peak E-velocity are left atrial pressure (LAP) and LV relaxation, several authors propose the ratio of E and v_p as an index of LAP, left ventricular end-diastolic pressure or pulmonary capillary wedge pressure (PCWP) (Firstenberg et al. 2000a, Garcia et al. 1999, Gonzalez-Vilchez et al. 1999, Nagueh et al. 1996, Nagueh et al. 1999). Hereby, v_p is believed to correct for the load-dependency of E. However, the effect of LV properties on v_p and the E/v_p ratio remains a matter of debate (Brun et al. 1992, Garcia 2001, Togni 2001).

Previous numerical (Flachskampf et al. 1992, McQueen et al. 1982) and hydraulic (Flachskampf et al. 1992) models have been very helpful in explaining the physiological determinants of E-wave velocity because they allow for the investigation of the isolated influence of LV properties without provoking

compensating mechanisms. In contrast, hydraulic models of LV filling (Bot et al. 1990, Shortland 1996, Steen and Steen 1994) were very helpful in understanding the hydrodynamic principles of LV filling but are not appropriate for simulating the influences of isolated changes in LV properties on the intracavitary flow field and v_p.

Therefore the aim of this study is (i) to explore in a new hydraulic model for LV filling the contributions of LV relaxation, filling pressure and compliance to changes in E, v_p and E/v_p and, (ii) to simulate E, v_p and E/v_p for different degrees of LV diastolic function using a general linear model.

2. Methods

A new hydraulic LV filling model is presented. Within this model the isolated influences of LV relaxation, filling pressure and LV compliance on E, v_p and E/v_p are investigated and E, v_p and E/v_p are predicted in four distinct stages of diastolic (dys)function: one reference situation (REF) next to delayed relaxation (DR), pseudonormal filling (PN) and restrictive filling (RF).

2.1. HYDRAULIC MODEL

The left heart model exists of an open rigid cylindrical perspex atrium (Figure 9.1, bottom: LA; diameter 30mm) connected to a truncated ellipsoidal LV (Figure 1, bottom: LV; zero-pressure equilibrium volume 100ml, base-apex length 75mm, short axis 50mm). The LV is composed of latex. In order to prevent inflation at the higher pressure ranges, the LV is surrounded by a gauze (Hydrolast® fixation bandage, Utermöhler Medical Care, Utrecht, The Netherlands). In between the two heart chambers a mitral tricuspid porcine xenograft is mounted (diameter 21mm, McNeilab Inc., Anaheim, California). A 70%-30% water-glycerin mixture (density 1080 kg/m³, viscosity 0.0035 Pa*s) was used as test-fluid. In the experimental setup, the LV is surrounded by a closed rectangular Perspex chamber (250mmx250mmx150mm, figure 1, bottom, PeCh). An early filling wave is initiated by bringing the LV to its end-systolic volume and pressure, starting from a filled LV in equilibrium under a fixed atrial pressure, i.e. for a fixed atrial fluid level. This is done by applying pressure (100 mmHg) in the perspex chamber around the LV, using a pneumatic system (Figure 9.1, top: PS) and compressed air. Because of the valve in mitral position, the fluid inside the LV can not freely migrate from the LV to the LA. Consequently, LV pressure rises until it equals the pressure in the surrounding Perspex chamber, causing leakage of the fluid round the bioprosthesis. When the LV has reached its end-systolic volume, the actual filling of the LV is initiated by switching an electromagnetic valve (Figure 9.1, top, EV) of the pneumatic system, releasing the air out of the surrounding chamber and allowing the LV to relax. Adapting the area of the air outlet (201-804 mm², figure 9.1, top: AiO's) changes the rate of relaxation. Filling pressure is adjusted by changing the fluid level in the atrium (0-

50 cm). Changing the thickness of the latex layer of the LV (0.8-3 mm) alters LV passive compliance.

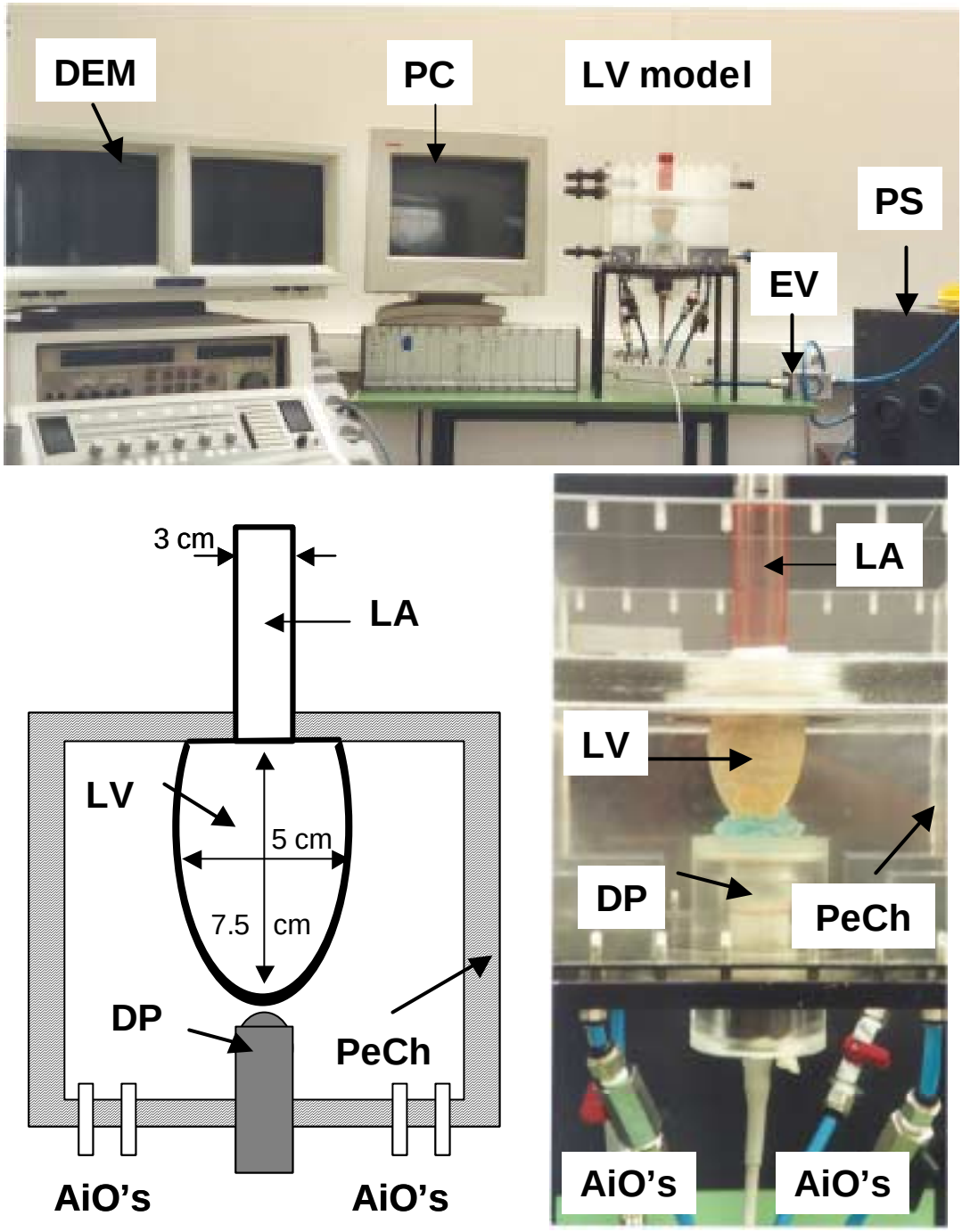

Figure 9.1. Hydraulic model of the left heart. **Top:** Overview of the experimental setup; DEM: Doppler-echo machine, PC: Personal Computer (pressure measurements and control of pneumatic system), EV: Electromagnetic valve, PS: Pneumatic system. **Bottom:** Schematic drawing (left) and picture (right) of the model; Left ventricle (LV) connected to a cylindrical perspex atrium (LA), Doppler probe (DP) is positioned at the ventricular apex., LV surrounded by perspex chamber (PeCh), Airoutlets (AiO's) in bottom of perspex chamber.

2.2. MODEL INSTRUMENTATION, PRESSURE ANALYSIS AND ANALYSIS OF CMD IMAGES

The model is instrumented with pressure transducers (Millar, Houston, TX, USA) in LA and LV. From the LV isovolumic pressure decay, the time constant of relaxation (τ) is calculated using an exponential model with non-zero pressure asymptote $p(t) = (p_0-p_\infty) \exp(-t/\tau) + p_\infty$ with P(t) LV pressure (in mmHg) as a function of time t (in s), p_0 the initial pressure (in mmHg) at maximum negative pressure derivative ($-dp/dt_{max}$), τ the constant of relaxation rate (in s), and p_∞ the pressure asymptote (in mmHg) (Bernardi et al. 1985). A 5.5 Mhz Doppler probe (Vingmed 800 CFM) is positioned at he LV apex (Figure 9.1, right panel: DP). CMD images and PWD images are captured and digitally stored on a magneto-optical disk (Sony, EDM-600B). The CMD images are analyzed and v_p measurements are done off-line in a semi-automatic way using customized software in the Matlab© 5.3 environment (The Mathworks inc., Natick, MA, USA). v_p is derived by measuring the slope of the line that can be identified with the front of the isovelocity contour of 50% of the maximum velocity (Firstenberg et al. 2000a, Garcia et al. 2000). Maximum E-velocity is obtained from the PWD image. Figure 7.2 shows three CMD images of LV filling, obtained in the experimental model (model LV latex layer thickness 3 mm) for varying filling pressures (LAP = 3 and 30mmHg) and relaxation (τ = 45 and 90 ms).

Velocity information along the Doppler scan line is encoded in the colored pixels of the CMD images with a high temporal resolution of 200 Hz. The isovelocity contours of 50% of the peak velocity are automatically detected (Figure 9.2, blue pixels). Using a least squares algorithm the best fitting lines with the front boundary of the isovelocity contours, starting at the mitral valve level and going 3cm into the LV, are determined. The v_p is defined as the slope of the lines. Compared to figure 9.2A (τ = 45ms, LAP = 3mmHg, v_p = 46 cm/s), v_p is increasing with increasing LAP (Figure 9.2B: τ = 45 ms, LAP = 30 mmHg, v_p = 55 cm/s) and decreasing with increasing τ (Figure 9.2C: τ = 90 ms, LAP = 3 mmHg, v_p = 37 cm/s).

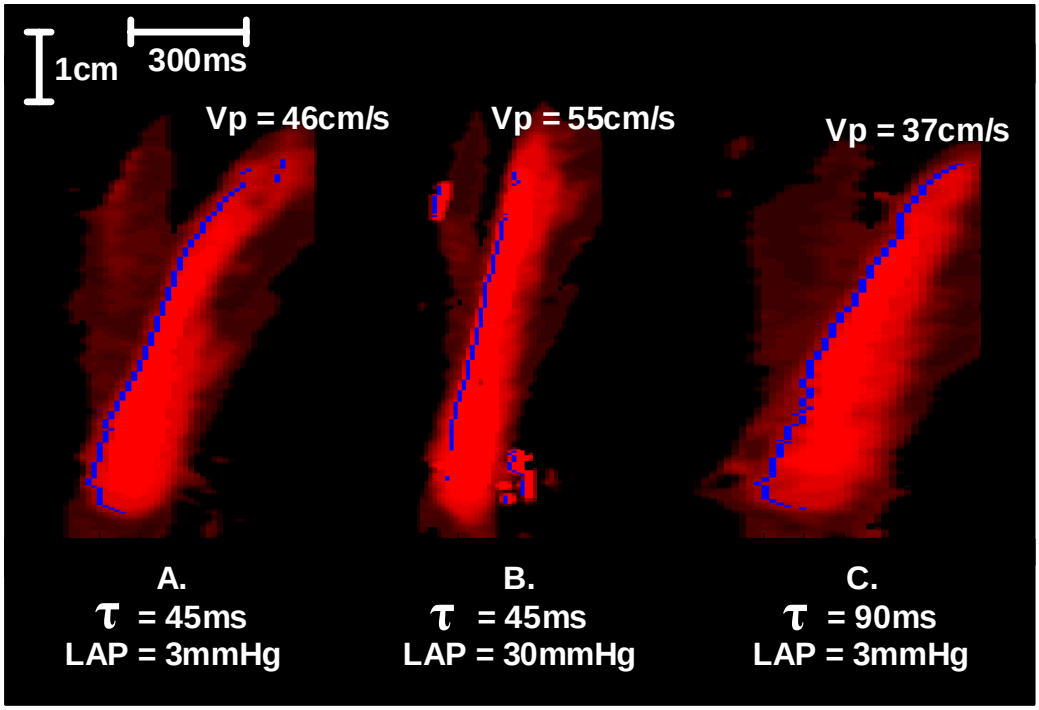

Figure 9.2. Color M-mode (CMD) images of ventricular filling in the experimental model for varying filling pressures and relaxation constants. The isovelocity contour of 50% of the peak velocity (blue pixels) is automatically detected. **Left panel (A):** CMD image for τ = 45 ms, P = 3 mmHg; **Middle panel (B):** CMD image for τ = 45 ms, LAP = 30 mmHg; **Right panel (C):** CMD image for τ = 45 ms, LAP = 3 mmHg. Flow propagation velocity (v_p) is increasing with increasing filling pressure and decreasing with decreasing relaxation constant.

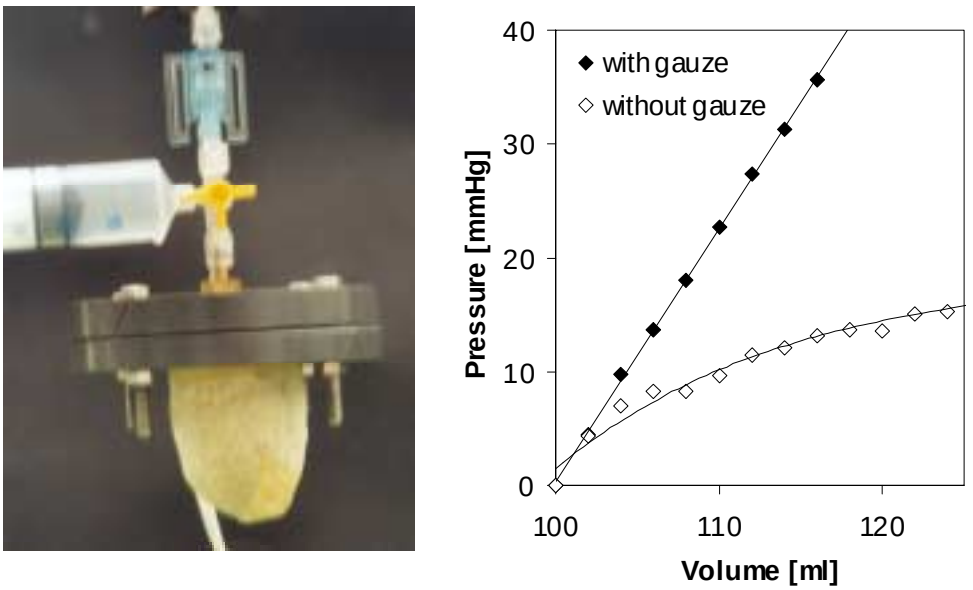

Figure 9.3. Left panel: Experimental set-up for measuring the passive LV pressure-volume relationship of the model left ventricles (experiment 1). **Right panel:** passive pressure-volume relationship of a model left ventricle with and without pericardium (gauze).

2.3. STUDY DESIGN

First, two different experiments are performed. Experiment 1 characterizes the passive LV properties, whereas experiment 2 explores the isolated influence of relaxation (τ), compliance (C) and filling pressure (LAP) on E, v_p and E/v_p during filling. Then, the results of the experiments are used to predict values of E, v_p and E/v_p for different stages of diastolic dysfunction.

Characterization of Passive LV Properties. To characterize the passive chamber properties of the model LV, the passive pressure-volume relationship is constructed. Figure 7.3 (left panel) shows the experimental set-up. The LV inlet is sealed and intraventricular pressure is measured while adding fluid into the LV in steps of 2 ml.

Isolated Influence of Relaxation, Compliance and Filling Pressure. Secondly E, v_p and E/v_p are studied in an orthogonal study design. E and v_p are measured using respectively PWD and CMD echocardiography. The measurements are done for varying filling pressures (LAP = 3, 10, and 30 mmHg) and LV relaxation constants (τ = 45, 60 and 90ms). Each measurement is repeated twice for each combination of the parameters. The experiments are performed in a compliant (model LV latex layer thickness of 0.8mm) and stiff LV (model LV latex layer thickness of 3mm).

Prediction of E, v_p and the E/vp Ratio for Different Stages of Diastolic Function. Finally E, v_p and the E/v_p ratio are predicted within their 95% confidence interval for different sets of LV characteristics, representing a reference situation (REF) on one hand, and delayed relaxation (DR), pseudo-normal (PN) and restrictive filling (RF) on the other hand.

2.4. STATISTICAL METHODS

A general linear model (GLM) multivariate procedure is used for simultaneous assessing the influence of LV characteristics on E and v_p in the experimental model. The GLM multivariate procedure provides regression analysis and analysis of variance for multiple dependent variables by one or more factor variables or covariates. E/v_p is not entered as a dependent variable in the multivariate model as it is a derived value from E and v_p. The influence of the LV characteristics on the E/v_p ratio is studied separately in a univariate model. Starting from a full factorial

model for both the multivariate and univariate model, the actual model is obtained using a backward elimination procedure. First all variables (i.e. compliance, relaxation and filling pressure) are entered as a full factorial model (including all second and third order interactions). Then, non-significant terms are removed one at a time. For each dependent variable, an F-value is calculated to estimate the overall significance of the model. F-values are also calculated to estimate the significance of each parameter accompanying the independent variables of the model. For each significant term, parameter estimates are produced including standard errors, t values and significance. The parameter estimates and accompanying variance-covariance matrices are used for predicting mean E and v_p values for different stages of diastolic dysfunction. A 95% confidence interval is calculated using the Working-Hotelling procedure, estimating the confidence region for the entire regression surface, and the Bonferroni approach, correcting for simultaneous prediction of several new observations (Neter et al. 1996). P values below 0.05 were considered to be statistically significant. All statistical calculations are performed using SPSS© 10.0 (SPSS inc., Chicago, Illinois, USA).

3. Results

3.1. Characterization of Passive LV Properties

Passive pressure-volume relationships of the tested LV's are constructed. Figure 9.3 (right panel) shows the pressure-volume relationships for the latex model LV (model LV latex layer thickness of 0.8mm) with (Figure 9.3, filled markers) and without gauze (Figure 9.3, open markers). Without gauze, the compliance (dV/dp) is increasing with increasing pressure, whereas with the gauze, this trend is changed. The influence of the gauze on the latex ventricle mimics the influence of the pericardium on the heart, as previously observed in vivo (Shintani and Glantz 1994). Within the pressure range occurring during diastolic filling in the LV (0-30mmHg), the pressure-volume relationship of the model LV with gauze approaches a linear function. Therefore, the compliance (C) of the model LV can easily be quantified with the inverse of the slope (C = dV/dp, (ml/mmHg)) of this linear relationship. Analysis of the passive pressure-volume relationship of the model LV with latex layer thickness of 0.8m m resulted in a compliance (C) of 1.35 ± 0.01 ml/mmHg (mean ± se, n = 9), whereas a latex layer thickness of 3 mm resulted in a C of 0.45 ± 0.01 ml/mmHg (mean ± se, n = 7).

3.2. Isolated Influence of Relaxation, Compliance and Filling Pressure

E, v_p and E/v_p are studied in the above mentioned compliant and stiff model LV for varying filling pressures (LAP = 3, 10, and 30 mmHg) and LV relaxation constants (τ = 45, 60 and 90 ms). Table 9.1 shows the GLM multivariate model that fits the measured E and v_p. The model F-values for E and v_p are respectively 421.3 and 82.9. The model predicts the measured E and v_p as illustrated in figure 9.4 (A) and 9.4 (B), showing the regression between measured and predicted values. The adjusted correlation coefficients (adj r^2) are respectively 0.96 and 0.82. A significant ($p < 0.001$) influence of relaxation (τ), compliance (C) and filling pressure (LAP) on E and v_p is observed. All interaction terms are removed as they exerted no significant influence ($p>0.05$). The vanishing of the interaction terms makes the interpretation of the parameter estimates (table 9.1, β values) more easy: a change of an independent variable with one unit will provoke a

change of the dependent variable with a magnitude that equals the according β value.

Influence of Relaxation. E and v_p are decreasing with increasing τ as can be concluded from the negative β values.

Influence of Filling Pressure. E and v_p are increasing with increasing LAP as indicated by the positive β values. v_p turned out to be less load dependent, compared to E as can be concluded from the significant different β values.

Influence of Compliance. Compliance (C) changes E and v_p in the opposite direction: whereas a rise in C increases v_p (positive β value), the same rise in C will decrease E (negative β value).

In a univariate model, the behavior of E/v_p is studied separately. Table 9.2 shows the parameter estimates of the model. As the dependent variable (E/v_p) is the ratio of two variables (E and v_p) that are affected by the LV characteristics (independent variables) in a different way, interactions are included in the final model. All interactions, except the two-way interaction between C and τ ($p=0.947$ in the full factorial model), are significant ($p<0.01$). The model has an F-value of 48.5 and predicts the measured values with an adjusted r^2 value of 0.84 (Figure 9.4 (C)). Because of the interaction terms, the interpretation of the according β values is not obvious: the effect on the E/v_p ratio of a change in one LV characteristic is dependent on the values of the other LV characteristics. The influence of LV characteristics on E/v_p will therefore be discussed in the next section.

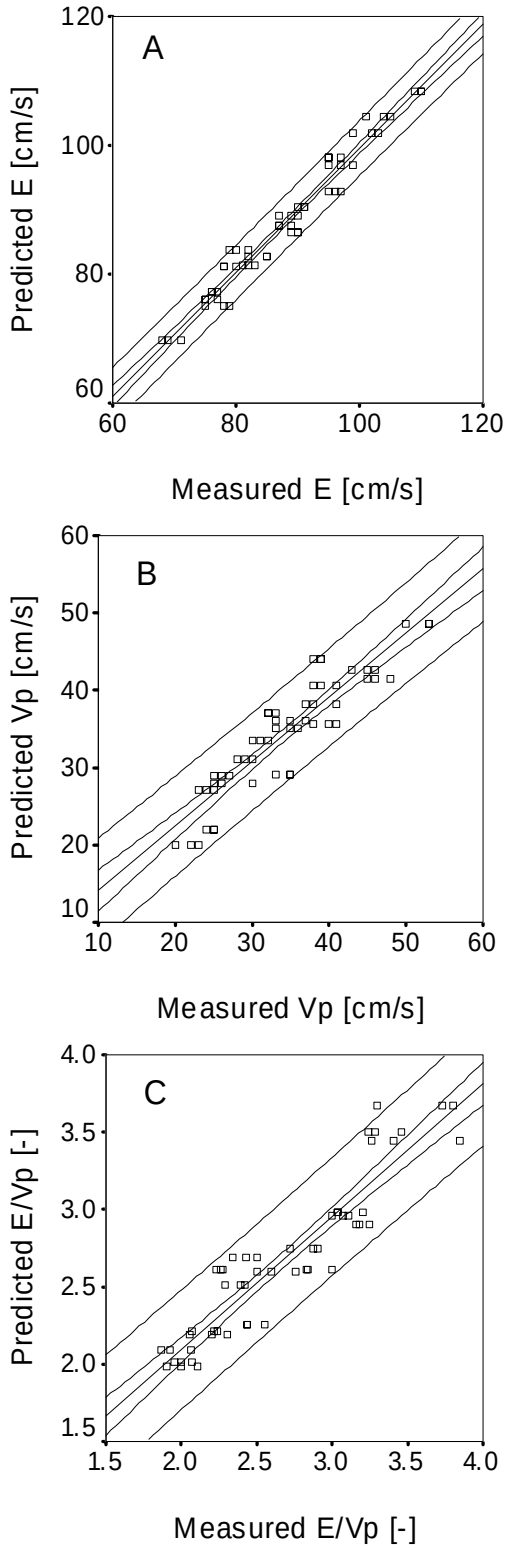

Figure 9.4. Upper panel (A): Regression between measured and predicted E-wave velocity (E) values using a GLM multivariate model. **Middle panel (B):** Regression between measured and predicted flow propagation velocity (v_p) values using a GLM multivariate model. **Lower panel (C):** Regression between measured and predicted E/v_p values using a univariate model.

Table 9.1: General Linear Multivariate model for E and v_p.

Dependent variable		β	SE	t-value	p
E [cm/s]	Constant	99.809	1.277	78.167	.000
	LAP [mmHg]	0.771	0.026	29.822	.000
	τ [ms]	-0.254	0.016	-16.082	.000
	C [ml/mmHg]	-7.078	0.657	-10.770	.000
v_p [cm/s]	Constant	42.667	2.047	20.849	.000
	LAP [mmHg]	0.297	0.041	7.157	.000
	τ [ms]	-0.302	0.025	-11.903	.000
	C [ml/mmHg]	7.860	1.053	7.462	.000

β: parameter estimate, SE: standard error, p: significance, LAP: filling pressure, τ: relaxation constant, C: compliance, E: peak early filling velocity, v_p: flow propagation velocity.

Table 9.2: General Linear univariate model for E/vp.

	β	SE	t-value	p
Constant	2.537	0.193	13.177	.000
LAP [mmHg]	-0.0430	0.015	-2.829	.007
τ [ms]	0.0142	0.002	5.721	.000
C [ml/mmHg]	-.890	0.104	-8.626	.000
τ x LAP [ms*ml/mmHg]	0.00062	0.000	2.866	.006
C x LAP [ml]	0.038	0.013	2.821	.007
τ x C x LAP [ms*ml]	-0.00053	0.000	-2.835	.007

β: parameter estimate, SE: standard error, p: significance, LAP: filling pressure, τ: relaxation constant, C: compliance, E/v_p: ratio of peak early filling velocity (E) and flow propagation velocity (v_p). τ x LAP, C x LAP and τ x C x LAP are the significant model interaction terms.

3.3. PREDICTION OF E, V_P AND THE E/V_P RATIO FOR DIFFERENT STAGES OF DIASTOLIC FUNCTION

The higher obtained GLM models are used to simulate E, v_p and E/v_p for different stages of diastolic function. Four distinct stages are created (Table 9.3) by varying

the LV properties within the ranges as applied during the previous experiment. For the reference situation (REF), τ was set at 50 ms, LAP at 5 mmHg and C at 1.20ml/mmHg. From this reference situation (REF), three typical stages of diastolic dysfunction are mimicked. A so called delayed relaxation pattern (DR) is obtained by increasing τ to 75 ms, keeping all the other variables constant, whereas an additional increase in LAP to 15 mmHg and a decrease in C to 0.90 ml/mmHg represents the so called pseudonormal case (PN). Finally, the so called restrictive filling (RF) pattern was mimicked by an additional increase in LAP (25 mmHg) and τ (85 ms) and a further decrease of C (0.60 ml/mmHg).

The bar plots of figure 9.5 (shaded bars) are showing the GLM predicted values of E, v_p and E/v_p for the reference situation (REF), delayed relaxation (DR), pseudonormal (PN) and restrictive filling (RF) pattern. The error bars are representing the 95% confidence interval (CI) as calculated using the conservative Working-Hotelling method.

Table 9.3: Parameter settings for the simulation of a reference situation, next to three different stages of diastolic dysfunction.

	REF	DR	PN	RF
LAP [mmHg]	5	5	15	25
τ [ms]	50	75	75	85
C [ml/mmHg]	1.20	1.20	0.90	0.60

LAP: filling pressure, τ: relaxation constant, C: compliance, REF: reference situation, DR: delayed relaxation, PN: pseudo-normal filling, RF: restrictive filling.

Compared to the REF stage, E is significantly ($p < 0.001$) lower in the DR stage, and higher in case of PN and RF. In contrast, v_p is significantly ($p < 0.001$) lower during DR, PN and RF, compared to the REF stage. Compared to the DR stage, v_p is higher in case of PN and lower in case of RF. Those differences are however not significant ($p > 0.05$). The difference between v_p in case of PN and RF however are significant ($p < 0.05$). The E/v_p ratio is monotonously increasing with the degree of diastolic dysfunction.

To unravel the isolated influence of the different LV characteristics in the different stages of diastolic dysfunction, E, v_p and E/v_p are also predicted, starting

from the reference situation, by only adjusting LAP and keeping the values of τ and C constant at the level of the reference situation (Figure 9.5, solid bars) and by adjusting LAP and C, only keeping the τ value at the reference level (Figure 9.5, white bars).

Isolated Increase in LAP. Nonetheless the negative β value accompanying LAP in the univariate model, an isolated rise in LAP increases E/v_p. This increase is however very small and not significant.

Combined Increase in LAP and Decrease in C. Because in normal physiology compliance and pressure are coupled by the pressure-volume relationship, this is a more realistic physiological scenario compared to the isolated increase in LAP. The combined influence of compliance and filling pressure significantly increases E/v_p, compared to the reference situation.

Combined Increase in LAP, C and τ. The additional influence of τ, covarying with the different stages of diastolic dysfunction, emphasizes the increase in the E/v_p ratio, compared to the combined influence of LAP and C as described above.

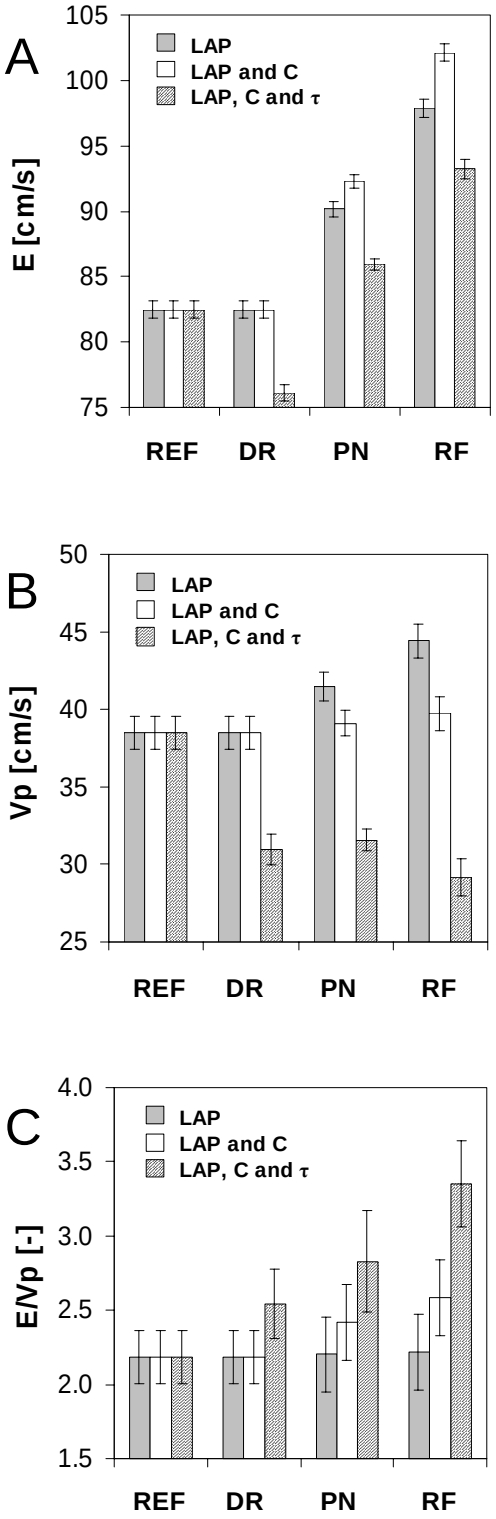

Figure 9.5. Predicted E-wave velocity (E) (**Upper panel (A)**), flow propagation velocity (v_p) (**Middle panel (B)**) and E/v_p (**Lower panel (C)**) for different combinations of LV characteristics, representing four distinct stages of diastolic dysfunction: a reference situation (REF), delayed relaxation (DR), pseudo-normal (PN) and restrictive filling (RF). The shaded bars show the combined influence of relaxation (τ), filling pressure (LAP) and LV compliance (C). The solid and white bars are isolating respectively the influence of LAP, and the combined influence of LAP and C.

4. Discussion

In this study we presented the first hydraulic model that allows the investigation of the isolated influence of LV properties on the intracavitary flow field.

4.1. Hydraulic Model

In previous hydraulic models of LV filling (Bot et al. 1990, Shortland 1996, Steen and Steen 1994), rapidly withdrawing water from a surrounding chamber using a piston pump filled the model ventricles. In those settings it was not possible to study the relationship between the inflow profile and flow propagation in the cavity. Also, it was difficult to translate results to a physiological situation as no exponential pressure decay preceded the filling and the passive compliance of the ventricle did not interfere because the filling process was completely controlled by the displacement of the piston pump. In this study, an attempt was made to design a model of LV filling that mimicked the physiological reality in more detail and comprised an exponential pressure decay preceding the filling, as well as LV compliance interfering with the filling. Nonetheless its simple concept, this model had the advantage that, in contrast to the in vivo situation, all characteristics could be adjusted individually without provoking compensating mechanisms. This allowed us to isolate the influence of the interfering variables one by one. In this way the model gave at least an indication of how LV characteristics are interfering with the intraventricular flow field.

4.2. CMD Echocardiography and Hydrodynamics of LV Filling

In the quest to differentiate between normal and pseudonormal LV filling patterns, different pathways are followed (Garcia et al. 1998). In this study we focussed on v_p as measured using CMD echocardiography. In order to understand the hydrodynamic underpinnings of v_p, some fundamental properties of the 3 dimensional flow field have to be considered. The formation of a ring vortex during LV filling is predicted by numerical (Iudicello et al. 1997, Vierendeels et al. 2000) and in vitro simulations (Bot et al. 1990, Shortland 1996, Steen and Steen 1994) and is in agreement with in-vivo observed characteristics of LV filling (Delemarre et al. 1990). In this concept v_p, obtained from a CMD image, can be associated with the propagation velocity of the ring vortex from base

towards the apex (Steen and Steen 1994, Vierendeels et al. 2000). A convincing argument in our and previous observations is that E always exceeded v_p, which strokes with the hydrodynamic principle that, due to the intrinsic circular motion of the particles in the ring vortex, the velocity of particles (E) in a vortex ring exceeds the velocity at which the whole ring travels (v_p). The CMD images of the early filling wave, obtained in the model, are composed of two phases (Figure 8.2). Phase I is straight upward and is provoked by the initial motion of the blood within the ventricle, whereas phase II can be associated with the filling of the ventricle and the propagation of the vortex, as described above. The biphasic early filling pattern is in accordance with previous observed filling patterns in vitro (Steen and Steen 1994), in vivo (Stugaard et al. 1993) and in numero (Vierendeels et al. 2000).

4.3. The Effect of LV Properties on E and v_P.

In our model the isolated influences of relaxation rate, LV compliance and filling pressure on E and v_p were studied. Our findings concerning the influences of relaxation (τ), filling pressure (P) and compliance (C) on E are in agreement with previous studies in animals (Appleton 1988, Choong et al. 1988, Ishida et al. 1986) and in hydraulic (Flachskampf et al. 1992) and numerical (Flachskampf et al. 1992, Ishida et al. 1986) models. E is decreasing with slowing of relaxation and LV compliance, and increasing with increasing filling pressure. The findings concerning v_p are in agreement with previous studies that found an inverse relationship between v_p and relaxation rate in humans and in animals (Brun et al. 1992, Garcia et al. 2000, Gonzalez-Vilchez et al. 1999, Steine et al. 1999, Stugaard et al. 1994, Stugaard et al. 1995, Takatsuji et al. 1996). A positive relationship between compliance and v_p is observed in our model. Duval-Moulin et al (Duval-Moulin et al. 1997) hypothesized that a stiff ventricle excerpts a stronger resistance on the flow, that enters the LV. Our findings provide direct evidence for this hypothesis.

Brun et al (Brun et al. 1992) reported a positive correlation between v_p and LV end-diastolic pressure. However, several studies have given evidence that v_p is a relatively preload insensitive index in humans and animals (Garcia et al. 1999, Garcia et al. 2000, Moller et al. 2000a). In our study, v_p is not independent of the filling pressure. However, compared to E, v_p is less dependent on filling pressure

as can be concluded from the different coefficients in the multiple linear regression models: an increase in LAP of 1 mmHg in the model will result in a mean increase in E of 0.771 ± 0.026 cm/s (mean ± se), whereas v_p will increase with 0.297 ± 0.041 cm/s (mean ± se). The, at first view, contradiction between the model results and clinical observations can possibly be explained by the constant compliance of the model LV. Because the pressure-volume relationship is linear within the applied pressure range, in the model a rise in pressure is not influencing the value of the compliance. In a physiologically more realistic situation, the passive LV pressure-volume relationship is exponential. Therefore, a rise in pressure is automatically coupled to a fall in compliance. Thus, in vivo the influence of filling pressure on v_p is counterbalanced by the simultaneous decrease in compliance. This phenomenon is also observed in our experiments: whereas the influence on v_p of an isolated rise in LAP (figure 7.5 (B), solid bars) is increasing v_p, compared to the reference values, the combined influence of LAP and C is bringing v_p values again to the level of the reference values (figure 7.5 (B), white bars).

4.4. The Effect of LV Properties on The E/v_P Ratio

As the main determinants of peak E-velocity are LA pressure and LV relaxation, the ratio of E and v_p is proposed as an index of LAP. Several studies have investigated the relationship between filling pressure and the ratio E/v_p using invasive pressure measurements and transthoracic Doppler echocardiography (Firstenberg et al. 2000a, Garcia et al. 1999, Gonzalez-Vilchez et al. 1999, Nagueh et al. 1996, Nagueh et al. 1999). All studies propose a linear relationship filling pressure = $\alpha * (E/v_p) + \beta$, where α and β are fitting constants. The filling pressures are quantified from either pulmonary capillary wedge pressure (PCWP), LV end-diastolic pressure, or LV pressure between the early filling and atrial contraction filling wave. Table 9.4 summarizes these literature data.

Overall a moderate to excellent correlation is reported (r = 0.62-0.81). In three studies, the coefficients α and β are reported. α varies between 0.039 and 5.28, whereas β varies between 1.02 and 4.6. Several factors may contribute to these differences. An obvious reason is the difference between the studies in quantifying filling pressure (CPWP vs. LV end-diastolic Pressure). However, a more fundamental reason can be derived from the results of our model. As

demonstrated, v_p is not completely load independent, though less load dependent, compared to E. This difference in load-dependency is responsible for a weak, not significant, positive correlation between load and E/v_p. However, the covarying variables compliance and relaxation are very strongly influencing the E/v_p ratio (Figure 9.5). As a result, in physiologically normal conditions, a rise in filling pressure causes a significant, though minor rise in E/v_p. This is in accordance with Firstenberg et al., reporting a relationship between load and E/v_p in a population of healthy volunteers (Table 9.4). As in this homogeneous population no substantial differences in relaxation and chamber compliance are expected between the different individuals, from the results of our model the positive, although flat, relationship between load and E/v_p is expected. On the other hand, in a group with different degrees of diastolic dysfunction, due to the covarying relaxation constant τ, differences in E/v_p are much more pronounced. Garcia et al. have studied a heterogeneous population of patients. In such a population, based on our model, it can be expected that differences in relaxation and chamber compliance are steeping the relationship between load and E/v_p. Literature data in table 9.4 confirm this hypothesis as the slope of the relationship between load and E/v_p in the patient population is a factor 139 steeper compared to the healthy population ($\alpha = 5.27$ vs. $\alpha = 0.039$).

Table 9.4: Literature data of the non-invasive estimation of filling pressure using the E/v_p ratio

	α	B	r	Population	reference
PCWP	-	-	0.65	atrial fibrillation	**(Nagueh et al. 1996)**
PCWP	5.27	4.6	0.80	Myocardial infarction	**(Garcia et al. 1999)**
LVP_{preA}	5.28	4.5	0.67	HCM	**(Nagueh et al. 1999)**
PCWP	-	-	0.62	miscellaneous	**(Gonzalez-Vilchez et al. 1999)**
PCWP	0.039	1.02	0.81	healthy volunteers	**(Firstenberg et al. 2000a)**

PCPW: capillary wedge pressure, LV_{preA}: LV end-diatolic pressure, HCM: hypertrophic cardiomyopathy, A and β: slope and intercept of the linear regression between filling pressure and the E/v_p ratio.

4.5. LIMITATIONS OF THE MODEL.

We have investigated the complex interaction between cardiovascular fluid mechanics and diastolic function of the LV in a hydraulic model. The latex ventricle, surrounded with a gauze, can not mimic the complex physiological processes in the normal and diseased heart. However, the aim of the model is not to mimic detailed processes at the cellular level, but to clarify the isolated influence of the relevant variables on the hydrodynamics of LV filling. We used a porcine xenographt mitral valve. The influences of the papillary muscles and chordae tendinae are not mimicked. Also, the simulation of the four stages of diastolic (dys)function is only an approximation. Other clinical influences, including chronotropic and inotropic changes, are interfering and can not be taken into account by the model.

5. Conclusion

A new hydraulic model for the LV filling is developed. In the model, isolated influences of relaxation, compliance and filling pressure in changes of E, v_p and E/v_p are studied. v_p is not completely preload independent, but less load dependent compared to E. A decrease in compliance causes a rise in v_p and a decrease in E. The effect of simultaneous changes in compliance and loading are counterbalancing changes in $v_{p.}$ Therefore, under normal physiologic conditions where load and compliance are coupled, v_p is apparently load insensitive and E/v_p is increasing with increasing filling pressure. Moreover, in the different stages of diastolic dysfunction, due to the interference of the covarying relaxation, the increase in E/v_p is more pronounced.

Acknowledgements

S. De Mey was a recipient of grant IWT-971096 from the Flemish Institute for the Promotion of Scientific-Technological Research in the Industry.

CHAPTER 10

Modeling of LV Filling: A Combined Hydraulic and Numerical Approach[†]

[†] The content of this chaper has been submitted for publication in Cardiovascular Engineering:
Modeling of LV Filling: A Combined Hydraulic and Numerical Approach.
S De Mey, J Vierendeels and P Verdonck.

1. Introduction

In previous work (cf. Chapter 9) a new hydraulic model for the study of left ventricular (LV) filling was presented and used to study LV filling. In the hydraulic model, significant interactions between the flow propagation velocity of the early filling wave (v_p) and LV diastolic variables, including left atrial (LA) filling pressure, the time constant of pressure fall during isovolumic relaxation (τ), and LV compliance were found. The aim of this study is to compare the findings in this new model with numerical simulations in a 2D axi-symmetric LV filling model.

2. Material and Methods

2.1. Hydraulic Model: Setup and Experiments

The left heart model (Figure 10.1) consists of an open rigid cylindrical Perspex atrium (Figure 10.1, LA, diameter 30 mm) connected to a truncated ellipsoidal left ventricle (Figure 10.1, LV, zero-pressure equilibrium volume 100ml, base-apex length 75 mm, short axis 50 mm). The LV is composed of latex. In order to prevent inflation at the higher pressure ranges, the ventricle is surrounded by a gauze. The compliance of the LV is proportional to the LV wall thickness. Experiments are performed using a compliant (wall thickness 0.8 mm) and a stiff (wall thickness 3 mm) model LV. To quantify the compliance of the model ventricles, passive pressure-volume relationships are measured by filling the ventricles in steps of 2 ml. Using linear regression the slope of the pressure-volume relationship was determined for the compliant and the stiff ventricle (1.35 and 0.45 ml/mmHg respectively).

In between the two heart chambers a mitral tricuspid porcine xenograft is mounted (diameter 21 mm, McNeilab Inc., Anaheim, CA). A 60%-40% water-glycerin mixture (dynamic viscosity 3.5 mPas) was used as test-fluid. In the experimental set-up, the ventricle is surrounded by a closed rectangular Perspex chamber filled with air (Figure 10.1, PeCh, 250 mm x 250 mm x 150 mm). An early filling wave is initiated by bringing the ventricle to its end-systolic volume and pressure, starting from a filled ventricle in equilibrium under a fixed atrial pressure, i.e. for a fixed atrial fluid level. This is done by applying pressure (100 mmHg) in the Perspex chamber around the LV, using a pneumatic system and compressed air. Because of the valve in mitral position, the fluid inside the LV can not freely migrate from the LV into the LA, but it leaks through the bioprosthesis until the LV has reached its end-systolic volume. The actual filling of the LV is initiated by switching an electromagnetic valve of the pneumatic system, releasing the air out of the surrounding chamber through air outlets (Figure 10.1, top, AiO's) in the bottom of the surrounding Perspex chamber and allowing the LV to relax. The rate of relaxation can be changed by adapting the area of the air outlets. Filling pressure is adjusted by changing the fluid level in the atrium.

The model is instrumented with a Doppler probe (Figure 10.1, DP; Vingmed, GE) in an apical position.

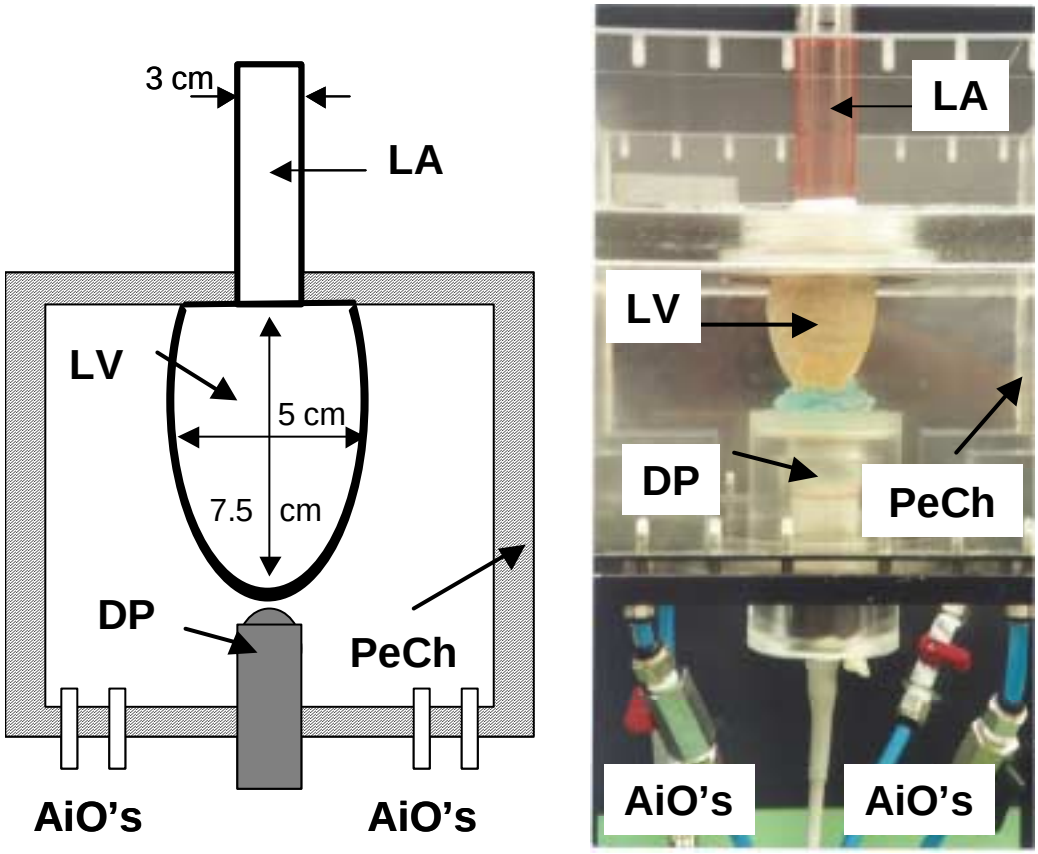

Figure 10.1: Hydraulic model of the left heart. **Left panel:** Schematic drawing. **Right panel:** Picture. The hydraulic model is composed of a cylindrical perspex atrium (LA) connected to a latex left ventricle (LV). The LV is surrounded by a perspex chamber (PeCh). In the bottom of the PeCh airoutlets (AiO's) are provided. LV filling velocities are measured using CMD echocardiography with Doppler probe (DP) in apical position.

Hydraulic model experiments of LV filling were done for varying hemodynamic settings, including variations in τ (45, 60 and 90 ms), LA pressure (3, 10 and 30 mmHg) and compliance (0.45 and 1.35 ml/mmHg). Each experiment is repeated three times.

2.2. Numerical Model

Computer models describing cardiac filling are mostly limited to the fluid dynamical process (1D lumped models based on electrical analogy, 2D analytical models or 2D and 3D numerical models) or are focused on the quantification of ventricular wall stresses and deformations (Verdonck et al. 1998). Peskin (Peskin

and McQueen 1989) was the first to model the blood-ventricular wall interaction using the immersed boundary method. The model of Vierendeels et al. used in this chapter is a 2D axi-symmetric numerical LV filling model, taking into account the interaction between the LV wall and the fluid (Vierendeels 1998).

Intraventricular Blood Model

The fluid domain of the LV is described by an axi-symmetrical model (Figure 10.1). The unsteady Navier-Stokes equations in a LV geometry with moving walls are solved. The computation starts at the onset of LV relaxation. During the relaxation phase, the fluid is assumed to be quiescent inside the LV. This assumption only holds for a homogeneous relaxation, which is assumed. When the LV pressure drops below the atrial pressure, the mitral valve opens immediately. From this moment on, a mitral velocity pattern is applied at the circular orifice (base) of the LV. After opening of the mitral valve, pressure in the LV is determined by both the relaxation and compliance of the LV wall and the dynamics of the blood inflow. Blood is assumed to behave as a Newtonian fluid with a density of 1050 kg/m^3 and a dynamic viscosity of 3.5 mPas.

Ventricular Wall Model

The LV wall is described by a truncated ellipsoid in the zero stress state (Figure 10.2). At the zero stress state and with blood at rest, the transmural pressure is zero. Away from the zero stress state, the shape of the LV is computed from equilibrium equations for the LV wall. A non-linear extension of the thin shell equations is used (Vierendeels 1998). The parameters involved are Young's modulus E, a non-linearity parameter α and LV wall thickness h. The mitral valve annulus is kept fixed, while the apical node can freely move in axial direction. This is in contrast with the living case where the mitral annulus is moving and the apical motion is limited.

During LV relaxation, the compliance of the LV is changing. This is modeled by a time dependent Young's modulus:

$$E = E_{start} + (E_{stop} - E_{start}) \cdot (1 - e^{-t/\tau}) \qquad \text{[Eq. 10.1]}$$

where t denotes the time and τ the time constant of LV relaxation. E_{start} is the modulus at the onset of relaxation and E_{stop} is the modulus in the passive state of

the heart muscle. Young's modulus E and the non-linearity parameter α are assumed to be constant along the heart wall. They are determined by the fitting of a pressure-volume relationship.

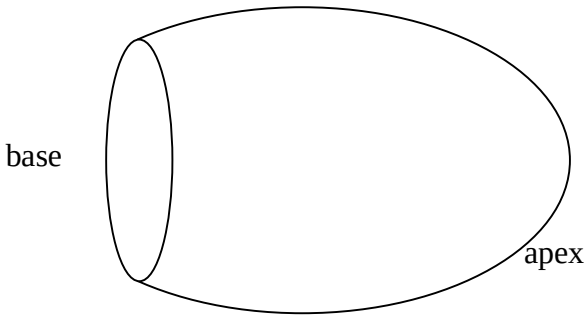

Figure 10.2: Axisymmetrical representation of the LV.

COUPLING PROCEDURE

The coupling of the heart wall displacement and the filling dynamics is based on an iterative approach (Vierendeels 1998). For each time step, the procedure alternates between the following steps: 1) calculation of the movement of the boundary, for a known pressure along the boundary, 2) determination of the position of the internal mesh nodes, for a known position of the boundary and 3) calculation of the flow field in a moving domain, which results in an updated velocity pattern and a new approximation of the pressure field to be used in step 1) until convergence for the time step is achieved.

SIMULATED CASES

Analogue to the hydraulic model experiments, in the numerical model 12 simulations were executed (Table 10.1). 9 simulations were executed in a LV model with compliance 1.35 ml/mmHg, varying τ (45, 60 and 90 ms), and varying LA filling pressure (10, 20 and 30 mmHg). 3 additional simulations were performed in a stiff model LV (compliance 0.45 ml/mmHg) for varying τ (45, 60 and 90 ms) on a fixed LA pressure level (30 mmHg). The passive pressure-volume relationships, measured in the hydraulic model LV with different compliances, are applied to the numerical model and account for differences in compliance. E_{start} is taken equal to E_{stop} because the material used in the

experiments stays in the passive state. Thus, according to Eq. 10.1, E remains constant and it appears that differences in τ are not simulated. However, in the hydraulic model, changing τ results in a change in inlet profile. Therefore, because the measured inflow profiles in the hydraulic model experiments are applied to the corresponding numerical simulations, the influence of τ can also be seen in the numerical outcome. The calculated flow patterns are transformed into the format of CMD echocardiograms.

Table 10.1: Settings of the time constant of LV relaxation (τ), LA pressure (LAP), and LV compliance (C) for LV filling in the Hydraulic model experiment and corresponding numerical simulations.

	τ, ms	**LAP, mmHg**	**C, ml/mmHg**
1	45	10	1.35
2	45	20	1.35
3	45	30	1.35
4	60	10	1.35
5	60	20	1.35
6	60	30	1.35
7	90	10	1.35
8	90	20	1.35
9	90	30	1.35
10	45	30	0.45
11	60	30	0.45
12	90	30	0.45

2.3. DATA ANALYSIS

CMD images from both the hydraulic experiments and numerical simulations are used for calculation of v_p using the Duval-Garcia method (cf. Chapter 6) (Duval-Moulin et al. 1997, Garcia et al. 1998). In brief, linear regression analysis is used for fitting a line with the isovelocity boundary of 50% of the maximum velocity, starting at the level of the mitral valve and going three cm into the LV. v_p is defined as the slope of the line in cm/s. Visual comparison between numerical

simulations and hydraulic experimental results is enhanced by displaying the numerical CMD simulations in the same format of the CMD images measured in the hydraulic model experiment, i.e. velocities are represented using a red to blue color lookup table.

The hydraulic experiment results are fitted to a multiple linear regression model (General Linear Model, GLM) with v_p the dependent variable and LA pressure, τ and LV compliance covarying factors to test for significant variables. Mean values of hydraulic experiment v_p values corresponding to the hemodynamic settings of the numerical model are determined using the GLM model. Numerical simulations and hydraulic experiment results are compared in terms of agreement using linear regression analysis.

3. Results

Figure 10.3. compares CMD images obtained in the hydraulic model experiment and the according numerical model simulations corresponding to cases 1, 7, 3 and 10 of table 10.1 (respectively corresponding with figure 10.3 (A), (B), (C) and (D). Overall, a good qualitative agreement is observed.

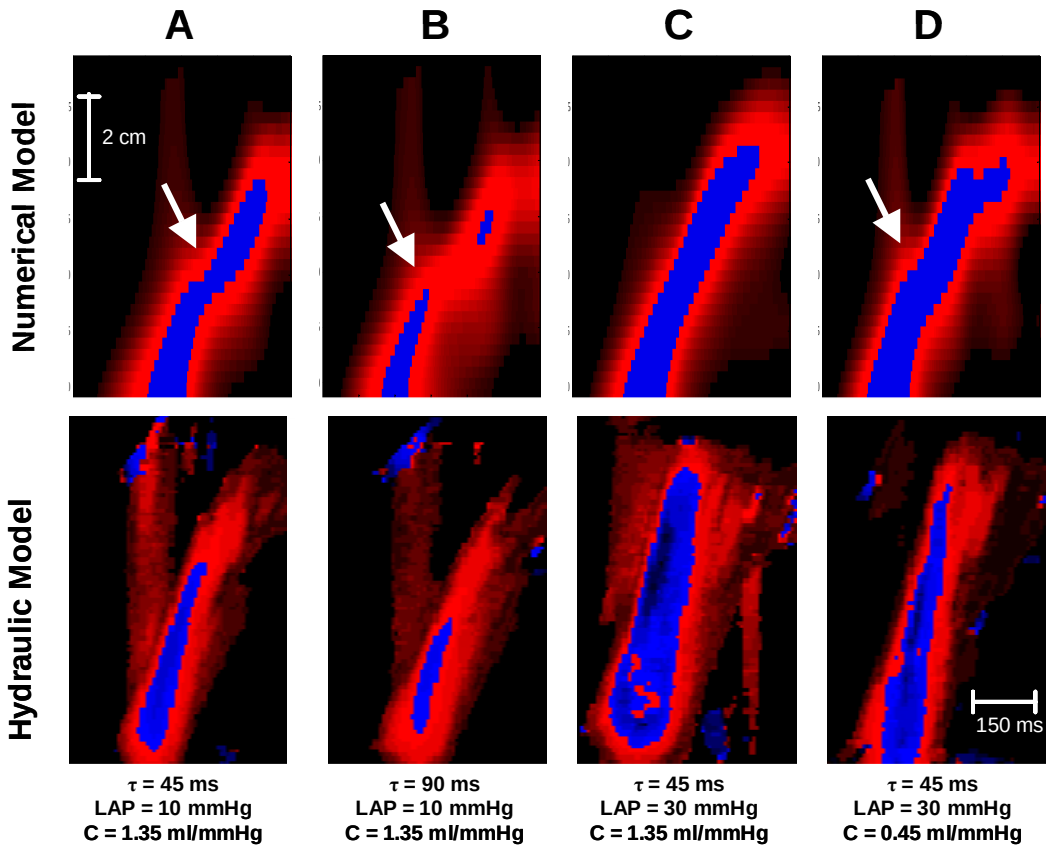

Figure 10.3: Calculated CMD images using the numerical model (**top**) and corresponding measured.CMD images in the hydrauloc model experiments (**bottom**) for varying time constant of relaxation (τ), LA pressure (LAP) and compliance (C). Arrows are indicating the positions where travelling vortices are stagnating.

The GLM model with dependent variable $v_{p,hydr}$ (v_p derived from hydraulic experiments) and covarying factors τ, compliance (C), and LA filling pressure (LAP) has a F-value of 82.9 (adjusted $r^2 = 0.82$, $p < 0.001$). A significant ($p < 0.001$) influence of τ, C and LAP is found. All interaction terms are removed as

they have no significant influence ($p > 0.05$). The according multiple linear regression equation is (Eq. 10.2):

$$v_p = 42.67 + 0.30 \cdot LAP - 0.30 \cdot \tau + 7.86 \cdot C \qquad \text{[Eq. 10.2]}$$

Figure 10.4 shows the regression between v_p derived from numerical simulations ($v_{p,num}$), and v_p derived from hydraulic model experiments ($v_{p,hydr}$) for the model LV with compliance 1.35 ml/mmHg. Overall, a moderate, but significant correlation coefficient is found ($r = 0.67$, $p < 0.01$). $v_{p,num}$ is consistently lower, compared to $v_{p,hydr}$.

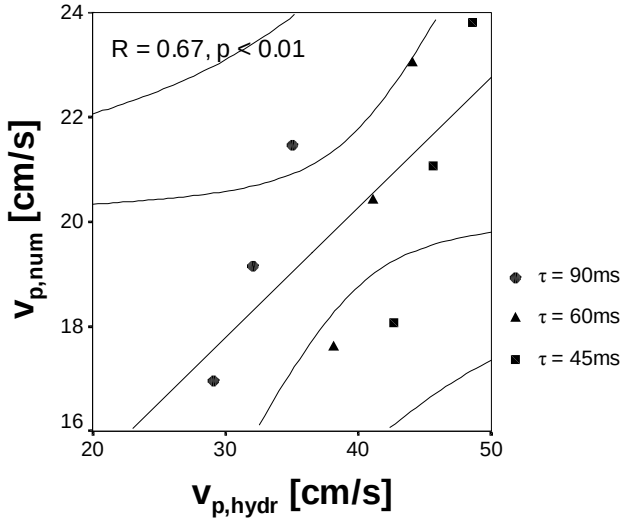

Figure 10.4: Regression, prediction and confidence intervals (p = 0.05) for numerical simulation results ($v_{p,num}$) versus hydraulic experiment results ($v_{p,hydr}$).

The relation between $v_{p,num}$ and τ (left), and $v_{p,hydr}$ and τ (right) for different levels of LA pressure is given in figure 10.5. $v_{p,num}$ decreases with increasing τ, and increases with increasing LA pressure. This is in agreement with the findings in the hydraulic model.

The left panel of figure 10.6 compares for different τ levels additional numerical simulations ($v_{p,num}$,) in a stiffer LV (Compliance = 0.45 ml/mmHg, squares) to the according simulations done in the LV with compliance 1.35 ml/mmHg (Triangles). In agreement with the hydraulic experiment results (Figure 10.6,

right), $v_{p,num}$ is higher in the more compliant model LV. However, in contrast to the hydraulic model results, this difference does not hold for all τ levels.

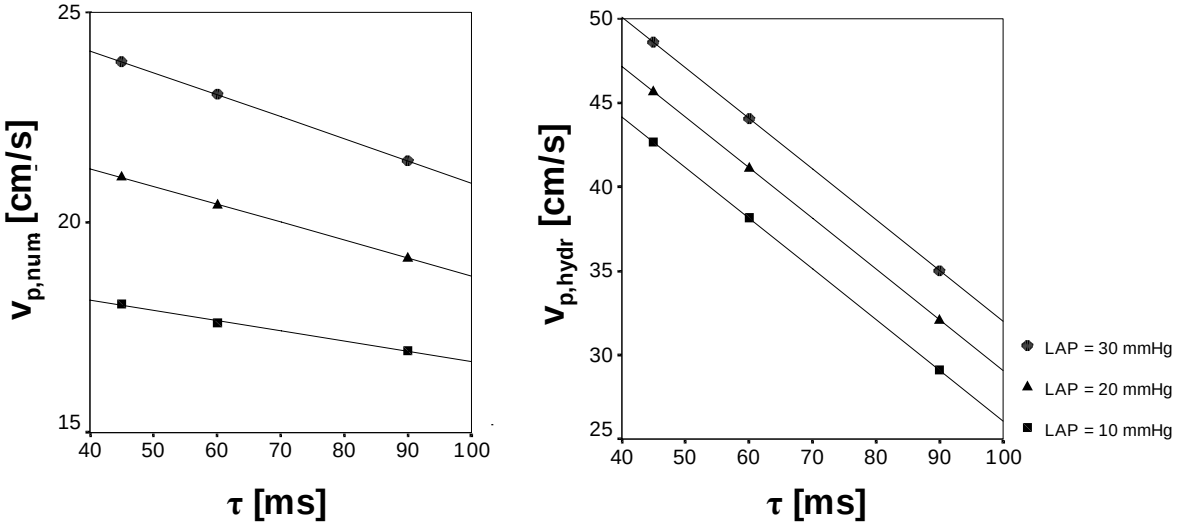

Figure 10.5: Numerical simulation results ($v_{p,num}$, **left**).and hydraulic experiment results ($v_{p,hydr}$, **right**) as a function of τ for different levels of LA pressure (LAP) in the LV model with compliance 1.35 ml/mmHg.

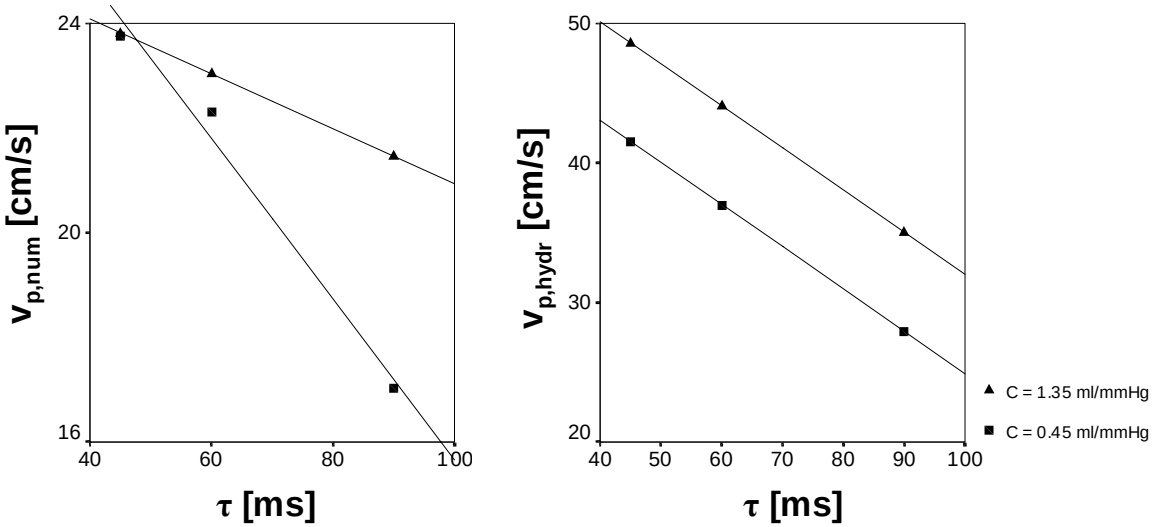

Figure 10.6: Numerical simulation results ($v_{p,num}$, **left**).and hydraulic experiment results ($v_{p,hydr}$, **right**) as a function of τ for different levels of LV compliance with LA pressure 30 mmHg.

4. Discussion

In this study numerical simulations corresponding to hydraulic model experiments have been compared.

v_p in the numerical simulations is consistently lower than v_p in the hydraulic experiments. Several aspects contribute to this aberration.

In the numerical model, gravity forces are not included in the equations. In contrast, in the hydraulic model, gravity interferes and, e.g., may cause a distortion of the LV geometry, compared to the numerical LV model. Further, in the numerical model, a homogeneous relaxation is assumed. Due to the position of the air outlets at the bottom level of the Perspex chamber that surrounds the hydraulic model LV, a homogeneous relaxation can not be guaranteed in the hydraulic experiments. Also, in the numerical model, inflow velocities are assumed to be orthogonal to the mitral valve plane. In the hydraulic model, as might be the case in vivo, this perfect alignment may not be present. Finally, the more pronounced curve-linear isovelocity lines in the numerical CMD output images, due to higher temporal and velocity resolution in the numerical simulations are also influencing derived v_p values.

In terms of changes in v_p as a result of changes in LV diastolic variables, hydraulic model experiments and numerical simulations agree well, especially for changes in τ and LA pressure. Concerning the influence of LV compliance, both models appear to show a deviant behaviour. In the hydraulic model ,compliance is positively correlated to v_p for all levels of τ, i.e. a more compliant LV leads to a higher v_p. This positive relationship between compliance and v_p is on one hand in contrast with the Moens-Korteweg equation, stating that wave propagation in a tube is related with the square root of the Young modulus E (i.e. an inverse relationship with compliance of the wall). On the other hand this finding supports the hypothesis that a stiff ventricle, not being an open tube, exerts a stronger resistance on the flow that enters the LV which fits with in vivo observations (Duval-Moulin et al. 1997) and in numero results (Vierendeels, 1998).

In the numerical model, there is an ambiguous influence of compliance on v_p, displayed in figure 10.6. Only for $\tau > 45$ ms, v_p is higher in the most compliant

model. Visual inspection of CMD images, especially from numerical simulations, shows a curved isovelocity contour that can be approximated in a bilinear way. Close to the base, the front is steeper (higher v_p) than further into the LV (lower v_p).

Reanalysing the simulated (numerical model) CMD images, only using the first cm of the isovelocity contour closest to the LV base, yields data given in figure 10.7. For all values of τ, the stiffer LV produces the highest v_p. in the first cm distal to the mitral valve, and seems to obey the Moens-Korteweg equation. Thus, close to the LV base, and in the early filling phase, the filling wave does not feel the resistance from the closed LV, as at this stage the reflection of waves at the LV apex did not has the occasion to influence hydrodynamics at the LV base.

Also, CMD images from the hydraulic experiments were reanalyzed, only taking into account the first centimeter of the isovelocity contour. However, due to noise in the images (which is completely absent in the numerical outcome), the fitting of lines to the 1 cm isovelocity contour using linear regression failed ($p > 0.05$) and derived v_p values were meaningless.

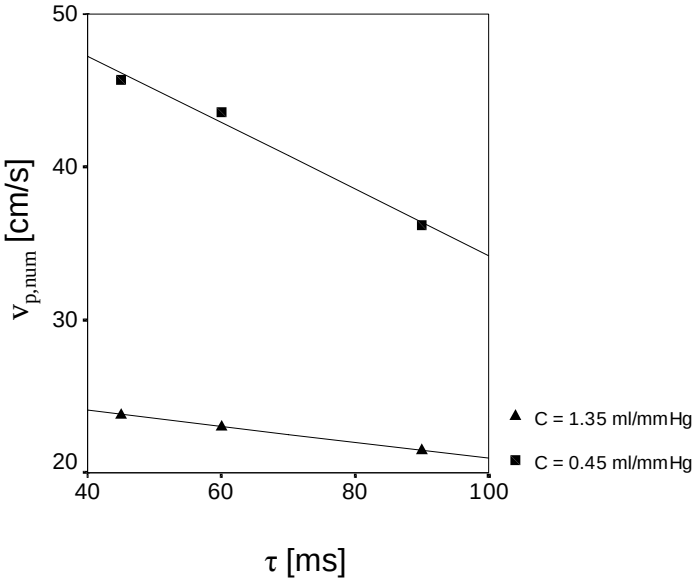

Figure 10.7: Numerical simulation results of v_p in the region of the LV base ($v_{p,num}$).as a function of τ for different LV model compliances.

The slower v_p, obtained when using the isovelocity contour that goes deeper in the LV can be explained by the stagnation point of the traveling vortices, occurring in the stiff LV (Figure 10.3 (D), see arrow), but not in the compliant LV (Figure 10.3 (C)). As can be verified in figures 10.3 (A) and (B), this stagnation point moves towards the apex with decreasing τ. Because the closer to the apex a stagnation point is situated, the less influence it has on calculated v_p values, this mechanism possibly explains the merging of v_p values for low τ values in the computer model.

5. Conclusion

The interaction between v_p and LV diastolic variables is studied in a numerical model and compared to corresponding hydraulic model results. Overall a good agreement is found. v_p increases with increasing LA filling pressure and decreases with increasing τ. A decrease in compliance augments v_p in the region of the LV base but decreases v_p due to stagnation of the vortex at the mid-level of the LV.

Acknowledgements

S. De Mey was supported by a grant of the Flemish Institute for the Promotion of Scientific-technological Research in Industry (IWT-971096).

CHAPTER 11

Regional Differences in the LV Time Constant of Relaxation: Its Relationship to Intraventricular Pressure Gradients in a Canine Model and Hydraulic Experiments †

† The content of this chaper has submitted for publication in Am J Physiol:
Regional Differences in the LV Time Constant of Relaxation: Its Relationship to Intraventricular Pressure Gradients in a Canine Model and Hydraulic Experiments.
S. De Mey, PM Vandervoort, JD Thomas, NL Greenberg, PR Verdonck.

Abstract

Introduction. The role of elastic recoil in producing intraventricular pressure gradients (IVPG) is well known. The influence of other physiologic variables however remains unclear. The aim of this study was therefore to investigate the role of regional differences in LV relaxation in producing IVPG.

Methods. Seven healthy adult mongrel dogs were used to measure pressures in the left atrium and at different locations in the left ventricle under baseline conditions and during infusion of isoproterenol and esmolol. To explore diastolic function in more detail and to support the findings in the canine model, analogue measurements are performed in a hydraulic model LV.

Results. In the canine model, the LV relaxation time constant τ was significantly shorter at the apex compared to the base of the LV at baseline ($\Delta\tau$ = 4.77±0.57%), during isoproterenol infusion ($\Delta\tau$ = 12.14±2.16%) and during esmolol infusion ($\Delta\tau$ = 1.40±0.11%). IVPG at baseline averaged 1.31 mmHg during isovolumic relaxation, rising significantly ($p < 0.001$) to 1.72 mmHg during early filling; these gradients rose significantly with isoproterenol and fell with esmolol, and multivariate analysis demonstrated both $\Delta\tau$ and τ to contribute significantly to predicting IVPG. These findings were supported by the hydraulic model, which showed IVPG to be closely related to $\Delta\tau$ ($r = 0.78$, $p<0.001$). In addition, the in vitro results suggested that higher LV compliance is associated with increased IVPG.

Discussion and conclusion. This study demonstrated that in addition to elastic recoil, regional relaxation differences significantly impact IVPG. The demonstration of shorter τ at the apex provides an additional link to explain variations in wall motion, IVPG and flow during the isovolumic relaxation period and early filling. Assessment of IVPG, now available non-invasively, could provide useful clinical insight into cardiac ischemia and diastolic dysfunction.

1. Introduction

Intraventricular pressure gradients (IVPG) and blood flow have been demonstrated during early diastole and during the isovolumic relaxation period (Courtois et al. 1988, Courtois et al. 1990, Falsetti et al. 1980, Firstenberg and al. 2001, Greenberg et al. 2001, Greenberg et al. 1995, Ling et al. 1979, Nikolic et al. 1995, Owen 1993, Verdonck et al. 1999, Vierendeels et al. 2000). Several mechanisms have been proposed to explain IVPG. Courtois and colleagues focused on the relationship between systolic function and diastolic IVPG by investigating the influence of regional ischemia-induced changes in LV function on IVPG (Courtois et al. 1990). Nikolic and coworkers (Nikolic et al. 1995) in a sophisticated animal experiment isolated elastic recoil as a source of IVPG in both filling and non-filling beats. Recently, Firstenberg et al. (Firstenberg and al. 2001) investigated IVPG for the first time in humans. Although a rigorous assessment of elastic recoil in terms of equilibrium volumes and suction volumes was not performed, the results of Firstenberg et al. were in accordance with the findings of Nikolic et al. and Courtois at al. in finding a significant relationship between changes in IVPG and changes in ESV. In addition, an important relationship between improvements in the time constant of LV relaxation (τ), an index for diastolic function, and increases in IVPG was observed.

Recently, Greenberg et al. (Greenberg et al. 2001) demonstrated the ability of directly and noninvasive quantifying IVPG using color M-mode Doppler echocardiography and digital image processing to apply the Euler equation, yielding potential application in the clinical setting. However, the inverse problem of assessing LV functional characteristics through analysis of IVPG requires knowledge of all mechanisms that produce and/or enhance IVPG. Because it is suggested that one or a combination of systolic and diastolic mechanisms are in effect, further investigation is required. The aim of this study was to focus on the possible role of diastolic function, specifically regional differences in τ within the left ventricular cavity, hypothesizing that these closely relate to regional LV wall motion and IVPG during the isovolumic relaxation period and during the early filling period. First, experiments were performed in a canine model under baseline conditions and during infusion of isoproterenol and esmolol. In order to separate

diastolic function from systolic function and to support the findings in the animal experiment, similar measurements were performed in a hydraulic LV filling model.

2. Methods

2.1. Animal Experiment and Data Acquisition

The investigation conforms to the Guide for the Care and Use of Laboratory Animals (NIH Publication No. 85-23, revised 1996). Seven healthy adult mongrel dogs weighing between 29.7kg ± 7.4kg (mean ± SD) of either sex were studied after animal care committee approval. The dogs were anaesthetized with 25mg/kg intravenous sodium pentobarbital. Anesthesia was maintained throughout the experiments with intermittent intravenous infusions of aliquots of pentobarbital. After tracheal intubation, positive pressure mechanical ventilation was instituted using room air. A peripheral vein was cannulated for crystalloid infusion in order to assist the maintenance of stable hemodynamics during pharmacological interventions. The right internal jugular vein was cannulated for hemodynamic monitoring with a 7.5F pulmonary artery catheter (Swan-Ganz; Baxter Healthcare Corporation, Irvine, CA, USA) and infusion of medication. The right femoral artery was cannulated for hemodynamic monitoring throughout the experiments. Following a midline sternotomy, the sternum was widely spread and the heart isolated and suspended in a pericardial cradle for exposure. At the end of all experiments on a given dog, the dog was sacrificed with an overdose of pentobarbital.

A dual sensor micromanometer catheter (Millar, Houston, TX, USA) was introduced into the left atrium (LA) through the left atrial appendage and positioned across the mitral valve with the distal pressure sensor in the apex of the left ventricle (LV) and the proximal pressure sensor at the level of the base of the left ventricle, 5 cm proximal from the catheter tip. The catheter was immersed in a saline solution for one hour prior to use to minimize pressure 'drift'. Prior to introduction, the transducers were calibrated relative to atmospheric pressure, 20 mmHg, and 100 mmHg gauge pressure. To account for hydrostatic pressure differences, LA and LV pressures were aligned during a long diastolic time interval. The pressure signals were amplified using a universal amplifier (Gould, Valley View, OH, USA) with a flat frequency response up to 500Hz. Six to twenty seconds, comprising a single data run, of both LA and LV pressures were digitized at 1000HZ using an AT-MIO-16 multifunctional data acquisition card

(National Instruments, Austin, TX, US) and transferred for storage to a personal computer (Gateway, North Sioux City, SD, USA) using a custom acquisition program developed in the Lab VIEW (National Instruments, Austin, TX, USA) environment.

Data acquisition was performed in stages at baseline (for each dog experiment), with isoproterenol infusion (for 6 dog experiments) and with esmolol infusion (for 3 dog experiments). Baseline data acquisition runs were initiated after allowing sufficient time for hemodynamics to stabilize before starting the experiment. Either esmolol or isoproterenol medication runs were initiated after completion of a satisfactory number of baseline acquisition runs. Isoproterenol was infused at 0.025 - 0.4 µg/kg/minute intravenously and data acquisition runs were initiated after allowing sufficient wash-in time for an appropriate heart rate response and hemodynamics to stabilize. Similarly, esmolol was infused at 0.2 - 0.3 mg/kg/minute intravenously with data acquisition after hemodynamic stabilization.

2.2. Hydraulic Model: Setup and Data Acquisition

The left heart model (Figure 11.1) exists of an open rigid cylindrical Perspex atrium (diameter 30 mm) connected to a truncated ellipsoidal ventricle (zero-pressure equilibrium volume 100 ml, base-apex length 75 mm, short axis 50 mm). The ventricle is composed of latex. In order to prevent overinflation at the higher pressure ranges, the ventricle is surrounded by a gauze. The compliance of the LV is proportional to the LV wall thickness. Experiments are performed using a compliant (wall thickness 0.8 mm) and a stiff (wall thickness 3 mm) model LV. To quantify the compliance of the model ventricles, a passive pressure-volume relationship is measured by inflating the ventricles in steps of 2 ml. Using linear regression the slope of the pressure-volume relationship was determined for the compliant and the stiff ventricle (1.35 and 0.45 ml/mmHg respectively).

In between the two heart chambers a mitral tricuspid porcine xenograft is mounted (diameter 21 mm, McNeilab Inc., Anaheim, California). A 60%-40% water-glycerine mixture (viscosity 3.5 10E-6 Pas) was used as test-fluid. In the experimental set-up, the ventricle is surrounded by a closed rectangular Perspex chamber (Figure 11.1, PeCh) with dimensions 250 mm x 250 mm x 150 mm.

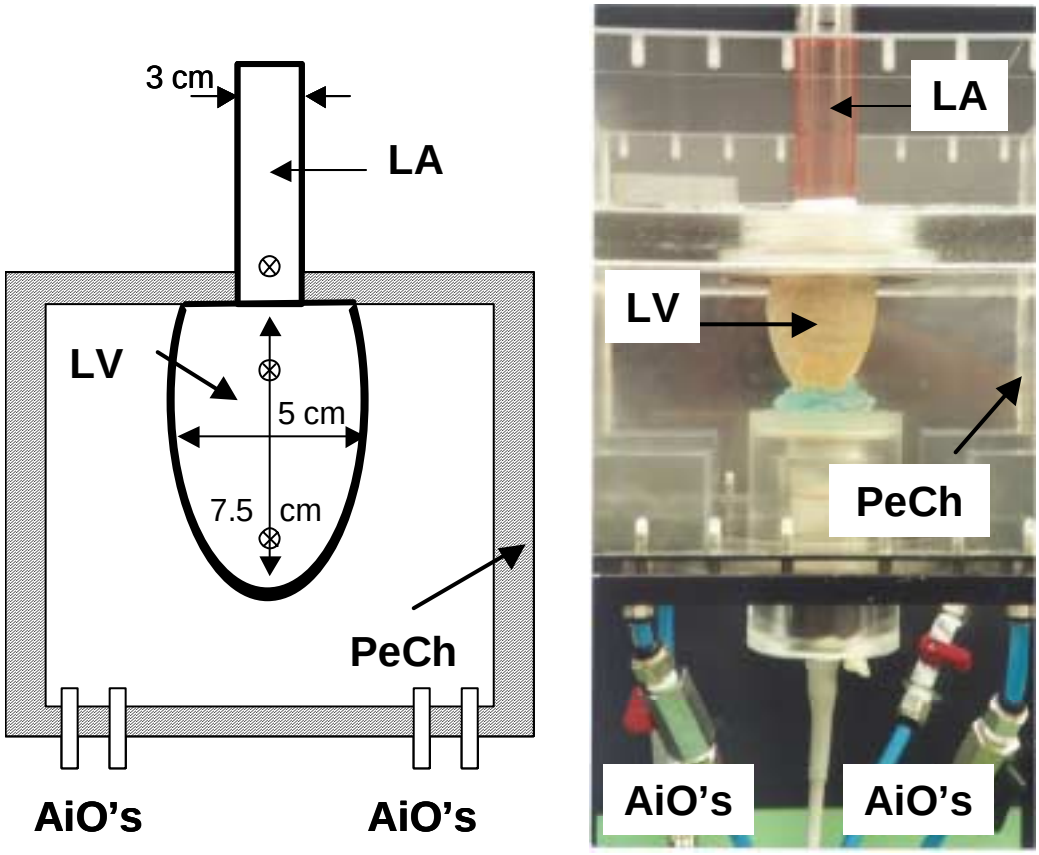

Figure 11.1: Hydraulic model of the left heart. **Left panel**: Schematic drawing. **Right panel**: According picture. The hydraulic model is composed of a cylindrical perspex atrium (LA) connected to a latex left ventricle (LV). The LV is surrounded by a perspex chamber (PeCh). In the bottom of the PeCh airoutlets (AiO's) are provided. ⊗: Location of pressure sensors in the model.

An early filling wave is initiated by bringing the ventricle to its end-systolic volume and pressure, starting from a filled ventricle in equilibrium under a fixed atrial pressure, i.e. for a fixed atrial fluid level. This is done by applying pressure (100 mmHg) in the Perspex chamber around the LV, using a pneumatic system and compressed air. Because of the valve in mitral position, the fluid inside the LV can not freely migrate from the LV to the LA. Consequently, LV pressure rises until it equals the pressure in the surrounding Perspex chamber, causing leaking of the fluid round the bioprosthesis. When the LV has reached its end-systolic volume, the actual filling of the LV is initiated by switching an electromagnetic valve of the pneumatic system, releasing the air out of the surrounding chamber through openings in the bottom op the surrounding Perspex chamber and allowing the LV to relax. The rate of relaxation can be changed by

adapting the area of the air outlets (Figure 11.1, AiO's). Filling pressure is adjusted by changing the fluid level in the atrium.

The model is instrumented with a multitip pressure transducer (Millar, Houston, TX, USA) in atrium and ventricle. Pressure transducers are located in the LA, the LV base and the LV apex. In the model pressure tracings are recorded for 3 settings of LA pressures (3, 10 and 30 mmHg), 4 settings of the time constant of ventricular relaxation between 55 and 160 ms, and 2 different LV compliances (0.45 – 1.35 ml/mmHg), yielding 3 x 4 x 2 = 24 different hemodynamic settings.

2.3. DATA ANALYSIS

Post acquisition numerical analysis of raw pressure data was performed using a custom numerical analysis program developed in the LabVIEW (National Instruments, Austin, TX, USA) environment. Figure 11.2 (A) illustrates typical pressure recordings in the canine model (left) and the hydraulic model (right). The period of isovolumic relaxation was defined as the time period between peak negative dp/dt and the opening of the mitral valve, defined as the first crossover of LA and LV pressure curves (Figure 11.2, reference line A). Reference line A and reference line B, positioned at the first crossover of LV basal and apical pressure after reference line A determined the early filling period. A mono-exponential LV pressure decay is assumed during the period of isovolumic relaxation: $p(t) = (p_0 - p_\infty) \exp(-t/\tau) + p_\infty$, with $p(t)$ the time-varying pressure, p_0 the pressure at maximum negative dp/dt, τ the time constant of relaxation and p_∞ the pressure asymptote. The time constant of relaxation (τ) was calculated under the assumption of a zero pressure asymptote as previously validated by Yellin and colleagues (Yellin et al. 1986) using the non-linear Levenburg-Marquardt algorithm. Pressure differences between base and apex are displayed in more detail in figures 11.2 (B) and (C). Figure 11.2 (B) plots the pressure differences between LA and the LV at the level of the base (LAP-LVPbase, dashed line) and the level of the apex (LAP-LVPapex, full line). The maximum instantaneous IVPG during isovolumic relaxation (IVPGivr) and early filling (IVPGe) were derived from the instantaneous pressure differences between the base and apex (Figure 11.2 (C)).

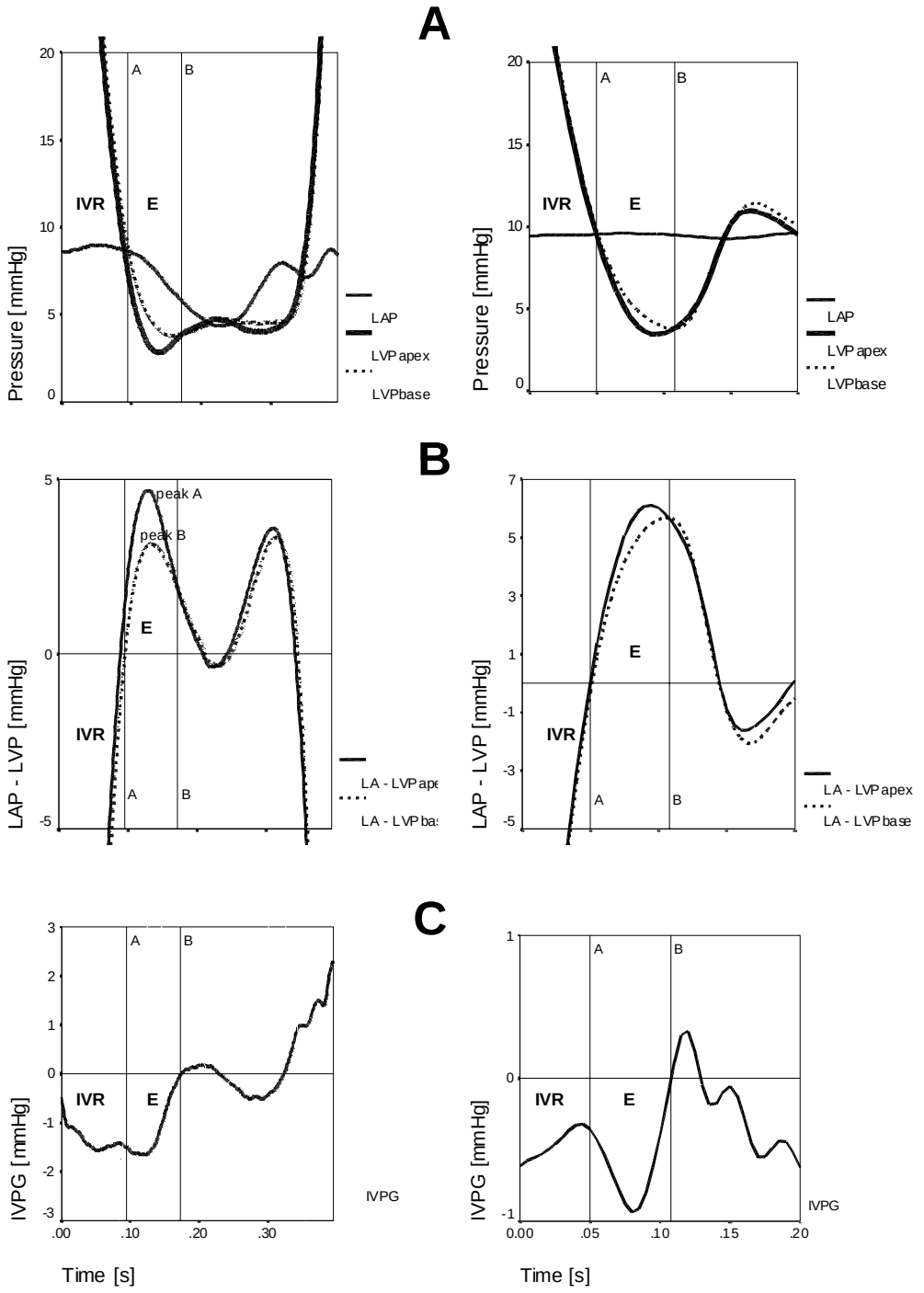

Figure 11.2: High fidelity pressure measurements in the dog experiment (left) and in the hydraulic experiment (right). Reference line A indicates the end of the isovolumic relaxation period (IVR), reference line B indicates the end of the early filling period (E). (A) Simultaneous LA pressure (LAP), LV pressure at the base (LVPbase) and LV pressure at the apex (LVPapex) recordings. (B) Pressure differences between LA pressure and LV basal pressure (LA - LVPbase) and LA pressure and LV apical pressure (LA - LVPapex). (C) Instantaneous intraventricular pressure gradients between left ventricular base and apex (IVPG).

2.4. STATISTICS

Mean values and standard errors (SE) of τ and IVPG are reported. A two tailed, paired t-test was used to compare τ at different locations within the LV and to compare IVPGivr and IVPGe. One way ANOVA was used to compare τ, IVPGivr, and IVPGe at baseline and during drug infusion. Post-hoc tests were performed using Bonferroni correction. Multivariate general linear models (GLM) were used to test for significant relations between variables. The GLM multivariate procedure provides regression analysis and analysis of variance for multiple dependent variables by one or more factor variables or covariates. The level of significance was set at a p-value of 0.05.

3. Results

3.1. Animal Experiment

LV base and apex values of τ under baseline, esmolol, and isoproterenol conditions are shown in Table 1. At baseline t is significantly shorter (Table 11.1, paired t-test, $p < 0.001$) at the apex compared to the base of the LV in 26 analyzed pressure recordings in all 7 dogs. The infusion of isoproterenol in 6 dogs with a total of 13 analyzed pressure recordings significantly shortened τ at both the base and the apex of the LV, whereas the infusion of esmolol in 3 dogs with a total of 8 analyzed pressure recordings significantly lengthened τ in comparison to baseline conditions (Table 11.1, ANOVA, post hoc Bonferroni correction, $p < 0.017$). τ became even more significantly shorter at the apex than at the base of the LV during isoproterenol infusion and less so during esmolol infusion (Table 11.1, paired t-test, $p<0.001$).

Table 11.1: τ values determined from pressure recordings obtained during the animal experiments at the LV base and apex at baseline, during isoproterenol infusion and during esmolol infusion.

	τ_{base} [ms]	τ_{apex}, [ms]	$\Delta\tau$, %
Baseline (n = 26)	74.8 ± 4.9	71.3 ± 4.8	4.8 ± 0.6*
Isoproterenol (n = 13)	53.8 ± 3.7†	47.7 ± 4.0†	12.1 ± 2.2$^{*, \ddagger}$
Esmolol (n = 8)	113.1 ± 5.9†	111.6 ± 4.3†	1.4 ± 0.1$^{*, \#}$

*: $p<0.001$, basis vs. apex, paired t-test; †: $p < 0.017$ vs baseline, ANOVA; ‡: $p < 0.001$ vs baseline, ANOVA; $^{\#}$: $p < 0.05$ vs baseline, ANOVA.

The maximum instantaneous pressure difference during isovolumic relaxation (IVPGivr) and the maximum instantaneous pressure difference during early filling (IVPGe) under baseline, isoproterenol, and esmolol conditions are shown in table 11.2. IVPGivr correlated significantly with IVPGe (Figure 11.3 (A), $r = 0.923$, $p < 0.001$). However, IVPGivr was significantly smaller than IVPGe (Table 11.2, paired t-test, $p < 0.001$). Under isoproterenol infusion, IVPGivr and IVPGe increased significantly compared to baseline values (Table 11.2, ANOVA, post hoc Bonferroni correction, $p < 0.003$). Under esmolol infusion IVPGivr and

IVPGe decreased significantly compared to baseline values (Table 11.2, ANOVA, post hoc Bonferroni correction, $p < 0.003$ and $p < 0.05$ respectively). Significant correlations between τbase and IVPGivr (Figure 11.3 (B), $r = -0.676$, $p < 0.001$), tbase and IVPGe ($r = -0.520$, $p < 0.001$), $\Delta\tau$ and IVPGivr ($r=0.709$, $p < 0.001$), and $\Delta\tau$ and IVPGe (Figure 3 (C), $r=0.733$, $p < 0.001$) were observed. In a multivariate regression model, both $\Delta\tau$ and τ were significant independent predictors for IVPGivr (corrected model F-value 41.1, $p < 0.001$; F-value $\Delta\tau$ 24.4, $P < 0.001$; F-value τ 18.7, $p < 0.001$) and IVPGe (corrected model F-value 29.7, $p < 0.001$; F-value $\Delta\tau$ 31.5, $p< 0.001$; F-value τ 3.9, $p = 0.054$).

Table 11.2: Instantaneous maximum intraventricular pressure gradients during isovolumic relaxation (IVPGivr) and early filling (IVPGe) at baseline during isoproterenol infusion and during esmolol infusion.

	IVPGivr, mmHg, mean ± SE	**IVPGe, mmHg, mean ± SE**
Baseline	$1.3 \pm 0.1^{*}$	1.7 ± 0.1
Isoproterenol	$2.1 \pm 0.2^{*,\dagger}$	$2.5 \pm 0.3^{\dagger}$
Esmolol	$0.5 \pm 0.1^{*,\dagger}$	$1.0 \pm 0.1^{\ddagger}$

*: $p<0.001$ vs IVPGe, paired t-test; †: $p<0.003$ vs baseline, ANOVA; ‡: $p<0.05$ vs baseline, ANOVA.

3.2. HYDRAULIC MODEL LV

Measurements are performed in 24 different hemodynamic settings of the hydraulic model. Figure 1 compares typical pressure tracings in the hydraulic model (right panels) with corresponding measurements in the animal model (left panel). Pressure tracings during the isovolumic relaxation period (IVR) and early filling (E) in the animal and hydraulic model are similar. Note that atrial contraction is not simulated in the hydraulic model. To compare the hydraulic model experiment to the animal experiment quantitatively, the hydraulic model results are categorized in three levels of τ using a standard “categorize” procedure of the SPSS software. The procedure converts continuous numeric data to a discrete number of categories based on percentile groups, with each group

containing approximately the same number of cases. Resulting group mean values of τ and differences in τ between base and apex are summarized in table 11.3.

Table 11.3: Categorized τ values from basal τ_{base} and apical τ_{apex} pressure tracings obtained in the hydraulic model. $\Delta\tau$: difference in τ.

	τ_{base}, [ms]	τ_{apex}, [ms]	$\Delta\tau$, %
Group 1 (n = 8)	59.5 ± 1.0	58.6 ± 1.0	$1.5 \pm 0.4^{*}$
Group 2 (n = 8)	74.6 ± 3.4^{NS}	73.3 ± 3.3^{NS}	$1.6 \pm 0.5^{*, NS}$
Group 3 (n = 8)	$140.1 \pm 12.0^{\dagger, \ddagger}$	$138.7 \pm 11.9^{\dagger, \ddagger}$	$1.0 \pm 0.3^{*, NS}$

*: $p<0.001$, paired t-test; †: $p<0.001$ vs Group 1, ANOVA; ‡: $p<0.001$ vs Group 2, ANOVA; ^{NS}: Not significant vs Group 1, ANOVA

The mean t values of the three groups are comparable to the values obtained in the animal experiment at baseline (~ Group 2), during isoproterenol (~ Group 1) infusion and during esmolol infusion (~ Group 3). The difference in τ along the base-apex axis is consistently directed from high to low. In contrast to the animal experiment, the magnitude of the differences do not differ significantly between the groups.

Table 11.4 summarizes IVPG obtained in the hydraulic model during isovolumic relaxation (IVPGivr) and early filling (IVPGe) for different levels of τ. Similar to the animal experiments, IVPGivr was significantly smaller than IVPGe (Table 4, paired t-test, $p<0.001$). In contrast to the animal experiments, no significant differences in IVPG are observed between the different groups.

Table 11.4. IVPG during isovolumic relaxation (IVPGivr) and early filling (IVPGe) obtained in the hydraulic model for different levels of τ

	IVPGivr, mmHg, mean ± SE	IVPGe, mmHg, mean ± SE
Group 1	$0.7 \pm 0.1^{*}$	1.2 ± 0.1
Group 2	$0.8 \pm 0.1^{*, NS}$	1.2 ± 0.1^{NS}
Group 3	$0.7 \pm 0.1^{*, NS}$	1.1 ± 0.1^{NS}

*: $p<0.001$ vs IVPGe, paired t-test; ^{NS}:Not significant vs Group 1 and 2, ANOVA.

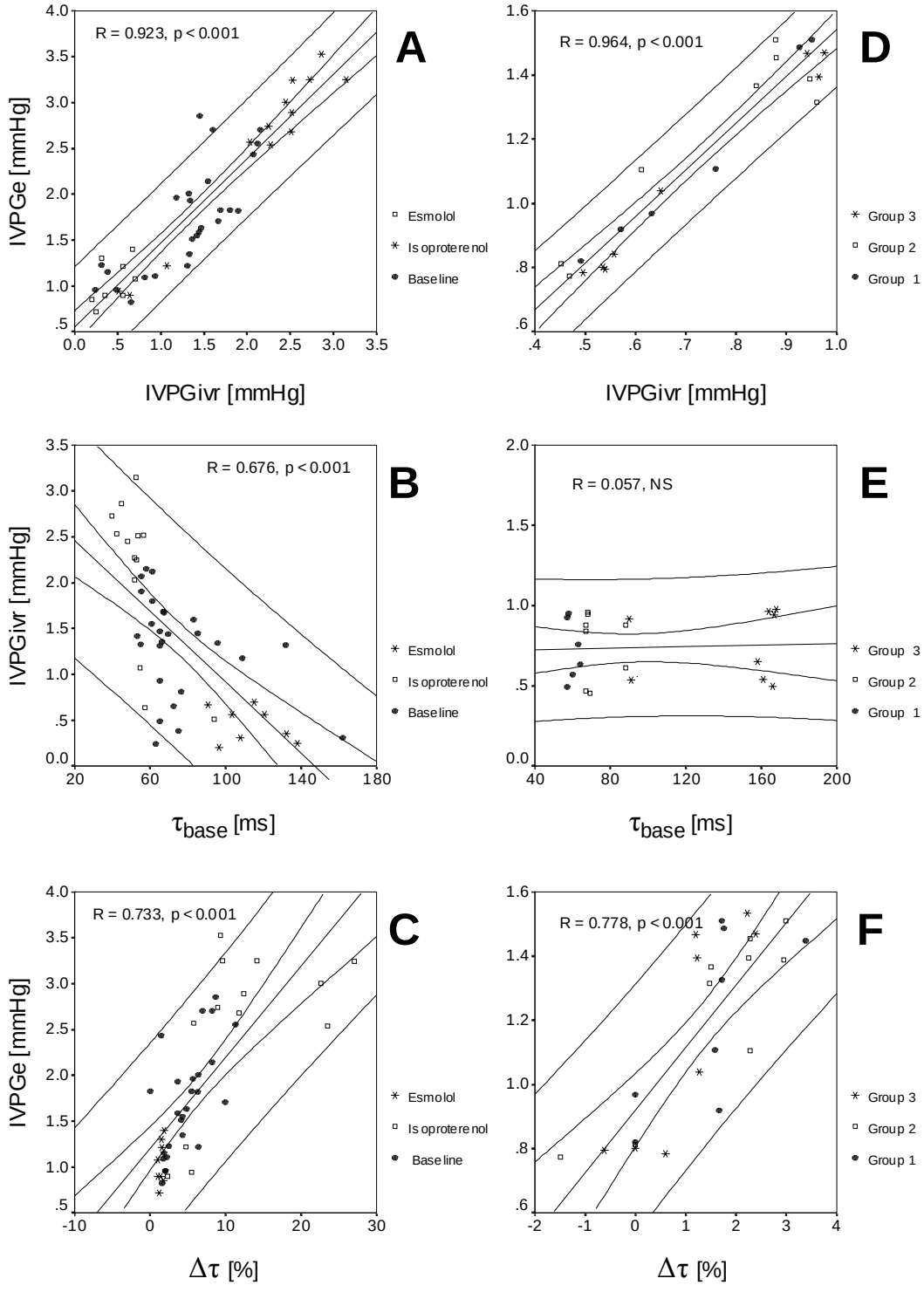

Figure 3: Regression of the instantaneous intraventricular pressure gradient during isovolumic relaxation (IVPGivr) and the instantaneous intraventricular pressure gradient during early filling (IVPGe) in the canine model (**A**) and the hydraulic model LV (**D**). Regression of $\Delta\tau$ and IVPGivr in the canine model (**B**) and the hydraulic model LV (**E**). Regression of $\Delta\tau$ and IVPGe in the canine model (**C**) and the hydraulic model LV (**F**).

Figures 11.3 (D), (E), and (F) display the regression plots corresponding to the regressions obtained in the animal experiment (Figure 11.3, (A), (B) and (C)). Compared to the animal experiment, in the hydraulic model analogue significant regressions are found between IVPGivr and IVPGe ($R = 0.964$, $P<0.001$), and $\Delta\tau$ and IVPGe ($R = 0.788$, $P<0.001$). In contrast, no significant correlation between τ and IVPGivr ($R = 0.058$, NS) was found.

In contrast to the animal model, an advantage of the hydraulic model was that several additional hemodynamic variables, including LA filling pressure and LV compliance, could be altered independently from each other. To test for significant variables that are influencing IVPGivr and IVPGe, both were entered as dependent variables in a multivariate model with covarying variables compliance, $\Delta\tau$, τbase, and LA filling pressure (LAP). Results are in table 11.5.

Table 11.5. Multivariate models predicting IVPGivr and IVPGe measured in the hydraulic model.

Dependent Variable	**Covarying parameter**	**β, mean ± SE**	**F**	**P**
IVPGivr [mmHg]	Model		94.2	0.000
	Intercept	0.390 ±0.030	173.9	0.000
	Compliance [ml/mmHg]	0.345 ± 0.039	78.64	0.001
	Δτ [%]	3.598 ± 1.562	5.306	0.032
IVPGe [mmHg]	Model		161.6	0.000
	Intercept	0.896 ± 0.075	141.7	0.000
	LAP [mmHg]	-0.005 ± 0.001	13.70	0.000
	Compliance [ml/mmHg]	0.480 ± 0.038	161.78	0.000
	Δτ [%]	6.506 ± 1.548	17.66	0.000

The β coefficient estimates the effect on the dependent variable of an isolated one unit increase in the corresponding covarying parameter. Non significant parameters are removed one by one. Compliance and $\Delta\tau$ remained significant for predicting the IVPG during isovolumic relaxation, whereas LA filling pressure,

next to compliance and $\Delta\tau$, remained significant for predicting the IVPG during early filling.

4. Discussion

In this study the influence of LV diastolic properties on intraventricular pressure gradients (IVPG) are investigated in a combined canine and hydraulic model experiment. In the animal experiment, the time constant of pressure fall during isovolumic relaxation (τ), spatial differences in τ ($\Delta\tau$), and their relationship with intraventricular pressure gradients during isovolumic relaxation (IVPGivr) and early filling (IVPGe) were measured. Because it is impossible to control all physiological variables in an animal model, a corresponding hydraulic model experiment was done. In the hydraulic LV model, each LV property can be changed and quantified, independently from other LV properties, while obviously sacrificing some physiologic features.

Animal experiment

Values of τ were consistently shorter at apical locations compared to basal locations in the canine LV. The direction of $\Delta\tau$ along the longitudinal axis of the LV from high to low was consistently base to apex under baseline condition, this gradient becoming even steeper during isoproterenol infusion (which shortened τ globally) and flatter during esmolol infusion (which lengthened τ globally). These findings are in agreement with the findings of previous authors (Bernardi et al. 1989, Burwash et al. 1993, Frederiksen et al. 1978, Gaasch et al. 1980, Karliner et al. 1977, Kettunen et al. 1986, Martin et al. 1984, Pagel et al. 1994). Under baseline conditions the magnitude of $\Delta\tau$ was 4.8% of the value at the base. During isoproterenol infusion the magnitude increased to 12.1%, whereas esmolol infusion caused an decrease of the magnitude to 1.4%. Based upon the findings of this study, the future reporting of values of τ in the literature should have the location of its determination with reference to fixed cardiac landmarks noted.

When the intraventricular pressure gradients were analyzed, both IVPGivr and IVPGe were observed to increase with isoproterenol infusion (decrease in τ) and to decrease with esmolol infusion (increase in τ), in comparison to baseline values. The inverse relation between τ and IVPG is also observed in humans by Firstenberg at al. (Firstenberg and al. 2001). In multivariate analysis, a positive relationship of $\Delta\tau$ with IVPGivr and IVPGe was demonstrated. To summarize, the earlier the apex relaxes relative to the base (as manifest by a high $\Delta\tau$), the higher

the base-to-apex pressure gradient during early diastole, an effect magnified at rapid overall relaxation, as manifest by a low τ.

Hydraulic model experiment

In order to isolate diastolic properties from systolic function and to interpret the findings in the animal experiment, measurements analogous to the canine model were performed in our hydraulic LV filling model.

Overall, good agreement between pressure tracings in the animal and hydraulic model experiments was observed, including the observation of a $\Delta\tau$, significant correlation between IVPGivr and IVPGe, and a significant relationship between $\Delta\tau$ and both IVPGivr and IVPGe.

In addition to τ and $\Delta\tau$, the influence of isolated changes in LV compliance and LA filling pressure was also tested. $\Delta\tau$ and overall LV compliance were positively correlated with IVPGivr, whereas LA filling pressure exerted an small additional effect on IVPG during early filling. The non-significant influence of LA pressure on IVPGivr is a logical consequence of the closed mitral valve during isovolumic relaxation.

The significant correlation between τ and IVPG, observed in the canine model, was not observed in the hydraulic model. Several aspects may explain this difference. On one hand, in the hydraulic model local differences in relaxation of the LV wall between basal and apical are solely a consequence of the position of the air outlets in the bottom of the model. Because further away from the outlets, relaxation of the LV at the level of the base is slower compared to the level of the apex. This fixed model setup explains the flat relationship between τ and $\Delta\tau$, observed in the hydraulic model ($r = -0.142$, $p = 0.488$), whereas the physiologically more integrated canine heart showed a significant correlation between $\Delta\tau$ and τ ($r = -0.476$, $p < 0.001$). For example, it is known that changing loading conditions may produce significant variations in τ (Gillebert et al. 1997, Leite-Moreira et al. 1999), while beta adrenergic modulation may have regional effects of differing magnitude within the heart.

Global determinants of IVPG

Several authors have demonstrated a pressure related intrinsic association between IVPG and changes in myocardial length during diastole (Hittinger et al. 1987, Nikolic et al. 1995, Owen 1993, Park et al. 1993). Nikolic at al. demonstrated that global elastic recoil is a major determinant of IVPG. However, it has also been suggested that the simple presence of IVPG is not in itself a rigorous proof of elastic recoil (Verdonck et al. 1999, Vierendeels et al. 2000). The present study demonstrated that other global LV diastolic properties, including compliance and LA pressure may also impact this.

Regional differences influencing IVPG

In this study, special attention is paid to local differences in τ within the LV cavity. $\Delta\tau$ is isolated in both canine and hydraulic model as an important determinant of IVPG. Mathematically speaking, IVPG can only occur if pressure falls faster in the LV apex than at the base. The finding in this study that the LV pressure decreases faster in the apex compared to the base during isovolumic relaxation, leading to an IVPG between base and apex both during isovolumic relaxation and early filling, provides a hemodynamic origin for the IVPG and subsequent blood flow that is not surprising. Interesting however is that the fact that the cross-over between basal and apical LV pressures already occurs during the course of isovolumic relaxation which supports the hypothesis that IVPG is not solely a consequence of a sudden phenomenon (e.g. the opening of the mitral valve and start of filling). These results support the hypothesis that during the isovolumic relaxation period the LV, besides bringing the LV pressure below LA pressure, also actively prepares for the subsequent early filling by producing IVPG during the isovolumic relaxation period, resulting in a redistribution of blood towards the apex.

Whereas the relevancy of $\Delta\tau$ in producing IVPG seems straightforward, the origin of $\Delta\tau$ remains a matter of debate. Differences in τ are a consequence of regional wall motion in the LV. Regional wall motion, especially during the isovolumetric relaxation period, is already reported by Altieri in 1973 (Altieri et al. 1973) and more recently by Kondo (Kondo et al. 1995). Unresolved, however, is the question of whether the regional difference in LV wall motion, and

consequentially $\Delta\tau$, is a reflection of faster cellular relaxation, earlier relaxation, regional differences in elastic recoil, or some combination of all three.

Assessment of $\Delta\tau$

Davis et al. (Davis et al. 1999) previously reported $\Delta\tau$ along the base-apex axis in a dog experiment, but in that study $\Delta\tau$ could only be demonstrated using a non-zero pressure asymptote in the relaxation model. Recently we investigated the accuracy of τ assessments using mono-exponential models with and without the assumption of a zero pressure asymptote (De Mey et al. 2001) and showed that the precision of t estimation was significantly worse in the non-zero asymptote model, which has an additional degree of freedom than the zero asymptote model. It was concluded that the zero asymptote method provides the most precise τ estimates when the actually pressure asymptotes of comparison runs (in this case the base and apex recordings) are similar. Because no significant difference in the actual pressure asymptote existed between basal and apical locations (mean difference 0.80 ± 0.61 mmHg, mean $\pm$ se, $p=0.59$, paired t-test), the zero asymptote mono-exponential model produces the most accurate estimates of $\Delta\tau$.

Clinical implications

Until recently all investigations of IVPG and $\Delta\tau$ required meticulous invasive catheterization with multiple high-fidelity transducers and thus had limited application in clinical cardiology. However, it is now possible to estimate IVPG entirely noninvasively by applying the Euler equation to the spatiotemporal blood velocity distribution within the LV inflow tract acquired by color M-mode Doppler echocardiography (Greenberg 1996; Greenberg 2001). This methodology has recently been applied to multiple clinical situations, including exercise testing (Vlassak et al. 2001a), myocardial revascularization (Firstenberg et al, Circ 2001), and septal myectomy in HOCM. The connection between $\Delta\tau$ and IVPG defined in this study should help in the nascent clinical application of IVPG imaging by color M-mode Doppler.

Limitations

This study has some limitations, which must be considered in interpreting the results. This canine model was an acute, open-chest, open pericardium model. While the effects of the pericardium are likely to be less important during isovolumic relaxation and early filling than at the end of diastole, future work should seek to confirm these findings in a closed chest model. The latex ventricle of the hydraulic model, surrounded with a gauze, can not mimic the complex physiological processes in the normal and diseased heart. However, the aim of the model is not to mimic detailed processes at the cellular level, but to clarify the isolated influence of the relevant variables on the hydrodynamics of LV filling. We used a porcine xenograph mitral valve. The influences of the papillary muscles and chordae tendinae are not mimicked.

5. Conclusion

The time constant of isovolumic relaxation t has long been regarded as a global cardiac index of diastolic function during the isovolumic relaxation period. This study demonstrated, under several different physiologic conditions, a consistent gradient in t along the longitudinal axis of the LV cavity, slower at the base, faster at the apex. The demonstration of a spatial t vector in the canine heart provides a plausible link to explain the presence of intraventricular pressure gradients and flow during the isovolumic relaxation period and early filling.

Acknowledgements

The first author is a recipient of a grant from the Flemish Institute for the Promotion of Scientific-Technological Research in the Industry [IWT-971096]. Also supported in part by Grants NCC 9-57 and NCC 9-60, National Aeronautics and Space Administration, Houston, TX (JDT) and R01-HL56688-01A1 from the National Institutes of Health National Heart, Lung and Blood Institute (JDT). Special regards to P. Segers for reviewing the manuscript.

CHAPTER 12

Diastolic Dysfunction, Infarct Size and Exercise Capacity in Remote Myocardial Infarction: A Combined Approach of Mitral E-wave Deceleration Time and Color M-mode Flow Propagation Velocity †

† The content of this chaper has been submitted for publication in Am J Cardiol:
Diastolic Dysfunction, Infarct Size and Exercise Capacity in Remote Myocardial Infarction: A Combined Approach of Mitral E-wave Deceleration Time and Color M-mode Flow Propagation Velocity.
J Sutter, S De Mey, J De Backer, O De Winter, S De Maeseneire, M De Buyzere, R Dierckx and P Verdonck.

Abstract

In 41 patients with remote myocardial infarction, both mitral E-wave deceleration time (d_t) and color M-mode Doppler flow propagation velocity (v_p) were related to infarct size evaluated by nuclear imaging. Especially pseudonormal and restrictive filling patterns (defined by the combination of d_t and v_p) were associated with greater infarct size and lower left ventricular ejection fraction. Although no direct correlation between d_t or vp and exercise capacity could be documented, exercise capacity was reduced in all stages of diastolic dysfunction as compared to patients with a normal diastolic filling pattern. Our findings support the combined use of d_t and vp to assess diastolic dysfunction in patients with remote myocardial infarction.

1. Introduction

A restrictive filling pattern, characterized by shortening of the mitral E-wave deceleration time (d_t), has been shown to be a strong, independent predictor of adverse left ventricular (LV) remodeling and a poor clinical outcome after myocardial infarction (Cerisano et al. 1999, Nijland et al. 1997, Oh et al. 1992). Yong et al. (Yong et al. 2001) recently suggested that these findings could be explained by the fact that a short d_t is related to a reduced amount of viable myocardium in patients with ischemic cardiomyopathy. Recently, color M-mode Doppler flow propagation velocity (v_p) has been introduced as a relatively preload-independent measure of LV relaxation (Garcia et al. 2000, Steine et al. 1998, Steine et al. 1999) that can be used in combination with d_t to define different abnormal filling stages (Garcia et al. 1998). Based on the combined use of d_t and v_p, Moller et al. (Moller et al. 2000a) showed that not only patients with a restrictive filling pattern, characterized by a short d_t, but also patients with a pseudonormal filling pattern, characterized by a normal d_t but a low vp are at increased risk for LV dilatation and cardiac death after myocardial infarction.

In normal subjects exercise capacity is clearly related to diastolic filling (Vanoverschelde et al. 1993, Vlassak et al. 2001b). In patients with previous myocardial infarction however, the association between exercise capacity and diastolic filling is less clear (Lewis et al. 1993, Sumimoto et al. 1997) and might be influenced by determinants such as infarct size and left ventricular ejection fraction (LVEF). Therefore, the aim of the present study was to compare exercise capacity in remote myocardial infarction, between patients with normal versus abnormal LV filling patterns (defined by d_t, v_p and the combination of d_t and v_p), stratified for infarct size and LVEF.

2. Methods

2.1. PATIENT POPULATION

We studied 41 patients (39 men, median age 56 years, range 40-77 years) with remote (more than 6 weeks old) myocardial infarction. All patients were in sinus rhythm and had no angina or ECG changes on exercise indicating reversible ischemia. Furthermore, no patients were included who had more than grade 2 mitral regurgitation on echocardiography. Thirty-four (83%) patients were on beta-blockers, 31 (76%) on ACE-inhibitors, 39 (95%) on aspirin, 3 (7%) on diuretics and 3 (7%) on digoxin.

2.2. STUDY PROTOCOL

All patients underwent within 2 days a resting echocardiography study, a resting 99Tc-Tetrofosmin gated Single Photon Emission Computed Tomography (SPECT) study and a symptom limited bicycle exercise stress test with expired gas analysis.

For the echocardiography examination a Hewlett-Packard 2500 Sonos system was used. Mitral inflow parameters including the early diastolic peak velocity (E), peak velocity at atrial contraction (A), E/A ratio and mitral deceleration time (d_t), were measured using pulsed Doppler (PWD) from the apical four-chamber position with the sample volume position at the tips of the mitral valve leaflets during diastole. For the analysis of the flow propagation velocity (v_p), color M-mode Doppler (CMD) recordings were performed in the apical 4-chamber view. The color sector was adjusted to fit only over the left ventricular chamber and the M-mode cursor was placed through the center of the flow from the base of the mitral annulus to the apex (De Mey et al. 2001a). All echocardiography parameters were digitally recorded for 3 consecutive beats at a speed of 100 mm/sec and were analyzed off-line by one investigator blinded to the results of the SPECT study and the exercise test. Off-line measurement of vp was done according to the method described by Garcia et al. (De Mey et al. 1998, Garcia et al. 2000). For all measurements the mean value for the 3 consecutive beats was calculated. For the classification of diastolic dysfunction, four stages of diastolic dysfunction were used as proposed by Garcia et al. (Garcia et al. 1998): normal

filling with d_t 150-200 ms and v_p > 45 cm/sec (stage I, n=9 patients, mean age 54±8 years), delayed relaxation with d_t > 200 ms (stage II, n=12 patients, mean age 61±10 years), pseudonormal filling with d_t 150-200 ms and v_p < 45 cm/sec (stage III, n=12 patients, mean age 57±10 years) and restrictive filling with d_t < 150 ms (stage IV, n=8 patients, mean age 56±8 years).

The resting 99Tc-Tetrofosmin gated SPECT study, the calculation of left ventricular ejection fraction (LVEF), LV volumes and infarct score (IS) as measurement of infarct size were performed as reported previously from our laboratory (De Sutter et al. 2000). Median LVEF was 48% (range 19-66%) and median infarct score was 17 (range 0-60).

Finally all patients performed an exercise test with gas exchange analysis as described previously (De Sutter et al. 1999). In brief, patients pedaled in upright position on an electrically braked cycle ergometer using a standardized protocol with 25-Watt increments every 2 minutes. Total Watts performed during the test were calculated. Respiratory gas exchange variables were acquired continuously throughout the exercise test using the Oxyconsigma (MEDA) metabolic system. Peak oxygen uptake ($V0_2max$) was the average oxygen uptake over the last minute of exercise. Median total Watts performed was 700 Watts (range 300-2200 Watts) and median VO_2max was 22 ml/kg/min (range 13-38 ml/kg/min).

For statistical analysis, Spearman rank correlation tests, unpaired student t-test and analysis of variance for comparison between groups were used. A p-value lower than 0.05 was considered statistically significant.

3. Results

Infarct Score (IS, r = -0.585, p = 0.001), resting LVEF (r = 0.420, p = 0.009), resting LV end-diastolic volumes (r = -0.330, p = 0.04) and LV end-systolic volumes (r = -0.382, p = 0.02) correlated with v_p. Mitral PWD parameters failed to correlate with LVEF, LV volumes and IS, except for d_t and IS (r = -0.374, p = 0.02). Figure 10.1 (A-D) shows the values of v_p and d_t when patients were divided according to the median of LVEF (48%) and IS (17).

When patients were divided into the 4 stages of diastolic dysfunction, stages III and IV of diastolic dysfunction were associated with a greater infarct size and a lower resting LVEF in comparison to stages I and II ($p<0.05$) (Figure 10.2 (A) and 10.2 (B)).

No diastolic parameter (E, A, E/A, d_t and v_p) correlated significantly with bicycle exercise capacity parameters including total Watts and VO_2max. However, when patients were divided into the four stages of diastolic dysfunction, patients with preserved diastolic function (stage I) had significantly higher total Watts compared to the other patients (mean total Watts 1282±313 in stage I versus 817±360 in stage II, 726±335 in stage III and 724±368 in stage IV, $p<0.05$, figure 10.2 (C)). Also VO_2max was significantly higher in stage I patients compared to the other patients (30.1±3.7 ml/kg/min in stage I versus 21.5±4.7 ml/kg/min in stage II, 22.6±3.4 ml/kg/min in stage III, and 19.2±5.3 ml/kg/min in stage IV, $p<0.05$, figure 10.2 (D)).

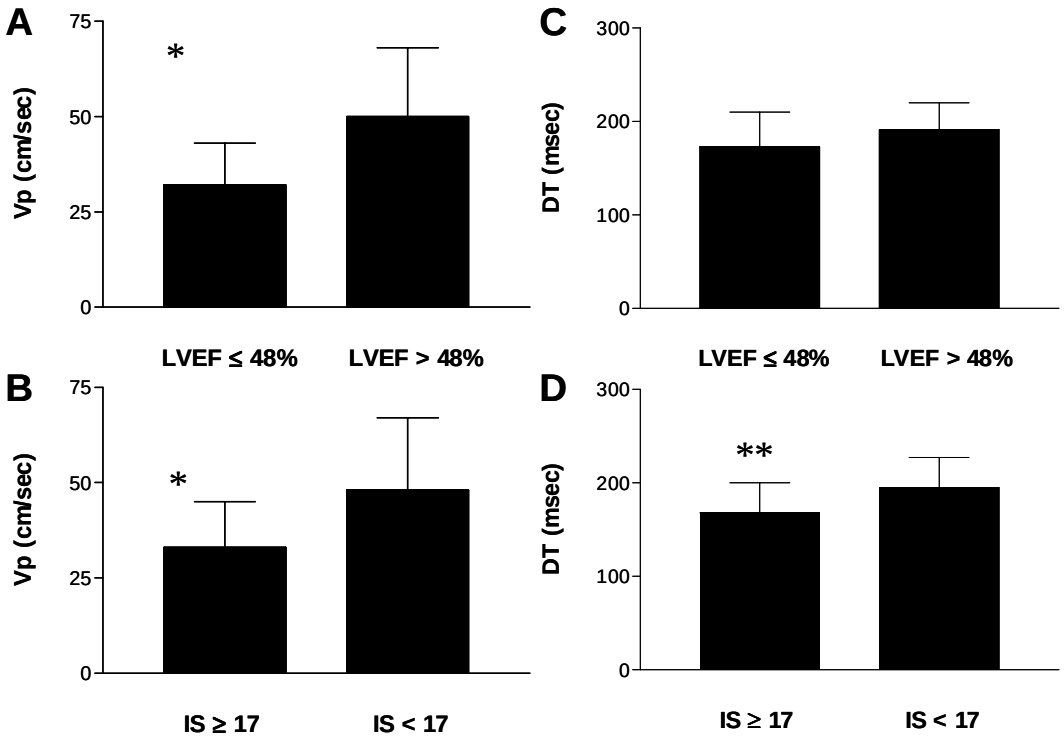

Figure 10.1. Flow propagation velocity (v_p) in patients with low versus high LVEF (**A**), and high versus low infarct score (IS) (**B**). Deceleration time (d_t) in patients with low versus high LVEF (**C**) and high versus low IS (**D**); (*): p<0.01 and (**): p<0.05.

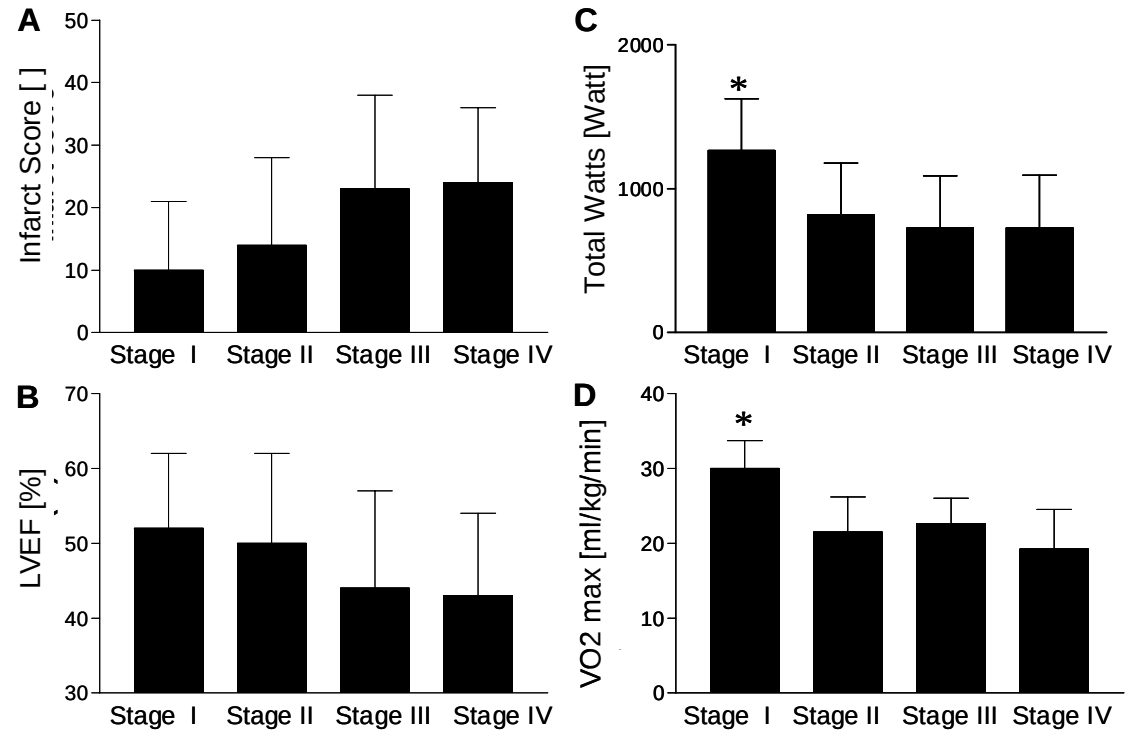

Figure 10.2: Relationship between stages of diastolic dysfunction (for definitions, see text) and Infarct Score (**A**), LVEF (**B**), Total Watts (**C**) and VO_2max (**D**).

4. Discussion

In this study we found a clear relationship between infarct size assessed by 99Tc-Tetrofosmin SPECT and CMD derived vp in patients with remote myocardial infarction. This finding expands the previously documented relationship between infarct size assessed by enzyme release and v_p during the acute stage of myocardial infarction by Steine et al. (Steine et al. 1998). Furthermore it can help to explain the findings that a lower vp is related to adverse left ventricular remodeling and a worse clinical outcome in patients after myocardial infarction (Moller et al. 2000a), since infarct size is a strong predictor of left ventricular remodeling and cardiac death in these patients (Dakik et al. 1996, Gibbons et al. 2000). Of note the relationship between v_p and infarct size was better than the relationship between d_t and infarct size. The fact that Yong et al. (Yong et al. 2001) recently reported a better relationship between d_t and the amount of viable myocardium in patients with ischemic cardiomyopathy is possibly related to the fact that in their study patients with more severely reduced LVEF and lesser amounts of viable myocardium were studied. We also found a relationship between the different stages of diastolic dysfunction and the amount of scar tissue and the reduction of LVEF. Interestingly, not only patients with a restrictive filling pattern but also patients with a pseudonormal filling pattern had a greater infarct score and lower LVEF compared to patients with an abnormal relaxation pattern or normal diastolic filling. These observations are in the same line as Moller et al. (Moller et al. 2000a) who showed that, when using d_t and v_p to define diastolic dysfunction, not only patients with a restrictive filling pattern but also patients with pseudonormal filling had a worse clinical outcome during follow-up.

In normal subjects exercise capacity is related to diastolic filling assessed by transmitral pulsed wave Doppler parameters (Vanoverschelde et al. 1993). More recently Vlassak et al. (Vlassak et al. 2001b) reported a relationship between exercise capacity and vp in normal individuals. The relationship between diastolic filling and exercise capacity in patients after myocardial infarction is however still a matter of debate (Lewis et al. 1993, Sumimoto et al. 1997). In the present study we could not document a significant relationship between any diastolic parameter, including d_t and v_p, and exercise capacity. However, when considering the

different stages of diastolic dysfunction defined by the combination of d_t and v_p, only patients with a preserved diastolic function had a preserved exercise capacity. All stages of diastolic dysfunction, including the delayed relaxation pattern, were associated with a significantly reduced exercise capacity as compared to the patients with preserved diastolic filling.

5. Conclusion

In patients with remote myocardial infarction, both d_t and v_p were related to infarct size and especially pseudonormal and restrictive filling patterns (defined by the combination of d_t and v_p) were associated with greater infarct size and lower LVEF. Although no direct correlation between d_t or v_p and exercise capacity could be documented, exercise capacity was reduced in all stages of diastolic dysfunction as compared to patients with a normal diastolic filling pattern. These findings support the combined use of d_t and v_p to assess diastolic dysfunction in patients with remote myocardial infarction.

Conclusion and Future Prospects

Congestive heart failure is an important cause of mortality in the Western community. Patients who meet the definition of CHF are a heterogeneous group and have diverse reasons for the occurrence of elevated filling pressure and/or low cardiac output. Stratification of CHF subjects into those with LV systolic dysfunction and those with predominantly LV diastolic dysfunction is important. Up to 40% of patients with congestive heart failure have isolated diastolic dysfunction. The definite diagnosis of diastolic heart failure remains challenging in the clinical setting.

SCIENTIFIC RESULTS

Within this thesis we have studied techniques, with the focus on color M-mode Doppler (CMD) echocardiography, for the assessment of diastolic function. Hydraulic and numerical models, next to animal experiments and clinical observations are used. Results have been obtained on two levels.

On one hand some *methodological issues* have been dealt with.

- When fitting an exponential function to the pressure decay during isovolumic relaxation, the trade-off between a fixed zero pressure asymptote and a free moving asymptote has been studied. A quantitative method was presented to balance bias (high when using a zero pressure asymptote) and variance (high when using a free floating asymptote) accompanying estimates of the time constant.

- Four different methods for the assessment of flow propagation velocity (v_p) have been implemented in new software algorithms and tested for intra-observer, inter-observer, and beat-to-beat variability in patients. The results indicated that the “Duval-Garcia” method is preferable in terms of repeatibility.

- In a preliminary study in a hydraulic model, the possibilities of the quantitative information in a CMD image has been studied. Longitudinal impedance, derived from CMD images of LV inflow, was identified in the model as an index, sensitive to valve diameter and test fluid.

- The limitations of pulsed Doppler echocardiography for the assessment of pressure differences using the simplified Bernoulli equation has been

addressed. The Seeley equation, an alternative expression taking into account geometry, was validated in a hydraulic model. Results were compared to data from post-operative coarctation patients.

On the other hand, basic mechanisms governing the interaction between LV *hemodynamics and LV diastolic variables* were investigated.

- A new hydraulic LV filling model has been developed. Significant relationships between v_p on one hand, and LV relaxation, LA filling pressure and LV compliance on the other hand have been demonstrated. The model predicts and explains variations in v_p observed in the clinical setting for the different stages of diastolic dysfunction.
- Hydraulic model results have been compared to analogue numerical simulations in a 2D axi-symmetric LV filling model. The numerical outcome supports the findings in the hydraulic model and provides a plausible link to unify the hydraulic experiment results with the Moens-Korteweg equation for wave propagation velocity.
- In a combined canine and hydraulic model it was demonstrated that in addition to elastic recoil, diastolic function parameters interfere in producing intraventricular pressure gradients (IVPG). Moreover, the existence of regional differences in relaxation in the canine heart provided an additional plausible link to explain variations in wall motion, IVPG and flow, not only during the isovolumic relaxation period, but also during early filling.

A clinical application concludes this thesis. In a well documented patient population of remote myocardial infarction, diastolic function, in terms of v_p, is linked to exercise capacity and infarct size.

FUTURE PROSPECTS

In this thesis, modeling has provided new insights into the fluid dynamics of the LV filling. Further elaboration of the models, e.g. by introducing a free moving mitral annulus ring or pathological valves may provide more information and reveal additional LV filling mechanisms.

The results of this work support the call for a standardized determination of v_p. The implemented semi-automatic algorithms are a first step towards standardization.

Intraventricular pressure gradients are identified as sensitive markers for changes in diastolic variables. Unifying this kind of pressure information with velocity information will provide additional information that can help in understanding the LV filling process and in judging diastolic function.

References

Aldousany, A. W., T. G. Di Sessa, B. S. Alpert, S. E. Birnbaum, and E. S. Willey. 1990. Significance of the Doppler-derived gradient across a residual aortic coarctation. Pediatr Cardiol 11: 8-14.

Altieri, P., S. Wilt, and R. Leighton. 1973. Left ventricular wall motion during the isovolumic relaxation period. Circulation 48: 499-505.

Appleton, C. 1988. Relation of transmitral flow velocity patterns to left ventricular diastolic function: new insights from a combined hemodynamic and doppler echocardiographic study. J Am Coll Cardiol 12: 426-40.

Appleton, C. 1997. Hemodynamic determinants of Doppler pulmonary venous flow velocity components: new insights from studies in lightly sedated normal dogs. J Am Coll Cardiol 30: 1562-74.

Appleton, C., J. Jensen, L. Hattle, and J. Oh. 1997. Doppler evaluation of left and right ventricular diastolic function: a technical guide for obtaining optimal flow velocity recordings. J Am Soc Echocardiogr 10: 271-91.

Apstein, C., and J. Morgan. 1994. Cellular mechanisms underlying left ventricular diastolic dysfunction. Pages 3-24 in W. Gaasch and M. LeWinter, eds. Left ventricular dysfunction and heart failure. Lea & Febiger, Philadelphia.

Arakawa, M., T. Nagano, T. Takaya, T. Noda, H. Miwa, K. Kagawa, T. Tanaka, M. Yamaguchi, and S. Hirakawa. 1987. Diastolic compliance of the left atrium in man: A challenging concept as a determinant of preload of the left vantricle. Automedica 9: 120.

Arakawa, M., T. Tanaka, and S. Hirakawa. 1989. Pressure-volume relation of the left atrium in man in M. Hori, H. Suga, J. Baan, and E. Yellin, eds. Cardiac mechanics and function in the normal and diseased heart. Springer-Verlag, Berlin.

Arts, T., F. Prinzen, and R. Reneman. 1993. Mechanics of he wall of the left ventricle. Pages 153-173 in J. Strackee and N. Westerhof, eds. The physics of heart and circulation. Institute of Physics Publishing, London.

Baker, D. 1978. Principles of Doppler in M. Fry, ed. Ultrasound, its applications in medicine and biology. Elsevier, New York.

Batchelor, G. 1967. An introduction to fluid dynamics. Cambridge University Press, London.

Baumgartner, H., T. Stefenelli, J. Niederberger, H. Schima, and G. Maurer. 1999. "Overestimation" of catheter gradients by Doppler Ultrasound in patients with aortic stenosis: a predictable manifestation of pressure recovery. J Am Coll Cardiol 33: 1655-61.

Bellhouse, B. 1972. Fluid mechanics of a model mitral valve an left ventricle. Cardiovasc Res 6: 199-210.

Beneken, J., and B. De Wit. 1967. A physical approach to hemodynamic aspects of the human cardiovascular system. Pages 1-46 in E. Reeve and A. Guyton, eds. Physical basis of circulatory transport. Saunders, Philadelphia.

Beppu, S., S. Izumi, and K. Miyatake. 1988. Abnormal blood pathways in left venricular cavity in acute myocardial infarction. Experimental observations with special reference to regional wall motion abnormality and hemostasis. Circulation 78: 157-64.

Bergsma, D. 1974. . Pages 103-104 in D. Bergsma, ed. Birth defects: atlas and compendium. Williams and Wilkins,, Baltimore.

Bernardi, L., S. Perlini, and F. Soffiantino. 1989. Acute heamodynamic effects of ibopamine and dopamine on isovolumic relaxation. European journal of pharmacology 164: 415-424.

Bernardi, L., B. Uretsky, P. Reddy, and R. Boudereau. 1985. Modeling the isovolumic relaxation period. Catheterization and Cardiovascular Diagnosis 11: 255-268.

Berry, C., D. Murdoch, and J. McMurray. 2001. Economics of chronic heart failure. Eur J Heart Failure 3: 283-291.

Bland, J., and D. Altman. 1986. Statistical methods for assessing agreement between two methods of clinical measurement. Lancet i: 307-310.

Bot, H. 1989. Mathematical models of diastolic blood flow patterns in the human left ventricle (PhD thesis). Department of Physiology. Vrije Universiteit, Amsterdam.

Bot, H., J. Verburg, B. J. Delemarre, and J. Strackee. 1990. Determinants of the occurrence of vortex rings in the left ventricle during diastole. J Biomech 23: 607-15.

Braunwald, E. 1992. Pathophysiology of heart failure in E. Braunwald, ed. Heart disease. Saunders, Philadelphia.

Braunwald, E., and J. Ross. 1963. The ventricular end-diastolic pressure. Am J Med 34: 147-150.

Brecher, G., and A. Kissen. 1957. Relation of negative intraventricular pressure to ventricular volume. Circ Res 5: 157.

Briguori, C., S. Betocchi, M. A. Losi, F. Manganelli, F. Piscione, L. Pace, M. Boccalatte, R. Gottilla, M. Salvatore, and M. Chiariello. 1998. Noninvasive evaluation of left ventricular diastolic function in hypertrophic cardiomyopathy. Am J Cardiol 81: 180-7.

British Standard Institution. 1979. Precision of test methods I: Guide for the determination and reproducibility for a standard test method (BS 5497, part I). BSI, London.

Bronzino, J. 1995. Biomedical Engineering Handbook. CRC Press, Boca Raton.

Brun, P., C. Tribouilloy, A. M. Duval, L. Iserin, A. Meguira, G. Pelle, and J. L. Dubois-Rande. 1992. Left ventricular flow propagation during early filling is related to wall relaxation: a color M-mode Doppler analysis. J Am Coll Cardiol 20: 420-32.

Brutsaert, D., U. Stanislas, and T. Gillebert. 1993. Diastolic failure: pathophysiology and therapeutic implications. J Am Coll Cardiol 22: 318-325.

Brutsaert, D., and S. Sys. 1989. Relaxation and diastole of the heart. Physiol Rev 69: 1228-1234.

Burwash, I., D. Morgan, C. Koilpillai, G. Blackmore, D. Johnstone, and A. J. 1993. Sympathetic stimulation alters left ventricular relaxation and chamber size. Am J Physiol 264: R1-R7.

Carvalho, J. S., A. N. Redington, E. A. Shinebourne, M. L. Rigby, and D. Gibson. 1990. Continuous wave Doppler echocardiography and coarctation of the aorta: gradients and flow patterns in the assessment of severity. Br Heart J 64: 133-137.

Cerisano, G., L. Bolognese, and N. Carabba. 1999. Doppler-derived mitral deceleration time: an early strong predictor of left ventricular remodeling after reperfused anterior acute myocardial infarction. Circulation 99: 230-6.

Chan, K. C., D. F. Dickinson, G. A. Wharton, and J. L. Gibbs. 1992. Continuous wave Doppler echocardiography after surgical repair of coarctation of the aorta. Br Heart J 68: 192-194.

Choong, C., V. Abascal, J. Thomas, J. Guerrero, S. McGlew, and A. Weyman. 1988. Combined influence of ventricular loading and relaxation on the transmitral flow velocity profile in dogs measured by Doppler echocardiography. Circulation 78: 672-683.

Cohen, G. I., J. F. Pietrolungo, J. D. Thomas, and A. L. Klein. 1996. A practical guide to assessment of ventricular diastolic function using Doppler echocardiography. J Am Coll Cardiol 27: 1753-60.

Coronel, R., J. de Groot, and J. van Lieshout. 2001. Defining heart failure. Cardiovesc Res 50: 419-422.

Courtois, M., B. Barzilai, A. Hall, and P. Ludbrook. 1997. Postextrasystolic left ventricular isovolumic pressure decay is not monoexponential. Cardiovasc Res 35: 206-16.

Courtois, M., S. Kovacs, and P. Ludbrook. 1988. The transmitral pressure-flow velocity relationship: the importance of regional pressure gradients in the left ventricle during diastole. Circulation 78: 661-671.

Courtois, M., S. Kovacs, and P. Ludbrook. 1990. The physiologic early diastolic intraventricular pressure gradient is lost during acute myocardial ischemia. Circulation 81: 1688-1696.

Dakik, H., J. Mahmarian, K. Kimball, M. Koutelou, R. Medrano, and M. Verani. 1996. Prognostic value of exercise thallium-201 tomography in patients treated with thrombolytic therapy during acute myocardial infarction. Circulation 94: 2735-2742.

Davie, A., C. Francis, L. Carvane, G. Sutherland, and J. Mc Murray. 1997. The prevalence of left ventricular diastolic filling abnormalities in patients with suspected heart failure. Eur Heart J 18: 981-984.

Davis, K., U. Mehlhorn, E. Schertel, H. Geissler, D. Trevas, G. Laine, and A. SJ. 1999. Variation in tau, the time constant for isovolumic relaxation, along the left ventricular base-to-apex axis. Basic Res Cardiol 94: 41-8.

De Maria, A., T. Wisenbaugh, M. Smith, M. Harrison, and M. Berk. 1991. Doppler echocardiographic evaluation of diastolic dysfunction. Circulation 84[suppl I]: I-288 - I-295.

De Mey, S., J. De Sutter, P. M. Vandervoort, and P. R. Verdonck. 2000a. A new model for the experimental validation of left ventricular filling characteristics (abstract). Circulation 102: 1775.

De Mey, S., J. De Sutter, J. Vierendeels, and P. Verdonck. 2001a. Diastolic filling and pressure imaging: Taking advantage of the information in a color M-mode Doppler image. Eur J Echocardiogr 1: (in press).

De Mey, S., K. Dumont, J. Geeraerts, P. Vandervoort, and P. Verdonck. 2000b. Noninvasive assessment of left ventricular longitudinal impedance using color M-mode Doppler echocardiography. Computers in Cardiology 27: 17-20.

De Mey, S., P. Segers, I. Coomans, H. Verhaaren, and P. Verdonck. 2001b. Limitations of Doppler echocardiography in the follow-up of aortic coarctation. J Biomech 34: 951-960.

De Mey, S., J. Thomas, N. Greenberg, P. Vandervoort, and P. Verdonck. 2001c. Assessment of the left ventricular time constant of relaxation: insights from simulations and hemodynamic measurements. Am J Physiol 280: H2936-H2944.

De Mey, S., P. Vandervoort, H. Pasteuning, N. Greenberg, and P. Verdonck. 1998. Quantification of wave propagation velocity from a colour M-mode Doppler image: implementation and analysis of different methods. Computers in Cardiology 25: 613-616.

De Mey, S., P. M. Vandervoort, and P. R. Verdonck. 1999. Preload (in)dependence of E-wave velocity and wave propagation velocity (abstract). Circulation 100: 1907.

De Sutter, J., C. Van de Wiele, Y. D'Asseler, P. De Bondt, G. De Backer, P. Rigo, and R. Dierckx. 2000. Automatic quantification of defect size using normal templates: a comparative clinical study of three available algorithms. Eur J Nucl Med 27: 1827-1834.

De Sutter, J., C. Van de Wiele, R. Dierckx, t. P. Gheeraer, M. De Buyzere, and Y. Taeymans. 1999. Reverse redistribution on Thallium-201 SPECT after primary angioplasty: a one-year follow-up study. Eur J Nucl Med 26: 633-639.

Delemarre, B., C. Visser, H. Bot, and D. AJ. 1990. Prediction of apical thrombus formation in acute myocardial infarction based on left ventricular spatial flow pattern. J Am Coll Cardiol 15: 355-60.

D'hooge, J., A. Heimdal, F. Jamal, T. Kukulski, B. Bijnens, F. Rademakers, L. Hatle, P. Suetens, and G. Sutherland. 2000. Regional strain and strain rate measurements by cardiac ultrasound: principles, implementation and limitations. Eur J Echo 1: 154-170.

Duval-Moulin, A. M., P. Dupouy, P. Brun, F. Zhuang, G. Pelle, Y. Perez, E. Teiger, A. Castaigne, P. Gueret, and J. L. Dubois-Rande. 1997. Alteration of left ventricular diastolic function during coronary angioplasty-induced ischemia: a color M-mode Doppler study. J Am Coll Cardiol 29: 1246-55.

Edwards, C. R. W., and S. Davidson. 1995. . Pages 303 in C. R. W. Edwards, ed. Davidson's principles and practice of medicine. Churchill Livingstone, Edinburgh.

European Study Group on Diastolic Heart Failure. 1998. How to diagnose diastolic heart failure. Eur Heart J 19: 990-1003.

Evans, D., W. McDicken, Skidmore, R, and J. Woodcock. 1989. Doppler ultrasound: physics, instrumentation and clinical applications. Wiley & Sons, New York.

Eyer, M., M. Brandestini, D. Phillips, and D. Baker. 1981. Color digital echo/Doppler image presentation. Ultrasound in Med Biol 7: 21-31.

Falsetti, H., M. Verani, C. Chen, and J. Cramer. 1980. Regional pressure differences in the left ventricle. Catheterization and cardiovascular diagnosis. Catheterization and cardiovascular diagnosis 6: 123-134.

Firstenberg, M., B. Levine, M. Garcia, N. Greenberg, L. Cardon, A. Morehead, J. Zuckerman, and J. Thomas. 2000a. Relationship of echocardiographic indices to pulmonart capillary wedge pressures in healthy volunteers. J Am Coll Cardiol 36: 1664-9.

Firstenberg, M., N. Smedira, N. Greenberg, D. Prior, P. McCarthy, M. Garcia, and J. Thomas. 2001. Relationship between early diastolic intraventricular pressure gradients, an index of elastic recoil, and improvements in systolic and diastolic function. Circulation (in press).

Firstenberg, M., P. Vandervoort, N. Greenberg, N. Smedira, P. McCarthy, M. Garcia, and J. Thomas. 2000b. Noninvasive estimation of transmitral pressure drop across the normal mitral valve in humans: importance of convective and inertial forces during left ventricular filling. J Am Coll Cardiol 36: 1942-9.

Flachskampf, F., L. Rodriguez, C. Chen, J. Guerrero, A. Weyman, and J. Thomas. 1993. Analysis of Mitral Inertance: a factor critical for early transmitral filling. J Am Soc Echocardiogr 6: 422-32.

Flachskampf, F., A. Weyman, J. Guerrero, and J. Thomas. 1992. Calculation of atrioventricular compliance from the mitral flow profile: analytic and in vitro study. J Am Coll Cardiol 19: 998-1004.

Frank, O. 1895. Zur Dynamik des Herzmuskels. Z Biol 32: 370. (Translation by Chapman C.B. and Wasserman F.: Frank, O. 1959. On the dynamics of cardiac muscle. Am Heart J 58: 282.)

Frederiksen, J., J. Weiss, and M. Weissfeldt. 1978. Time constant of isovolumic pressure fall: determinants in the working ventricle. Am J Physiol 235: H701-H706.

Gaasch, W. 1994. Passive elastic properties of the left ventricle. Pages 143-149 in W. Gaasch and M. LeWinter, eds. Left ventricular dysfunction and heart failure. Lea & Febiger, Philadelphia.

Gaasch, W., A. Blaustein, C. Andrias, R. Donahue, and B. Avitall. 1980. Myocardial relaxation II: hemodynamic determinants of rate of left ventricular isovolumic pressure decline. Am J Physiol 239: H1-H6.

Gaasch, W., A. Blaustein, and M. LeWinter. 1994. Heart failure and clinical disorders of LV diastolic function. Pages 245-258 in W. Gaasch and M. LeWinter, eds. Left ventricular diastolic dysfunction and heart failure. Lea and Febiger, Philadelphia.

Gaasch, W., and M. Le Winter, eds. 1994. Left Ventricular Diastolic Dysfunction and Heart Failure. Lea & Febiger, Philadelphia.

Galderisi, M., E. Benjamin, J. Evans, R. D'Agostino, D. Fuller, B. Lehman, P. Wolf, and D. Levy. 1992. Intra- and interobserver reproducibility of Doppler-assessed indexes of left ventricular diastolic function in a population-based study (the Framingham heart study). Am J Cardiol 70: 1341-1346.

Garcia, M., M. Firstenberg, N. Greenberg, N. Smedira, L. Rodriguez, D. Prior, and J. Thomas. 2001. Estimation of left ventricular operating stiffness from Doppler early filling deceleration time in humans. Am J Physiol 280: H554-H561.

Garcia, M. J. 2001. Color M-mode Doppler flow propagation velocity in cardiac tamponade: reply. J Am Coll Cardiol 37: 329.

Garcia, M. J., M. A. Ares, C. Asher, L. Rodriguez, P. Vandervoort, and J. D. Thomas. 1997. An index of early left ventricular filling that combined with pulsed Doppler peak E velocity may estimate capillary wedge pressure. J Am Coll Cardiol 29: 448-54.

Garcia, M. J., R. T. Palac, D. J. Malenka, P. Terrell, and J. F. Plehn. 1999. Color M-mode Doppler flow propagation velocity is a relatively preload-independent index of left ventricular filling. J Am Soc Echocardiogr 12: 129-37.

Garcia, M. J., N. G. Smedira, N. L. Greenberg, M. Main, M. S. Firstenberg, J. Odabashian, and J. D. Thomas. 2000. Color M-mode Doppler flow propagation velocity is a preload insensitive index of left ventricular relaxation: animal and human validation. J Am Coll Cardiol 35: 201-8.

Garcia, M. J., J. D. Thomas, and A. L. Klein. 1998. New Doppler echocardiographic applications for the study of diastolic function. J Am Coll Cardiol 32: 865-75.

Gibbons, R., T. Miller, and T. Christian. 2000. Infarct size measured by single photon computed tomographic imaging with 99Tc-Sestamibi. A measure of the efficacy of therapy in acute myocardial infarction. Circulation 101.

Gillebert, T., A. LeiteMoreira, and S. DeHert. 1997. The hemodynamic manifestation of normal myocardial relaxation - A framework for experimental and clinical evaluation. Acta Cardiol 52: 223-246.

Gillebert, T., and S. Sys. 1994. Physiologic control of relaxation in isolated cardiac muscle and intact left ventricle. Pages 25-42 in W. Gaasch and M. LeWinter, eds. Left ventricular dysfunction and heart failure. Lea & Febiger, Philadelphia.

Gonzalez-Vilchez, F., M. Ares, J. Ayuela, and L. Alonso. 1999. Combined use of pulsed and color M-mode Doppler echocardiography for the estimation of pulmonary capillary wedge pressure: an empirical approach based on an analytical relation. J Am Coll Cardiol 34: 515-23.

Gorcsan, J. d., V. K. Gulati, W. A. Mandarino, and W. E. Katz. 1996. Color-coded measures of myocardial velocity throughout the cardiac cycle by tissue Doppler imaging to quantify regional left ventricular function. Am Heart J 131: 1203-13.

Greenberg, N., P. Vandervoort, M. Firstenberg, M. Garcia, and J. Thomas. 2001. Estimation of diastolic intraventricular pressure gradients by Doppler M-mode echocardiography. Am J Physiol 280: H2507-H2515.

Greenberg, N., P. Vandervoort, and J. Thomas. 1995. Noninvasive assessment of diastolic intraventricular pressure gradients using color Doppler M-mode echocardiography. Computers in Cardiology 22: 1-4.

Greenberg, N. L., P. M. Vandervoort, and J. D. Thomas. 1996. Instantaneous diastolic transmitral pressure differences from color Doppler M mode echocardiography. Am J Physiol 271: H1267-76.

Gulati, V. K., W. E. Katz, W. P. Follansbee, and J. Gorcsan. 1996. Mitral annular descent velocity by tissue Doppler echocardiography as an index of global left ventricular function. Am J Cardiol 77: 979-84.

Hatle, L., and B. Angelsen. 1985. Doppler Ultrasound in Cardiology. Physical principles and clinical applications (2nd ed.). Lea & Febiger.

Henry, F. S., A. P. Shortland, F. Iudicello, R. A. Black, J. C. Jarvis, M. W. Collins, and S. Salmons. 1997. Flow in a simple model skeletal muscle ventricle: comparison between numerical and physical simulations. J Biomech Eng 119: 13-19.

Hirai, T., S. Sasayama, T. Kawasaki, and S. Yagi. 1989. Stiffness of systemic arteries in patients with myocardial infarction. Circulation 80: 78-86.

Hirota, Y. 1980. A clinical study of left ventricular relaxation. Circulation 62: 765-63.

Hittinger, L., B. Crozatier, J. Belot, and M. Peirrot. 1987. Regional ventricular segmental dynamics in normal conscious dogs. Am J Physiol 253: H713-H719.

Isaaz, K. 2000. Expanding the frontiers of Doppler echocardiography for the noninvasive assessment of diastolic hemodynamics. J Am Coll Cardiol 36: 1950-1952.

Isaaz, K., A. Thompson, G. Ethevenot, J. Cloez, B. Brembilla, and C. Pernot. 1989. Doppler echocardiographic measurement of low velocity motion of the left ventricular posterior wall. Am J Cardiol 66-75.

Ishida, Y., J. Meisner, K. Tsujioka, J. Gallo, C. Yoran, W. Frater, and E. Yellin. 1986. Left Ventricular filling dynamics: influence of left ventricular relaxation and left atrial pressure. Circulation 74: 187-196.

Iudicello, F., F. Henry, M. Collins, S. Salmons, A. Sarti, and C. Lamberti. 1997. Comparison of haemodynamic structures between a skeletal muscle ventricle and the human left ventricle. Internal Medicine 5: 1-10.

Kannel, W. 1999. Current status of the epidemiology of heart failure. Current Cardiology Reports 1: 11-19.

Kappetein, P. A., G. L. Guit, A. J. Bogers, H. W. Weeda, K. H. Zwinderman, J. P. Schonberger, and H. A. Huysmans. 1993. Non-invasive long-term follow-up after coarctation repair. Ann Thorac Surg 5: 1153-1159.

Karliner, J., M. LeWinter, F. Mahler, R. Engler, and R. O'Rourke. 1977. Pharmacologic and hemodynamic influences on the rate of isovolumic left ventricular relaxation in the normal conscious dog. Journal of Clinical Investigation 60.

Kasai, C. 1985. Real-time two-dimensional blood flow imaging using an autocorrelation technique. IEEE Trans Sonics Ultrasonics 32: 458-464.

Kettunen, R., J. Timisjarvi, P. Ramo, E. Kouvalainen, J. Heikkila, and H. L. 1986. Time constant of isovolumic pressure fall in the intact canine left ventricle. Cardiovascular Research 20: 698-704.

Kondo, H. T. Masuyama, et al. 1995. Digital substraction high-frame-rate echocardiography in detecting delayed onset of regional left ventricular relaxation in ischemic heart disease [see comments]. Circulation 91: 304-12.

Kovacs, S., B. Barzilai, and J. Perez. 1987. Evaluation of diastolic function with Doppler echocardiography: the PDF formalism. Am J Physiol 252: H178-H187.

Lamb, H. 1932. Hydrodynamics. Cambridge University Press, London.

Lee, C., and L. Talbot. 1979. A fluid mechanical study of the closure of heart valves. J Fluid Mech 91: 41-63.

Leite-Moreira, A., J. Correia-Pinto, and T. Gillebert. 1999. Afterload induced changes in myocardial relaxation: A mechanism for diastolic dysfunction. Cardiovasc Res 43: 344-353.

Lenihan, D. 1995. Mechanisms, diagnosis and treatment of diastolic heart failure. Am Heart J 130: 153-66.

Lewis, B., S. Emmott, J. Smyllie, A. MacNeill, J. Lubsen, and a. t. D. S. Group. 1993. Left ventricular systolic and diastolic function, and exercise capacity six to eight weeks after acute myocardial infarction. Am J Cardiol 73: 149-153.

Ling, D., S. Rankin, C. Edwards, P. McHale, and R. Anderson. 1979. Regional diastolic mechanics of the left ventricle in the conscious dog. Am J Physiol 236: H323-H330.

MacFadyen, R., C. MacLeod, P. Shiels, W. Smith, and T. MacDonald. 2001. Isolated diastolic heart failure as a cause of breathlessness in the community: the Arbroath study. Eur J Heart Failure 3: 243-248.

Mandinov, L., F. Eberli, C. Seiler, and O. Hess. 2000. Diastolic heart failure. Cardiovasc Res 45: 813-825.

Martin, G., J. Gimeno, J. Cosin, and M. Guillem. 1984. Time constant of isovolumic pressure fall: new numerical approaches and significance. Am J Physiol 247: H283-H294.

Marx, G. R., and H. D. Allen. 1986. Pitfalls of Doppler evaluation of the pressure gradient in aortic coarctation. J Am Coll Cardiol 7: 1379-1385.

Matsubara, H., J. Araki, M. Takaki, S. Nakagawa, and H. Suga. 1995. Logistic time constant of isovolumic relaxation pressure-time curve in the canine left ventricle. Better alternative to exponential time constant. Circulation 92: 2138-26.

McLeod, F. 1974. Multichannel pulsed Doppler techniques in R. Renenman, ed. Cardiovascular applications of ultrasound. North Holland Publishing, Amsterdam.

McQueen, D., C. Peskin, and E. Yellin. 1982. Fluid dynamics of the mitral valve: physiological aspects of a mathematical model. Am J Physiol 242: H1095-H1110.

Mego, D. M., V. S. DeGeare, S. Y. Nottestad, V. P. Lamanna, L. C. Oneschuk, B. J. Rubal, and M. Zabalgoitia. 1998. Variation of flow propagation velocity with age. J Am Soc Echocardiogr 11: 20-5.

Meisner, J. 1986. Left atrial role in left ventricular filling: dog and computer studies (PhD thesis). Albert Einstein College of Medicine. Yeshiva University, New York.

Meisner, J., D. McQueen, Y. Ishida, H. Vetter, U. Bortolotti, J. Strom, R. Frater, C. Peskin, and E. Yellin. 1985. Effects of timing of atrial systole on LV filling and mitral valve closure: computer and dog studies. Am J Physiol 249: H604-H619.

Milde, J., M. Sessoms, J. Lisauskas, A. Bowman, M. Courtois, and S. Kovács. 2000. Ventricular diastolic impedance: a new index of global diastolic function. J Am Coll Cardiol 35: 185 (abstract).

Milnor, W. R. 1989. Hemodynamics. Williams & Wilkins, Baltimore, MD.

Mirsky, I., and A. Pasipoularides. 1990. Clinical assessment of diastolic function. Progress in cardiovascular diseases 32: 291-318.

Miyashita, T., Y. Okano, H. Takaki, T. Satoh, Y. Kobayashi, and Y. Goto. 2001. Relation between exercise capacity and left ventricular systolic versus diastolic function during exercise in patients after myocardial infarction. Coronary Artery Disease 12: 217-225.

Miyatake, K., M. Yamagishi, N. Tanaka, M. Uematsu, N. Yamazaki, Y. Mine, A. Sano, and M. Hirama. 1995. New method for evaluating left ventricular wall motion by color-coded tissue Doppler imaging: in vitro and in vivo studies. J Am Coll Cardiol 25: 717-24.

Moller, J., E. Sondergaard, S. Poulsen, and K. Egstrup. 2000a. Pseudo-normal and restrictive filling patterns predict left ventricular dilation and cardiac death after a first myocardial infarction: A serial color M-mode Doppler echocardiographic study. J Am Coll Cardiol 36: 1841-6.

Moller, J. E., S. H. Poulsen, E. Sondergaard, and K. Egstrup. 2000b. Preload dependence of color M-Mode doppler flow propagation velocity in controls and in patients with left ventricular dysfunction. J Am Soc Echocardiogr 13: 902-909.

Moller, J. E., E. Sondergaard, J. B. Seward, C. P. Appleton, and K. Egstrup. 2000c. Ratio of left ventricular peak E-wave velocity to flow propagation velocity assessed by color M-mode Doppler echocardiography in first myocardial infarction: prognostic and clinical implications. J Am Coll Cardiol 35: 363-70.

Mosterd, A., A. Hoew, M. De Bruyne, J. Deckers, D. Linker, A. Hofman, and D. Grobbee. 1999. Prevalence of heart failure and left ventricular dysfunction in the general population: the Rotterdam study. Eur Heart J 20: 447-455.

Muhler, E. G., J. M. Neuerburg, A. Ruben, R. G. Grabitz, R. W. Gunther, B. J. Messmer, and G. von-Bernuth. 1993. Evaluation of aortic coarctation after surgical repair: role of magnetic resonance imaging and Doppler ultrasound. Br Heart J 70: 285-290.

Murdoch, D., and J. McMurray. 1998. Epidemiological perspective on heart failure: Common, costly, disabling, deadly.

Nagueh, S., K. Middleton, H. Kopelen, W. Zoghbi, and M. Quinones. 1997. Doppler tissue imaging: a noninvasive technique for evaluation of left ventricular relaxation and estimation of filling pressures. J Am Coll Cardiol 30: 1527-33.

Nagueh, S. F., H. A. Kopelen, and M. A. Quinones. 1996. Assessment of left ventricular filling pressures by Doppler in the presence of atrial fibrillation. Circulation 94: 2138-45.

Nagueh, S. F., N. M. Lakkis, K. J. Middleton, W. H. Spencer, W. A. Zoghbi, and M. A. Quinones. 1999. Doppler estimation of left ventricular filling pressures in patients with hypertrophic cardiomyopathy. Circulation 99: 254-61.

Nakatani, S., M. Firstenberg, N. Greenberg, P. Vandervoort, N. Smedira, P. McCarthy, and J. Thomas. 2000. Mitral inertance in humans: critical factor in Doppler estimation of transvalvular pressure gradients. Am J Physiol 280: H1340-H1345.

Nakatani, S., M. Garcia, M. Firstenberg, L. Rodriguez, R. Grimm, N. Greenberg, P. McCarthy, P. Vandervoort, and J. Thomas. 1999. Noninvasive assessment of left atrial maximum dP/dt by a combination of transmitral and pulmonary venous flow. J Am Coll Cardiol 34: 795-801.

Neter, J., M. H. Kutner, C. J. Nachtsheim, and W. Wasserman. 1996. Applied Linear Statistical Models. IRWIN.

Nichols, W., and M. O'Rourke. 1990. McDonald's Blood Flow in Arteries. Edward Arnold, London.

NIH Publication N° 8. 1996. Pages 23.

Nijland, F., O. Kamp, A. Karreman, M. Van Eenige, and C. Visser. 1997. Prognostic implications of restrictive left ventricular filling in acute myocardial infarction: a serial Doppler echocardiographic study. J Am Coll Cardiol 30: 1618-24.

Nikolic, S., M. Feneley, O. Pajaro, J. Rankin, and E. Yellin. 1995. Origin of regional pressure gradients in the left ventricle during early diastole. Am J Physiol 268: H550-H557.

Nikolic, S., E. Yellin, K. Tamura, H. Vetter, T. Tamura, J. Meisner, and R. Frater. 1988. Passive properties of canine left ventricle: Diastolic stiffness and restoring forces. Circ Res 62: 1210-1222.

Nishihara, K., T. Mikami, H. Takatsuji, H. Onozuka, N. Saito, S. Yamada, K. Urasawa, and A. Kitabatake. 2000. Usefulness of early diastolic flow propagation velocity measured by color M-mode doppler technique for the assessment of left ventricular diastolic function in patients with hypertrophic cardiomyopathy. J Am Soc Echocardiogr 13: 801-8.

Nishimura, R., and J. Tajik. 1997. Evaluation of diastolic filling of the left ventricle in health and disease: Doppler echocardiography is the clinician's Rosetta stone. J Am Coll Cardiol 30: 8-18.

Oh, J., Z. Ding, B. Gersh, K. Bailey, and T. AJ. 1992. Restrictive left ventricular diastolic filling identifies patients with heart failure after acute myocardial infarction. J Am Soc Echocardiogr 5: 497-503.

Owen, A. 1993. A numerical model of early diastolic filling: importance of intraventricular pressure wave propagation. Cardiovascular Research 27: 255-261.

Pagel, P., D. Hettrick, and D. Warltier. 1994. Left ventricular mechanical consequences of dihydropyriding calcium channel modulation in conscious and anesthetized chronically instrumented dogs. Aenesthesiology 81: 190-208.

Park, M. K., D. Lee, and G. A. Johnson. 1993. Oscillometric blood pressures in the arm, thigh and calf in healthy children and those with aortic coarctation. Pediatrics 91: 761-5.

Pasipoularides, A., J. Murgo, J. Miller, and W. Craig. 1987. Nonobstructive left ventricular ejection pressure gradient in man. Circ Res 61: 220-7.

Paulus, W., P. Vantrimpont, and M. Rousseau. 1992. Diastolic function of the nonfilling human left ventricle. J Am Coll Cardiol 20: 1524-1532.

Peronneau, P. 1970. Velocimetre sanguin par effet Doppler a emission ultrasonore pulsee. Onde Electrique 50: 369.

Peskin, C., and D. McQueen. 1989. A three-dimensional computational method for blood flow in the heart I. immersed elastic fibers in a viscous incompressible fluid. J Comp Phys 81: 372-405.

Price, S., and L. Wilson. 1992. Pathophysiology, clinical concepts of disease processes (4th ed.). Mosby-Year Book inc, Philadelphia.

Raff, G., and S. Glantz. 1981. Volume loading slows left ventricular isovolumic relaxation rate: evidence of load-dependent relaxation in the intact dog heart. Circ Res 48: 813-24.

Rajagopalan, N., M. Garcia, L. Rodriguez, R. Murray, C. Apperson-Hansen, M. Stugaard, J. Thomas, and A. Klein. 2001. Comparison of new Doppler echocardiographic methods to

differentiate constrictive pericardial heart disease and restrictive cardiomyopathy. Am J Cardiol 87: 86-94.

Rao, P. S. 1995. Coarctation of the aorta. Sem in Nephr 15: 87-105.

Robinson, P. J., R. K. Wyse, J. E. Deanfield, R. Franklin, and F. J. Macartney. 1984. Continuous wave Doppler velocimetry as an adjunct to cross sectional echocardiography in the diagnosis of critical left heart obstruction in neonates. Br Heart J 55: 552-556.

Rodevand, O., R. Bjornerheim, T. Edvardsen, O. A. Smiseth, and H. Ihlen. 1999. Diastolic flow pattern in the normal left ventricle. J Am Soc Echocardiogr 12: 500-7.

Rusconi, C., G. Ghizzoni, T. Sabatini, C. Oneglia, and P. Faggiano. 1998. Pathophysiology of diastole and left ventricular filling in humans: noninvasive evaluation in G. Drzewiecki and J. Li, eds. Analysis and assessment of cardiovascular function. Springer, New York.

Sagawa, K., W. Maughan, H. Suga, and K. Sunagawa. 1988. Cardiac contraction and the pressure-volume relationship. Oxford University Press, New York.

Salisbury, P., C. Cross, and P. Rieben. 1963. Chordae tendinae tension. Am J Physiol 25: 385.

Satomora, S. 1959. Study of the flow patterns in peripheral arteries by ultrasonics. J Acoust Soc 15: 151-158.

Scalia, G. M., N. L. Greenberg, P. M. McCarthy, J. D. Thomas, and P. M. Vandervoort. 1997. Noninvasive assessment of the ventricular relaxation time constant (tau) in humans by Doppler echocardiography. Circulation 95: 151-5.

Schmailz, K., and O. Ormerod, eds. 1998. Ultrasound in Cardiology. Blackwell Science, Cambridge.

Seeley, B. D., and D. F. Young. 1976. Effect of Geometry on pressure losses across models of arterial stenoses. J Biomechanics 9: 439-448.

Segers, P., F. Dubois, D. De Wachter, and P. Verdonck. 1998. Role and relevancy of a cardiovascular simulator. J Cardiovasc Eng 3: 48-56.

Segers, P., and C. Fronteau. 1991. Fluidodynamische modellering van de stroming doorheen de mitraalklep. Pages 297. Civil Engineering. Ghent University, Ghent.

Senni, M., C. Tribouilly, R. Rodeheffer, S. Jacobsen, H. Evans, K. Bailey, and M. Redfield. 1998. Congestive heart failure in the community: a study of all incident cases in Olmsted County, Minnesita, in 1991. Circulation 98: 2282-2289.

Senzaki, H., B. Fetics, C. Chen, and D. Kass. 1999. Comparison of Ventricular Pressure Relaxation Assessments in Human Heart Failure. J Am Coll Cardiol 34: 1529-36.

Shintani, H., and S. Glantz. 1994. The left ventricular diastolic pressure-volume relation, relaxation, and filling in W. Gaasch and M. LeWinter, eds. Left ventricular dysfunction and heart failure. Lea & Febiger, Philadelphia.

Shortland, A. 1996. Factors influencing vortex development in a model of a skeletal muscle ventricle. Artificial Organs 20: 1026-1033.

Smiseth, O. A., K. Steine, G. Sandbaek, M. Stugaard, and T. Gjolberg. 1998. Mechanics of intraventricular filling: study of LV early diastolic pressure gradients and flow velocities. Am J Physiol 275: H1062-9.

Solomon, S., P. Barbier, and S. Glantz. 1999. Changes in porcine transmitral flow velocity pattern and its diastolic determinants during partial coronary occlusion. J Am Coll Cardiol 33: 854-866.

Starling, E.H. 1918. The Linacre lecture on the Law of the Heart given at Cambridge. London, Longmans Green.

Steen, T., and S. Steen. 1994. Filling of a model left ventricle studied by colour M-mode Doppler. Cardiovasc Res 28: 1821-7.

Steen, T., K. Steine, O. A. Smiseth, and H. Ihlen. 1994. Repeatability of colour M-mode Doppler measurements of left ventricular filling. Int J Cardiol 43: 79-85.

Steine, K., T. Flogstad, M. Stugaard, and O. A. Smiseth. 1998. Early diastolic intraventricular filling pattern in acute myocardial infarction by color M-mode Doppler echocardiography. J Am Soc Echocardiogr 11: 119-25.

Steine, K., M. Stugaard, and O. A. Smiseth. 1999. Mechanisms of retarded apical filling in acute ischemic left ventricular failure. Circulation 99: 2048-54.

Stugaard, M. 1994. Intraventricular filling pattern and diastolic function. Clinical and experimental studies by color M-mode echocardiography (PhD thesis). Medical Department B and Institute for surgical research. University of Oslo, Oslo.

Stugaard, M., L. Greenberg Neil, J. Zhou, and D. Thomas James. 1997. Automated eigenvector analysis for quantification of color M-mode Doppler filling patterns of the left ventricle in an ischemic canine model. Computers in Cardiology 24: 61-64.

Stugaard, M., C. Risoe, H. Ihlen, and O. A. Smiseth. 1994. Intracavitary filling pattern in the failing left ventricle assessed by color M-mode Doppler echocardiography. J Am Coll Cardiol 24: 663-70.

Stugaard, M., O. A. Smiseth, C. Risoe, and H. Ihlen. 1993. Intraventricular early diastolic filling during acute myocardial ischemia, assessment by multigated color m-mode Doppler echocardiography. Circulation 88: 2705-13.

Stugaard, M., O. A. Smiseth, C. Risoe, and H. Ihlen. 1995. Intraventricular early diastolic velocity profile during acute myocardial ischemia: a color M-mode Doppler echocardiographic study. J Am Soc Echocardiogr 8: 270-9.

Suga, H. 1995. How we view systolic function of the heart: Emax and PVA in N. Ingels, G. Daughters, J. Baan, J. Covell, R. Reneman, and F. Yin, eds. Systolic and diastolic function of the heart. IOS Press, Amsterdam.

Sumimoto, T., T. Jikuhara, T. Hattori, F. Yuasa, M. Kaida, M. Hisokaka, K. Takehana, T. Tamura, T. Sugiura, and T. Iwasaka. 1997. Importance of left ventricular diastolic function on maintenance of exercise capacity in patients with systolic dysfunction after anterior myocardial infarction. Am Heart J 133: 87-93.

Takatsuji, H., T. Mikami, K. Urasawa, J. Teranishi, H. Onozuka, C. Takagi, Y. Makita, H. Matsuo, H. Kusuoka, and A. Kitabatake. 1996. A new approach for evaluation of left ventricular diastolic function: spatial and temporal analysis of left ventricular filling flow propagation by color M-mode Doppler echocardiography. J Am Coll Cardiol 27: 365-71.

Takeuchi, M., K. Fujitani, K. Kurogane, and e. al. 1985. comparison of two exponential models of the time constant during left ventricular isovolumic pressure decay in coronary artery disease. Jap Circ Journal 49: 1225-1234.

Taylor, R., and A. Waggoner. 1992. Doppler assessment of left ventricular diastolic function: a review. J Am Soc Echocardiogr 5: 603-12.

Teien, D. E., H. Wendel, J. Bjornebrink, and L. Ekelund. 1993. Evaluation of anatomical obstruction by Doppler echocardiography and magnetic resonance imaging in patients with coarctation of the aorta. Br Heart J 69: 352-355.

Teien, D. E., H. Wendel, S. Holm, and M. Hallberg. 1991. Estimation of Doppler gradients at rest and during exercise in patients with coarctation of the aorta. Br Heart J 65: 155-157.

Thomas, J. 1994. Doppler echocardiography and left ventricular diastolic function. Pages 192-218 in W. Gaasch and M. LeWinter, eds. Left ventricular dysfunction and heart failure. Lea & Febiger, Philadelphia.

Thomas, J., J. Newel, C. Choong, and A. Weyman. 1991. Physical and physiological determinants of transmitral velocity: numerical analysis. Am J Physiol 260: H1718-H1730.

Thomas, J., and A. Weyman. 1989. A fluid dynamics model of mitral valve flow: description with in vitro validation. J Am Coll Cardiol 13: 221-233.

Thomas, J., and A. Weyman. 1991. Echo-Doppler evaluation of left ventricular diastolic function: physics and physiology. Circulation 84: 977-999.

Thomas, J. D., M. J. Garcia, and N. L. Greenberg. 1997. Application of color Doppler M-mode echocardiography in the assessment of ventricular diastolic function: potential for quantitative analysis. Heart Vessels Suppl 12: 135-7.

Thompson, D., C. Waldron, D. Coltart, B. Jenkins, and M. Webb-Peploe. 1983. Estimation of time constant of left ventricular relaxation. British Heart Journal 49: 250-258.

Togni, M. 2001. Color M-mode Doppler flow propagation velocity in cardiac tamponade (letter). J Am Coll Cardiol 37: 328-329.

Tsui, B. Single-photon emission computed tomography. Pages 1055-1076 in J. Bronzino, ed. Biomedical engineering handbook. CRC press, 1995.

Udelson, J., and R. Bonow. 1994. Radionuclide angiographic evaluation of left ventricular diastolic function. Pages 167-191 in W. Gaasch and M. LeWinter, eds. Left ventricular dysfunction and heart failure. Lea & Febiger, Philadelphia.

Urheim, S., T. Edvardsen, H. Torp, B. Angelsen, and O. Smiseth. 2000. Myocardial strain by Doppler echocardiography - Validation of a new method to quantify regional myocardial function. Circulation 102: 1158-1164.

Van Dantzig, J. M., B. J. Delemarre, H. Bot, R. W. Koster, and C. A. Visser. 1995. Doppler left ventricular flow pattern versus conventional predictors of left ventricular thrombus after acute myocardial infarction. J Am Coll Cardiol 25: 1341-6.

Vandervoort, P. M., N. L. Greenberg, P. M. McCarthy, and J. D. Thomas. 1993. Estimation of left ventricular filling gradients using digital analysis of color Doppler M-mode velocities. Computers in Cardiology 20: 293-296.

Vanoverschelde, J., B. Essamri, R. Vanbutsele, A. d'Hondt, J. Cosyns, J. Detry, and J. Melin. 1993. Contribution of left ventricular diastolic function to exercise capacity in normal subjects. J Appl Physiol 74: 2225-33.

Vasan, R., E. Benjamin, and D. Levy. 1995. Prevalence, clinical features and prognosis of diastolic heart failure: an epidemiologic perspective. J Am Coll Cardiol 26: 1565-1574.

Vasan, R., M. Larson, E. Banjamin, J. Evans, C. Reiss, and D. Levy. 1999. Congestive heart failure in subjects with normal versus reduced left ventricular ejection fraction. J Am Coll Cardiol 33: 1948-1955.

Vasan, R., and D. Levy. 2000. Defining diastolic heart failure. A call for standardized diagnostic criteria. Circulation 101: 2118-2121.

Verdonck, P., A. Kleven, R. Verhoeven, B. Angelsen, and J. Vandenbogaerde. 1992. Computer-controlled in vitro model of the human left heart. Med & Biol Eng & Comput 30: 656-659.

Verdonck, P., P. Segers, L. Missault, and R. Verhoeven. 1996. In vivo validation of a fluid dynamics model of mitral valve M-mode echocardiogram. Med & Biol Eng & Comp 34: 192-198.

Verdonck, P., P. Segers, and R. Verhoeven. 1994. Mitral valve M-mode echocardiogram and left ventricular (dys)function. J Cardiovasc Diagn Proc 13: 7-13.

Verdonck, P., J. Vierendeels, and P. Dierickx. 1998. Cardiac Mechanical models. Pages 1-50 in P. Verdonck, ed. Intra and Extracorporeal Cardiovascular Fluid Dynamics - General Principles in Application. WITTpress, Southampton, UK.

Verdonck, P., J. Vierendeels, K. Riemslagh, and E. Dick. 1999. Left ventricular pressure gradients: a computer-model simulation. Med Biol Eng Comput 37: 1-6.

Verhaaren, H., S. De Mey, I. Coomans, P. Segers, D. Matthys, D. De Wolf, and P. Verdonck. 2001. Fixed region of nondistensibility after coarctation repair: in vitro validation of its influence on Doppler peak velocities. J Am Soc Echo 14: 580-587.

Vierendeels, J. 1998. Een numeriek model voor de vulling van de linkerhartkamer. Pages 293. Mechanical Engineering. Ghent University, Ghent.

Vierendeels, J., K. Riemslagh, E. Dick, and P. Verdonck. 2000. Computer simulation of intraventricular flow and pressure gradients during diastole. J Biomech Eng 122: 667-674.

Vitarelli, A., and M. Gheorghiade. 1998. Diastolic heart failure: standard Doppler approach and beyond. Am J Cardiol 81: 115G-121G.

Vlassak, I., L.M. King, N.L. Greenberg, M.S. Firstenberg, J.D. Thomas, M.J. Garcia. 2001a. Earlier apical relaxation increases ventricular suction during exercise in normal volunteers (abstract). J Am Coll Cardiol 37: 442A.

Vlassak, I., L. King, N. Greenberg, J. Thomas, and M. Garcia. 2001b. Color M-mode propagation velocity predicts exercise capacity (abstract). J Am Soc Echocardiog 2001, in press.

Weisfeldt, M., H. Scully, and J. Frederiksen. 1974. Hemodynamic determinants of maximum negative dP/dt and periods of diastole. Am J Physiol 227.

Weiss, J., J. Frederiksen, and M. Weisfeldt. 1976. Hemodynamic Determinants of the Time-Course of fall in canine left ventricular pressure. J Clin Invest 58: 751-760.

Wells, P. 1977. Doppler methods in P. Wells, ed. Biomedical Ultrasonics. Academic Press, New York.

Wendel, H., D. Teien, D. G. Human, and M. A. Nanton. 1992. Doppler echocardiographic and morphologic evaluation of patients following operative repair of aortic coarctation. Acta Paediatr 81: 247-252.

Weymann, A., ed. 1994. Principles and Practices of Echocardiography. Lea & Febiger, Philadelphia.

Wonnacot, and Wonnacot. 2000. Statistics. .

Wyse, R. K. H., P. J. Robinson, J. E. Deanfiled, D. S. Tunstall Pedoe, and F. J. Macartney. 1984. Use of continuous wave Doppler ultrasound velocimetry to assess the severity of coarctation of the aorta by measurement of aortic flow velocities. Br Heart J 52: 278-283.

Yamakado, T., E. Takagi, S. Okubo, Y. Imanaka, T. Tarumi, M. Nakamura, and T. Nakano. 1997. Effects of ageing on left ventricular relaxation in humans. Analysis of left ventricular isovolumic pressure decay. Circulation 95: 917-23.

Yellin, E. 1995. The momentum of mass, the momentum of ideas, and diastolic function in N. Ingels, G. Daughters, J. Baan, J. Covell, R. Reneman, and F. Yin, eds. Systolic and diastolic function of the heart. IOS Press, Amsterdam.

Yellin, E., M. Hori, C. Yoran, E. Sonnenblick, S. Gabbay, and R. Frater. 1986. Left ventricular relaxation in the filling and nonfilling intact canine heart. Am J Physiol 250: H620-H629.

Yellin, E., and S. Nikolic. 1994. Diastolic suction and the dynamics of left ventricular filling. Pages 89-102 in W. Gaasch and M. LeWinter, eds. Left ventricular dysfunction and heart failure. Lea & Febiger, Philadelphia.

Yellin, E. L., S. D. Nikolic, and R. W. Frater. 1994. Left ventricular diastolic function and mitral valve flow. J Heart Valve Dis 3: 41-4.

Yoganathan, A., J. Hopmeyer, and R. Heinrich. 1995. Mechanics of heart valves in J. Bronzino, ed. Biomedical engineering handbook. CRC press.

Yong, Y., S. Nagueh, S. Shimoni, K. Shan, Z. He, M. Reardon, G. Letsou, J. Howell, M. Verani, M. Quinones, and W. Zoghbi. 2001. Deceleration time in ischemic cardiomyopathy. Relation to echocardiographic and scintigraphic indices of myocardial viability and functional recovery after revascularization. Circulation 103: 1232-1237.

Zamorano, J., D. R. Wallbridge, J. Ge, J. Drozd, J. Nesser, and R. Erbel. 1997. Non-invasive assessment of cardiac physiology by tissue Doppler echocardiography. A comparison with invasive haemodynamics. Eur Heart J 18: 330-9.

Symbolenlijst / Symbols

Abbreviations / Afkortingen

A	Atrial Contraction	Atriale Contractie
ACE	Angiotensin Converting Enzyme	Angiotensin Converting Enzyme
AiO	Air Outlet	Luchtuitlaat
ANOVA	Analysis Of Variance	Variantie Analyse
AoF	Aortic Valve Flow	Aortadebiet
AR	Atrial Reversal Flow	Atriale Omkeer Stroming
ATP	Adenosine Triphosphate	Adenosine Trifosfaat
AV	Atrioventricular	Atrio-Ventriculair
BPM	Beats Per Minute	Slagen Per Minuut
BSA	Body Surface Area	Lichaamsoppervlakte
CHF	Congestive Heart Failure	Congestief Hartfalen
CI	Coarctation Index	Coarctatie Index
CMD	Color M-mode Doppler	Kleuren M-mode Doppler
CO	Cardiac Output	Hartminuutvolume
CT	Computed Tomography	Computed Tomography
DBP	Diastolic Blood Pressure	Diastolische Bloeddruk
DHF	Diastolic Heart Failure	Diastolisch Hartfalen
DP	Doppler Probe	Doppler Probe
DR	Delayed Relaxation	Vertraagde Relaxatie
E	Early Filling	Vroege vulling
ECG	Electrocardiogram	Electrocardiogram

EDPVR	Enddiastolic Pressure-Volume Relationship	Eind-diastolisch Druk-Volume Verband
EDV	Enddiastolic Volume	Eind-diastolisch Volume
EF	Ejection Fraction	Ejectiefractie
ESPVR	Endsystolic Pressure-Volume Relationship	Eind-systolisch Druk-Volume Verband
ESV	Endsystolic Volume	Eind-systolisch Volume
EV	Electromagnetic Valve	Electromagnetische KLep
GLM	General Linear Model	Algemeen Lineair Model
HR	Heart Rate	Hartritme
IS	Infarct Score	Infarctscore
IVRT	Isovolumic Relaxation Time	Isovolumetrische Relaxatietijd
IVPG	Intraventricular Pressure Gradients	Intraventriculaire Drukgradiënten
IVPGe	IVPG During Early Filling	IVPG Tijdens Vroege Vulling
IVPGivr	IVPG During Isovolumic Relaxation	IVPG Tijdens Isovolumetrische Relaxatie
LA	Left Atrium	Linker Atrium
LAP	LA Pressure	LA Druk
LM_2	Mono-exponential Model with Fixed Zero Pressure Asymptote	Mono-exponentieel Model met Vaste Nul-Drukasymptoot
LM_3	Mono-exponential Model with Floating Pressure Asymptote	Mono-exponentieel Model met Vrije Drukasymptoot
LV	Left Ventricle	Linker Ventrikel
LVP	LV Pressure	LV Druk
MiF	Mitral Valve Flow	Mitraaldebiet
MRI	Magnetic Resonance Imaging	Magnetische Resonantie Beeldvorming
MSE	Mean Squared Error	Gemiddelde Kwadratische Afwijking
NA	Not Available	Niet Beschikbaar
NS	Not Significant	Niet Significant
NYHA	New York Heart Association Class Of Disease Severity	New York Heart Association Ziektegraad Classificering
PCWP	Pulmonary Capilary Wedge Pressure	
PeCh	Perspex Chamber	Perspex Kamer
PET	Positron Emission Tomography	Positron Emission Tomography
PN	Pseudo-normal Filling	Pseudo-normale Vulling
PRF	Pulse Repitition Frequency	Puls Herhalingsfrequentie
PS	Pneumatic Systel	Pneumatisch Systeem

PWD	Pulsed Wave Doppler	Gepulste Doppler
RA	Right Atrium	Rechter Atrium
RE	Relative Efficiency	Relatieve Efficiëntie
REF	Reference Stage	Referentie Toestand
RF	Restrictive Filling	Restrictieve Vulling
RV	Right Ventricle	Rechter Ventrikel
SA	Sinoatrial	Sino-Atriale
SBP	Systolic Blood Pressure	Systolische Bloeddruk
SD	Standard Deviation	Standaardafwijking
SE	Standard Error	Standaardfout
SHF	Systolic Heart Failure	Systolisch Hartfalen
SPECT	Single Photon Emission Computed Tomography	
STFT	Short-time Fourier Transform	Korte-tijd Fouriertransformaie
SV	Stroke Volume	Slagvolume
TD	Time Delay	Tijdsvertraging
TDI	Tissue Doppler Imaging	Weefsel Doppler Beeldvorming
VAR	Variability	Variabiliteit

Symbols / Symbolen

A	velocity of the atrial contraction wave	snelheid van de atriale contractie golf	[cm/s]
a	acceleration	acceleratie	[cm/s²]
a	diameter vortex core	vortex-kern diameter	[cm]
b	parameter	parameter	
b	diameter vortex annulus	vortex ring diameter	[cm]
c	speed of sound	geluidssnelheid	
C	compliance	compliantie	[ml/mmHg]
Ca	calcium	calcium	
D	diameter	diameter	[cm]
D	diastolic flow	diastolische stroming	[cm/s]
d_t	deceleration time	deceleratietijd	[ms]
e	Euler constant	Eulerconstante	
E	velocity of the early filling wave	snelheid van de vroege vullingsgolf	[cm/s]
E	time varying elastance	tijdsafhankelijke elastantie	[mmHg/ml]

E	Young's modulus	modulus van Young	[kPa]
f	frequency	frekwentie	[1/T]
F	frame rate	beeldherhalingssnelheid	[1/T]
F	energy losses	ladingsverliezen	[m]
g	gravity constant	graviteitsconstante	[L/T²]
h	LV wall thickness	LV wanddikte	[mm]
k	pulses per scanline	pulsen per scanlijn	
k_c	LV stiffness index	LV stijfheidsindex	[1/ml]
K	Kalium	Kalium	
K_l	geometry parameter	geometrie afhankelijke parameter	
K_v	geometry parameter	geometrie afhankelijke parameter	
n	count	aantal	
Na	Natrium	Natrium	
p	pressure	druk	[mmHg]
p	level of significance	significantieniveau	
Q	flow	debiet	[l/min]
r	LV radius	LV straal	[cm]
r	correlation coefficient	correlatiecoëfficiënt	
r	target range	doelbereik	[L]
Re	Reynolds number	Reynoldsgetal	[ ]
s	line coordinate	lijncoördinaat	[L]
S	stiffness index	stijfheidsindex	[mmHg]
S	systolic flow	systolische stroming	[cm/s]
S	base-apex distance	base-apex afstand	[cm]
t	time unit	tijdseenheid	[T]
Tc	Technetium	Technetium	
Th	Thallium	Thallium	
v	velocity	snelheid	[cm/s]
v_p	flow propagation velocity	stromingvoortplantingssnelheid	[L/T]
V	volume	volume	[ml]
V_0	LV equilibrium volume	LV evenwichtsvolume	[ml]
V_φ	LV intercept	LV intercept	[ml]
VO_2max	peak oxygen uptake	piek-zuurstofopname	[ml/kg/min]
z	altitude	hoogte	[m]
Z	impedance	impedantie	[mmHg·s/ml]

Greec Symbols / Griekse Symbolen

α	parameter	parameter	
β	arterial stiffness index	arteriële stijfheidsindex	[ ]
β	parameter	parameter	
β	GLM parameter estimate	GLM parameterschatting	
θ	angle	hoek	
μ	dynamic viscosity	dynamische viscositeit	[Pa·s]
ν	kinematic viscosity	kinematische viscositeit	[cm²/s]
ξ	energy loss coefficient	ladingsverlies coëfficiënt	[ ]
ρ	density	massadichtheid	[kg/m³]
σ	LV wall tension	LV wandspanning	[mmHg]
τ	LV relaxation time constant	LV relaxatie tijdsconstante	[ms]
ω	harmonic number	harmonisch nummer	

Subscripts

adj	adjusted	aangepast
BTB	Beat-To-Beat	slag-tot-slag
d	diastolic	diastolisch
d	distal	diastaal
D	Doppler	Doppler
hydr	hydaulic	hydraulisch
inter	Between observers	tussen waarnemers
intra	within observer	eigen aan een waarnemer
m	myocard	myocardium
max	maximum	maximum
n	negative	negatief
num	numerical	numeriek
Nyq	Nyquist	Nyquist
p	proximal	proximaal
p	positive	positief
R	receiver	ontvanger
s	systolic	systolisch
s	in situ	in situ
0	equilibrium	evenwicht

0	reference section	referentie sectie
0	start time	starttijd
0	source	bron
1	study section	studieplaats
∞	asymptote	asymptote

Operators / Wiskundige Operatoren

$\partial/\partial x$	partial derivative with respect to variable x	partiële afgeleide naar de veranderlijke x
d/dx	derivative with respect to variable x	afgeleide naar de veranderlijke x
Δ	difference	verschil
$\int$	integral operator	integraal
$\sum$	summation	sommatie
$\bar{}$	mean	gemiddelde

Units / Eenheden

m	[L]	meter	
µm	[L]	micrometer	10^{-6} m
mm	[L]	millimeter	10^{-3} m
cm	[L]	centimeter	10^{-2} m
s	[T]	second	
µs	[T]	microsecond	10^{-6} s
ms	[T]	millisecond	10^{-3} s
min	[T]	minute	60 s
Pa	$[M/T^2/L]$	Pascal	
mmHg	[L]	millimeter Mercury	133.3 Pa
g	[M]	gram	
kg	[M]	kilogram	10^{3} g
Hz	[1/T]	Herz	
kHz	[1/T]	kiloHertz	10^{3} Hz
MHz	[1/T]	megaHerz	10^{6} Hz
°C		degrees Celsius	

Diastology:
Insights from Model Studies and Clinical Observations using Color M-Mode Doppler Echocardiography.

Stefaan De Mey

AJ 2001-2002